ABSTRACTS

Nikat Akkus, Garip Genc, Cemal Girgin
Control of the pretension in filament winding process

A tension control system which simulates the effect of tension force in the filament winding machines has been designed and implemented in the present study. Filament Winding (FW) machines are widely used in Fiber Reinforced Plastic (FRP) composite production systems in which they have a pretensioning system to optimize the tension of the fiber during winding process. The precise control of the winding path needs highly mechatronic systems. The designed control system consists of magnetic break, servo motor, a PID control unit, a load cell and a data converter. The tension of the carbon fiber was measured by a load cell and compared to the preset value to keep the tension of the carbon fiber in predefined certain range.

Orest Bazylevych, Orest Ivakhiv, Roman Velgan
Procedure of distances evaluation for surface inspection

In the context of developing automated optical inspection system, this work brings into focus the aspect of development of evaluation algorithms for thickness distribution extraction from the object model reconstructed after surface scanning. Within this work an algorithm for the evaluation of local differences between two triangle meshes is presented. The pair of triangular meshes is representing the front and backside of a scanned 3D-object. The resulting array of differences vector corresponds to the shortest local distances (i.e. local thickness) between sides of object.

Ivars Beinarts, Anatoly Levchenkov, Peteris Balckars
Control of heating processes in transport mechatronic system using sigmoidal feed forward neural network

In this article interest is concentrated on the climate parameters optimization in passengers' interior of mechatronic systems (public electric transportation vehicles- train, tram or trolleybus). Idea is to use feed forward artificial neural network to create an algorithm and coordination mechanism for heating system parameters control to save electrical energy, and to increase the level of comfort for passengers. A special interest for investigations and further development is devoted to intelligent HVAC system allowing more flexible control of the system's compressor, fan and heater operation, and, therefore, improvement of efficiency and energy saving. This paper provides the mathematical model and algorithm for optimal control of the climate control system.

Mariusz Bogdan
Computer processing of some surface images of technical objects after influence of the high temperature conditions

Computer processing of the image of surface of operating gas turbine blades was proposed in order to make the method of the evaluation of the condition of these blades more objective. The dependences and connections between the degree of blade material overheating and the colour of analyzed surfaces were shown on the basis of images registered in visible range of electromagnetic wave (digital image – Charge Coupled Device matrix). The proposal of methodology to assign the overheated areas on the blade's surface in order to assess the range (of degradation) of thermal usage of the blade and to forecast it's working resources, might be useful to monitor the situation in the operating conditions. Moreover in the article the problematic of acquisition of the form digital images dates was presented by showing physical basis of analysis of reflected signal from metallic surface are showed in aspect of recording by photoelectric light sensor (matrix CCD).

Norbert Chamier-Gliszczyński
Disassembly modeling of the mechatronic systems for reuse and recycling

This paper presents processes modeling disassembly of the mechatronic systems for reuse and recycling. Typical steps in modeling and analyzing disassembly processes consist of the following: the objective of the model is stated, a mass flow diagram consisting of acquisition, sorting, disassembly processes, and recycling process of the facility in developed, modeling disassembly processes, disassembly process planning, optimal disassembly sequences: (generation of feasible disassembly sequences, adaptive disassembly processing, selective disassembly, destructive disassembly).

Agata Dudek
Investigation on the microstructure of the HAP and YSZ composites

Group of bioceramic materials includes, among others, hydroxyapatites (HAp, OHAp, HA), which, due to their specific properties are widely applied. These compounds are currently present in bone systems of human and animal bodies. One of the solutions for improvement of poor properties of HAp is addition of zirconium oxide which is characterized

by high biological tolerance and enhanced mechanical properties. Application of bioceramic materials as coatings for implants introduced into human body due to their bioinertness and biocompatibility enables overcoming immunology barriers. One of the fundamental advantages of ceramic materials is their positive impact on human tissues. The investigations involved creation of composites through single-axial compaction of two ceramic powders (HAp+YSZ) and then their sintering at the temperature of 1300oC for two hours. The aim of the investigations was to determine thermal stability of hydroxyapatite (Fig. 1) and HAp + YSZ (Partially Stabilized Zirconia) (Fig. 2) and impact of addition of YSZ (8%wt. Y2O3 stabilizing ZrO2) on phase composition of the prepared composites after the process of sintering.Investigations of the structure have been performed using JEOL JSM 5400 (Fig. 4, 5) scanning microscope while phase composition have been carried out by means of Seifert 3003 T-T X-ray diffractometer (Fig. 6, 7).

Aleksandr Gubarev, Oleg Jachno, Oksana Ganpantsurova
Cyclic-modular approach to development of electronically-mechanical control systems of the pneumatic drive

The module approach for build-up of cyclic action systems is considered. The main property of approach is system decomposition on cyclic action subsystems (modules). All modules have same structure: actuating device (drive), control device (directional valve), status sensors. Methods of approach application are realized by means of graphs. Advantage of module approach is possibility of physically heterogeneous devices combination (devices with pneumatic or hydraulic control, electro-relay or PLC) not only in all system, but also inside of each modulus, that reduced a number of signal conditioning devices. Such synthesis is possible owing to a minimal structure of each modulus.

Marek Hryniewicz, Jan Anthonis, Herman Ramon
3D apple modeling with the use of the structured light method

The geometrical fruit model could affect many physical phenomena, such as heat, mass and moisture transfer, pneumatic transport and mechanical vibrations which occur during handling and processing fruits (Jancsok, 1999). The fruit geometrical model could be further studied by the Finite Element Method (FEM) (Jancsok, 1999). Incidence of bruises is the most important type of postharvest mechanical injury (van Zeebroeck, 2005). The reason for this is that the causes and mechanisms of impact and vibration are complex and interrelated (van Zeebroeck, 2005). In mechanical engineering a geometrical model of the structure to be analyzed is usually available as CAD drawing which can be imported directly in FE software (Jancsok, 1999). However, for agricultural-, bio- and food- materials there are no geometrical models available so they have to be defined manually, which is complicated by the complex shape and the shape variability of these products (Jancsok, 1999). Dintwa (Dintwa, 2006) stated that the 3D simplified models used in the dynamic experiments were not accurate enough, most certainly because of the coarse discretization used with these models. This paper describes a system for complex shapes geometrical modeling. The system was implemented in real apple modeling. It was developed on structured light method elaborated by Sitnik (2002). The method has advantages and disadvantages. Advantages: modeling of complex shapes, recalculation of many points at one moment, at least only 3 views for one figure, measurements without object touching.
Disadvantages: problems with light reflection.

Tatjana Ivanova, Janis Rudzitis
Traceability and capability control of mass measurement equipment and drift statistical analysis of national mass standards in Latvia

LNMC is highest metrological institute of Latvia. The paper describes national mass standards currently in use, their traceability, stability, mass measurement equipment and related techniques.

Roman Z. Kacprzak
Applicability estimation of a low-cost haptic device for the purpose of steering the mobile platform

In this paper a concept of using an easily accessible (i.e. commercially available for common home user) model of enhanced user interface – Haptic Device – for purpose of steering a mobile platform is presented. The functional requirements for the investigated device are specified based upon literature sources and verified empirically by author by performing real-time experiments in Matlab\Simulink.

Bronius Karaliunas
Computer modeling of the characteristics and magnetic field of single - phase commutator motor

The article presents some calculation results of dynamic characteristics of the single – phase series – excited commutator motors and magnetic field analysis. Single – phase commutator motors in up – to – date literature are called universal motors, because they can be used in both alternating current (AC) and direct current (DC) systems. The single – phase AC small power commutator motors are widely used in different vacuum cleaners, electric tools, drives

of household, electrical, medical and hygienic equipments and porta-ble electrical hand tools. However, the principal defect of those motors is worse commutation with sparkling between brushes and the collector, and high enough level of radio interferences on wide frequency range. In this article obtained expressions compounds the mathematical model of the single – phase series – excited commutator motor. The model of the dynamic processes of the motor and its block diagram are compiled according to the differential equations which were derived from the equations of voltage balance. The software of Matlab/Simulink is applied here which has integrated the methods of the solution of differential equations for the motor. For modeling the magnetic field of a AC series – excited commutator motor there was used the software JMAG. The program is complied by means of finite elements, by attaching on the computer separate geometric figures their titles and character-ristics. Since the magnetic field in the air gap between the salient poles and armature is not homogeneous, so the density of the grid has to be the highest. The obtained results of modeling describe a very complicated structure of a magnetic field of a commutator motor for the analysis of which are required new and comparatively accurate mathematical models.

Gabriel Kost, Daniel Reclik
The 2 ½D algorithm in robot workspace analysis

In this paper there is presented the method of 3D manipulator's workspace analysis. The analysis of robot's work-space is necessary for generation the safety movement path. There was 2 ½ D method, which is based on algorithm of following sections defining in robot work area. Those sections are explored by flat analysis, but the results are transposed into graph form. This graph is the record of all possible movements, so to get the optimum movement there must be used Floyd's algorithm. This, shortest trace is optimized and smoothed by using B-Spline curves.

Mustafa Kurt, Hasan Geyik, Bilçen Mutlu, Yaşar Tatar , Ergun Nart
Design, prototype and experimental evaluation of a wheelchair treadmill

Generally, wheelchair users cannot move easily within buildings since living areas in architectural structures are not suitable for them to maintain or to improve their physical capabilities. Because living area restrictions affect the physical performance of the users outside during the day, the reduced mobility causes several health problems. These problems become more intense by the time. Especially heart and lung related illnesses are common among the wheelchair users since the immobility decreases respiration capacity. The aim of this research is to design and prototype a wheelchair treadmill to help wheelchair users improve their upper extremity system. In this study, CAD was employed for the design of wheelchair treadmill. Then finite element analysis (FEA) was carried out for the parts of the wheelchair treadmill and the prototype was manufactured based on the results. The prototype was tested under the conditions the product was originally intended to function. In the experiments, the speeds of wheelchair and wheelchair treadmill were measured. The distances taken by users were also recorded, and the results were evaluated with respect to road surface conditions.

Dmitry Litvinov, Janis Rudzitis
High frequency vibration monitoring and diagnostics of high-speed pump rolling bearings

Evolution of modern industry makes great demands to reliable work of pump equipment with large revolutions number of rotating parts. Under special supervision must be the centrifugal high-speed pumps. One of the major and hardly loaded units of high-speed pump equipment are rolling bearings, therefore it is very important to conduct monitoring and early diagnostics works to find out defects in them. For the high-frequency vibration detection and analysis it is possible to use both stationary and portable systems of monitoring and diagnostics. This diagnostics advantage is early detection of aberration from normal operation of rolling bearings and transition from equipment service and repair on-schedule to real situation service and repair, which is determined on periodic diagnostics results.

Cristina Pana, Viorel Stoian
A fault-tolerant control system for a hexapod mobile robot

This paper presents a fault-tolerant control system for a hexapod mobile robot. First, a description of the dynamic model of the hexapod mobile robot by a system of differential equations is made and after that, a representation of the system in state variable space is obtained. A fault detection and identification algorithm is proposed. The modality used here is an analytical redundant process, which supposes that the processing of the information is made at a superior level for the identification of the changes due to the faults. By this method, the actualized model obtained by the on-line identification of the system, is permanent compared with nominal model (without faults). The adaptive control system for uncertain non-linear systems proposed here has two main blocks: adaptation mechanism block which implements the mathematical model of the adaptation error and control law accommodation block which changes the characteristics of the control law. Finally, the authors propose the hexapod mobile robot which is open to fault events, to be a variable structure system and analyze a specific control method.

Ilhan Tarimer, Serkan Örücü, Rıza Gürbüz
Developing an educational software controlling data transfer of serial and parallel ports

In this study, it has been examined whether computer-based teaching software is applicable in today's electronic and computer teaching. By the improvement of today's computer teaching, people are able to reach information easily. Both indoor and outdoor of classroom works, teaching software, which supports learning, has been aimed to help both teachers and students. The educational software prepared in this study that can be used in the area of controls with parallel and serial computer ports. In this study, basic properties of parallel-serial ports, to use them in mechatronics and their using facilities have been explained. How to program these ports together with their connections have been embedded into the educational teaching software. Thus, according to its algorithm and frame, this educational software interface developed can be used for general mechatronics training

Abdullah Uzun, Fahri Vatansever
Ismail Al Jazari machines and new technologies

Al-Jazari was a 12th Century Turkish Scientist, Engineer and writer. His full name was Badi Al-Zaman AbulI-Izz Ibn Ismail Ibn Al-Razzaz Al-Jazari. He lived in Diyarbakir region in Turkey (1206 AD). As his town name is Cizre, the modern Turkish scripting of Jizra , his last name is known as Jazari (Uzun, 1997). Badi Al Zaman means "prodigy of the Age" and was applied to other well-known men (Hill, 1974). He served the Artuks a Seljuks dynasty in Diyarbakir, as a chief engineer – as did his father before him. He invented the crankshaft and some of the first mechanical clocks, driven by water and weights- used water power. He authored and drawed 60 inventions in his book "Al-Jami Bain Al-Ilm Wal-Amal Al-Nafi Fi Sinat'at Al-Hiyal" (The Book of Know-ledge of Ingenious Mechanical Devices). Kitab al-Hiyal is an interesting work on automatic control mechanism, fountains, devices, pipes, valves and siphons. The importance and originality of Kitab al-Hiyal is due to its being an earlier example of the automatic control studies in the history. There are a number of ma-nuscripts of Jazari's work in Oxford, Leiden, Paris, Dublin and İstanbul. Equally cranks may have first been documented by Al Jazari – 300 years before western engineers achieved this (Francesco di Giorgio Martini and Leonardo Da Vinci). He used some kind of symbols for understanding of his drawings like using of electronic circuits. We found that his machine drawings and manufacturings quite qualified understanding (http://orionrobots.co.uk/tiki-index.php?page=Al+Jazari). The aim of this study is to review and examine Al Jazari's drawings and then, to compare and examine with the new technology period.

Marius Vasylius, Vytautas K. Augustaitis, Vytautas Barzdaitis, Marijonas Bogdevicius
Dynamics of the air blower with gyroscopic couple

To avoid damaging of tilting pad journal bearings, the problem of safety shut down of high speed air blower cantilever rotor becoming important in modern industry. The experimental testing, modeling and simulation of dynamic behavior of rotating system was run to directly evaluate gyroscopic negative effect damaging journal bearings. A dynamic model of air blower rotating system was designed and simulated. A simulation and experimental measurement results of rotating system were used to optimize the shut down regime of machine. Gyroscopic effect influences of rotor bearing stability are confirmed. Results of numerical simulation confirm results of experimental vibration measuring. The theoretical research results are given and conclusions are made. Experimental testing and simulations results was applied to typical air blower rotating systems for elimination of huge negative forces acting on new bearings during shut down of the machine.

Arkady S. Yuschenko, Dmitry N. Morozov, Andrey A. Zhonin
Speech control for mobile robotic systems

The experience and intelligence of human are necessary to fulfill the hazardous and responsible operations by mobile robot in undetermined environment. To make the control process more effective and simple for human the speech control may be used. The operator's interface in this case may be created using the linguistic variables both for commands formalization and for information presentation. The speech controlled robot has to be an autonomous intelligent system capable to re-cognize the current situation and to adopt its behavior to real environment. To adopt the artificial intelligence to the human impression and reasoning the fuzzy logic principles may be used to create the knowledge base of a speech controlled robot. The simple manipulation and locomotion operations may be presented in form of fuzzy production rules. For complicated modes of behavior the procedure of fuzzy AI – planning have been proposed. The procedure of robot learning on the base of fuzzy neural networks has been developed .for the situations when human-operator can not formalize the fuzzy rules of robot behavior beforehand.

CONTROL OF THE PRETENSION IN FILAMENT WINDING PROCESS

Nikat AKKUS[*], Garip GENC[**], Cemal GIRGIN[***]

[*]Marmara University, Faculty of Technical Education, Mechatronics Dep.,Goztepe Campus 34722, Istanbul, Turkey
[**] Marmara University, Vocational School of Technical Sciences, Mechanical Dep. Goztepe Campus 34722, Istanbul, Turkey
[***] TEKO Electronics & Technical Educational Systems, Mechanical Dep. Goztepe Campus 34722, Istanbul, Turkey

nakkus@marmara.edu.tr, ggenc@marmara.edu.tr , cemal.girgin@tekoelektronik.com.tr

Abstract: A tension control system which simulates the effect of tension force in the filament winding machines has been designed and implemented in the present study. Filament Winding (FW) machines are widely used in Fiber Reinforced Plastic (FRP) composite production systems in which they have a pretensioning system to optimize the tension of the fiber during winding process. The precise control of the winding path needs highly mechatronic systems. The designed control system consists of magnetic break, servo motor, a PID control unit, a load cell and a data converter. The tension of the carbon fiber was measured by a load cell and compared to the preset value to keep the tension of the carbon fiber in predefined certain range.

1. INTRODUCTION

Composite systems which consist of fibers and resins have high usage in industrial areas as new structural materials. Composites are strong and light, thus they are mostly used where the mobility is important. There are many types of manufacturing process such as Sheet Molding, Compression Molding, Pultrusion, Resin Transfer Molding, Prepreg forming to create structural parts. Most of the manufactured One of the important composite forming processes is the Filament Winding (FW) process, which needs high path control of the continuous fiber. The winding pattern in the FW process should be precisely controlled to have better wound product with high quality. Thus the FW machines which are used to produce mostly axisymetric and symmetrical parts are mostly accepted as a type of mechatronics machines. The main parts of the FW machines are;

- Winding machine body, similar to that of lathe machine,
- Control unit (mostly by NC, CNC or DNC unit),
- Heat controlled resin impregnation system,
- Roving storage and pretensioning unit.

The FW machine is an integrated system of the above sub systems and needs to be run by control and coordination of the sub systems.

The brittle structure of the fiber especially that of carbon fiber affected very much from the pretensioning pro-cess. Optimizations of the above parameters are very important to lessen the damage caused on the fiber roving. Thus a servo motor controlled PID control system was designed and manufactured to carry out the necessary experiment. The task of the PID control was to keep the pretensioning force in a certain range under various tension forces.

Mainly, pre tension control for filament winding is the interest of researchers. In the literature some studies exist on the influence of winding tension on composite part quality, even if they are referred to symmetric part shapes that may be obtained by traditional filament winding (Cogen, 1997; Lauke and Friedrich, 1993; Mertiny and Ellyin, 2002). All studies stated that once the tension value has been set, it is necessary to assure that the tension acting on the roving during winding is as near as possible to the set nominal value for best strength of the final product.

Chan et al. (1996) described the evaluation of a robot based filament winding cell consisting of an industrial robot. They studied accuracy vs. speed relationships of the robotic winding cell for more prices winding of the fiber bundles. Sharon and Lin (2001) suggested the development of a fully automated fiber optic winding machine capable of accurately winding several different coil patterns, incorporates active tension control during winding, and includes a vision-based, automated error detection and correction system for improved reliability. Choi and et al. (1997) proposed that, a feedback controller for a moving tape tensioning system which uses an ER (electro-rheological) brake actuator. Yeung and et al. (1995) suggested a new drive system with fuzzy control and a synchronized compensator has been incorporated in the system to achieve these results. A low-displacement, high-bandwidth filament tension sensor has been developed as an integral part of the system.

Kudo and et al. (2000) proposed a new automated sewing system is described, consisting of two robots handling the fabric on the table in a similar manner as does a human operator during sewing. To enable user-friendly operation of the system operation, particularly in the phase of preparing new tasks, the original Multi-arm Robot Control (MRC) system has been developed. The control of hand coordination and the fabric tension has also been developed and implemented. To control seam path and its deviation from the desired trajectory, visual feedback was adopted. Sauter and et al. (2005) proposed a method for

fault-tolerant control in dynamic systems. The proposed approach is composed of two stages. The first stage is the detection and isolation of the failed component using a directional filter designed under a particular eigenstructure assignment. The second stage is represented by the reconfiguration mechanism which makes possible the compensation of the fault effects. Polini and Sorrentino (2005) studied a new type of robotized winding cell in which the winding tension tried to be kept constant. They equipped the cell with a dynamometer that has been mounted under the winding die. Components of the force along three orthogonal directions (Fx, Fy and Fz) were aimed to be measured in the system and the data of tension were managed by Labview software of National Instrument. Polini and Sorrentino (2006) suggested system to keep the winding tension on roving near to the nominal value and to avoid collision occurrence. Carrino and et al. (2003) studied a modular structure of a new feed-deposition head for a robotized cell able to manufacture complex shape parts in composite material by means of the filament winding technology. Imamura and et al. (1999) purpose two kinds of winding tension control methods, and implement them using PID or I-PD control and they proposed tension control methods, which make use of the rotational velocity diffe-rence between the mandrel and nip-roll parts, performed well in trials. Carrino and et al. (2004) suggested an original method to optimize and to compare alternative winding trajectories for robotized filament winding.

Another fiber tensioning system with a conventional load cell (Kyowa Instruments) was used to check the correctness of the developed servo-mechanic pretensioning system Carbon fibers were wound under various pretension forces using the developed system [Fig. 1 and 2]. Tension tests were carried out to understand several tensioning parameters on the carbon fiber strength using Instron tension machines.

2. DESIGN OF SERVO CONTROLLED TENSION SYSTEM

A pretension control system for filament winding process was designed and manufactured to understand the effect of the pretension system parameters in the present this study. The diameter of the single fiber is around 10 micrometer. The fibers are not used as single fiber but they are used generally as bundle whose fiber numbers are changed from 1000 (1K) to 48000 (48K). They are brittle and can be easily damaged if any friction or bending forces are in present during winding process. To simulate the friction and bending of the fibers, an experimental set up was designed and manufactured as it is in real situations.

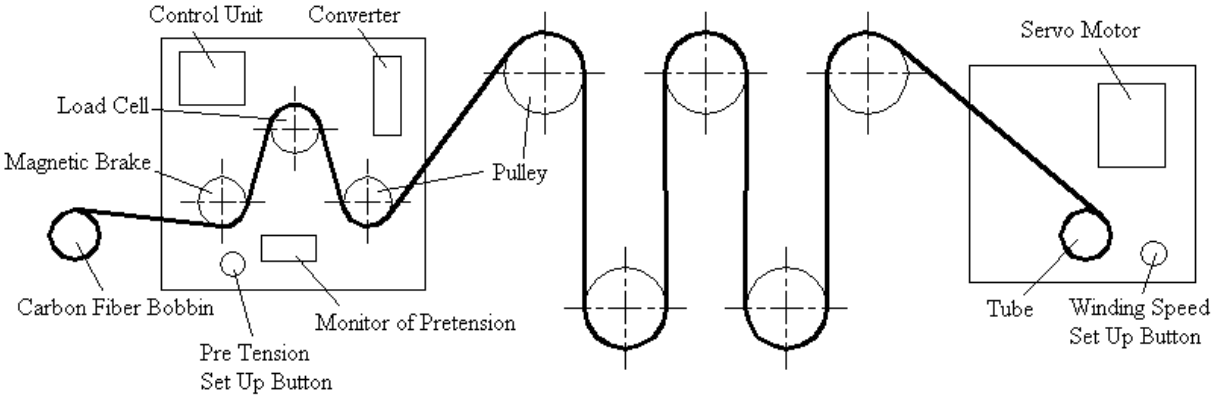

Fig. 1. Servo System Controlled Filament Winding System (a – Magnetic Brake Unit, b – Pre Tension Unit, c – Servo Motor Unit)

Tensioners which are the main object in the present study are used to pull the fiber so that the fiber could follow precisely the winding pattern path which it is supposed to go. The parameters which affect the winding are;

- The pretensioning force,
- The diameter of the pulleys which the fibers goes trough,
- The angle of the fiber between pulleys.

To control of the some of the above parameters are important to prevent strength loss in fibers caused by breakage. To do this, the strength loss measurement of the fiber bundle is important task. Bending strength in the fibers is mostly caused by vertical distance between pulleys and angle which defined by pulley diameter. A pulley system
in which the above parameters can be changed was manufactured. The tension force on the fiber body was measured by a torque controlled servo motor which was located at one end of the tension system. At the end of the system, there was a winding roll to pull the fiber. The tension force on the fiber was measured by a load cell which is located juts prior to last roll. The first unit is tension setup of carbon fiber
by magnetic brake with indicator of tension value.

Servo system controlled filament winding tension system which is seen in Fig. 1. consist of mainly from 3 units.

1. Magnetic brake unit which adjusted the speed of the fiber. This is also resulted the increase or decrease on the tension force in the fiber body (Fig. 2.).
2. The second unit is consisted of pulleys. The unit has two kind pulleys which are different in diameter. The

pulleys task was to transfer the fibers to the FW machine in a proper manner and create a room for tensioning adjustment (Fig. 1.b). The other task of the pulley was to change the travel angle of the fiber by changing the a and b distance between pulleys.

3. the third unit is fiber roll out unit. The task of the unit was to pull out of the fiber according to the predefined speed and wound it on a roll.

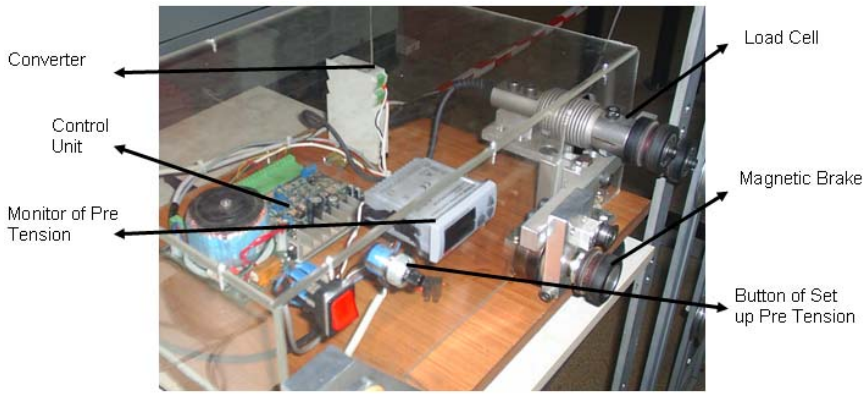

Fig. 2. Magnetic Brake Unit

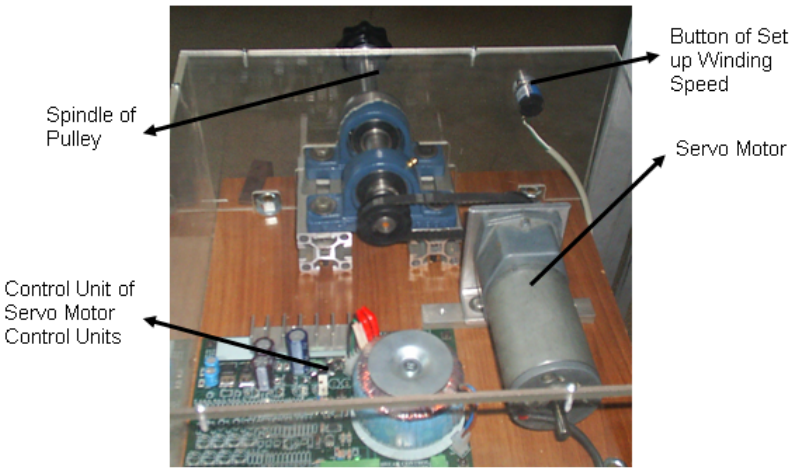

Fig. 3. Servo Motor Unit

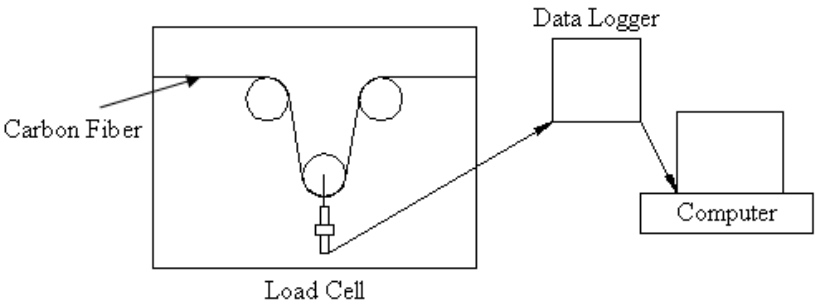

Fig. 4. Schematic Load Cell System

Pre tension unit which has pulleys – that can change positions is the second unit (Fig. 1b.). The third unit which can be change winding speed during filament winding. However this unit has bobbin for winding (Fig. 3).

During winding, converter takes the measured load signal and converts it to signal between 0 – 10 V and transmits the parameter to the control unit. A proportional–integral–derivative controller (PID controller) was used as control loop feedback mechanism. As it is well known, the PID controller calculation involves three separate parameters; the Proportional, the Integral and Derivative values. The Proportional value determines the reaction to the current error, the Integral determines the reaction based on the sum of recent errors and the Derivative determines the reaction

to the rate at which the error has been changing. The weighted sum of these three actions is used to adjust the brake movement. The PID controller attempted to correct the error between a measured tension force and a desired set point of tension force by calculating and then outputting a corrective action that can adjust the process accordingly.

The tuning of the PID controller was performed manually. According to the manual tuning, if the system must remain online, one tuning method is to first set the I and D values to zero. Increase the P until the output of the loop oscillates, and then the P should be left set to be approximately half of that value for a "quarter amplitude decay" type response. Then increase D until any offset is correct in sufficient time for the process. However, too much D will cause instability. Finally, increase I, if required, until the loop is acceptably quick to reach its reference after a load disturbance. However, too much I will cause excessive response and overshoot. A fast PID loop tuning usually overshoots slightly to reach the set point more quickly; however, some systems cannot accept overshoot, in which case an "over-damped" closed-loop system is required, which will require a P setting significantly less than half that of the P setting causing oscillation. The contributors of the PID control scheme is correcting terms, whose sum constitutes the manipulated variable (MV). That is:

$$MV(t) = Pout + Iout + Dout \quad (1)$$

Where Pout, Iout, and Dout are the contributions to the output from the PID controller from each of the three terms.

The effectiveness of the PID control system was also checked by a conventional measurement system which was consisted of a load cell, high speed data logger and a computer. A three pulley system with a load cell (Kyowa Instruments), originally proposed by Horide et al.(1999) was employed. The schematic of the load cell system is given in Fig. 4.

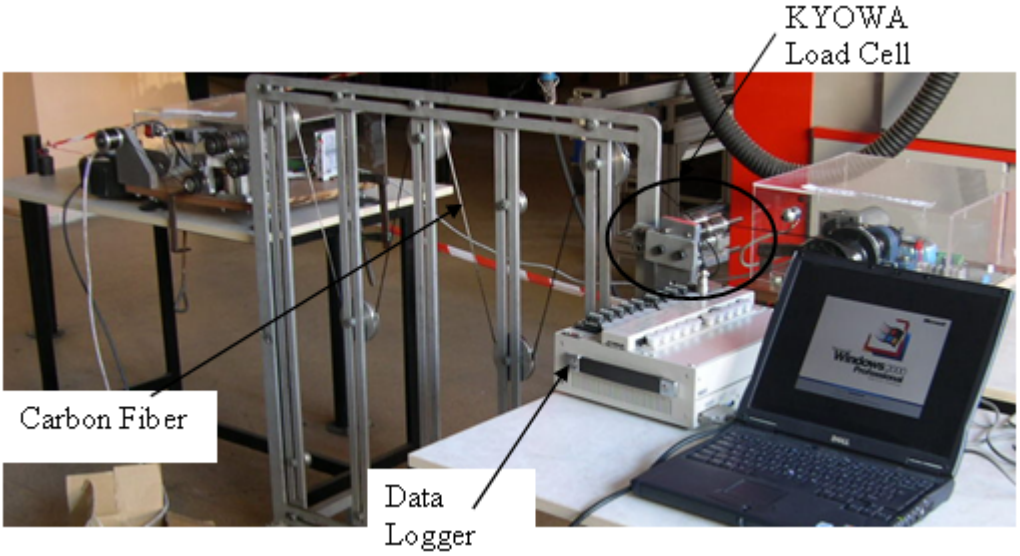

Fig. 5. Calibration System with KYOWA-UCAM 21 Measure System

The pre tension load on the fiber during winding process must be constant on acceptable value. Pre tension load, which is set up during filament winding process, compare with is measured value by system which had accepted the correctness. Fiber tensioning system with a conventional load cell (Kyowa Instruments) was used to check the correctness of the developed servo-mechanic pretensioning system Carbon fibers were wound under various pretension forces using the developed system [Fig. 5]. The loads, which are measured by KYOWA-UCAM 21, are saved to computer as shown in Fig. 5.

3. RESULT AND DISCUSSION

In this study, the effect of the primary manufacturing parameter ‘winding tension’ on filament winding process which widely uses on composite manufactured. It was designed to handle carbon fibers at high speeds while maintaining exact and very uniform tension. But it can be used with any type of fiber in composite manufacturing of continuous fiber. In composite winding, exact tension of each fiber is critical in order to achieve a finished product which has a high quality and good strength-to-weight ratio. Thus, an advanced tension control system with real-time control of the winding tension for filament-winding machine has been designed, manufactured and tested. Two kinds of winding tension control methods namely PID control and direct load cell control were used in the experiments. Imamura et al. has proposed a tension control methods, which make use of the rotational velocity difference between the mandrel and nip-roll parts. Rotational velocity is undirected parameters in case of fiber tensioning. Any sliding between pulley and fiber may cause an incorrect data. Thus, in the present study, the tension force on the fibers body was directly measured by a load cell and the value was evaluated by a PID controller to keep the tensioning constant. A conventional load cell system

with a very high sampling rate (80 microsecond-1) was also used to check the effectiveness of the PID controlled load cell system. Fig. 5. shows the comparison of the tension force measurements data obtained from PID controller tensioning system with the conventional load cell system. This figure indicates that the tensioning can be kept within 10 % variation of the set value which is generally acceptable.

With the implementation of the better tensioning system such as one proposed in the present study, it may be possible to have advantage in the FW machines. Those advantages may be:

– Production cost reduction may be possible,
– Less row material loss during winding may occurs,
– Production speed can be increased,
– Better product quality may be available.

To have better winding pattern with optimized fiber waviness more winding parameters should be included in the control system, especially in the wet winding process. The fibers are always tending to slide on the mandrel during the placement in the machine.

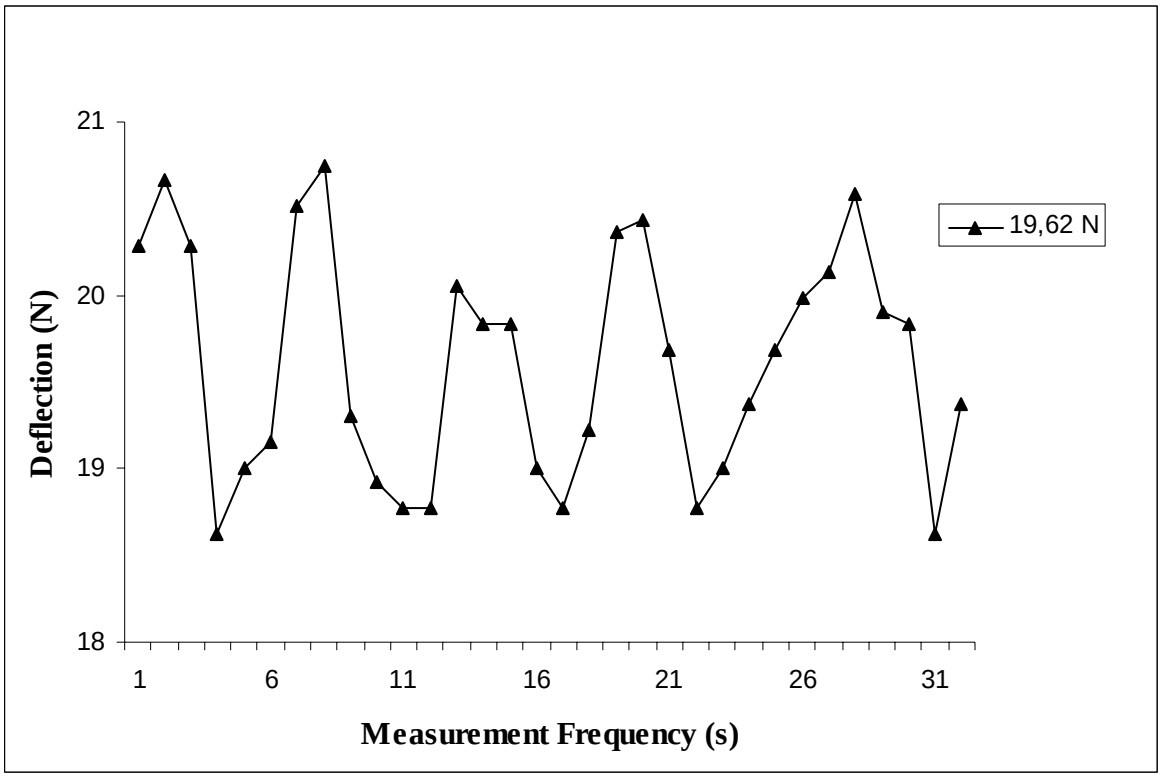

Fig. 6. Variation of the Tension Force in the Fiber during Winding

Fig. 6. shows deflections of the pre tension and measurement frequency per second. Like 19,62 N load which are set up during winding process. This value are taken approximately ± 1 N deflections values as shown in Fig. 6. As the pretension load are taken on the acceptable constant value breaking of the fiber are handicapped and the pre tension value are set up during winding process on the desirable values.

4. CONCLUDING REMARKS

A pretension control system with PID control for filament winding process was designed and manufactured to understand the effect of the pretension system parameters in the present this study. Tension controls of this process are important factors in beter winding paterns which is the main reson of high strength. A proportional–integral–derivative controller (PID controller) was used as control loop feedback mechanism. Proportional, integral, and derivative (PID) control requires real-time system feedback. PID is a sophisticated control technique which monitors the error between a desired variable value and the actual value, and adjusts the control accordingly (proportional).The aim of the fiber control was to keep fiber tension force constant in a pre-defined value. The tested pre-tension control system for filament winding led to the following conclusions:

– Pretension was controlled in variable value successfully during filament winding.
– The primary test of the system showed that the fiber tension may be kept constant within the 10% of aimed tension value.

REFERENCES

1. **Cohen, D.** (1997), Influence of filament winding parameters on composite vessel quality and strength, *Composites*, Part A 28A, 1035-1047

2. **Lauke B., Friedrich K.** (1993), Evaluation of processing parameters of thermoplastic composites fabricated by filament winding, *Compos Manuf.* Vol. 4 (2), 93-101.
3. **Mertiny, P., Ellyin, F.** (2002), Influence of the filament winding tension on physical and mechanical properties of reinforced Composites, *Applied Science and Manufacturing*, Composites: Part A 33, 1615-1622.
4. **Chan S., Munro M., Fahim, A.** (1996), Accuracy-speed relationships of a robotic filament winding cell, *Robotics and Computer-Integrated Manufacturing*, Vol. 12, Issue 1, 3-13.
5. **Sharon, A., Lin, S.** (2001), Development of an automated ber optic winding machine for gyroscope production, *Robotics and Computer Integrated Manufacturing*, 17, 223-231.
6. **Choi, S. B., Cheong, C.C., Kim, G.W.** (1997), Feedback control of tension in a moving tape using an er brake actuator, *Mechatronics*, Vol. 7, No. I, 53-66.
7. **Yeung, M.F., Falkner, A.H., Gergely, S.** (1995), The control of tension in textile filament winding, *Mechatronics*, Vol. 5, Issues 2-3, 117-131.
8. **Kudo, M., Nasu, Y., Mitobe, K., Borovac, B.** (2000), Multi-arm robot control system for manipulation of flexible materials in sewing operation, *Mechatronics*, 10, 371-402.
9. S**auter, D., Jamouli, H., Keller, J. Y., Ponsart, J.C.** (2005), Actuator fault compensation for a winding machine, *Control Engineering Practice*, 13, 1307–1314.
10. **Polini, W., Sorrentino, L.** (2005) Influence of winding speed and winding trajectory on tension in robotized filament winding of full section parts, C*omposites Science and Technology*, 65, 1574–1581.
11. **Polini, W., Sorrentino, L.** (2006), Actual safety distance and winding tension to manufacture full section parts by robotized filament winding, *Journal of Engineering Materials and Technology*, Vol. 128, Issue 3, 393-400.
12. **Carrino, L., Polini, W., Sorrentino, L.** (2003), Modular structure of a new feed-deposition head for a robotized filament winding cell, *Composites Science and Technology*, 63, 2255-2263.
13. **Imamura, T., Kuroiwa, T., Terashima, K., Takemoto, H.** (1999), Design and tension control of filament winding system, *Systems, Man, and Cybernetics, IEEE SMC '99 Conference Proceedings, IEEE International Conference*, Vol.2, 660-670.
14. **Carrino, L., Polini, W., Sorrentino, L.** (2004), Method to evaluate winding trajectories in robotized filament winding", *Journal of Composite Materials*, Vol. 38, No. 1, 41-56.
15. **Akihiro, H., Shuichi, W., Masanori, K.** (1999), Evaluation of strength in FW-FRP composites using ring burst test (Effects of winding tension on fracture behavior and strength)", *Transactions of the Japan Society of Mechanical Engineers*, Vol. 65, No. 631, 635-642.

PROCEDURE OF DISTANCES EVALUATION FOR SURFACE INSPECTION

Orest BAZYLEVYCH[*], Orest IVAKHIV[*], Roman VELGAN[*]

[*]Precision Mechanics Department, L'viv Polytechnic National University, 12 Bandery str., 79013 L'viv, Ukraine

oresti@polynet.lviv.ua, velgan@gmail.com

Abstract: In the context of developing automated optical inspection system, this work brings into focus the aspect of de-velopment of evaluation algorithms for thickness distribution extraction from the object model reconstructed after surface scanning. Within this work an algorithm for the evaluation of local differences between two triangle meshes is presented. The pair of triangular meshes is representing the front and backside of a scanned 3D-object. The resulting array of differences vector corresponds to the shortest local distances (i.e. local thickness) between sides of object.

1. INTRODUCTION

To guarantee the quality of parts produced by sheet metal forming the inspection of products geometrical form, surface defects, thickness and possible tearing is needed. The strong demands for cost reduction, shortened development cycle and high quality involve the necessity of a fast, exact and robust measurement procedure at the stages of forming tool development, procedure and product optimisation and during mass production. Especially, the inspection at production starts lead to important conclusions on the production process (e.g., the influence of tool modifications on the manufactured parts). Used in the industry visual inspection by trained personnel can't satisfy recent requirements to the accuracy and objectivity of inspection procedure. Moreover, many relevant surface defects on sheet metal parts are not visible to the human eye. For successful surface defects detection using machine vision inspection instruments a great number of points with high spatial density as well with required evaluation precision is needed. Existing coordinate measuring machine not always satisfy demands for scanning velocity caused by the necessity of online inspection. Instrumentation for fast, automated, user-independent, with high density of measuring points thickness estimation of sheet metal parts is currently not available. It is known optical instrumentation using photogrammetry and grid analysis method (Höflin and Feldmann, 2002; Schmidt et al., 2004). Regular grid (usually circles) is applied on a sheet metal part before forming. Strain and thickness changes are evaluated from the grid analysis (analysis of marks form changing after forming). The resolution for such method is restricted by mark raster and there is some methodical error due to indirect thickness estimation. Most of instrumentation for formed sheet metal inspection specialised for one or two parameters evaluation and instruments combining the geometrical form parameters inspection, defect detection and thickness estimation currently are not available.

2. INSTRUMENTATION FOR SURFACE INSPECTION

Optical measuring technologies in sheet metal forming and tooling have been used more and more in the industry during recent years. Using optical systems considerably decreases the development time for products and production while improving the quality. Good prospects for application for the inspection of sheet metal parts have fringe projection optical systems. The availability of highly capable three-dimensional optical sensor systems based on the image triangulation principle using fringe projection method creates the possibility of fast digitising of object surface resulting in a large set of measuring points with high resolution. Existing on the market fringe projection systems enable check up of geometrical form and examination of surface structure of digitised object (Ernst et al., 2003).

The highly accurate and fast sensor system reliably detects even the smallest relevant surface defects such as dents, bumps, sink marks, waviness, constrictions and cracks etc. with a defect resolution down to 10 µm (Steinbichler Optotechnik GmbH). To assure the stability of formed sheet metal parts, additionally to form and surface structure the thickness fluctuations in the critical zones of formed component and defects like necking, thinning (with the future risk of tear) or wrinkling should be considered. New possibilities of defect detection reveals with the elaboration of measuring procedure enabling two-side surface scanning and creation of digital object model (Weckenmann et al., 2004). To realise the evaluation of thickness fluctuations an algorithm for distances between surfaces estimation is to be elaborated.

3. ALGORITHM DESCRIPTION

3.1. Definitions

To ensure the stability of a part created by sheet metal forming procedure is very important to guarantee that the

minimal local thickness of a part is greater as the defined (for concrete material and work load conditions) critical value. From this point of view we define evaluated distance as the closest distance in local surrounding of an analysed surface point. Note that after a surface scanning an object is represented in form of point clouds (3D-data sets). As is the convention in coordinate metrology, thickness is estimated as length of the perpendicular from a point of one work piece surface side to the nearest interpolated surface element at the opposite side. The special feature of surface data is that the nearest point at the opposite side is included in several surface elements, so it is needed to find the surface element perpendicular on which is the shortest. Given a point p at one side of object surface and surface element S at opposite side, we define the distance $c(p,S)$ as

$$c(p,S) = \min_{p' \in S} d(p, p'), \quad (1)$$

where $d()$ is the Euclidean distance between two points in R^3 and p' - the projection of p onto surface element S. In local surrounding of surface elements S_1, S_2 (for two object sides, correspondingly) the one-directional distance E is defined as

$$E(S_1, S_2) = \min_{p \in S_1} c(p, S_2). \quad (2)$$

Note that often in such way estimated distance is not symmetric, i.e. $E(S_1,S_2) \neq E(S_2,S_1)$. A two-sided distance may be obtained taking the minimum of $E(S_1,S_2)$ and $E(S_2,S_1)$ in local neighbouring of surface elements.

3.2. Evaluation procedure

The process of nearest element searching is complicated for data sets obtained by optical systems due to large number of scanning point presence. These data are non-sorted sets, i.e. without information about neighbouring relations between data points. So the first step in evaluation procedure (Fig. 1) is the estimation of topology information of 3D-data. Such information allows fast searching of the neighbouring elements and creates the necessary prerequisites for surface modelling (in current work a linear interpolation of triangle meshes is used). For topology estimation the Delaunay triangulation is used. The Delaunay triangulation realises space division with the following merging
of nearest points in triangles and demonstrates the optimal properties after circumscribed circles and angle maximization criteria. Moreover, there is a possibility to approximate a plane through each three nearest points and in such way to create a surface model (Fig. 2).

Using of Delaunay triangulation gives an opportunity to significantly reduce the number of searching operations and increase the efficiency of data processing algorithm. By means of such a structure, for point of one side, it is possible to quickly find a nearest point at the opposite side. But such a point can belong to several triangles. So, to find a triangle, projection on which gives the shortest distance, the algorithm for nearest point searching should be extended to the nearest element searching by the following steps:

– searching for adjacent triangles, containing the found nearest point;
– evaluation of projection points onto planes of adjacent triangles;
– rejection of the planes if projected point is not inside of triangle;
– estimation of the shortest perpendicular length, which corresponds to the local one-directional distance E.

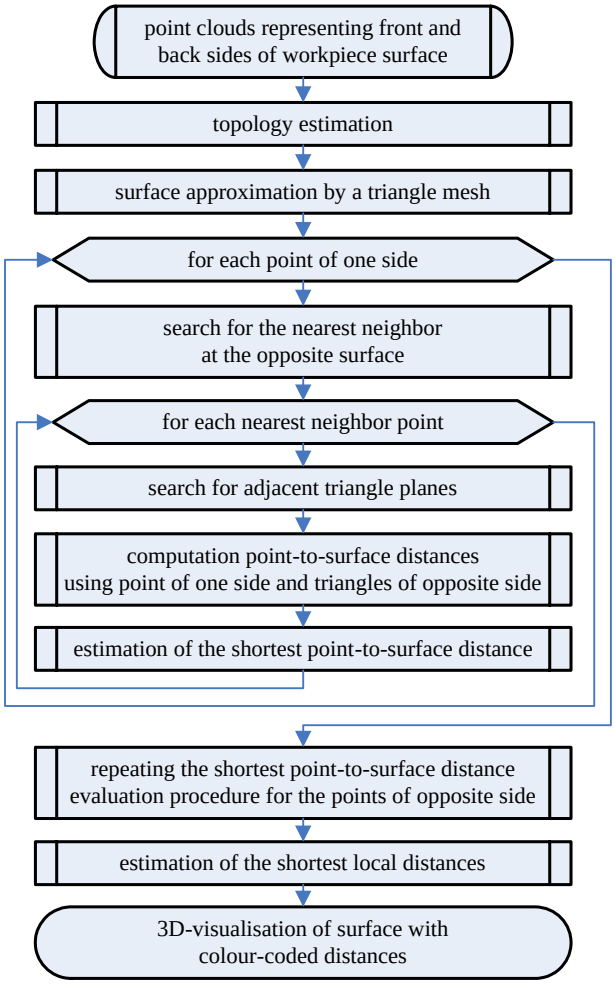

Fig. 1. Procedure for evaluation of distances between surfaces

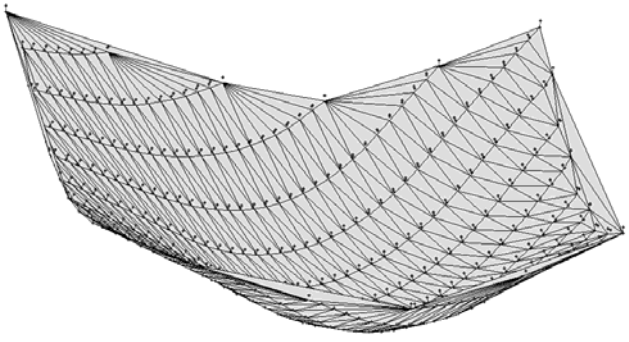

Fig. 2. Example of surface triangulation

For the efficiency of shortest element searching pointer indication triangles, containing current point is created.

For each triangle with points *P1*, *P2*, *P3* described by 3D-coordinates the normal vector is calculated from cross product of two triangle edges (Fig. 3)

$$\vec{n} = \left[(P2 - P1) \times (P3 - P1)\right]. \quad (3)$$

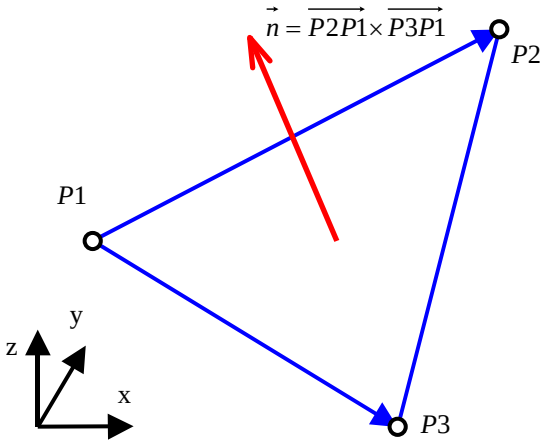

Fig. 3. Computation of normal vector for a triangular surface element

The elements of normal vector $\vec{n} = \{A; B; C\}$ are the coefficients of plane equation $Ax + By + Cz + D = 0$, where the coefficient D means the plane offset from the coordinate origin in the line of plane normal. If coefficients A, B and C are known the D is easy to find if put the coordinates of one of triangle points into the line equation. This operation can be described by dot product of vectors $\vec{n} = \{A; B; C\}$ and $P1 = \{x_1; y_1; z_1\}$

$$D = -(n \cdot P1). \quad (4)$$

Now it is possible to evaluate the distances from each point of one side P_{1i} to the triangle plane at opposite side (to the corresponding projection point) containing the found nearest point. We evaluate this distance as difference between projection of P_{1i} to the normal of triangle plane (corresponding to the distance to the origin) and distance from triangle plane to the origin:

$$d = \mathrm{proj}_n P_{1i} - D = (n \cdot P_{1i}) - D. \quad (5)$$

At the next step the similar procedure in inverse direction, i.e. from the work piece opposite side, is run out. Analysing the results of the bi-directional procedures we find the smaller one of the above calculated distances located nearby defined points.

3.3. Procedure realisation

The elaborated algorithm realizes the method for estimation of local closest distances between sides of digitised formed sheet metal part. An example of measured part with colour-coded thickness information is shown at the Fig. 4.

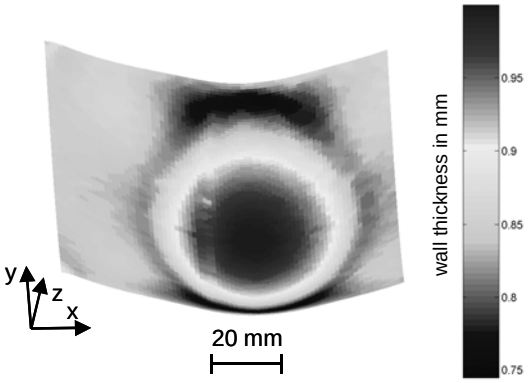

Fig. 4. Colour-coded distances distribution

4. SUMMARY

The evaluation module returns both numerical (array of local distances vectors) and visual results in form of coloured reference surface according to the estimated local distances. The estimated area-wise thickness is visualized over the one of measured surfaces as a colour-coded map. This kind of representation enables easy localization and documentation of the smallest wall thickness. Furthermore, the direct visualization helps to find reference of the wall thickness corresponding to the measured surface zone.

REFERENCES

1. **Ernst R., Weckenmann A., Velgan R.** (2003), Local wall thickness measurement of formed sheet metal using fringe projection, In: *D. Ilic, M. Boršic, J. Butorac: XVII IMEKO World Congress*, Proceedings, 1802-1805.
2. **Höfling R., Feldmann P.** (2002) Strain Analysis by Automatic Grid Evaluation, *Technisches Messen*, Vol. 69, 10/2002, 437-442.
3. **Schmidt T., Tyson J., Galanulis K.** (2004) Total Area Strain Mapping Improves Total Quality of Stampings, *Two- and Three-Dimensional Vision Systems for Inspection, Control, and Metrology, Proceedings of the SPIE*, Vol. 5265, 157-162.
4. **Steinbichler Optotechnik GmbH**. Surface Inspection of Sheet Metal Parts with ABIS II at KIA Slovakia. http://www.steinbichler.com/en/detail/news,3985.htm
5. **Weckenmann A., Ernst R., Velgan R., Gall P., Nalbantic K.** (2004) Detection of Defects in Sheet Metal by using Fringe Projection System, In: *8th International Symposium on Measurement and Quality Control in Production*, VDI-Berichte 1860, 231-236.

CONTROL OF HEATING PROCESSES IN TRANSPORT MECHATRONIC SYSTEM USING SIGMOIDAL FEED FORWARD NEURAL NETWORK

Ivars Beinarts[*], Anatoly Levchenkov[*], Peteris Balckars[*]

[*] Riga Technical University, Kronvalda blvd. 1-202, Riga, LV-1010, Latvia

ivars.beinarts@latnet.lv, levas@latnet.lv, peteris@dzti.edu.lv

Abstract: In this article interest is concentrated on the climate parameters optimization in passengers' interior of mechatronic systems (public electric transportation vehicles- train, tram or trolleybus). Idea is to use feed forward artificial neural network to create an algorithm and coordination mechanism for heating system parameters control to save electrical energy, and to increase the level of comfort for passengers. A special interest for investigations and further development is devoted to intelligent HVAC system allowing more flexible control of the system's compressor, fan and heater operation, and, therefore, improvement of efficiency and energy saving. This paper provides the mathematical model and algorithm for optimal control of the climate control system.

1. INTRODUCTION

Nowadays great attention is paid to increasing level of passengers' comfort in public electric transport. The aim of it is to provide passengers with a transportation service of a high quality. Elaboration of new HVAC (heating, ventilation and air conditioning) systems has to be performed in order to provide it. Effective work of them can be provided by elaborating control systems with usage of artificial intellect methods and progressive algorithms.

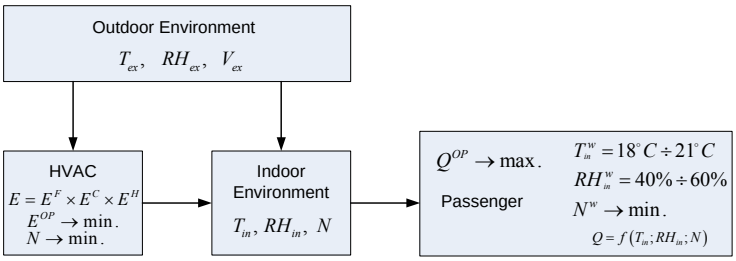

Fig. 1. Environment and HVAC system connection (Q – passengers comfort level, E – energy consumption, RH – air humidity, N – acoustic noise, V – air velocity, T – temperature, ^{OP} – optimal choice of parameters, $_{in}$ – indoor, $_{ex}$ – outdoor. Ability of HVAC system to provide optimal level of comfort Q^{OP} is directly dependent on energy consumption E of HVAC system)

Indoor environment parameters of vehicle passengers' interior to large extent depend on outdoor environment parameters (Fig. 1), frequency and intensity of both environments connecting (when opening doors and windows) as well as on effectiveness of HVAC system (Beinarts and Levchenkov, 2007).

2. PROBLEM FORMULATION

The main purpose of the paper is to develop structure scheme of HVAC intellectual control system and to describe its working algorithm, as well as to define the optimal HVAC system working regime, taking into account priorities of consumers, and trying to reduce consumption of electric energy as much as possible.

Deep and detailed investigation of the behaviour of such a system, its operation and running processes requires its generalized mathematic modelling, taking into account all possible regimes of the operation of compressor, fan motors, heater and setting an algorithm of their control under any condition. Possible problem solution is intelligent coordination mechanism – intelligent control system with the artificial neural network, which gives possibility to save the electrical energy min., at the same time providing high level of comfort to passengers max.

3. HVAC SYSTEM

The modelling and investigation are based on the typical architecture of HVAC system (Sauer et al., 1994) with a traditional application of AC induction motors for driving both compressor and fan of the conditioner. The well-known field-oriented method (Bimal and Bose, 2002) has been considered for the modelling.

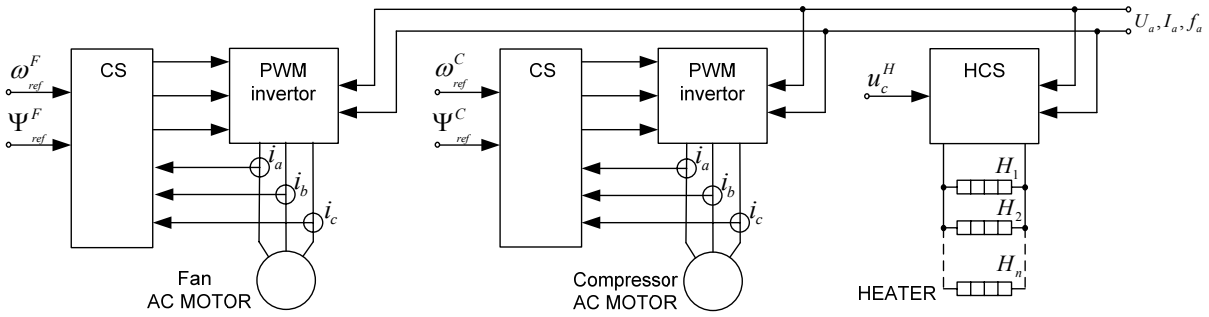

Fig. 2. Power part of HVAC system (CS – control system, ω – speed control, ψ – flux linkage, T_{sx}, u – voltage, u_c^H – heater control signal)

There are two control systems (CS) – one is for compressor motor control and the other – for fan motor control (Fig. 2). Heater control system (HCS) is used for control of electric heaters, control of which is realized according to signal.

4. CONTROL SYSTEM DESIGN

HVAC system control is performed using computer system. Processing of environmental parameters and passengers' wishes regarding climate parameters is realised using program agents.

Overall structure scheme of control system is given in Fig. 3. Passengers' wishes of necessary level of comfort are described as fuzzy variables and processed with fuzzy logic controller (FLC) which is described in (Beinarts and Levchenkov, 2008).

Signal Q_P^S, characterising wishes of passengers, is produced on FLC output. Environmental parameters of passengers' interior are controlled using suitable sensors, which are connected to ANN inputs $x_1 - x_6$. Inputs $x_8 - x_{10}$ are connected to separate power elements (cooler, fan, heater) of HVAC system for acquiring data about summary energy consumption E from electro energy power supply (EPS) that is characterized by signals E^C, E^F, E^H respectively. Information acquired from sensors and FLC are processed by ANN and according ANN rules respective output signals y^C, y^F, y^H are generated, which contain information on necessary work regimes of air conditioner, cooler and heater.

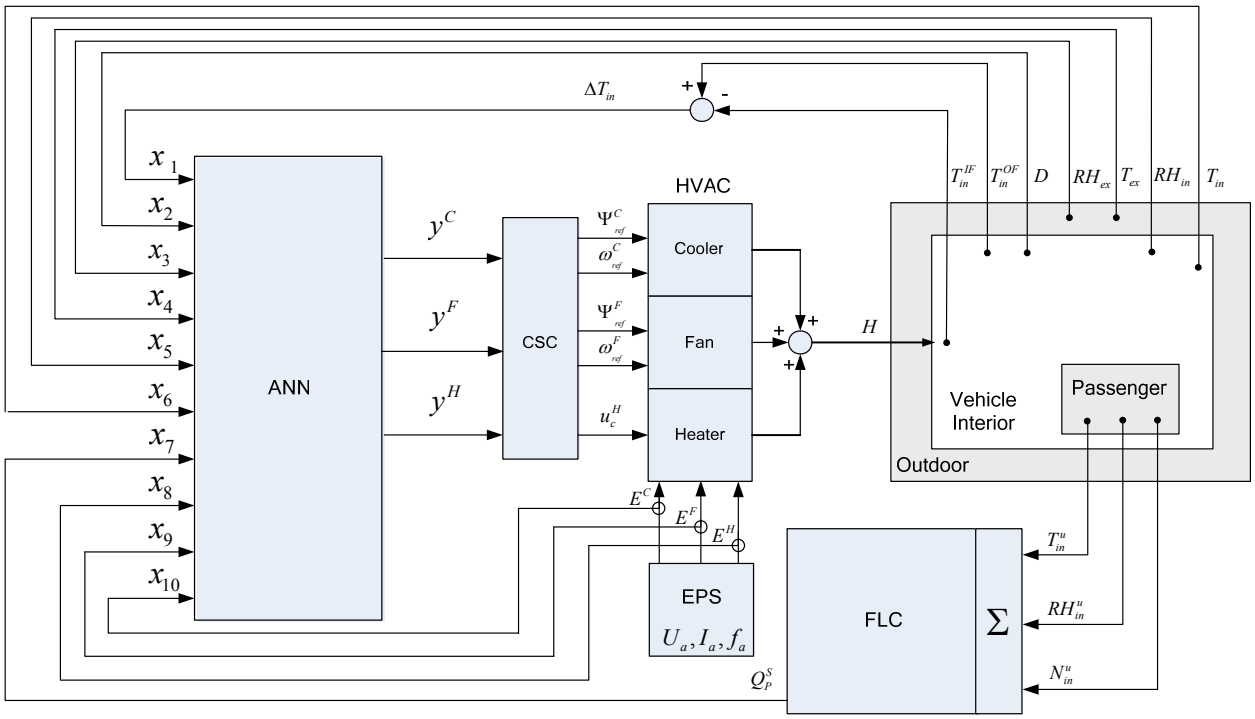

Fig. 3. Heating control system structure

ANN outputs are connected to the input of control signal controller (CSC). CSC performs HVAC power part control with signals ω_{ref}, ψ_{ref} and u_c^H.

EPS provides HVAC system with controlled flow of electric energy: $E = E^F \cdot E^C \cdot E^H$, size of which is controlled and data on its value E are passed to ANN, which provides an optimal control regime of energy consumption.

5. PROBLEM DECISION METHODOLOGY

5.1. Artificial neural network

In the paper there is used a sigmoidal type feed forward artificial neural network, which is also known as Multi-Layer Perceptron (MLP) (Haykin, 1998). Structure of three-layer MLP is given in (Fig. 4).

Sigmoidal (logistic) neuron activation function is used in the network:

$$f(s) = \frac{1}{1 + e^{-as}}, \tag{1}$$

where s – output value of neuron inputs sum, a – steepness parameter.

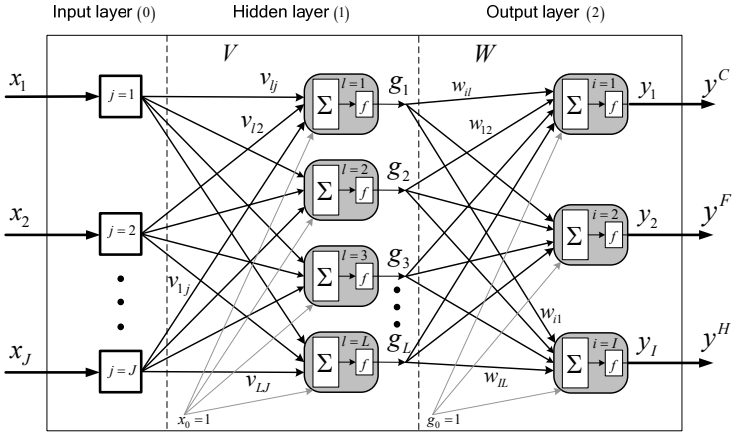

Fig. 4. Feed-forward MLP type artificial neural network (Input layer signals: $x_j \in \{ x_1, x_2, \ldots, x_J\}$, hidden layer output signals: $g_l \in \{ g_1, g_2, \ldots, g_L\}$, output layer signals: $y_i \in \{ y_1, y_2, \ldots, y_I\}$, hidden layer weights: v_{lj} – output layer weights: w_{il} – neuron activation function: f – um of input signals: Σ, HVAC system control signals: $\{y^C, y^F, y^H\}$, C – cooling, F – fan, H – heat process)

Sigmoidal expression shows that values of neuron output can be in range [0, 1]. As one of the most important characteristics of the function is simplicity of its derivation:

$$f'(s) = a \cdot f(s) \cdot \left[1 - f(s)\right] \tag{2}$$

In order to simplify description an extended designation of the input vector of the network is used described as $x = [x_0, x_1, \ldots, x_J]^T$, where $x_0 = 1$ corresponds to a signal of polarization. Input vector x is interconnected with the real output signal vector $y = [y_0, y_1, \ldots, y_I]^T$ and the desired output vector $d = [d_0, d_1, \ldots, d_I]^T$.

Output signal of the hidden layer neuron is calculated according to formula:

$$g_l = f\left(\sum_{j=0}^{J} v_{lj} \cdot x_j\right) \tag{3}$$

where index $j = 0$ corresponds to the signal and weights of polarization, and $x_0 \equiv 1$, $g_0 \equiv 1$.

Output signal of the output layer neuron is calculated according to formula:

$$y_i = f\left(\sum_{i=0}^{I} w_{il} \cdot g_l\right) = f\left(\sum_{i=0}^{I} w_{il} \cdot f\left(\sum_{j=0}^{J} v_{lj} \cdot x_j\right)\right) \tag{4}$$

5.2. Neural network training

The aim of the training is to adjust such values of weights v_{lj} and w_{il} for all layers of the network so that when input vector x is set, then such output signal values y_i are obtained which would match with necessary precision with desired values d_i, when $i = 1, 2, \ldots, I$. If to look at the polarization signal as to the one of the components of the input vector then polarization weights can be added to the vectors weights of corresponding neurons of both layers.

5.3. Error back propagation algorithm

The error back propagation algorithm (Kecman, 2001) for multilayer ANN defines weights adjusting strategy using gradient methods of optimization. It is considered as a one of the most effective training algorithms at the moment. Algorithm is based on the target function which is formulated as a square sum of difference between desired and real output signals values:

$$E(w) = \frac{1}{2}\sum_{i=1}^{I}\left(d_i - y_i\right)^2 \tag{5}$$

$$E(w) = \frac{1}{2}\sum_{p=1}^{P}\sum_{i=1}^{I}\left(d_j^{(p)} - y_i^{(p)}\right)^2 \tag{6}$$

Making more precise weights values can be done each time after presenting of each training pattern p according formula (5) (regime „On-Line“), or one time after presenting of all training patterns when many training patterns are presented $p = 1, 2, \ldots, P$ according formula (6) (regime „Off-Line“). There is „On-Line“ training regime used in the paper.

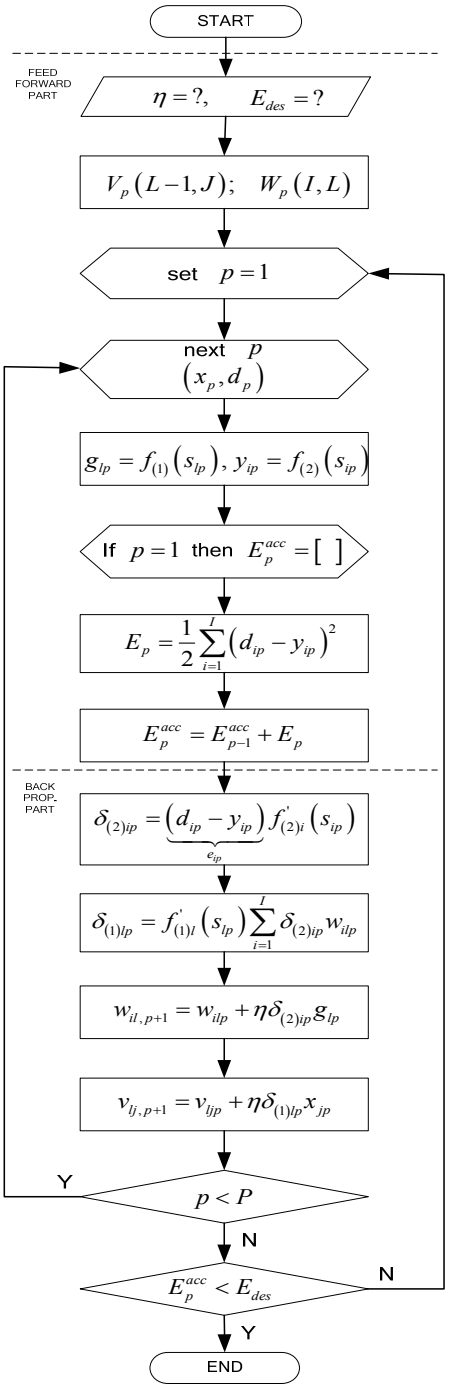

Step1. Choose the learning rate η and predefine the maximally allowed, or desired, error E_{des}.
Step 2. Initialize weights matrices.
Step 3. Start new learning epoch.
Step 4. Perform the on-line training, apply the new training pair (x_p, d_p) in sequence or randomly to the hidden layer neurons.
Step 5. Consecutively calculate the outputs from the hidden and output layer neurons.
Step 6. Initialize E_p^{acc} = [ ]. Perform only in the first step of an epoch (p = 1).
Step 7. Find the value of the sum of errors square cost function E_p for the data pair applied and the given weights matrices V_p and W_p.
Step 8. Value of the cost function is accumulated over all the data pairs.
Step 9. Calculate the output layer neurons' error signals. i = 1, …, I.
Step 10. Calculate the hidden layer neurons' error signal l = 1, …, L – 1.
Step 11. Calculate the updated output layer weights.
Step 12. Calculate the updated hidden layer weights.
Step 13. Compare actual p with P.
Step 11. The learning epoch is completed: $p = P$. For $E_p < E_{des}$, terminate learning.

Fig. 5. „On-Line" version of error back propagation algorithm

If assume that the target function is continuous then gradient methods of optimization are the most effective for the network training. Adjusting of weight vectors is done according to formula:

$$w(i+1) = w(i) + \Delta w \quad (7)$$

where $\Delta w = \eta p(w)$, and η – training coefficient, $p(w)$ – direction in space w. Structure of error back propagation algorithm is given in Fig.5.

A set of P measured data pairs that are used for training is given: $X = \{x_p, d_p, p = 1, \ldots, P\}$, consisting of the input pattern vector: $x = [x_1, x_2, \ldots, x_J + 1]^T$ and the output desired responses: $d = [d_1, d_2, \ldots, d_K]^T$.

6. PROBLEM DECISION ALGORITHM

Step 1. Initialization. In the object O (vehicle passengers' interior) HVAC system provides minimal necessary climate parameters Q_O^S set by an operator.
Step 2. ANN is trained using error back propagation algorithm on the base of training data pattern set P prepared by a supervisor.
Step 3. Passengers' climate parameter perception slopes T_{in}^u, RH_{in}^u, N_{in}^u are determined, and the comfort level set-point Q_S^P is defined by FLC.
Step 4. ANN is processing information obtained from environmental parameters' sensors placed in the interior of an object and comparing energy consumption values of HVAC system power plant, and in the result it activates ANN output signals y^C, y^F, y^H. Target is minimization of electrical energy consumption $E = E^C \cdot E^F \cdot E^H \rightarrow$ min. in compressor, fan motors and heater, considering consumer wishes Q_S^P with control regime C with ANN decision making D under control procedure $C_w^{DM}(t)$ during time t.
Step 5. ANN output signals y^C, y^F, y^H that contain information about the necessary changes of HVAC system power elements' parameters are processed by CSC. In the result, CSC forms control signals of HVAC system ω^C_{ref}, ψ^C_{ref}, u^C_{ref} and address of destination power unit.
Step 6. Work regime of HVAC system $C_w^{DM}(t)$ is set according computation results.
Step 7. HVAC system, according to CSC control signals, provides changes of climate parameters in the object, taking into account optimal consumption of electro energy: $E(t) \rightarrow$ min. with comfort level of passengers' $Q(t) \rightarrow$ min.

7. SUMMARY

The provided results prove that the use of feed forward ANN of sigmoidal type (MLP) with application of the proposed algorithms can be useful for solving HVAC technology control problems in the public electric transport. Usage of the created models and algorithms in the climate parameters control system in the passengers' interior will raise possibility to increase efficiency of electro energy usage, so exploitation costs of transport will reduce as well as passengers' comfort level will be increased. Appropriate for this purpose are systems working using control core, developed on the basis of artificial intelligence, which can control the current condition of all system, environment parameters independently on operator, and taking into account predictable changes of these conditions, it can take decision on the necessary system actions. The elaborated system model can be used for sustaining microclimate in different facilities, public electric transport vehicles and buildings.

REFERENCES

1. **Beinarts I., Levchenkov A.** (2007), Intelligent Systems for Transport Climate Parameters Optimization Using Multi Criteria Decision Making, *Proceedings of 48th RTU international scientific conference "Power and Electrical Engineering",* RTU press, Latvia, Riga.
2. **Beinarts I., Levchenkov A.** (2008), Usage of Fuzzy Logic Controller for Passengers' Interior Heating System of Railway Electric Transport". *Proceedings of 16th International Symposium "EURNEX-Zel2008",* Slovakia, Zilina.
3. **Bose B. K.** (2002), *Modern Power Electronics and AC Drives,* Prentice Hall PTR, Upper Saddle River.
4. **Greivulis J., Firago B.** (1993), *Principles of Electrical Drives in Questions and Answers*, RTU press, Latvia, Riga.
5. **Haykin S.** (1998), *Neural Networks: A Comprehensive Foundation,* Prentice Hall.
6. **Kecman V.** (2001), *Learning and Soft Computing: Support Vector Machines. Neural Networks, and Fuzzy Logic Models*, Massachusetts Institute of Technology.
7. **Kröse B., Smagt P.** (1996), *An Introduction to Neural Networks,* The University of Amsterdam.
8. **Leonhard W.** (1996), *Control of Electrical Drives,* Springer-Verlag, Berlin.
9. **Murphy J. M. D., Turnbull F. G.** (1985), *Power Electronic Control of AC Motors,* Pergamon Press, Oxford.
10. **Ribickis L., Rankis I.** (1996), *Electrical Drive,* RTU. Latvia, Riga.
11. **Sauer H. J., Howell R. H.** (1994), *Principles of Heating Ventilating and Air Conditioning,* ASHRAE, Atlanta.

COMPUTER PROCESSING OF SOME SURFACE IMAGES OF TECHNICAL OBJECTS AFTER INFLUENCE OF THE HIGH TEMPERATURE CONDITIONS

Mariusz BOGDAN*

* Białystok Technical University, Faculty of Mechanical Engineering, Department of Automatics and Robotics, ul. Wiejska 45c, 15-351 Białystok, Poland

marbog@doktoranci.pb.edu.pl

Abstract: Computer processing of the image of surface of operating gas turbine blades was proposed in order to make the method of the evaluation of the condition of these blades more objective. The dependences and connections between the degree of blade material overheating and the colour of analyzed surfaces were shown on the basis of images registered in visible range of electromagnetic wave (digital image – Charge Coupled Device matrix). The proposal of methodology to assign the overheated areas on the blade's surface in order to assess the range (of degradation) of thermal usage of the blade and to forecast it's working resources, might be useful to monitor the situation in the operating conditions. Moreover in the article the problematic of acquisition of the form digital images dates was presented by showing physical basis of analysis of reflected signal from metallic surface are showed in aspect of recording by photoelectric light sensor (matrix CCD).

1. NATURE OF THE UNDERTAKEN DIAGNOSTIC PROBLEM

During the operating process of technical objects such as: airplane, traction, as well as marine of propulsion, all kinds of failures of their turbine sets take place. Most common defects are material overheating, as well as thermal fatigue of jet and rotor blades. These kinds of defects lead to faulty engine operation, and sometimes in case of airplane engines to tragic accidents. Elimination of this kind of defects is always carried out as a major engine repair, which results in high costs (Błachnio, 2005; Dudziński 1987; Poznańska, 2000).

At present, the evaluation of the condition of turbine blades is carried out based on the registered image of the diagnosed element's surface and compared to the standard images of operational and nonoperational analogical blades surfaces. Such condition evaluation criteria are very subjective, because they depend on the knowledge as well as the vision of the diagnostician. Verification of diagnostician's decision is carried out through destructive method. Tested element undergoes microstructure analysis on metallographic section. Errors in the subjective evaluation by the diagnostician can lead to mistaking an overheated blade for a suitable one, or a not-overheated one for unsuitable. Up until now, a non-destructive method of evaluation of the degree of overheating of blade's material based on objective criteria hasn't been developed.

Objectivity, sensitivity and reliability increasing of evaluation condition of the tested technical element will be possible thanks to disclosure of dependences and connections between the colour change of the analyzed surfaces and the change of material microstructure owing to influence of working factor of high temperature (Błachnio and Bogdan, 2008; Bogdan and Błachnio, 2006).

On the grounds of problem analysis the following hypothesis is assumed: in visible band of electromagnetic wave the digital images processing of surfaces gas-turbine can be used for the evaluation of the condition of microstructure after effecting of working factor of high temperature.

The task of the conducted researches is aimed to demonstration of the relationship between the parameters change of surface image of gas-turbine blade and changes of the material microstructure. The data presented in form of the digital images is recorded by optical system with light-sensitive detector (photodetector) – matrix CCD (digital camera).

2. PHYSICAL BASIS OF METHOD ANALYSIS IN VISIBLE LIGHT

Blade surface is recognized by light-sensitive detector (matrix CCD with optical system) thanks to the light reflected – reemitted from blade surface (light source secondary). It makes possible the indirect method of tested object recognition through processing and analysis of the data presented in form digital images (Rafałowski, 2004; Sanecki, 2006; Manaybe and Inkokuchi, 1996). A small part of incident luminous flux is captured at metallic surface. Majority of light (90% – 95%) emitters from surface in form of visible light with the same length like incident light. Rest of energy (5-10%) is scattered in heat form (in agreement with principle of conservation of energy) (Sanecki, 2006):

$$I_o = I_r + I_p + I_e \tag{1}$$

where:

I_o – intensity light incidence, I_r – intensity light reflection, I_p – intensity light transmission, I_e – intensity light dispersion

Property of metallic surface are characterized by numerical coefficients. When we apply these characteristics to the wave length of used radiation the properties are presented by spectrum coefficients. Most interesting light incidence coefficient is presented like ratio of luminous flux Φ_ρ reflected by illuminated surface to Φ luminous flux incidence.

$$\rho = \frac{\Phi_\rho}{\Phi} \tag{2}$$

Every kind of surface reflection that occurs in practice can be considered as a combination of regular and diffusion reflection.

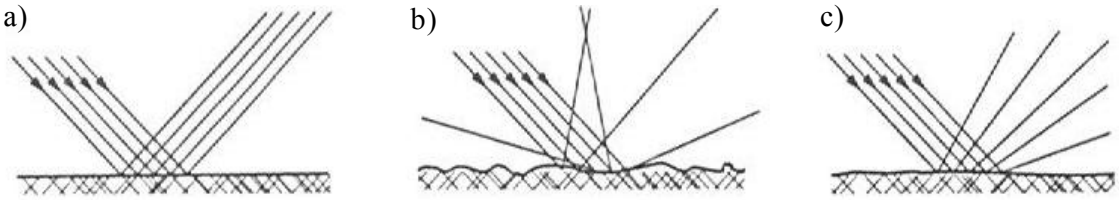

Fig. 1. Method of light reflection from different surfaces: a) polished surface, b) matted surface c) smoothed surface (Sanecki, 2006)

Depending on the structure of metallic surfaces, light reflected from them can farther propagate in the form of:

- directional reflected light (from polished surface);
- transmitted light (from matted surface);
- directional transmitted light (from smoothed surface no mirror surface).

Defined in physical sense the intensity of shinning (brightness) of metallic surface that is the source of reflected light, is described by introduction of luminance term. This term is understood as light radiation of shining surface (own, reflected, passed light) that depends on its area, value of radiated luminous flux and its light distribution in various directions.

Polish standards define luminance at a given time and direction as a ratio of quantity of the light that is at given direction, being generated from infinitesimal element of the surface which surround the given point to this element projection on orthogonal plain (Rafałowski, 2004; Sanecki, 2006):

$$L = \frac{E}{S \cdot \cos\alpha} \tag{3}$$

Formula (3) results that the luminance of shining surface attains maximum in perpendicular direction and it decreases when the observation deviation changes.

Chemical constitution of matter which covers surface of metallic objects defined the suppression individual of wave length in radiation spectrum of shinning object and mix of selectively light reflected from its surface defines its colour (specified metals can have colour owing to selectively of light reflecting – gold, copper). To characterize the spectral properties of testing surface it is possible to use the graph ratio of spectral luminance coefficient to wave length (curve of reflection ability).

3. PROBLEM OF IMAGINING BY THE MATRIX

Matrix CCD is sensitive light detector (photodetector). Simplifying in a measure, we can say that it is built out of pixels and every pixel is an elementary part of whole registered image (single point). Task of pixels (elements of processing and accumulation) is photons capturing (measure of light intensity). In order to capture photons the pixels realize photoelectric effect, i.e. electrons freeing under influence of photons energy reaching to the centre (scheme of this conversion as well as forming losses illustrated in Fig. 2). Next, the assembled signal reaches amplifier through the electrodes assembled at the end of every rank of pixels. With the rise in gain the level of noises is also increasing. It is presented if form of graininess as well as perturbations of colour of processing images.

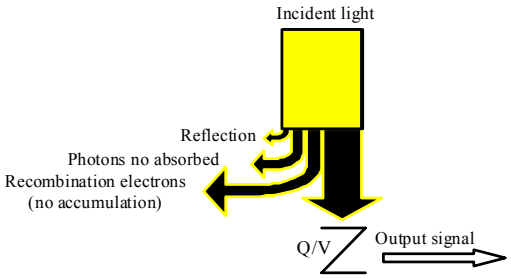

Fig. 2. Block diagram of losses in process of conversion from optical signal into CCD electric signal (Rafałowski, 2004)

Matrix CCD itself doesn't differentiate (can't differentiate) colours. It only counts photons incident (the light radiations incident on particular pixels). In front of detector the colour filter is placed, it consist of 3 primary (basic) colour: red, green and blue (this scheme of basic colour is called RGB – from first letters of English name). This is the most often applied colours system of filter which is called as Bayer's (filter) scheme.

The image acquisition process using CCD matrix and quality of imaging quantification are influenced by the following factors and parameters:

- too low sensitivity of CCD matrix – big noised (graininess);

- image defect – less onerous error mainly results from lens construction – the defect of image dimensions is among this kind of errors;
- vignetting – lightly (delicate) raising shade of images edges;
- chromatic aberration – delicate broadering of thin lines colour – the lines remind then a rainbows miniature;
- noise level – (visible on photographs as irregular bright and dark light spots which appear while photographing of uniform colour surfaces);
- accuracy of colours and brightness mapping – that is technique of reading-out of deep red and black colours as well as fragments of very high brightness by the matrix.

4. INVESTIGATIONS OF JET TURBINE BLADES

Fifteen blades of blades ring of turbine jet were examined. The recording was carried out using digital camera. On special measuring position, for the purpose of avoidance of errors at images recording, following conditions are stipulated, i.e. angle of light incidence is 45º, light dispersion is achieved by application of special diaphragms, the recorded light is in range of visible light, angle of image detection is 90º, images are of the same picture resolution. Preliminary classification according to evaluation used before was accepted. Generally, fifteen photos for each state were carried out. The examined region of interest along the edge of attack was selected (format: JPEG, size: 250x750 pixels, depth of colour: 24 bits – true colour).

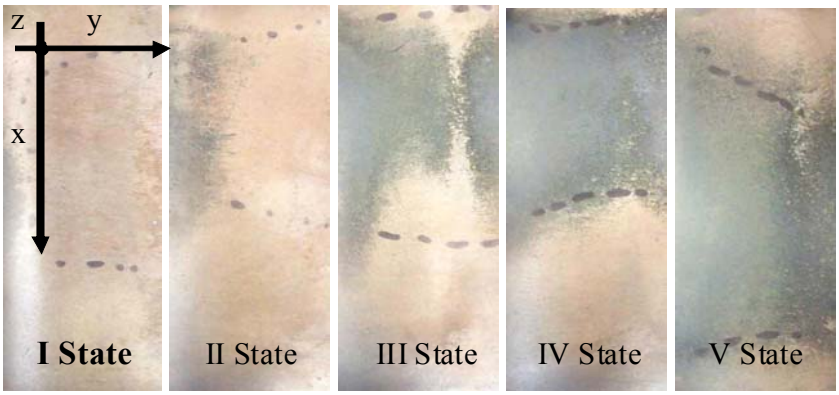

Fig. 3. Accepted classification the degree of overheating blades (according to evaluation used before) - acquisition of the digital camera

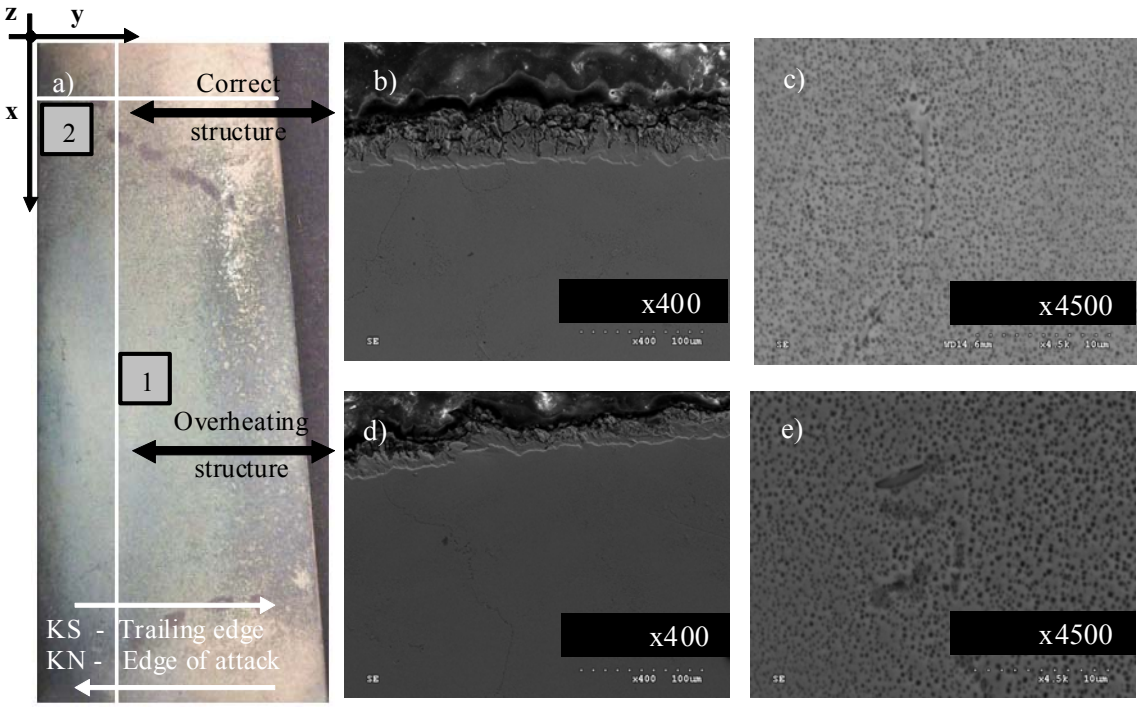

Fig. 4. Metallographic researches of blade of ring made from ŻS6 K alloy: a) cutting lines (number 1, 2) of turbine blades; b, c) example of non overheating structure of surface layer and subsurface layer; d, e) example of overheating structure of surface layer and subsurface layer

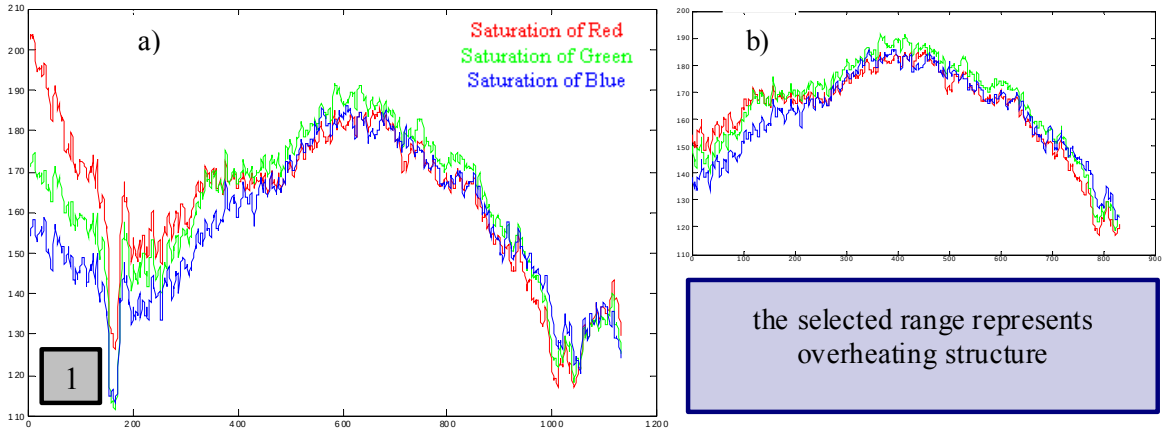

Fig. 5. Average RGB colour profiles: a) along line number 1 – parallel to edge of attack (KN), b) selected range of overheated structure

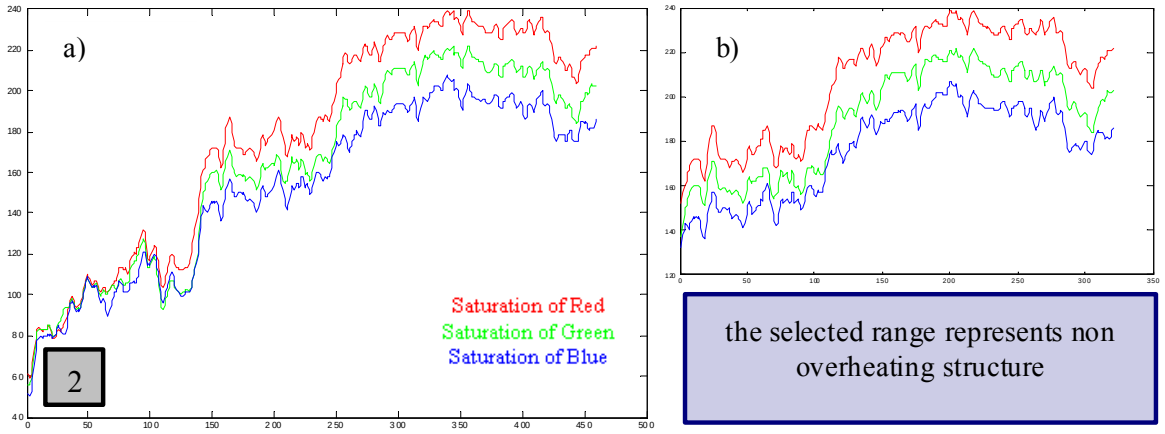

Fig. 6. Average RGB colour profiles: a) along line number 2 – perpendicular to edge of attack (KN), b) selected range of non overheated structure

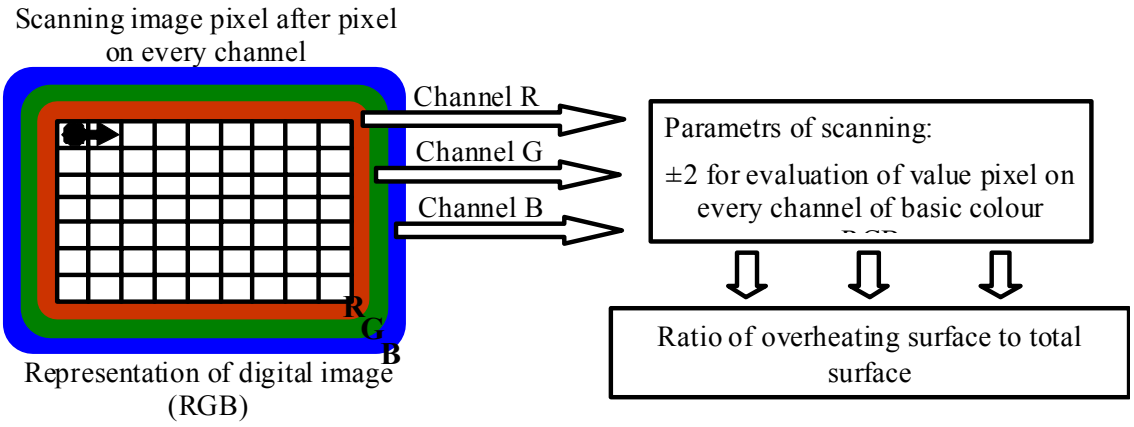

Fig. 7. Scheme of scanning images of surface blades

Blades have been working at the range of temperatures from 990K to 1123K (overheated occurred as a result of exceeding of the working temperature limit). The fifth state according to classification used before is defined as overheating blade. For the purpose of this evaluation verification the metallographic examinations were carried out along 2 cutting lines (Fig. 4).

Changes of thickness of surface layer (aluminium) and changes of quantity of precipitates and spacing of strengthening γ' phase (materials were examined with a scanning electron microscope – computer analysis

of metallographic images) were defined. Changes of these both parameters have decisive effect on thermal property (heat-resisting and high-temperature creep resisting) of tested alloy (Błachnio and Bogdan, 2008; Błachnio, 2008). It makes possible presenting of graph of average colour profile which presents both the overheating structure (selected range of along line number 1 – Fig. 5 a, b) and non overheated structure (selected range of along line number 2 – Fig. 6 a, b).

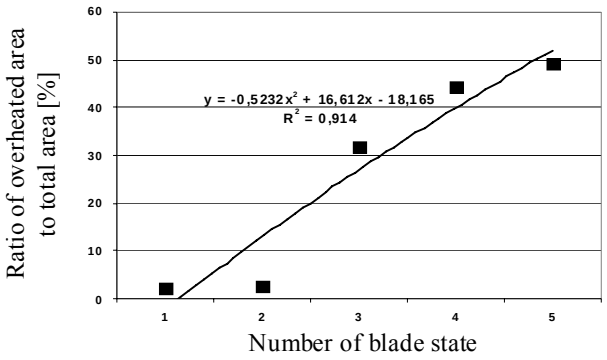

Fig. 8. Effect of scanning of surface images

On the basis of two ranges of average colour profiles (Fig. 5b, Fig. 6b) every surface element (pixel after pixel) of states (I-V) of turbine blade was tested. It was made from point of view of occurrence of colour points (RGB) which describe the overheating and non overheating structures (with tolerance ± 2 of value for each pixel from selected range) (see Fig. 7). The condition fulfillment means that pixel belongs to the range of graph 5b and the unit should be set in resulting matrix. Furthermore, in case of the range of non-overheated structure, the unit was set for pixels which out of the range of graph 6b. The final result for every state was obtained as a logical sum of two matrix. Both matrixes represent the points recognized as overheating points and the values of second matrix, as it was described above, were obtained as a result of negation of colourful points which represent the non overheating structure (= point overheating).

The points (image pixels) recognized as overheated were summed for every state and this sum was related to the total number of pixels. As a result of ratio of overheated area to total selected area (Fig. 8) is obtained.

5. FINAL CONCLUSION AND SUMMARY

As a result of scanning of blades of image surfaces for the states I - V ratio of overheating surface to total surface (expressed in percents) was obtained. The above presented graph shows that the blade from state 3 should be recognised as to be overheated. The above investigation process may contribute to the increase of credibility (growth of objectivism) of evaluation of the blade condition. Automated image acquisition along with the programme for the surfaces image recognition would also lead to rationalization and more precise diagnostics of this technical object. Moreover, the use of sight-glass devices (videscoops) for image acquisition may be applied to the investigation of the changes during the monitoring of the blade condition and damage development, i.e. technical state of examined elements during operating process (periodic researches) without the need of engine disassembly.

To get know the influence of working factor on the state of blade surface it is necessary to describe the environment of the blade turbines, i.e. the working time of the engine that includes the starting and acceleration time, while the most destructive heat loads of the engine are thermal shocks which mainly (affect) have an impact on structural elements of so-called hot part of engine, caused by the large gas temperature changes, characteristics of environment. That is, the rotation speed increase (accretion) during engine starting, distribution of temperature behind turbine, distribution of real average temperature in front of turbine (Wiatrek, 1982). The important factor which has an influence on colour of tested surfaces is the composition of fuel and correct working of injector.

REFERENCES

1. **Błachnio J.** (2005), Non-destructive testing methods as applied to the diagnosing of turbine engines, *IV International Scientific – Technical Conference*, Gdańsk – Kopenhaga.
2. **Błachnio J., Bogdan M.**: The assessment of the jet gas-turbine blade condition, *Archives of Transport* (in print).
3. **Błachnio J.**, The effect of high temperature on the degradation of heat-resistant and high-temperature alloys, *MSM2008* (in progress).
4. **Bogdan M.**: Błachnio J.(2006), Analiza sygnału świetlnego odbitego od powierzchni w diagnostyce obiektów technicznych, VI Krajowa Konferencja Diagnostyka techniczna urządzeń i systemów DIAG'2006, Ustroń, *Diagnostyka* Nr 2/38/2006, 175÷186.
5. **Dudziński A.** (1987), Analiza rentgenostrukturalna stopu EI-929 poddanego długotrwałemu wygrzewaniu, *Doctor's Disseration*, WAT, Warszawa.
6. **Manabe Y.**: Inokuchi S. (1996), *13th International Conference on Pattern Recognition (ICPR'96)*, Vol. 1, 840÷843.
7. **Poznańska A.** (2000), *Żywotność łopatek silników lotniczych ze stopu EI-867 w aspekcie odkształcenia niejednorodnego i zmian strukturalnych*, Ph.D. Disseration, Politechnika Rzeszowska, Rzeszów.
8. **Rafałowski M.** (2004), Scalone analizatory w pomiarach techniki świetlnej i oceny kształtu obiektów, *Rozprawy naukowe* Nr 114, Wydawnictwo Politechniki Białostockiej, Białystok.
9. **Sanecki J.** (2006), *Teledetekcja - pozyskiwanie danych*, WNT, Warszawa.
10. **Wiatrek R.** (1982), *Napędy Lotnicze: Zespoły wirnikowe silników turbinowych*, WKŁ, Warszawa.

DISASSEMBLY MODELING OF THE MECHATRONIC SYSTEMS FOR REUSE AND RECYCLING

Norbert CHAMIER-GLISZCZYŃSKI *

*Technical University of Koszalin, Institute of Mechatronics, Nanotechnology and Vacuum Technique,
ul. Racławicka 15-17, 75-620 Koszalin, Poland

norbert.chamier-gliszczynski@tu.koszalin.pl

Abstract: This paper presents processes modeling disassembly of the mechatronic systems for reuse and recycling. Typical steps in modeling and analyzing disassembly processes consist of the following: the objective of the model is stated, a mass flow diagram consisting of acquisition, sorting, disassembly processes, and recycling process of the facility in developed, modeling disassembly processes, disassembly process planning, optimal disassembly sequences: (generation of feasible disassembly sequences, adaptive disassembly processing, selective disassembly, destructive disassembly).

1. INTRODUCTION

Using the mechatronic systems in the electronic and car industry it caused that he was recycling process regulating: the European Waste Electrical and Electronic Equipment (WEEE) directive and the End of Life Vehicle (ELV) directive. To basic parameters one should get which during one should rank processes of the recycling of these mechatronic systems were determined by the rate of reuse-recovery and reuse-recycling, which value in directives (WEEE, ELV). Big material diversifying (Fig. 1) under construction individual mechatronic systems contributed for extending their process of the recycling (Fig. 2).

A process of disassembly is deserving the distinction, which in big step is contributing to getting planned rates of reuse-recovery and reuse-recycling. About the major part of disassembly in the process of the recycling of products they are providing numerous publications. For example: Johnson and Wang, 1998 (Economical evaluation of disassembly operations for recycling, remanufacturing and reuse), Lambert and Gupta, 2005 (Disassembly modeling for assembly, maintenance, reuse, and recycling), Shih, Chang and Lin, 2006 (Intelligent evaluation approach for ele-ctronic product recycling via case-based reasoning).

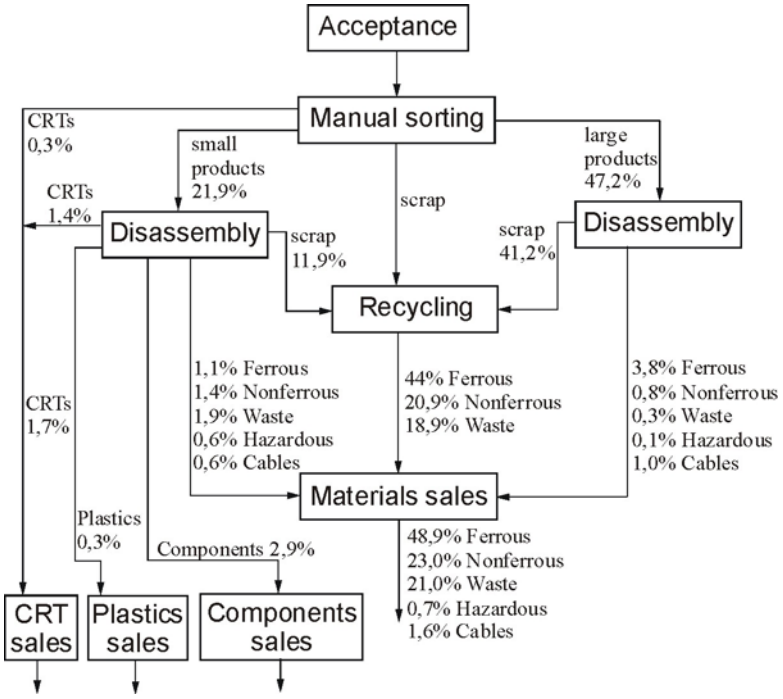

Fig. 1. Example of a scrap mechatronic system recycling facility (Spengler at al., 2003)

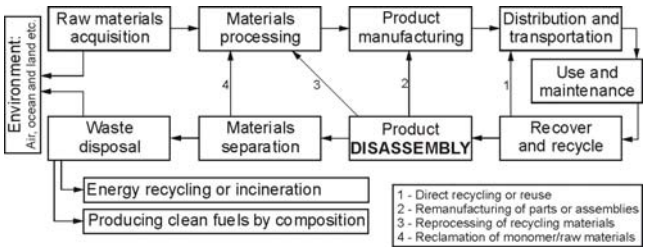

Fig. 2. Different forms for recycling (Kuo, 2006)

2. DISASSEMBLY MODELING

Structure of the disassembly process of mechatronic systems we will be introducing with help of the graph, which every disassembly operation is copied in the form of the connection in of graph. However elements to regaining and are regained, copied in the form of nodes of this graph. This graph is enrolling in the form Ambroziak, 1998; Jarzębińska-Dziegciar, 2004; Korzan, 1978:

$$G=\langle W,O,R\rangle \tag{1}$$

W – node set (of elements) of graph G, O – connection set (of disassembly operations) of graph G, R – relation R⊆ W×O×W.

For the explicitness of conducting more further deliberations, we are receiving the following notation of sets and connections in the graph G:

$$W=\{w(i)\equiv i:\quad i=1,2,...,I\};\qquad i=\{1,2,...,i,\quad j,...,I\} \tag{2}$$

$$O=\left\{\begin{matrix}(w(i),w(j)):\quad w(i),w(j)\in W,\\ w(i)\neq w(j)\qquad i,j\in I\end{matrix}\right\} \tag{3}$$

From above he is resulting that the examined process of disassembly has I nodes graph and K connections of the graph.

However mapping R is the Cartesian product W×O×W no the set {0, 1} (Ambroziak, 1998; Jarzębińska-Dziegciar, 2004):

$$R:W\times O\times W\rightarrow\{0,1\} \tag{4}$$

Any triple (w(i), o(k), w(j))∈ W×O×W taką, że R(w(i), o(k), w(j))=1 we are interpreting in the following way: o(k) bow linking w(i) node with the w(j) node, w(i)◷ w(j) or o(k) bow is contained between w(i) node and w(j)node. However any triple (w(i), o(k), w(j))∈ W×O×W so, that R(w(i), o(k), w(j))=0 we are interpreting as follows: o(k) bow isn't linking w(i) node with the w(j) node, w(i)◷ w(j) or o(k) bow isn't contained between w(i) node and w(j) node.

In the disassembly process of mechatronic systems a right order of making the operation, resulting from structure of this systems and technology taken on of its disassembly is required. Therefore a directed graph is being used for the description of this feature (Ambroziak, 1998; Jarzębińska-Dziegciar, 2004).

In the coincidence realization of the recovery materials and elements from mechatronic systems, a need of defining quantitative characterizations for elements of the structure of the disassembly process of mechatronic systems. Therefore recover materials of elements from mechatronic systems we are defining the ordered triple(Ambroziak, 1998; Jarzębińska-Dziegciar, 2004; Korzan, 1978):

$$S=\langle G,F_W,F_O\rangle \tag{5}$$

G – mapping graph structure of the disassembly process of mechatronic systems, F_W – functions set defined on the node set of the graph G,

$$F_W=\{\varphi_1,\varphi_2,...,\varphi_u\},\qquad u=1,2,...,U \tag{6}$$

U – number mapping definite onto node set graph G, F_O – set of functions defined on the connection set of the graph G,

$$F_O=\{\gamma_1,\gamma_2,...,\gamma_z\},\qquad z=1,2,...,Z \tag{7}$$

Z – number mapping definite onto connection set of the graph G.

In the examined recovery materials and elements from mechatronic systems graph G, described is formula 1 with two-part and full graph what means that node set W in it is possible to divide in two disjoint subsets: for the elements sets EO for recovery and the set of regained elements and materials OEM. We are accepting, that:

$$W=EO\cup OEM \tag{8}$$

$$EO\cup OEM=\varnothing \tag{9}$$

For the lucidity of the record let A, A⊆ W, a harvest means elements for recovery EO and B, B⊆ W means the harvest regained elements and materials OEM. At the same time we assume that A of elements for recovery numbered a = 1, 2,…, A and B of elements and materials regained numbered b = 1, 2,…,B. However connection among the pair tidied up of tops of sets A and B is making the relation of the A×B record. We are determining the set of all relations of the RD record as:

$$RD\subset(A\times B)=\{(a,b):\quad a\in A,\quad b\in B\} \tag{10}$$

3. STRUCTURE OF THE SET RECOVERED ELEMENTS AND MATERIALS

Recovered elements from mechatronic systems considering the criterion of their reuse they divided in two groups: 1) elements form the first group to the reuse and the regeneration, 2) elements form the second group, which the

criterion is in of kind of material, from which they were made.

A model of the structure of recovered elements and materials will be used to the description of mentioned groups from the mechatronic systems defined as:

$$OEM_d = (OE, OM) \tag{11}$$

OEM – recovered elements and materials from mechatronic systems, d – identification number of the mechatronic systems, OE – set recovered elements from the mechatronic systems,

$$OE = OEP \cup OER \tag{12}$$

OEP – set reuse elements, OER – set regeneration elements, OM – set recovered materials from the mechatronic systems,

$$OM = OZ \cup OPM \tag{13}$$

OZ – set recovered scrap metal,

$$OZ = OZS \cup OZK \cup OZMS \tag{14}$$

OZS – set recovered scrap ferrous metals, OZK – set recovered scrap nonferrous metals, OZMS – set recovered scrap precious metals, OPM – set recovered other materials,

$$OPM = OTS \cup OG \cup OPO \tag{15}$$

OTS – set recovered plastics, OG – set recovered rubber, OPO – set recovered waste.

4. CRITERIA OF THE ENVIRONMENTAL ASSESSMENT

Rate of the reuse-recovery:

$$PO_d = \frac{MOE + MMO}{M} \times 100\% \tag{16}$$

PO – rate of the reuse-recovery, d – identity number, M – mass of the mechatronic systems, MOE – mass of the recovered elements,

$$MOE_d = \sum_{k=1}^{m} moe_k \tag{17}$$

MMO – mass of the recovered materials,

$$MMO_d = \sum_{l=1}^{n} momo_l + MFO \tag{18}$$

MFO – masses of the fraction from bulk recycling which is being counted to recovery.

Rate of the reuse-recycling:

$$PR_d = \frac{MOE + MMR}{M} \times 100\% \tag{19}$$

PR – rate of the reuse-recycling, MOE – mass of the recovered elements, MMR – mass of the recycling materials,

$$MMR_d = \sum_{p=1}^{q} momr_p + MFR \tag{20}$$

MFR – masses of the faction from the bulk recycling process,

$$MFR = mozs_4 \times \left(\frac{f_{r1} + f_{r2} + f_{r3}}{100} \right) \tag{21}$$

$mozs_4$ – mass for the bulk recycling process, f_{r1} – percentage share of the ferrous metals fraction, f_{r2} – percentage share of the nonferrous metals fraction, f_{r3} – percentage share of the plastics fraction.

5. PROBLEM THE OPTIMIZATION DISASSEMBLY OF MECHATRONIC SYSTEMS

This task consists in fixing the optimal strategy of process disassembly of the mechatronic systems, which the function of the purpose is accepting the maximum value for:

$$f_c = (\sum_{i=1}^{e} oep_i + \sum_{i=1}^{f} oer_i + \sum_{i=1}^{g} ozs_i + \sum_{i=1}^{h} ozk_i + \sum_{i=1}^{k} ozms_i + \sum_{i=1}^{l} ots_i + \sum_{i=1}^{m} og_i + \sum_{i=1}^{p} opo_i) \rightarrow \max \tag{22}$$

Limiting conditions:

- rate of the reuse-recovery,

$$PO \geq 0,85 \tag{23}$$

- rate of the reuse-recycling,

$$PR \geq 0,80 \tag{24}$$

- balance conditions of recovered mass of elements and materials from the mechatronic systems,

$$\forall a \in A \qquad \sum_{a=1}^{A} m^{(a,b)} \leq m_a \tag{25}$$

$$\forall b \in B \qquad \sum_{b=1}^{B} m^{(a,b)} \leq m_b \tag{26}$$

A – set recovered elements, $m^{(a,b)}$ – mass recovered in the relation (a, b), m_a – mass of the element to recovering, B – set of regained elements and materials, m_b – mass of the recovered elements.

6. CONCLUSION

Of optimization research and experimental research findings in the comparative assessment received of process disassembly of mechatronic systems a criterion of the environmental assessment was used. Analysis of received results pointed for intentional carrying out the optimization of disassembly of mechatronic systems which led to the height of rate PO (rate of the reuse-recovery) and PR (rate of the reuse-recycling) (Fig. 3).

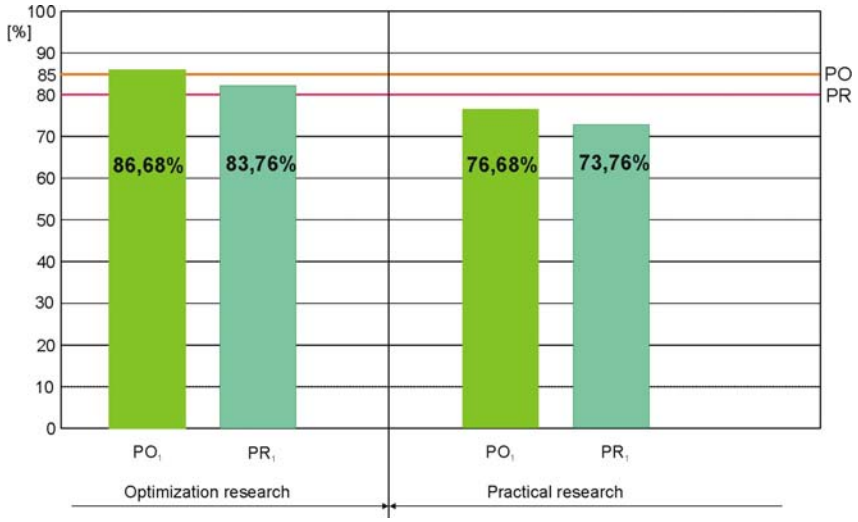

Fig. 3. Analysis of get rates: PO_1 – rate of the reuse-recovery from the mechatronic systems , PR_1 – rate of the reuse-recycling from the mechatronic systems, PO – rate of reuse-recovery in directives WEEE and ELV, PR – rate of reuse-recycling in directives WEEE and ELV

REFERENCES

1. **Ambroziak T.** (1998), *Modelowanie procesów technologicznych w transporcie*, Prace Naukowe, Transport z. 40 Politechniki Warszawskiej, Oficyna Wydawnicza Politechniki Warszawskiej, Warszawa.
2. **Fred Lambert A. J. D., Gupta S. M.** (2005), *Disassembly modeling for assembly, maintenance, reuse, and recycling*, CRC Press.
3. **Jarzębińska-Dziegciar A.** (2004), *Optymalizacja nieliniowych sieci transportowych z wykorzystaniem algorytmów genetycznych*, Rozprawa doktorska, Politechnika Warszawska, Wydział Transportu, Warszawa.
4. **Johnson M. R., Wang M. H.** (1998), Economical evaluation of disassembly operations for recycling, remanufacturing and reuse, *Int. J. Prod. Res*., Vol. 36 (12).
5. **Korzan B.** (1978), *Elementy teorii grafów i sieci. Metody i zastosowania*, Wydawnictwa Naukowo-Techniczne, Warszawa.
6. **Kuo T. C.** (2006), Enhancing disassembly and recycling planning using life-cycle analysis, *Robotics and Computer-Integrated Manufacturing*, 22.
7. **Shih L., Chang Y., Lin Y.** (2006), Intelligent evaluation approach for electronic product recycling via case-based reasoning, *Advanced Engineering Informatics*, 20.
8. **Spengler T., Ploog M., SchrOter M.** (2003), Integrated Planning of Acquisition, Disassembly and Bulk Recycling; *A Case Study on Electronic Scrap Recovery*, OR Spectrum, 25(3).

CONTENTS

INVESTIGATION ON THE MICROSTRUCTURE OF THE HAP AND YSZ COMPOSITES

Agata DUDEK *

* Institute of Materials Engineering, Częstochowa University of Technology,
ul. A. Krajowej 19, 42-200 Częstochowa, POLAND

dudek@mim.pcz.czest.pl

Abstract: Group of bioceramic materials includes, among others, hydroxyapatites (HAp, OHAp, HA), which, due to their specific properties are widely applied. These compounds are currently present in bone systems of human and animal bodies. One of the solutions for improvement of poor properties of HAp is addition of zirconium oxide which is characterized by high biological tolerance and enhanced mechanical properties.
Application of bioceramic materials as coatings for implants introduced into human body due to their bioinertness and biocompatibility enables overcoming immunology barriers. One of the fundamental advantages of ceramic materials is their positive impact on human tissues.
The investigations involved creation of composites through single-axial compaction of two ceramic powders (HAp+YSZ) and then their sintering at the temperature of 1300°C for two hours.
The aim of the investigations was to determine thermal stability of hydroxyapatite (Fig. 1) and HAp + YSZ (Partially Stabilized Zirconia) (Fig. 2) and impact of addition of YSZ (8%wt. Y_2O_3 stabilizing ZrO_2) on phase composition of the prepared composites after the process of sintering.
Investigations of the structure have been performed using JEOL JSM 5400 (Fig. 4, 5) scanning microscope while phase composition have been carried out by means of Seifert 3003 T-T X-ray diffractometer (Fig. 6, 7).

1. INTRODUCTION

Recent years have seen considerable improvement in development of special-purpose properties used in medicine. In particular, this encompasses group of materials used for implants.

Application of bioceramic materials as coatings for implants introduced into human body due to their bioinertness and biocompatibility enables overcoming immunology barriers. One of the fundamental advantages of ceramic materials is their positive impact on human tissues.

European Society for Biomaterials clearly defines biomaterials as a group of natural or synthetic substances which can replace or overcome functions of parts or a whole tissue or organs (Hartmann and Jager, 2001).

A group of minerals such as hydroxyapatites (HAp, OHAp, HA), due to their specific properties covers wide application range in biotechnology. They are the compounds which, from chemical and mineralogy point of view, are similar to inorganic substances which form human bone tissue or teeth.

Considerations of human bone system issues is by all measures justified due to progressing demand for a variety of implants.

Literature studies enable statement that a threshold of opportunities of improvements in biotolerance and properties of applied bioceramic implants has already been reached. Currently the most promising materials for prosthetics are composites (Khalil et al., 2007; Chevalier et al., 2005; Inzuka et al., 2005; Sung and Kim, 2003; Cheng et al., 2005; Rapacz-Kmita et al., 2005; Yoshida et al., 2006; Chiu et al., 2007; Kalkura, 2003; Heimann, 2006.

2. MATERIALS AND INVESTIGATIONS METHODOLOGY

Hydroxyapatite powder of $Ca_{10}(PO_4)_6(OH)_2$ (Sulzer-Metco) (with 99% purity and the ratio of Ca/P = 1.67) and ZrO_2 zirconium oxide powder modified with 8%wt. Y_2O_3 (YSZ) were used for investigations.

Morphology for the applied powders are presented in Fig. 1, 2.

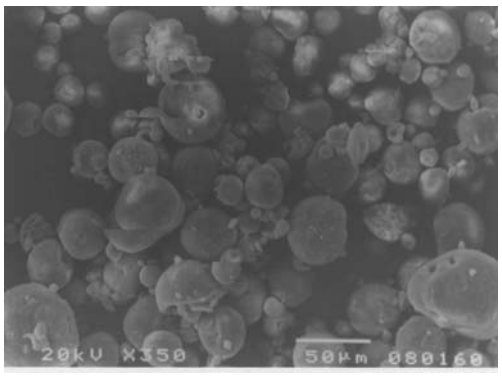

Fig. 1. Morphology of hydroxyapatite powder, magn. 350x

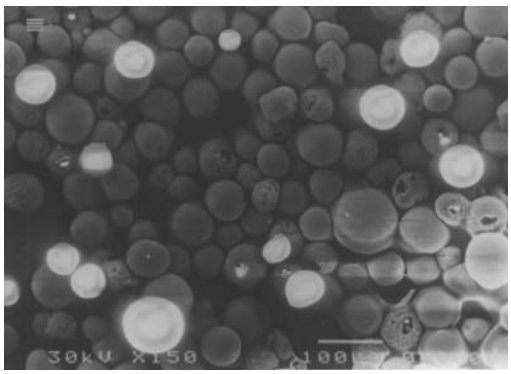

Fig. 2. Morphology of YSZ powder, magn. 350x

In order to prepare composites the following granulation values for the powders were used: HAp – ca 50 μm, ZrO_2 – 80 μm. Both powders have regular, spheroid shape of grains.

Powders were then subject to grinding in ball grinder in order to obtain even mixing of both powders.

The purpose of the investigation was to obtain bioceramic composites with the following rates by weight: 100 % HAp , HAp + 10% wt. YSZ, HAp + 30% wt. YSZ. These powders were formed through their single-axis compaction inside a die with load of 70 MPa (Fig. 3).

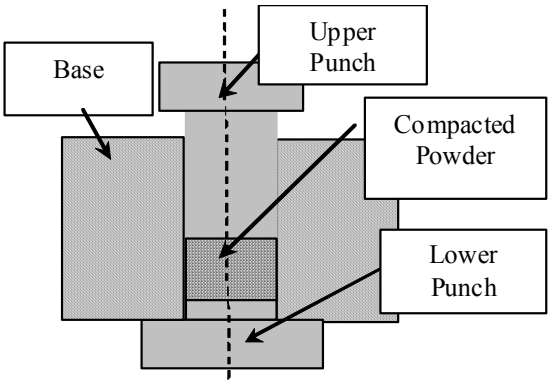

Fig. 3. Diagram of the die used for powder compaction

A result of compaction was a form, commonly referred to as 'moulded piece'. Compaction of the powders was carried out in the following stages:

- dislocation of particles in relation to each other,
- plastic strain of particles,
- crushing of particles.

The particles moving in relation to each other as a result of the compaction pressure had to overcome friction forces and than the breaking of 'bridges' which had appeared during powder loading occurred.

Next stage of bioceramic composite preparation was sintering of the prepared moulded pieces. This process consisted in soaking of the compacted powder at the temperature lower than melting point of the applied components in order to compact it into a solid piece. Sintering temperature was determined as 1300 ^oC for 2 hours.

As a result of physical and chemical processes which accompany the process of sintering a change in properties and dimensions of moulded pieces was observed.

During investigations some microscopic tests of moulded pieces before and after the sintering process in order to analyse one phase system were carried out. Microstructure of moulded piece before sintering is presented in Fig. 4, while after sintering – Fig. 5.

Analysis of one phase system (100 % HAp) before and after sintering reveals that the grains after the process of densification were partially crashed and they adhered to each other. After the process of sintering a visible reduction in porosity occurred.

In order to analyse phase stability of the produced composites (which is necessary in the aspect of their prospective application) after sintering, a phase analysis was carried out using Seifert 3003 T-T X-ray diffractometer using radiation with wavelength of $\lambda_{K\alpha Co}$=0.17902 nm. The results of investigations for all created composites are presented in Fig. 6 and 7.

Hydroxyapatite begins changing its phase composition over the temperature of 900 ^oC due to loss of water and appearance of partially or totally dehydrated oxyhydroxyapatite.

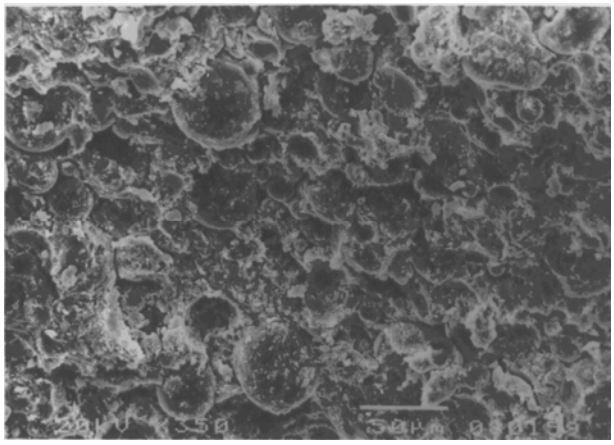

Fig. 4. Microstructure of the compacted powder with 100 % HAp

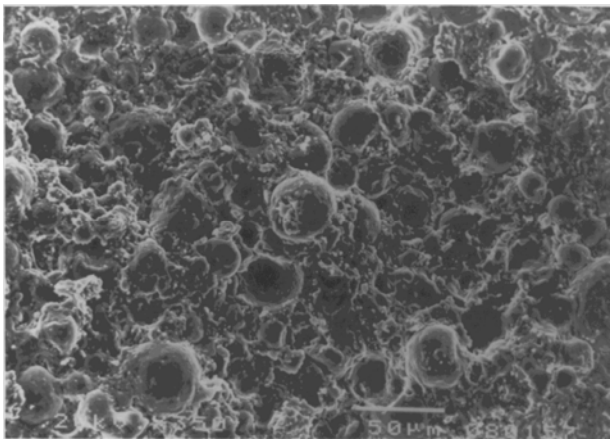

Fig. 5. Microstructure of the compacted and sintered powders with 100 % HAp

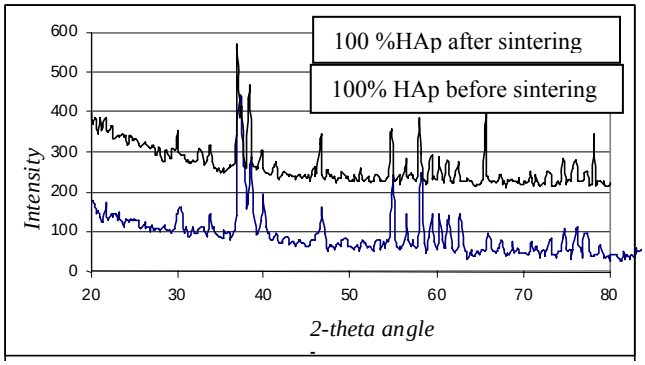

Fig. 6. Diffractogram of 100% HAp moulded piece before and after sintering at the temperature 1300^0C for 2 hours

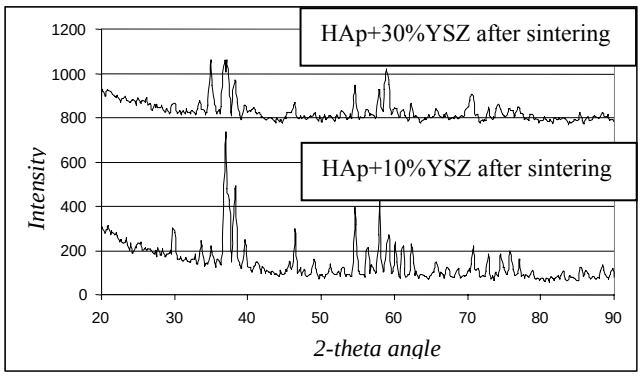

Fig. 7. Diffractogram of moulded piece HAp +10 %wt. PSZ and HAp + 30 %wt. PSZ sintered at the temperature of 1300^0C for 2 hours

Phase analysis of the samples made of 100% hydroxyapatite, both before and after the process of sintering, have not revealed any phase changes (Fig. 6). HAp phase (hydroxyapatite) with $Ca_{10}(PO_4)_6(OH)_2$ formula occurred throughout the volume; it crystallises in hexagonal system with the following unit cell parameters: a=b=9.418 nm, c= 6.884 nm and space group of P63/m.

Diffractograms obtained for HAp +10 %wt. and HAp +30 %wt. composites revealed presence of two phases: HAp and ZrO_2 with tetragonal cell (Fig. 7). Moreover, X-ray tests excludes the fact of the presence of β-TCP phase, described by Yun-Mo Sung and Dae-Hee Kim's team in Sung and Kim (2005); the authors argued that its contents increased as a result of rise in YSZ percentage value.

3. CONCLUSIONS

Subject of investigations was composites made of HAp powder and HAp +YSZ powders with granulation of 50 μm and 80μm, respectively. Composites were created by single-axis compaction in die and then sintering at the temperature of 1300 ^{o}C during two hours.

Macro- and microscopic observations of samples before and after sintering revealed contraction in volume as a result of reduction in porosity, maintaining primary shape of samples.

On the basis of X-ray analysis no phase decomposition in hydroxyapatite or in HAp – based composites with addition of YSZ (ZrO_2 – zirconium oxide stabilized with 8%wt. yttrium oxide Y_2O_3) after the process of sintering at the temperature of 1300 ^{o}C has been revealed.

The applied sintering temperature and addition of ZrO_2 have not caused appearance of unfavourable, from the chemical stability point of view, β-TCP phase.

Analysis of X-ray and structural tests proved thermal stability of the applied hydroxyapatite powder.

REFERENCES

1. **Piconi C., Maccauro G.** (1999), Zirconia as a ceramic biomaterial, *Biomaterials*, 20, 1-5.
2. **Hartmann P., Jager C.** (2001), *Journal of Solid State Chemistry*, 160, 460-468.
3. **Khalil K.A., Kim S., Kim H,Y.** (2007), *Materials Science and Engineering*, 456, 368-372.
4. **Chevalier J., Deville S., Munch E., Jullian R., Lair F.** (2005), *Biomaterials*, 25, 5539-5545.
5. **Inuzuka M., Nakamura S., Kisi S.** (2004), *Solid State Ionic's*, 172, 509-513.
6. **Sung Y.M., Kim D.H.** (2003), *Journal of Crystal Growth*, 254, 411-417.
7. **Cheng G., Pirzada D., Cai M., Mohanty P., Bandyopadhyay A.** (2005), *Materials Science and Engineering C*, 541-547.
8. **Rapacz-Kmita A., Paluszkiewicz C., Ślósarczyk A., Paszkiewicz Z.** (2005), *Journal of Molecular Structure*, 744-747, 653-656.
9. **Yoshida K., Hashimoto K., Toda Y., Udagawa S., Kanazawa T.** (2006), *Journal of the European Ceramic Society*, 26, 515-518.
10. **Chiu C.Y., Hsu H.C., Tuan W.H.** (2007), *Ceramics International*, 33, 715-718.
11. **Kalkura S.N.** (2003), *Materials Letters* 57, 2066-2070.
12. **Heimann R.B.** (2006), *Surface and Coatings Technology*, 201, 2012-2019.

CYCLIC-MODULAR APPROACH TO DEVELOPMENT OF ELECTRONICALLY-MECHANICAL CONTROL SYSTEMS OF THE PNEUMATIC DRIVE

Aleksandr GUBAREV[*], Oleg JACHNO[*], Oksana GANPANTSUROVA[*]

* National Technical University of Ukraine "KPI", 37, Peremogy av., Kiev, 03056, Ukraine

gubarev@i.ua

Abstract: The module approach for build-up of cyclic action systems is considered. The main property of approach is system decomposition on cyclic action subsystems (modules). All modules have same structure: actuating device (drive), control device (directional valve), status sensors. Methods of approach application are realized by means of graphs. Advantage of module approach is possibility of physically heterogeneous devices combination (devices with pneumatic or hydraulic control, electro-relay or PLC) not only in all system, but also inside of each modulus, that reduced a number of signal conditioning devices. Such synthesis is possible owing to a minimal structure of each modulus.

1. INTRODUCTION

Modern production lines of an industrial automation are bound with making of heterogeneous systems. Methods of design, representative for one field, for example, pneumatics, should be matched with other technical means, including control algorithms for PLC. Good results display methods, based on logic model of system, which one is invariant to kind of realization technique in execute and control means (Ciskowski at al., 2007; Ebel and von Terzi, 2000; Schmidt, 2002; Woźniak and Jędrzejkiewicz, 2007).

2. PREMISES OF THE APPROACH

The tendered approach originally was intended for the hydraulics and the pneumatics cyclic systems for which one application of traditional methods was limited by number of drives and steps of system operation, by cost, response and asynchronous actions of the hydraulic and pneumatic apparatuses. The approach allows: propagation of reengineering problems, necessity of fast junction to issue of other product modifications, shortening of the testing and adjusting time.

2.1. Problems

- Decomposition of large systems on a projecting phase.
- Rational combination of an algorithmic, electronic, electric, pneumatic and hydraulic tool.
- Diagnostics, navigation of errors, troubleshooting.
- Build-up of systems with the open structure.

2.2. Physical premises

- The automation object consists of the fixed number of elements.
- Each element fulfills the action entering in an operating procedure multiply.
- Process of object activity can be represented in the form of operation or of a work cycle completely consisting of actions of object elements.
- Deflections from a cycle can be represented as alternative actions of some elements.

2.3. Theoretical premises

Cyclical process can be considered, as the functional form of product description (result of system operation) (Губарев, 1997).

Premise 1. Correspondence of product (purpose), process (technology of production), object (manufacturing system):

$$O(*,*,*,T) \oplus W \Leftrightarrow \exists P : \forall p \in P \Rightarrow W \oplus O \xrightarrow{G} p \qquad (1)$$

$$\forall \tau \in T \exists \Phi : O(*,*,*,\tau) \xleftarrow{\Phi} O(*,*,*,\tau - 1), \qquad (2)$$

where: W - the medium of object operation; O (E, Φ, F, T) – object; $E = \{e_1, \ldots, e_n\}$ – an object state as a set of states *n* of its elements; $\Phi = \{\varphi_1, \ldots, \varphi_m\}$ – control functions by object; $F = \{f_1, \ldots, f_m\}$ – unctions of actions (working off of control); $T = \{\tau_1, \ldots, \tau_k\}$ – the discrete time (argument of cause-effect relationship between actions); $P = \{p_1, \ldots, p_r\}$ – a product (a result of object interacting with exploitation medium);

Premise 2. The technology for production line does not vary during operation:

$$\exists O(E,\Phi,F,T) \Rightarrow \forall(\tau_i \neq \tau_j):$$
$$\begin{cases}\exists n : E(\tau_i) \equiv (F(\Phi(E(\tau_j))))^{(n)} \\ \exists m : E(\tau_i) \equiv (F(\Phi(E(\tau_i))))^{(m)}\end{cases}. \quad (3)$$

Premise 3. There is an unequivocal correspondence between set of functional elements e_i and set of segments of process φ_i:

$$\begin{cases}\forall e_i \in E \exists \varphi_j \in \Phi : e_i \leftarrow \varphi_j \\ \forall \varphi_j \in \Phi \exists e_i \in E : \varphi_j \rightarrow e_i\end{cases}. \quad (4)$$

The model of elements system is reduced to a process model from actions. Then, system as process can be decomposed to actions and logical connections between them. Each modulus (an action plus connection), in consequence of (4), simultaneously is function and building block of object:

$$\{e_i\}_n = \{(f,\varphi)_i\}_n = \{(x,y)_i\}_n, \quad (5)$$

where $X = \{x_1, \ldots, x_n\} = \{X\}_n$ – process and result of fulfilment of the actions caused by logic functions in system:

$$\left(\left.\begin{matrix}x_i=0\\ e_i\\ y_i=1\end{matrix}\right|_{\tau \equiv 0} \xrightarrow{f_i} \left.\begin{matrix}x_i=1\\ e_i\\ y_i=1\end{matrix}\right|_{\tau+1 \equiv 1}\right) \Leftrightarrow \xrightarrow{X_i}$$

$Y = \{y_1, \ldots, y_m\} = \{Y\}_n$ – the logic functions, which connect following actions with previous, where argument are results before the fulfilled actions $y_i = y_i(\{X\}_n)$.

$$\begin{cases}\forall(\tau_j, x_i)\exists! y_i : x_i(\tau_j) \Leftarrow y_i(\{X(\tau_j - 1)\}_n) \\ \forall(\tau_j, y_i)\exists! x_i : y_i(\{X(\tau_j - 1)\}_n) \Rightarrow x_i(\tau_j)\end{cases}. \quad (6)$$

Premise 4. Each action should iterate many times because of a process repetition:

$$\forall x_i \exists(\tau_{i1} < \tau_{i2} < \tau_{i3} < \tau_{i4}) \subset \{T\}: \\ : x_i(\tau_{i1}) \neq x_i(\tau_{i2}) \neq x_i(\tau_{i3}) \neq x_i(\tau_{i4}). \quad (7)$$

Analogously, and the reasons causing these actions, also should iterate. But, as to each action, before its repetition, the "return" action of the same modulus precedes, then should iterate and reasons of this action.

Therefore, and reasons of the modulus actions constitute couples, and mutually exclusive conditions:

$$\forall y_i \in \{Y\}_n \exists! y_j \in \{Y\}_n : \begin{cases}\overline{x_i} \Leftarrow y_j(\{X\}_n) \\ \overline{x_j} \Leftarrow y_i(\{X\}_n)\end{cases}. \quad (8)$$

With allowance for (1) – (8):

1. The model of the cyclic system of drives is uniform (all modules have an equal constitution);
2. The model consists of cyclical modules which contain two inverse actions and two logic functions, setting a context of fulfilment of these actions.

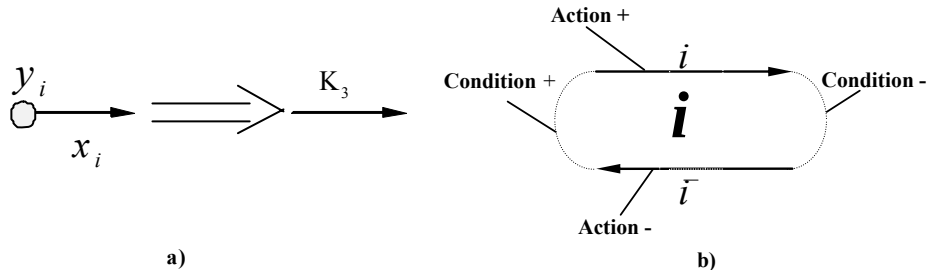

Fig.1. The scheme of one action (a) and of cyclical modulus for this action (b)

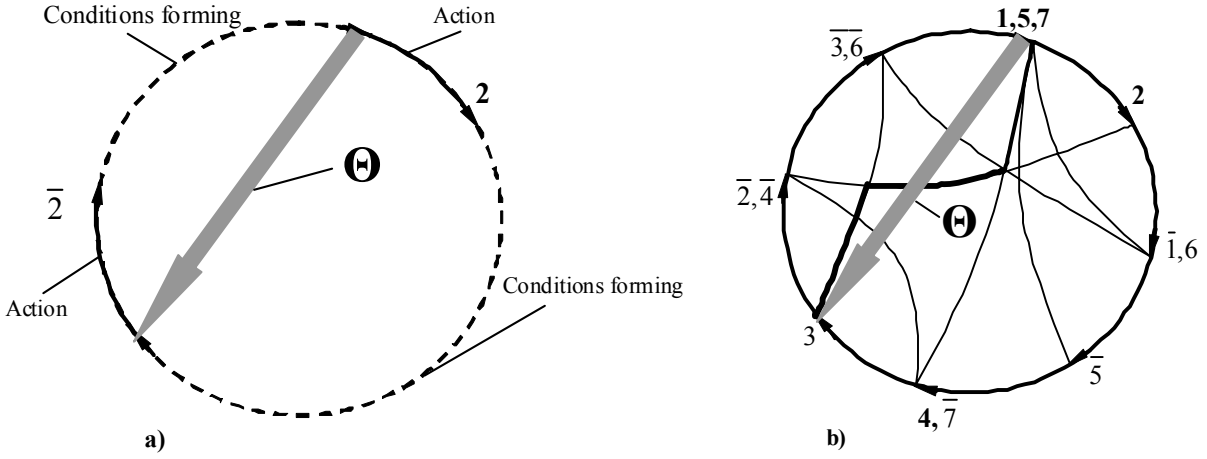

Fig. 2. The cyclical sequence of operations represented in the form of a closed digraph: for one modulus (a) and for cyclic system (b)

Each action is marked out by number of the modulus and represented by an arc referred from a reason to result (Fig. 1a), where y_i – a logic function caused this action; x_i – action; i – a name of the modulus. The modulus consolidates two inverse actions and conditions of their running in to the form of a cycle (Fig. 1b).

Process of object activity consists of segments. Each segment is represented by a directional action of one modulus or simultaneous actions of several modules. The segment of process is represented by the directional arc with names of actions. Cyclical process receives form of a cycle or of the closed digraph, if there are parallel line-ups of actions. Arcs of the graph are segments $\{x_i\}$ of cyclical modules (9). Sections of conditions forming $\{y_i\}$ in cyclical modules (are marked out by a dot line) match to system operation between result of fulfilment back action and he beginning of the main action of the modulus (Fig. 2a).

Pictorially the model of system consists of a functional graph figuring an operational process:

$$G = \{P, L, \mathrm{M}\}, \tag{9}$$

where $P = \{p\}_n : \forall p_i \exists (l_{i-1}, l_i) \in L \Rightarrow l_{i-1} \to p_i \to l_i$ – set of the vertexes matching completion of the previous actions and forming of a condition of the beginning of following actions;

$L = \{l\}_m : \forall l_i \exists (p_{i-1}, p_i) \in P \Rightarrow p_{i-1} \to l_i \to p_i$ – set of the arcs matching fulfilment of actions;

$\mathrm{M} = \{\mu\}_m : \forall l_i \exists \mu_i = (k_{\mu 1}, k_{\mu 2}, \cdots) \neq \varnothing$ – et of marks for the arcs matching names of actions.

Inside of a functional graph there is a subgraph of connection which one adds actions of each modulus up to a cycle (Fig .2b).

Imitation of object activity realized by fulfilment of the graph under rules of an input, an output and traversal through arcs and vertexes. In this case, action can be considered as result of fulfilment of conditions (y_i=1), sufficient for its beginning. That is actions are an integral from conditions on a segment of one arc:

$$L(\tau) \Leftrightarrow \{x_1(\tau), x_2(\tau), \cdots, x_n(\tau)\}; \tag{10}$$

$$L'(\tau) \Leftrightarrow \{y_1(\tau), y_2(\tau), \cdots, y_n(\tau)\}; \tag{11}$$

$$L(\tau_k) = \begin{cases} *: ((L(\tau_k - 1) = 1) \wedge (L'(\tau_k) = \overline{1})) \vee \\ \vee (L(\tau_k - 1) = 0) \wedge (L'(\tau_k) = 1)) \\ L(\tau_k - 2) + \int\limits_{\tau_k - 1}^{\tau_k} L'(\tau_k - 1) \partial\tau \end{cases}; \tag{12}$$

$$\frac{\partial L(x_i(\tau))}{\partial \tau}\Big|_{\tau_k} = \begin{cases} 1: ((x_i(\tau_k + 1) = 1) \wedge (x_i(\tau_k) = 0)) \\ \overline{1}: ((x_i(\tau_k + 1) = 0) \wedge (x_i(\tau_k) = 1)) \\ (0 \vee y_i(\tau_k - 1)): x_i(\tau_k) = x_i(\tau_k + 1) \end{cases}. \tag{13}$$

Analysis of systems model has displayed, that the information about finished actions is recorded in value $\{\mathrm{X}\}_\mathrm{n}$ in the alphabet (0, *, 1). With other words, $\{\mathrm{X}\}_\mathrm{n}$ is an expression of system memory, distributed on static component (value 0 and 1 – fulfilled actions) and dynamic component (value * – running actions):

$$L(\tau_i) = \int\limits_{\tau_o}^{\tau_i} L'(\tau) \partial\tau = L(\tau)\Big|_{\tau_o}^{\tau_i - 1} + ,$$

$$+ \int\limits_{\tau_i - 1}^{\tau_i} L'(\tau) \partial\tau = L_c(\tau_o, \tau_i) + L_v(\tau_i) \tag{14}$$

where – the static component of memory accumulated on the interval $L_C(\tau_o, \tau_i)$; $L_V(\tau_{i/o})$ – dynamic component of memory.

It is displayed, that memory distribution on $L_C(\tau_o, \tau_i)$ and $L_V(\tau_{i/o})$ depends on interval limits (τ_o, τ_i). It is established, that the availability of an interval (τ_o, τ_i) for which one the memory value is zero follows to separation of object into independent units (from τ_o up to τ_i and from τ_i up to τ_o). The informational completeness of object is mirrored with closed system measure:

$$\forall \tau_i \exists (L(\tau)\Big|_{\tau_i}^{\tau_i + 1} + L(\tau)\Big|_{\tau_i + 1}^{\tau_i}) \equiv 0 \tag{15}$$

and integrities measure:

$$\begin{cases} \forall (\tau_i, \tau_j): \tau_i \neq \tau_j \pm 1 \Rightarrow S_{i/j} \neq 0 \\ \forall \tau_k \overline{\exists} L: (L(\tau_k) = 1) \wedge (L(\tau_k + 1) = \\ = \overline{1}) \vee (L(\tau_k) = \overline{1}) \wedge (L(\tau_k + 1) = 1). \end{cases} \tag{16}$$

For the system, which satisfy these measures its development is reduced to build-up of a cyclical modules complete set. For build-up of one modulus it is necessary to realize two actions and two conditions. To the main actions there match arcs of the graph at which one transmission value x_i each time varies from 0 through * up to 1. To the back action - variation x_i^- from 0 through * up to 1. In the real system to it there matches fulfilment of productive function (for example, activity of a drive, connection of pressure).

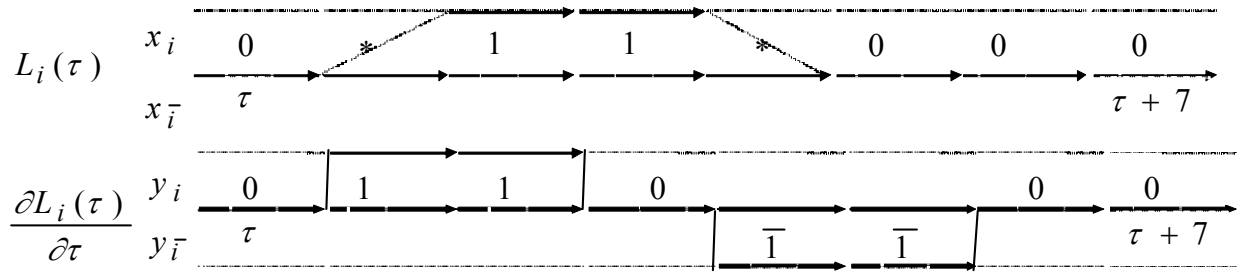

Fig. 3. The diagram of control and state for one cyclical modulus

Conditions are the vector which one closed up arcs and constituted from other actions segments (Fig. 2b). Conditions consist of several components: proximate causes, a context of action, a condition of a repetition and others. The procedure of deriving of minimum logic conditions is reduced to build-up of a closing vector:

$$y_{i(5)} \Leftarrow \bigcup_{v}\bigcup_{k=1}^{m}[\bigcap_{p}^{R1,R2}((x_{k,1(i)}+\{x\}_{k,1c})_p * \cdots * (x_{k,n(i)}+\{x\}_{k,nc})_p * \{x\}_{k-\bar{k}})_p] * \{x\}_{k-\bar{m}}$$

$$y_{i(4)} \Leftarrow \bigcup_{k=1}^{m}(x_{k,1(i)}+\{x\}_{k,1c}) * \cdots * (x_{k,n(i)}+\{x\}_{k,nc}) * \{x\}_{k-\bar{k}} * \{x\}_{k-\bar{m}} \supset$$

$$\supset y_{i(3)} \Leftarrow \bigcup_{k=1}^{m} x_{k,1(i)} * \ldots * x_{k,n(i)} * \{x\}_{k-\bar{k}} * \{x\}_{k-\bar{m}} \supset \quad ; \quad (17)$$

$$\supset y_{i(2)} \Leftarrow \bigcup_{k=1}^{m} x_{k,(i)} * \{x\}_{k-\bar{k}} * \{x\}_{k-\bar{m}} \supset \quad ;$$

$$\supset y_{i(1)} \Leftarrow \bigcup_{k=1}^{1} x_{(i)} * \{x\}_{i-\bar{i}} \quad ,$$

where

$\bigcup_{v}$ - union of expressions of one modulus for alternate modes of system operation; $\bigcup_{k=1}^{m}$ - the total of expressions for operating modes of the modulus; $\bigcap_{p}^{R1,R2}$ - product of expressions of context reasons from alternate modes of system R1 and R2; $x_{k,\,j(i)}$ – state signal of proximate causes of k-th mode of i-th modulus; $\{x\}_{k,\,jc}$ – the logical expression enlarging a signal $x_{k,j(i)}$ before completion of action y_i; $\{x\}_{k-\bar{k}}$ – the logical expression ensuring a repetition of the modulus; $\{x\}_{k-\bar{m}}$ – the logical expression ensuring reasonableness of inverse actions of the modulus.

3. TECHNICAL PERFORMANCE OF SYSTEM

3.1. Actions of one modulus (X_i and $X_{\bar{i}}$)

In technical performance the drive is arranged with tools of controlling and the supervision of a given function fulfilment. For example, the pneumatic cylinder fulfilling a hold-down tool of a two details during its pasting together. (Fig. 4). The control device is the pneumatic directional valve. Monitoring devices - the pressure transducer (gain of a hold-down tool), position sensors (initial and working), an interval timer (an assembly time in gluing of details). The pasting together is finished if: the drive has transited the midposition sensor X'_{2S}, is not discontinued stroke of the cylinder, after achievement of gain of a pasting together drive has transited a technological time interval.

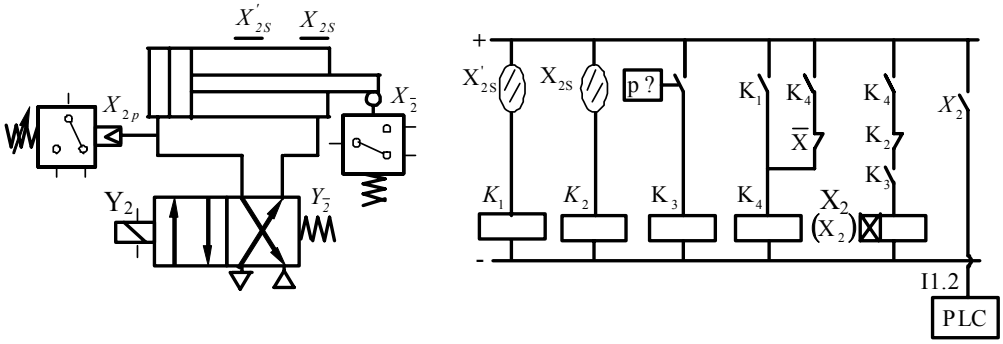

Fig. 4. Actuating part of modulus No 2 (the pneumatic cylinder fulfilling a hold-down tool of a two details during its pasting together)

2.4. Conditions of one modulus (Y_i and $Y_{\bar{i}}$)

In technical performance to conditions there match control diagrams (relay, pneumatic, hydraulic) or algorithms of PLC programs. Conditions are constituted for all modules in the minimum form (17). Procedures of drawing up of conditions allow for application of bistable and monostable valves. For example, for build-up of a logic control
command for the main action of the second modulus (Fig. 2b) the vector Θ, which one goes from the beginning of the main action ***2*** to the beginning back-action $\bar{2}$, is plotted. The vector Θ is made by segments of connection lines of modules: $7+2\cdot\bar{3}$. The first condition is added by proximate causes $7 \to 7\cdot 5\cdot 1$, the last condition is invertible $\bar{3} \to 3$. Then we write down a logic function which one is a control command:

$$Y_2 = X_1 \cdot X_5 \cdot X_7 + X_2 \cdot \overline{X_3}\,.$$

This expression matches to build-up of command in case of application as the control device of a monostable valve.

Thus the drive control diagram can be realized depending on technical specifications and demands as by means of pneumatic, hydraulic tools, and by means of the program or to consolidate in it physically heterogeneous devices (Fig. 5).

3.2. The modules connecting up to a system

Process of modules connecting in to a system is fulfilled under the asynchronous circuit: each modulus provided by status signals, which dimensioned the logic conditions for its start and stop (Y_i and Y_i-), all system components provided with foreseen power supply. As well as by any alternative version of the circuit structure, engaging devices of system, a possibility of a stopping and alternative versions of control are provided. Further, each modulus operates under the logic rules set for it, and actions of modules, following these rules, constitute an operation period of system. Such method of modules connecting can be used as a tool for modernization and systems reengineering (Chrostowski et al., 2004; Ebel and von Terzi, 2000).]

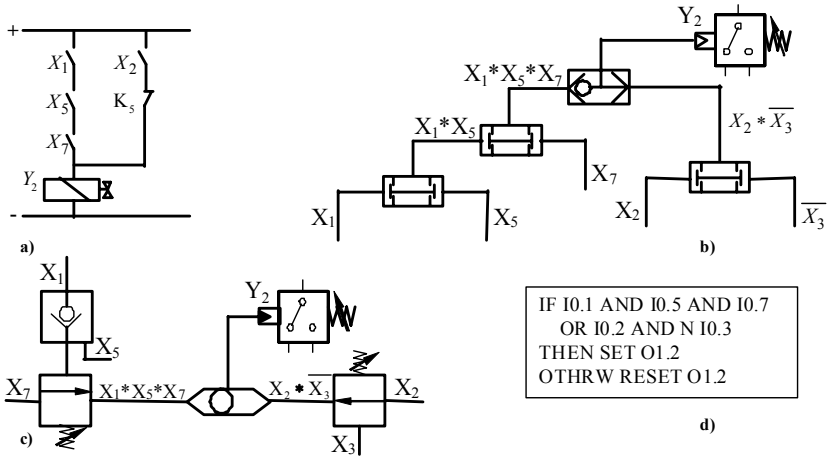

Fig. 5. Variants of realization of a conditional part of the modulus No 2: a) by means of the relay circuit; b) by a pneumatic tools; c) by hydraulic apparatuses; d) by making algorithm of the PLC program

The main segment of algorithm has view of a cyclic kernel. In this segment are displayed the complete set of modules description in the same form. For example, the STL algorithm for bistable control valve in modulus No 2 has such view:

```
IF          X1 AND  X5   AND    X7
   OR         X2  AND   N     X3
THEN  SET      Y2
        RESET  YN2
OTHRW       RESET   Y2
            SET     YN2
```

or monostable control valve:

```
IF        X1   AND   X5   AND   X7
    OR    X2   AND    N     X3
THEN      SET       Y2
OTHRW     RESET     Y2
```

The same forms for flag, timer, counter, multi-positional drive are designed. By making the algorithm this allows to have the same description method for all system components. Advantages of this method is: reduction of program list, simplicity of new modulus addition in to a system, possibility to consolidate alternative versions of system operation in one program, the program "watch" all modules all the time by a cyclic kernel.

4. SUMMARY

The cyclic-modular approach is effective at making systems with close to cyclical process of operation and quantity of actuating devices 5 and more. Efficiency of the approach is raised, if it uses at all phases - from development of the preliminary specifications, before drawing up of operating instructions, production of references on navigation and trouble-shooting. The method has formal measure for estimation of systems logic completeness, the algorithm of account of measure linearly depends on number a subsystem. The cyclic-modular constitution of systems simplifies the matching of various means in one object that get the possibility for addition the system by new modules and fulfilment of reengineering.

REFERENCES

1. **Chrostowski H., Domagala Z, Kedzia K**. (2004), Napędy i sterowania hydrauliczne w pierwszej dekadzie XXI wieku. *Hydraulika i Pneumatyka*, z. 2, 22-27.
2. **Ciskowski S., Dworzak L., Ganczarek M**. (2007), Modelowanie i programowanie metodą Grafpol pracy napędów pneumatycznych, I*nternational Scientific-Technical Conference: Hydraulics and Pneumatics*, 56-63.
3. **Ebel F., von Terzi M.** (2000), *Festo Didactic*, Mechatronics.: Festo Didactic GmbH&Co., D73770 Denkendorf.
4. **Guzowski A., Sobzyk A**. (2005), Modernizacja sterowania manipulatorów pneumatycznych, *Hydraulika i Pneumatika*, z. 1, 20-23.
5. **Schmid D.** (2002), *Mechatronika* – Polish edition REA, Warshawa.
6. **Wozniak M., Jedrzykiewicz Z.** (2007), Projektowanie układów hydraulicznych z wykorzystaniem algorytmów genetycznych, *Hydraulics and Pneumatics*, 126-132.
7. **Губарев А.П.** (1997), Дискретно-логическое управление в системах гидропневмоавтоматики: Учебное пособие.- К.: ИСМО.

3D APPLE MODELING WITH THE USE OF THE STRUCTURED LIGHT METHOD

Marek HRYNIEWICZ[*,*], Jan ANTHONIS[**], Herman RAMON[***]**

[*]Institute for Building, Mechanization and Electrification of Agriculture, ul. Rakowiecka 32, 02-532 Warszawa, Poland
[**]LMS Engineering Innovation Research Park Z1, Interleuvenlaan 68, B-3001 Leuven, Belgium
[***]Division of Mechatronics, Biostatistics and Sensors, KU Leuven University, Kasteelpark Arenberg 30, B-3001 Heverlee, Belgium

marek.hryniewicz@wp.pl, jan.anthonis@lmsintl.com, Herman.Ramon@biw.kuleuven.be

Abstract: The geometrical fruit model could affect many physical phenomena, such as heat, mass and moisture transfer, pneumatic transport and mechanical vibrations which occur during handling and processing fruits (Jancsok, 1999). The fruit geometrical model could be further studied by the Finite Element Method (FEM) (Jancsok, 1999). Incidence of bruises is the most important type of postharvest mechanical injury (van Zeebroeck, 2005). The reason for this is that the causes and mechanisms of impact and vibration are complex and interrelated (van Zeebroeck, 2005). In mechanical engineering a geometrical model of the structure to be analyzed is usually available as CAD drawing which can be imported directly in FE software (Jancsok, 1999). However, for agricultural-, bio- and food- materials there are no geometrical models available so they have to be defined manually, which is complicated by the complex shape and the shape variability of these products (Jancsok, 1999). Dintwa (Dintwa, 2006) stated that the 3D simplified models used in the dynamic experiments were not accurate enough, most certainly because of the coarse discretization used with these models.
This paper describes a system for complex shapes geometrical modeling. The system was implemented in real apple modeling. It was developed on structured light method elaborated by Sitnik (2002). The method has advantages and disadvantages.
Advantages: modeling of complex shapes, recalculation of many points at one moment, at least only 3 views for one figure, measurements without object touching.
Disadvantages: problems with light reflection.

1. INTRODUCTION

Precision Agriculture uses the best available technologies to tailor soil and crop management to fit the specific conditions found within an agricultural field or tract. It needs collecting huge amount of data from the field from many sensors. The Division of Mechatronics, Biostatistics and Sensors, KU Leuven University in Belgium has elaborated a concept of unmanned crop cultivation. This concept is based on unmanned autonomous machines which would do every activity on the field. There are for example sensors needed for machine guidance. The most challenging task is plant inspection, especially fruits in orchards during the growing season. This task needs a method which could inspect fruit dimension, shape of surface and colour. Information about fruit dimension is very valuable for yield prediction. Shape of surface and colour information is very important for fruit health investigation. From all fruit shape information fruit volume could be calculated as a result. This would be useful for precise dosage of spraying. It should limit usage of herbicides and fertilizers, which is very important for human health. However the fruit shape investigation must be done without touching the fruit. Each touch of fruit is a source of mechanical damage of the surface. Bacterials, pathogens and fungi are developing very well in these places, resulting in fruit damage and decrease in yield. It is the same mechanism as postharvest mechanical injury described by Zeebroeck (van Zeebroeck, 2005). The fruit shape is also very important for simulations of heat, mass and moisture transfer, pneumatic transport and mechanical vibrations which occur during handling and processing fruits (Jancsok, 1999). However, for agricultural-, bio- and food- materials there are no geometrical models available so they have to be defined manually, which is complicated by the complex shape and the shape variability of these products (Jancsok, 1999). Dintwa (Dintwa, 2006) stated that the 3D simplified models used in the dynamic experiments were not accurate enough, most certainly because of the coarse discretization used with these models. The fruit geometrical model could be further studied by the Finite Element Method (FEM) (Jancsok, 1999) or Discrete Element Method (DEM) (Dintwa, 2006). In mechanical engineering a geometrical model of the structure to be analyzed is usually available as CAD drawing which can be imported directly in FE software (Jancsok, 1999). This paper describes a system for complex shapes geometrical modeling. The system was implemented for real apple modeling, based on the method of structured light, elaborated by Sitnik (2002). This method is used in reverse engineering for mechanical parts modeling. In this paper, this method is tested on biological models in laboratory conditions before using it on the field.

2. METHOD JUSTIFICATION

The right method choice is very important because the appropriate method is going to be implemented in orchard or greenhouse. Thus the real conditions must be taken into consideration during the choice.

There is limited area of camera movement in real conditions due to plants structure (leafs, stems) and close distance to other plants. The ideal method should give an opportunity to measure the biggest part of fruit surface without any camera movement.

Existing methods based on vision techniques are passive or active according to Curless (2000). The term passive is used for sensing to refer to the measurement of visible radiation that is already present in the scene, in contrast to active techniques that project light into the scene. The active methods have an advantage above passive methods because they can be implemented in places with bad illumination. This is very important issue for measurements in orchard or greenhouse. Numerous shadows from leaves and natural change of illumination conditions from clouds are typical challenge for computer vision in agriculture. Additionally the best active methods generally produce more accurate reconstructions than is possible using passive techniques as stated Seitz (1999).

There is a set of active triangulation methods which belongs to active methods (Trucco and Verro, 1998). The simplest method with Light Spot Projection is illustrated on Figure 1. There is needed a laser and a camera. It is easy to find the point P distance from the camera when we know the distance between the laser and the camera, and appropriate angles, according to description given by Klette and others (1998) .The Z axis coincides with the optical axis of the camera.

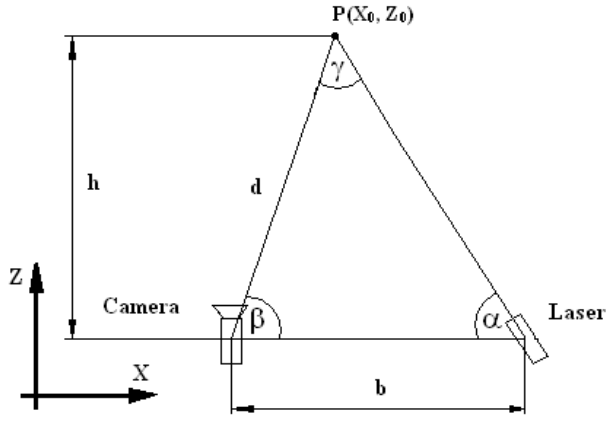

Fig. 1. Principle of Light Spot Projection detection in 3D

On Figure 1: b – distance between laser light source and camera along X axis, h – distance between camera and point P in space along Z axis, d – absolutely distance between camera and point P in space, α – angle between laser ray and X axis, β – angle between X axis and section between camera and point P, γ – angle between laser ray and section between camera and point P, X_0 – P point coordinate along X axis, Z_0 – P point coordinate along Z axis.

There are the next trigonometrical proportions (1):

$$d/\sin(\alpha) = b/\sin(\gamma) \quad (1)$$

From (2)

$$\gamma = \pi - (\alpha + \beta) \quad (2)$$

and (3)

$$\sin(\pi - \gamma) = \sin(\gamma) \quad (3)$$

it follows that (4)

$$d/\sin(\alpha) = b/\sin(\pi - \gamma) = b/\sin(\alpha+\beta) \quad (4)$$

Thus, the distance d is given as (5):

$$d = b*\sin(\alpha)/\sin(\alpha+\beta) \quad (5)$$

The location of the point $P(X_0, Z_0)$ can be represented in XZ coordinates as follows (6), (7):

$$X_0 = d*\cos(\beta) \quad (6)$$

$$Z_0 = h = d*\sin(\beta) \quad (7)$$

The Light Spot Projection Method detects only one point coordinates of laser from one image. It must be done change of laser point position or all setup position for detecting another point on investigated object. It is a technical trouble for apples surface investigation. This method can be improved by throwing a laser line onto the object. It is so called Light Line Projection Method and it principle is shown on Fig. 2.

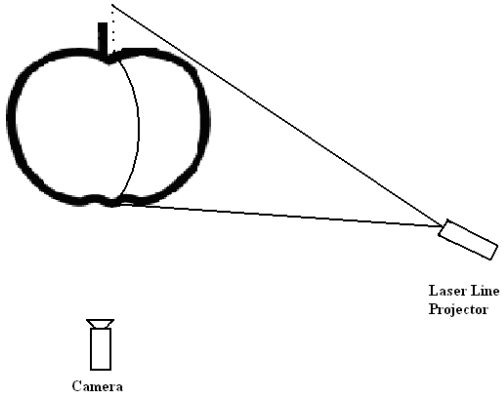

Fig. 2. Light Line Projection Method principle

The Light Line Projection Method improves amount of calculated points from one image but it is limited only to one stripe. Extension of this Method is projecting of several light planes at the same time on the examined apple surface. It is so called Static Light Pattern Projection Method. Fig. 3 presents the Method concept.

The Static Light Pattern Projection Method reduces number of images needed to the investigated apple surface representation. The Method gives only points coordinates represented on stripes. The points coordinated between the strips are unknown. The all setup should be moved and other images should be registered for calculation of the points coordinates. It is inconvenient for field circumstances.

The Structured Light Method can give a surface of all visible part of fruit without any camera movement. The Method idea is widely described in Sitnik (2002) and presented on Fig. 4. A sequence of fringe patterns is projected from DLP projector on the apple. The images are captured without any setup movement. This Method can give points coordinates of all visible part of the apple.

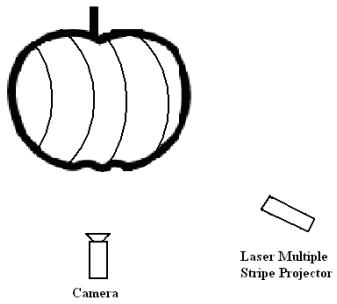

Fig. 3. Static Light Pattern Projection Method concept

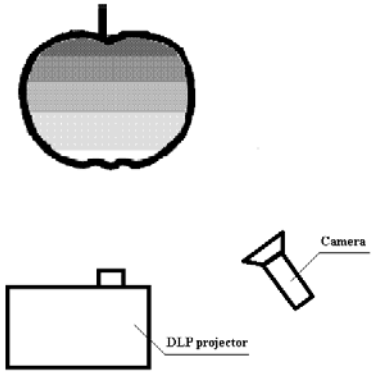

Fig. 4. Structured Light Method idea

In conclusion, potentially the Structured Light Method is the best method among other existing methods. But it should be checked with use of real apples with different textures and colours. Skin of apple has quite different optical properties than metals surface with or without painting. There is a threat of reflections or other unknown side effects. Industry deals with this problem by powdering of measured metal objects. Powder layer has a few micrometers (10^{-6} m) thickness. The measured object has dimension of a few centimeters (10^{-2} m) and more. The change of dimensions for a few micrometers (powder layer thickness) is comparable with change of object dimensions according to temperature. Thus powder layer dimension can be neglected during measurements. But the powder layer gives any reflections from measured surface.

3. AIMS OF THE RESEARCH

The research should answer the following questions:

– Is the structural light method convenient for apples surface measurement by an unmanned autonomous machine?
– Are there any side effects (reflections without powdering, etc.)?
– Is the method enough precise for apple measurement?
– How is an apple shape in reality?

4. MATERIALS AND METHOD

4.1. Materials

A set of apples is investigated. It consists of eight pieces of Gala apples and eight pieces of Russet apples. Gala apples have smooth surface. Russet apples have rough surface. Their volume is measured by checking a change of water level in a vessel. The vessel has a label scaled in volume. Thus it is easy to obtain an apple volume as difference of water volume after immersing the apple in water and water volume before the apple immersing in water. It is presented on Fig. 5.

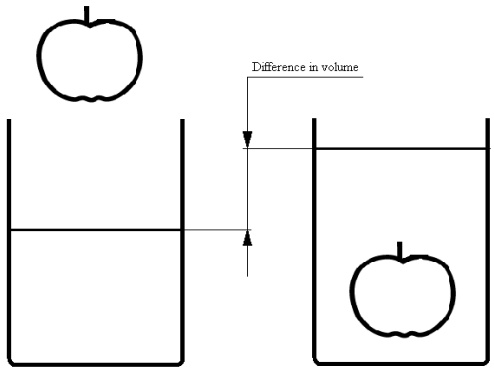

Fig. 5. Apple volume measuring

Then the apples are measured by making use of the Structural Light Method. It is assumed that all errors in the Method are distributed in the same way along each axis. Thus it is very simple error estimation.

The system idea (described by Sitnik (2002)) is based on throwing structured pattern light on an object, taking object picture with pattern image on object surface and analyzing it by the software. The result is the information about surface shape. Full fruit volume is obtained from a few camera points of view.

The hardware consists of one megapixel camera, digital light projector (DLP) with spatial resolution 1024x768 pixels, computer for images processing and calculations.

4.2. Shape and volume measurement with use of the Structural Light Method

Full apple volume can be obtained when the full apple shape is measured. It can be done by using an AutoCAD function which automatically calculates volume for closed three dimensional objects. The steps for data collecting are described in the Algorithm for receiving full shape of fruit.

The data are further processed according to the Algorithm for one camera position. This algorithm is the core of the method.

4.3. Algorithm for receiving full shape of the apple

The algorithm can be summarised in a few points:

1. Set the first apple position, collect the data and process them according to the algorithm for one fruit (camera) position.
2. Move the apple to the next position and collect the data and process them according to the algorithm for one fruit (camera) position.
3. Repeat point 2 until all the required data will be collected and processed.
4. Merge the data from multiple positions in one object:
   – unify systems of coordinates,
   – make triangulation,
   – simplify the mesh.
5. Write and export the data in an appropriate format.

The physical operations in the algorithm are illustrated on Figure 6.

4.4. Algorithm for one camera position

The algorithm can be summarized in a few points:

1. Throw a structured pattern light (a sequence of sinusoidal patterns shifted in phase) on an object.
2. Take the picture of the object.
3. Shift the phase in the structured pattern light and throw it on the object.
4. Take the picture of the object.
5. Repeat steps 2-4 times, minimum twice.
6. Analyze the pictures – map registered phase from taken picture into (x, y, z) coordinates.
7. Operations with points in (x, y, z) coordinates:
   – bad points elimination,
   – smoothing,
   – simplification.

The computer prepares an image of fringe patterns which is sent into DLP. The DLP throws the image on the measured object. The camera captures a picture, and then the computer with appropriate software does all recalculations.

The system core consists of very sophisticated software. It is based on an analysis of fringe patterns. Sitnik (2002) stated that it has been proven by several authors (Halioua and Liu, 1986; Kowarschik et al., 2000) that the most efficient and accurate way to perform phase determination in shape measurement systems applied for analysis of an arbitrary static 3D object should be performed by: temporal phase shifting (TPS) method (Schwider at al., 1983) followed by hierarchical unwrapping, specifically by Gray code method (Osten et al., 1996). The temporal phase shifting technique requires a projection of a sequence of sinusoidal patterns shifted in phase on a measured object. Intensity of each pixel for a real fringe pattern of the prepared image is usually represented by equation (7):

$$I_n(i, j) = A(i, j) + \Sigma\, B(i, j) * \cos[m*(\Phi(i, j) + n*\Delta\alpha)] \qquad (7)$$

where: I – generated image pixel intensity, n – number of image, i – generated image row number, j – generated image column number, A – background function value, B – modulation function value, Φ – unknown phase value, m – order of harmonics in signal, Δα – phase shift step.

The phase shift step Δα can be expressed as (8):

$$\Delta\alpha = 2\pi/(m+2) \qquad (8)$$

where: m – order of harmonics taken into consideration in signal.

The image with pattern previously described is thrown on the object by the DLP projector, which is presented on Fig. 6.

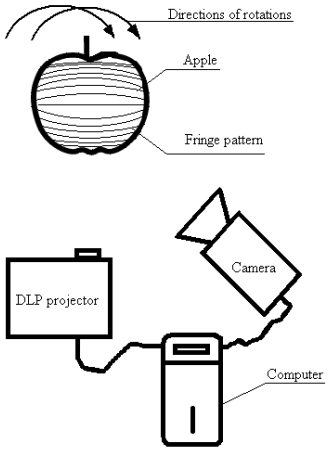

Fig. 6. Measurement system

The unknown phase value Φ consists of two parts (9):

$$\Phi = \Phi\mathrm{mod}2\pi + \Phi\mathrm{FN}2\pi \qquad (9)$$

Then the phase modulo2π is calculated for each pixel of camera separately from the intensity values of a captured sequence in this pixel. Minimum three images must be taken for calculations. The phase modulo2π is calculated according to formula (10):

$$\Phi\mathrm{mod}2\pi = \arctan(\Sigma I n \sin(n\Delta\alpha)/\Sigma I n \cos(n\Delta\alpha)) \qquad (10)$$

where: I – generated image pixel intensity, n – number of image, Δα – phase shift step (as in formula (8)).

Each fringe in the sine pattern is coded (numbered) in conjunction with phase according to formula (11):

$$\Phi\mathrm{FN}2\pi = \mathrm{FN} * 2\pi \qquad (11)$$

where:

$\Phi_{FN2\pi}$ – stepped phase, FN – fringe number.

Exemplary coded sine patterns thrown on investigated apple are presented on Fig. 7.

This final unwrapped phase map is a base for mapping it into (x, y, z) coordinations according to formula (12):

$$(x, y, z) = CM(\Phi, i, j) \qquad (12)$$

where: x, y, z – Cartesian co-ordinates of pixel in the calibration matrix space, i, j – pixel indices in the source image taken from the camera, CM – function related to calibration matrix determined experimentally, Φ – phase value calculated for pixel (i, j).

However the set is not ideal. It needs some improvements as: bad points elimination, smoothing and simplification.

The calculations are repeated for each apple position resulting in multiple sets of points. These sets are merged into one by: systems of coordinates unification, triangulation, making triangulation with mesh creation and simplifying the mesh. The data are written in an appropriate format at the end.

Fig. 7. Exemplary images of four Gray coded sine patterns with phase FN2π calculated from them

The investigated object is then moved as previously described in the Algorithm for receiving full shape of the apple.

5. RESULTS

Gala apples must be covered by powder before measurements with use of the Structural Light Method because of reflexes from smooth surface. The apples are naturally covered by a very thin layer which is optically similar to a wax surface. This surface reflects light what makes measurements of structured light impossible. This phenomenon is present for both red and green colours on apples. The apples surface must be covered by a very thin antireflective layer from powder. Then it enables good pictures registration.

Russet apples have rougher surface in compare with Gala apples. They can be measured by the Method without powdering. It is expected that other fruits with surface similar (or rougher) to Russet apples can be measured by this Method.

The exemplary shapes of one apple are presented on Fig. 8. A few different apples shapes are presented on Fig. 9. The standard deviation for volume difference between volumes measured in water and computed by AutoCAD is 5 ml, which is equivalent to 1,7 mm of linear distance along each axis. A possible explanation for this error can be by reading the volume of water. Sitnik (2002) claims that the uncertainty of measurement from a single direction is 10^{-4} m for measurement of volume dimensions. For sorting apples in different dimension classes, the required precision is about 5 mm, according to Commission regulation (EC) laying down the marketing standards for apples (Commission regulation (EC) No 85/2004).

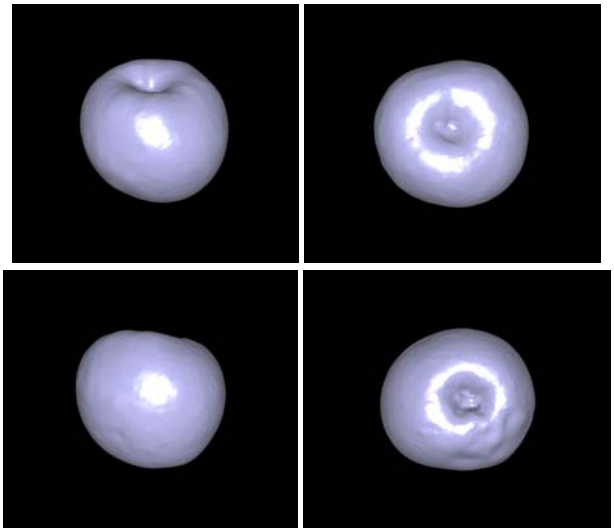

Fig. 8. Exemplary shapes of one apple

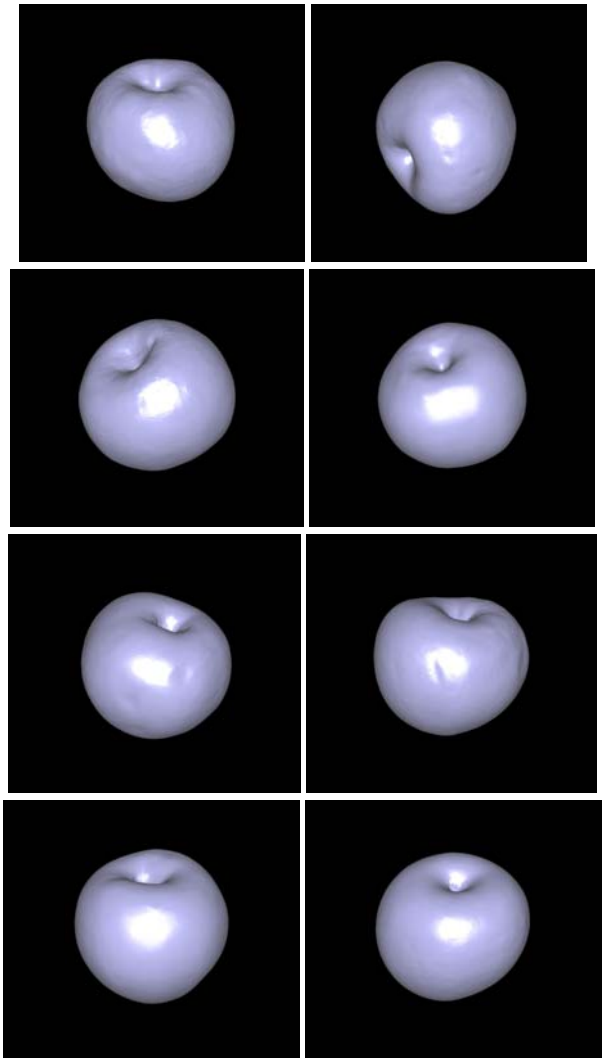

Fig. 9. A few different apples shapes

6. CONCLUSIONS

The Structural Light Method use for apples measurement is limited to varieties with surface similar or rougher to Russet apples. Apples (or fruits) with smoother surface (similar to Gala) must be covered by antireflective powder for shape and surface measurements. The method is independent from colour and measures the shape with high fidelity for apples covered by powder. The method can be used for apples and other fruits surface measurements in laboratory conditions. It measures apples with sufficient precision according to marketing standard for apples (Commission regulation (EC) No 85/2004).

Digital pictures of apples show that shapes are very complicated what is one from many problems to resolve in Finite Element Method or Discrete Element Method. Results of the measurements (the very precise real digital shapes of apples) are very valuable for modeling in these methods.

REFERENCES

1. **Curless B.** (2000), Overview of Active Vision Techniques, *SIGGRAPH 2000 Conference Los Angeles*, Course on3D Photography,
2. **Dintwa E.** (2006), *Development of accurate contact force models for use with Discrete Element Method (DEM) modelling of bulk fruit handling processes*, PhD work, Doctoraatsproefschrift Nr. 726 aan de Faculteit Faculteit Bio-ingenieurswetenschappen van de K.U. Leuven.
3. **Halioua M., Liu H.-Ch.** (1986), Optical sensing techniques for 3D machine vision, *Proc. SPIE* 665, p. 150-161.
4. **Jancsok P.** (1999), *Geometrical model generation for Finite Element Meshes of biological products based on digital image processing*, PhD work, Doctoraatsproefschrift Nr. 413 aan de Faculteit Faculteit Landbouwkundige en Togepaste Biologishe Wetenschappen van de K.U. Leuven.
5. **Klette R., Schluns K., Kosh A.** (1998) *Computer Vision Three-Dimensional Data*, Image Springer.
6. **Kowarschik R., Kühmstedt P., Gerber J., Schreiber W., Notni G.** (2000), Adaptive optical three-dimensional measurement with structured light, *Opt. Eng.*, 39, p. 150-158.
7. **Osten W., Nadeborn W., Andrae P.** (1996), General hierarchical approach in absolute phase measurement, *Proc SPIE*, 2860.
8. **Schwider J., Burow R., Elssner K.E., Grzanna J., Spolaczyk R., Merkel K.** (1983), Digital wave-front measuring interferometry: some systematic errors sources, *Appl. Opt.*, 22, p. 3421-3432
9. **Seitz S.** (1999), An Overview of Passive Vision Techniques, *SIGGRAPH 1999 Conference Los Angeles*, Course on 3D Photography.
10. **Sitnik R. (2002),** *A fully automatic 3D shape measurement system with data export for engineering and multimedia systems*, PhD work, Mechatronics Department of the Warsaw University of Technology.
11. **Trucco E., Verro A.** (1998), *Introductory Techniques for 3-D Computer Vision*, Prentice Hall.
12. **van Zeebroeck M.** (2005), *The Discrete Element Method (DEM) to Stimulate Fruit Impact Damage during Transport and Handling*, PhD work, Doctoraatsproefschrift Nr. 643 aan de Faculteit Faculteit Bio-ingenieurswetenschappen van de K.U. Leuven.
13. Commission regulation (EC) No 85/2004 of 15 January 2004 laying down the marketing standards for apples.

TRACEABILITY AND CAPABILITY CONTROL OF MASS MEASUREMENT EQUIPMENT AND DRIFT STATISTICAL ANALYSIS OF NATIONAL MASS STANDARDS IN LATVIA

Tatjana IVANOVA[*], Janis RUDZITIS[**]

[*]Latvian National Metrology Centre, Kr. Valdemara iela 157, LV–1013, Riga, Latvia
[**]Riga Technical University, Kalku iela 1 Riga, LV–1658, Latvia

puchkova@inbox.lv, aria@latnet.lv

Abstract. LNMC is highest metrological institute of Latvia. The paper describes national mass standards currently in use, their traceability, stability, mass measurement equipment and related techniques.

1. INTRODUCTION

Latvian National Metrology Centre (State Agency) is a public organization with legal liability. Its main task is to ensure uniformity of measurement throughout the country and provide metrological services to persons and organizations. LNMC is highest metrological institute of Latvia. Main tasks of State Agency are to maintain uniformity and traceability of physical units, verification and calibration of measuring instruments and standards (weights etc.). Department of mass measurement of State Agency is a holder of national mass standards. These are 1 kg mass standard in stainless steel and two sets of mass standards (from 1 mg to 500 g). Laboratory performs periodic calibration and statistical analysis of mass standards. The Department of mass measurement ensures traceability between national mass standards (with values derived from the International Prototype of the kilogram) and weights of class E_1 and lower. Once in two years national mass standards are carried to DFM (Dansk Fundamental Metrologi, Denmark) or other laboratory for calibration. Department of mass measurement of State Agency has probably the best mass measurement equipment in Latvia, such as "Sartorius" comparator (high-precision mass measurement instrument). ScalesNet32 is the software used for data acquisition and analysis. Computer running ScalesNet32 is connected to both comparator and climate control system of the lab. This equipment allows LNMC to perform calibration of E1 class weights (most accurate ones).

Department of mass measurement of State Agency does participate in various international interlaboratory comparisons schemes: "839 EUROMET", "EUROMET 786", "LNMC (Latvia) -METROSERT (Estonia) - MIKES (Finland)", "832 EUROMET" and others.

Tab. 1. Interlaboratory comparisons of LNMC

Project Id	**Year**	**Description**	**Standard, range**	**Framework reference number**
510 EUROMET. M.M-K4	15.04.2002.-02.05.2002.	Comparison of mass standards	Standard (Stainless steel) **1 kg**	European metrology programme EUROMET 510
445 EUROMET. M.M-K2	27.03.2003.-21.05.2003.	Comparison of mass standards	A set of standarts (Stainless steel) **10 kg,500 g, 20 g, 2 g, 100 mg**	European metrology programme EUROMET 445
832 EUROMET	14.12.2004.-17.01.2005.	Comparison of mass standards	Standard (Stainless steel) **50 kg**	EUROMET 832
V/a LNMC (LATVIA) – METROSERT (ESTONIA) –	05.09.2006.	Calibration of non-automatic weighing instruments	1) Mettler-Toledo, AX504, *Max* 510 g, *d*= 0,1 mg 2) Mettler-Toledo, KB50-2, *Max 60* kg, *d*= 0,01 g	VM1-2006
V/a LNMC (LATVIA) – METROSERT (ESTONIA) – MIKES (FINLAND)	09.÷23.11. 2006.	Comparison of mass standards	Standard 500 kg	-
EUROMET 786 (M.M-K2.1)	04.01.2007.-02.02.2007.	Comparison of mass standards	A set of standards (Stainless steel) **10 kg, 500 g, 20 g, 2 g, 100 mg**	European metrology programme EUROMET 786

At present, the laboratory is planning interlaboratory comparison of mass measurement capability between various Latvian laboratories. Department of mass measurement will be the pilot laboratory of the comparison. Comparisons like this have never been carried out before. This comparison will be first such project in Latvia. We have to adapt existing methods and procedures for our needs or develop new ones. Major complication is that there is strong competition between some of participants. However, small size of Latvia makes transfer of standards less complex and expensive task. Interlaboratory comparisons allow laboratories to validate measurement capability, identify and correct measurement errors, assess technical proficiency and calibration procedures, verify adequacy of laboratory environment, provide evidence of measurement traceability and demonstrate measurement comparability between laboratories.

2. TRACEABILITY OF MEASUREMENTS

The international definition of 'traceability' is: *property of the result of a measurement or the value of a standard whereby it can be related to stated references, usually national or international standards, through an unbroken chain of comparisons all having stated uncertainties*. As said above, mass is unique amongst the base quantities of the SI because its unit definition, the kilogram, is based on a physical artifact; a cylinder of platinum iridium alloy, held at the Bureau International des Poids et Measures BIPM near Paris, is defined as being exactly one kilogram in mass. All mass measurements undertaken in the World should be traceable to this single artefact – the international prototype of the kilogram (known as K – see history of the kilogram) – and this is achieved by regularly comparing its mass with the official 'copies' of the Kilogram held in national measurement institutes, such as NPL.

2.1. Elements of traceability

Traceability is characterized by a number of essential elements: an unbroken chain of comparisons going back to a standard acceptable to the parties, usually a national or international standard; measurement uncertainty; the measurement uncertainty for each step in the traceability chain must be calculated according to defined methods and must be stated so that an overall uncertainty for the whole chain may be calculated; documentation; each step in the chain must be performed according to documented and generally acknowledged procedures; the results must equally be documented; competence; the laboratories or bodies performing one or more steps in the chain must supply evidence for their technical competence (e.g. by demonstrating that they are accredited); reference to SI units; the "appropriate" standards must be primary standards for the realization of the SI units; recalibrations; calibrations must be repeated at appropriate intervals; the length of these intervals depends on a number of variables, (e.g. uncertainty required, frequency of use, way of use, stability of the equipment).

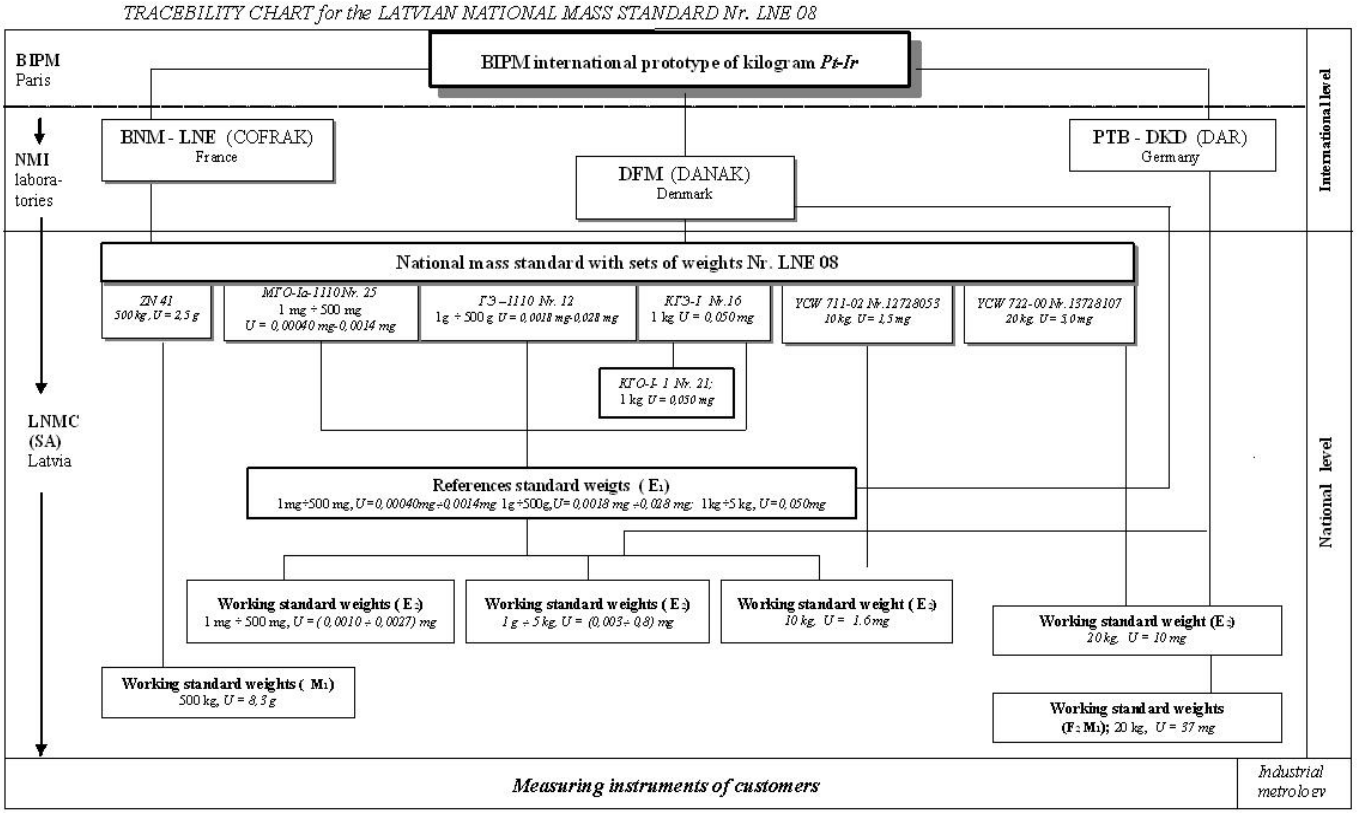

Fig. 1. Standard calibration procedure

At the international level, decisions concerning the International System of Units (SI) and the realization of the primary standards are taken by the Conférence Générale des Poids et Mesures (CGPM). The Bureau International des Poids et Mesures (BIPM) is in charge with coordinating the development and maintenance of primary standards and organizes intercomparisons on the highest level.

The National Metrology Institutes are the highest authorities in metrology in almost all countries. In most cases they maintain the "national standards" of the country which are the sources of traceability for the associated physical quantity in that country. If the National Metrology Institute has facilities to realize the corresponding SI unit of measurement (the term SI units includes all derived units), the national standard is identical to or directly traceable to the primary standard realizing the unit. If the Institute does not have this facility, it has to ensure that the measurements are traceable to a primary standard maintained in another country. The National Metrology Institutes ensure that the primary standards themselves are internationally comparable. They are responsible for disseminating the units of measurement to users. They are the top level of the calibration hierarchy in a country.

Department of mass measurement of LNMC (SA) is a holder of national mass standards. These are 1 kg mass standard in stainless steel and two sets of mass standards (from 1 mg to 500 g). Laboratory performs periodic calibration and statistical analysis of mass standards. This ensures traceability between Latvian national mass standards (with values derived from the International Prototype of the kilogram) and weights of class E1 and lower. Once in two years national mass standards are carried to DFM (Dansk Fundamental Metrology, Denmark) or other laboratory for calibration.

2.2. Weighing cycles

In the weighing cycles, *"A'* represents weighing the reference weight and *"B"* represents weighing the reference weighing the test weight. The cycles *ABBA* and *ABA* are normally used when calibrating E and F class weights. The cycle $AB_1 \ldots B_nA$ is often used when calibrating M class weights, but generally not recommended for E and F class weights. If, however, a mass comparator with an automatic weight exchange mechanism is used and if the system is installed in a protecting housing, this cycle can also be accepted for class E and F weights calibrations. Only cycles ABBA and ABA are useful in subdivision weighing. More than one reference weight can be used; in this case the weighing cycles can be applied for each reference weight separately; the reference weights may then be compared against one another.

Tab. 2. Minimum number of weighing cycles

Class	E_1	E_2	F_1	F_2	M_1, M_2, M_3
Minimum number of *ABBA*	3	2	1	1	1
Minimum number of *ABA*	5	3	2	1	1
Minimum number of $AB_1 \ldots B_nA$	5	3	2	1	1

2.3. Data analysis

Average difference of conventional mass – One test weight. For cycles *ABBA* and *ABA*, the conventional mass difference, Δm_c, between the test weight and the reference weight of a cycle, I, is:

$$\Delta m_c = m_{ct} - m_{cr} \tag{1}$$

$$\Delta m_{ci} = \Delta I_i + m_{cr} \cdot C_i \tag{2}$$

where

$$C_i = (\rho_{ai} - \rho_0) \cdot (\frac{1}{\rho_t} - \frac{1}{\rho_r})$$

The average difference of conventional mass for n cycles is:

$$\overline{\Delta m_c} = \frac{1}{n} \sum_{i=1}^{n} \Delta m_{ci} \tag{3}$$

If the density ρ_t or ρ_r of a weight is not known, but the material is known, the appropriate assumed density from mean value of hand-book should be used. If it is only known that the density of a weight is within the allowed limits then the value 8000 $kg \cdot m^{-3}$ should be used. In cases where air buoyancy correction is estimated to be negligible, i.e., if the term $m_0 \cdot C_i$ can be omitted.

$$\left| C_i \right| \le \frac{1}{3} \cdot \frac{U}{m_0} \tag{4}$$

If only one or an averaged value of the air density is available, the buoyancy correction $m_{cr} \cdot C$ can be applied after averaging.

Average difference of conventional mass – Several test weights. If several test weights are calibrated according to weighing cycle $AB_1 \ldots B_nA$, the average mass difference for weight k is obtained from equation (3) by replacing ΔI_i with $\Delta I_{i(k)}$ in equation (2).

Average difference of conventional mass – Several series of measurements. If there are several (J) identical series of measurements with average values $\overline{\Delta m_j}$ and with approximately equal standard deviations the average value of all measurements is:

$$\overline{\Delta m_c} = \frac{1}{J} \cdot \sum_{j=1}^{J} \overline{\Delta m_{cj}} \tag{5}$$

Several series of measurements are usually performed only in calibration of class E weights, when the reproducibility of weighing has to be investigated.

Conventional mass of the test weight. The conventional mass of the test weight can be calculated from the formula:

$$m_{ct} = m_{cr} + \overline{\Delta m_c} \tag{6}$$

In verification, the conventional mass of the reference weight is not always known. In these case, its nominal value should be used.

The standard uncertainty $u(m_{cr})$, of the mass of the reference weight should be calculated from the calibration certificate by deviling the quoted expanded uncertainty, U, by the coverage factor k (usually k=2) and should be combined with the uncertainty due to the instability of the mass of the reference weight, $u(m_{cr})$.

$$u(m_{cr}) = \sqrt{(\frac{U}{2})^2 + u_s^2(m_{cr})} \tag{7}$$

The uncertainty due to instability of the reference weight, $u_s(m_{cr})$, can be estimated from observed mass changes after the reference weight has been calibrated several times.

The uncertainty of air buoyancy correction can be calculated from

$$u_b^2 = \left[m_{cr} \cdot \frac{(\rho_r - \rho_t)}{\rho_r \cdot \rho_t} \cdot u_{\rho_a} \right] \tag{8}$$

Where ρ_a is the air density during the (previous) calibration of the reference weight by use of a higher order reference weight. When using equation (8) be sure to use the same value for the uncertainty of the density of the reference weight $u(\rho_\gamma)$, that was used in the uncertainty calculation of the previous calibration. If the air density is not measured and the average air density for the site is used, than the uncertainty for the air density is to be estimated as:

$$u(\rho_a) = \frac{0{,}12}{\sqrt{3}} \left[kg \cdot m^{-3} \right] \tag{9}$$

At sea level the density of air should be assumed to be 1,2 $kg{\cdot}m^{-3}$.

Uncertainty of the balance u_{ba}. The recommended approach to determine this component is to test the balance and mass comparators at reasonable time intervals and use the results from the test in the uncertainty calculations. If the balance is calibrated with a sensitivity weight (or weights) of mass m_s, and of standard uncertainty $u(m_s)$, the uncertainty contribution due to sensitivity is

$$u_S^2 = (\overline{\Delta m_c})^2 \cdot (\frac{u^2(m_S)}{m_S^2} + \frac{u^2(\Delta I_S)}{\Delta I_S^2}) \tag{10}$$

Where ΔI_S is the change in the indication of the balance due to the sensitivity weight; $u(\Delta I_S)$ is the uncertainty of ΔI_S; and, $\overline{\Delta m_c}$ is the average mass difference between the test weight and the reference weight. If the sensitivity is not constant with time, temperature, and load, its variation must be included in the uncertainty. If the weight does not have the form of a perfect cylinder, then additional corrections or an expanded uncertainty may be required. For a digital balance with the scale interval d, the uncertainty due to resolution is

$$u_d = (\frac{d/2}{\sqrt{3}}) \cdot \sqrt{2} \tag{11}$$

The factor $\sqrt{2}$ comes from the two readings, one with the reference weight and one with the test weight.

Uncertainty due to eccentric loading u_E. If this contribution is known to be significant, the magnitude must be estimated and if necessary the contribution must be included in the uncertainty budget.

$$u_E = \frac{(d_1/d_2) \cdot D}{2 \cdot \sqrt{3}} \tag{12}$$

Where D is the difference between maximum and minimum values from the eccentricity test performed according to OIML R 72-6; d_1 is the estimated distance between the centres of the weights, and d_2 is the distance from the centre of the load receptor to one of the corners. In most cases, the uncertainty contribution u_E is already covered by the uncertainty u_w of the weighing process and may be neglected. When using balances with automatic weight exchange mechanism, the indication difference ΔI, between two weights may be different when the positions are interchanged: $\Delta I_1 \neq \Delta I_2$. This may be interpreted as an eccentric loading error and the corresponding uncertainty should be estimated using equation (13). This uncertainty contribution is applicable, if it is known from previous interchanging measurements with weights of the same nominal value. In case that the interchange is performed during a calibration procedure, the average of the two indication differences shall be taken as the weighing results and u_E can be neglected.

$$u_E = \frac{|\Delta I_1 - \Delta I_2|}{\sqrt{3}} \tag{13}$$

Combined standard uncertainty of the balance u_{ba}. The uncertainty components are added quadratic ally as follows:

$$u_{ba} = \sqrt{u_S^2 + u_d^2 + u_E^2 + u_{ma}^2} \tag{14}$$

Expanded uncertainty $U(m_t)$. The combined standard uncertainty of the conventional mass of the test weight is given by:

$$u_c(m_t) = \sqrt{u_w^2(\overline{\Delta m_c}) + u^2(m_{cr}) + u_b^2 + u_{ba}^2} \tag{15}$$

The expanded uncertainty U, of the conventional mass of the test weight is as follows:

$$U(m_t) = k \cdot u_c(m_t) \tag{16}$$

Where the coverage factor k = 2, should be used.

Tab. 3 - 6. Instability analysis of national mass standards

Type of weights ***МГО – 1 а – 1110*** No ***25*** *(1 mg-500 mg)* *1989 -2006 years*

No.	Nominal value of the weights, m_N *mg*	$\overline{\Delta m_D}$ *mg*	E_1 *mpe (OIML R 111)* *mg*	Drift $u_S(\overline{\Delta m_D})$ *mg*
1.	**1**	**-0,00003**	0,003	0,000017
2.	**2**	**0,00003**	0,003	0,000017
3.	**2***	**0,00008**	0,003	0,000046
4.	**5**	**0,00003**	0,003	0,000017
5.	**10**	**0,00006**	0,003	0,000035
6.	**20**	**-0,00002**	0,003	0,000012
7.	**20***	**0,00008**	0,003	0,000046
8.	**50**	**0,00010**	0,004	0,000058
9.	**100**	**0,00005**	0,005	0,000029
10.	**200**	**0,00015**	0,006	0,000087
11.	**200***	**0,00008**	0,006	0,000046
12.	**500**	**0,00033**	0,008	0,000191

Type of weights ***ГЭ - 1110*** No ***12*** *(1 g-500 g)* *1989 -2006 years*

		mg	*mg*	*mg*
1	**1**	**-0,00031**	0,010	0,000179
2	**2**	**-0,00038**	0,012	0,000219
3	**2***	**-0,00027**	0,012	0,000156
4	**5**	**-0,00027**	0,016	0,000156
5	**10**	**-0,00029**	0,020	0,000167
6	**20**	**-0,00031**	0,025	0,000179
7	**20***	**-0,00062**	0,025	0,000358
8	**50**	**-0,00107**	0,030	0,000618
9.	**100**	**-0,00280**	0,05	0,001617
10.	**200**	**-0,00495**	0,10	0,002858
11.	**200***	**-0,00359**	0,10	0,002073
12.	**500**	**-0,00793**	0,25	0,004578

Type of weights ***КГЭ - 1*** No ***16*** *(1 kg)* *1985 -2006 years*

No	Nominal value of the weights, m_N *кg*	$\overline{\Delta m_D}$ *mg*	E_1 *mpe (OIML R 111)* *mg*	Drift $u_S(\overline{\Delta m_D})$ *mg*
1.	**1**	0,00677	0,5	0,003909

Type of weights ***КГО – 1 -1*** No ***21*** *(1 kg)* *1984 -2006 years*

No	Nominal value of the weights, m_N *кg*	$\overline{\Delta m_D}$ *mg*	E_1 *mpe (OIML R 111)* *mg*	Drift $u_S(\overline{\Delta m_D})$ *mg*
1.	**1**	0,01707	0,5	0,009855

Remark: Where m_N is nominal value of the weights, m_c – conventional mass of the weights, $U(m_c)$ – expanded uncertainty of the conventional mass of the test weigh, $u_S(\overline{\Delta m_D})$ – drift (instability of the test weight)

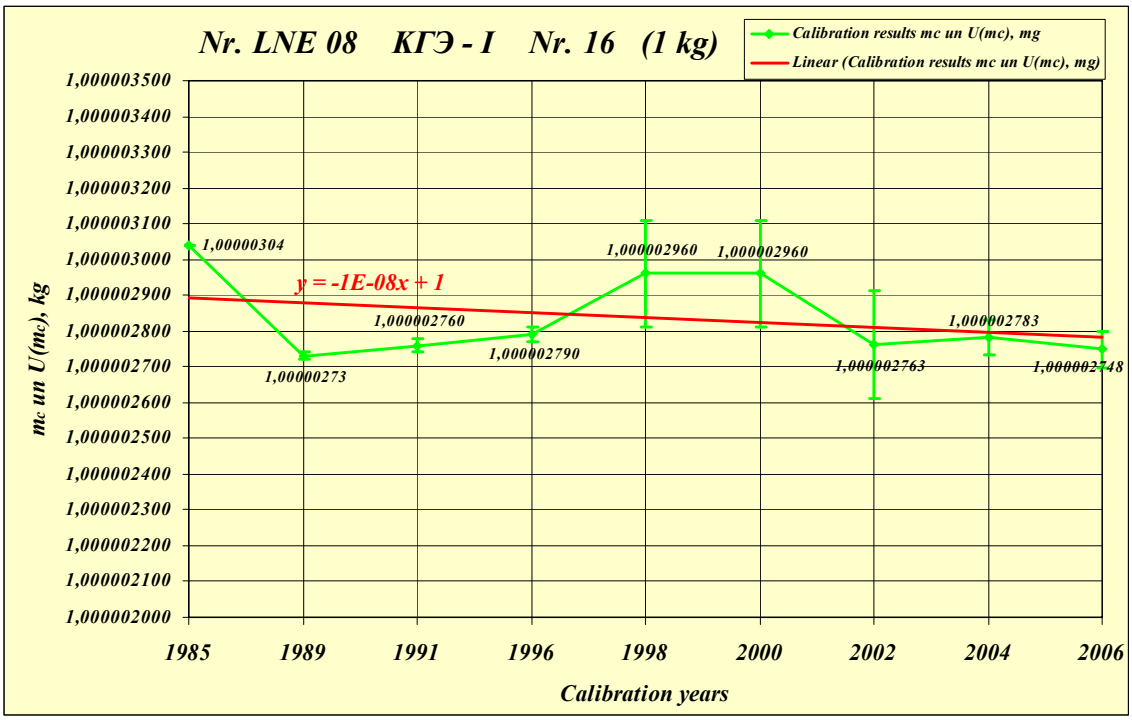

Fig. 2. Calibration results of national standards and approximation

Measurement equipment of Department of mass measurement of State Agency. Department of mass measurement of State Agency has probably the best mass measurement equipment in Latvia (Table 7), such as "Sartorius" comparator (high-precision mass measurement instrument). ScalesNet32 (Figure 3) is the software used for data acquisition and analysis. Computer running ScalesNet32 is connected to both comparator and climate control system of the lab. This equipment allows LNMC to perform calibration of E1 class weights (most accurate ones).

Tab. 7. Mass comparators and balances in Department of mass measurement of State Agency

Mass comparators				
No.	Type	Manufacturer / Productions year	Calibrations weights	
1.	**CC 6**	"Sartorius" Germany, 2003	**E1 ;E2 ;F1 ;F2**	***1 mg ÷ 5 g***
2.	**CC 50**		**E1**	***500 mg ÷ 50 g***
			E2 ;F1 ;F2	***1 mg ÷ 50 g***
3.	**CC 1 000 S-L**		**E1 ;E2 ;F1**	***100 g ÷ 1 kg***
4.	**CC 10 000 U-L**		**E1 ;E2 ;F1**	***1 kg ÷ 10 kg***
5.	**CC 50 002**		**E2**	***20 kg ÷ 50 kg***
			F1	***10 kg ÷ 50 kg***
			F2	***5 kg ÷ 50 kg***
			M1	***1 kg ÷ 50 kg***
6.	**KC 600 sHR**	Mettler-Toledo", Sweden - MSE Systems, Germany, 2003	**M1**	***100 kg, 200 kg ÷ 500 kg***
7.	**CCS 3 000 K**	"Sartorius" Germany, 2006	**M1**	***2 t ÷ 3 t***
Balances				
No.	Type	Manufacturer / Productions year	Calibrations weights	
8.	**ВЛО-200g-Ia**	«Госметр», Russia, 1968		***50 g ÷ 200 g***
9.	**ВЛО-200g-I**	«Госметр», Russia, 1978		***50 g ÷ 200 g***
10.	**ВЛО-1kg-I**	«Прибор», Ukraine, 1988		***200 g ÷ 1 kg***
11.	**ВЛО-5kg-I**	«Госметр», Russia, 1975		***500 g ÷ 5 kg***
12.	**ВЛО-20kg-II**	"Etalon", Latvia, 1955		***5 kg ÷ 20 kg***

ScalesNet32 fulfils the requirement of a quality management system, regulated by national standards. Calibration of weights always relates to a project or a customer, serial number and type of the weights, and others essential parameters, creating a unique description of the test object. The weight date is saved in a database, assuring the avail-

ability of the weights history at all times. The balances used for testing user supplied weights are calibrated in pre-defined intervals. These calibration data is recorded in the database. ScalesNet32 controls the used reference weights and climate stations with a set of connected sensors. The software will inform the user of *necessary routine* calibrations of the reference weights used for testing. The calibration intervals for the balances and reference weights are entered into the system by the user. The following modules are available: calibration of customer weights; external calibration of customer weights; calibration of reference weights; calibration of weights with dissemination of mass scale; quick calibration of weights; calibration of weights with row data output; manual input of weighing data; calibration of Balance; Collection of environment data.

Most important features of Scales Net

- Centralized SQL Database to record all measurements and data;
- Auto-read of process data via a Balance-port. Port parameter can be configured according to the specifications of the scales manufacturer;
- Automatic measurement of the labs environmental parameters during weighing cycles;
- Adjustment of weighing cycles and measurement profiles (ABBA or ABA) in classes;
- Selection of classes according to OIML R111, ASTIM 617, or other national standards;
- Simultaneous testing of weights, belonging to one set of weights, using different Comparators in a Laboratory environment;
- Plausibility test for reference weights and balance (testing if selection of weights and balance matches pre-defined classes);
- Each tested weight is provided with a test certificate, recording all test results (reference weights and balance used, temperature, humidity, air pressure, etc.);
- Optional history report for each tested weight;
- User definable Word templates to create calibration and/or test protocols, or DKD protocols. Data to be represented will be positioned via text markers within the word document. During printing the text markers will be replaced by the actual measurement data. DKD protocols can be generated in 2 languages;
- Automatic inventory generation, listing all used balances reference weights.

External System Hardware

- **Scales-Controller**
  Microprocessor controlled terminal to perform all necessary steps of the calibration procedures for weights and test equipment. Connectivity to the ScalesNet32 database is provided via CAN bus.
- **Climate Station**
  Collects all environment data of the laboratory. During a measurement cycle the environment data will be delivered and combined with the actual weighing data. A data logger-converter is needed to convert the environment data into a ScalesNet32 readable format. If a third party system is used instead.

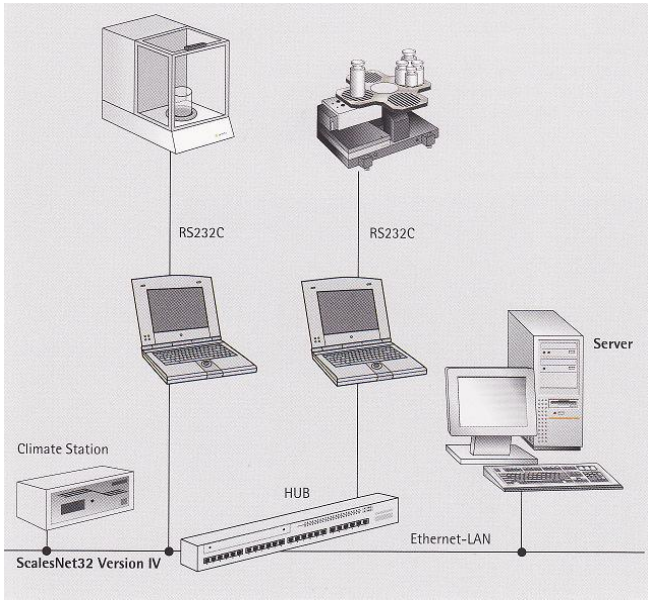

Fig. 3. ScalesNet32

2.4. Mass comparators

Mass determinations of the highest accuracy are carried out with mass comparators. These are used in laboratories high up in the hierarchy of the dissemination of the unit of mass, starting with the international prototype of the kilogram. In particular, the International Bureau of Weights and Measures (BIPM) in Sevres near Paris and the national metrological institutes (NMI) which generally have the national prototypes at their disposal belong to this hierarchy. Mass comparators are based on the compensation principle. This means that the weight force is largely balanced by force acting in the opposite direction. The range of the balance's display is therefore limited, and corresponds to the remaining difference of the weight forces. Only mass standards of the highest quality are used on such balances. Most comparators are based on the principle of the beam balance, where the weight force of a mass standard is compensated by the weight force of a counter weight via a lever. A comparator that works on the hydrostatic weighing principle has been realised, the compensation being effected by the buoyancy in a liquid. In the older beam ba-lances, the knife-edges and bearing blocks form pivots, and in more recent models it is the flexure-strip. Some of these mass comparators were developed in the laboratories of national metrological institutes, and others in workshops with many years experience in the construction of balances. Today, comparators are industrially manufactured that have a standard deviation of up to 10^{-9}. The best comparators in NMI reach up to 5×10^{-12}.

Fig. 4 shows the characteristic quantities of a beam balance in a general two dimensional representation. The axes of rotation are reduced to pivots i.e. assumed to be parallel. The beam's bearing is at point S'; the weight force of its mass m_S acts at its centre of gravity S. The masses m_L and m_G hang at points L and G. The broken line represents the gravitational horizon; the line connecting L and G forms an angle α with the horizon and is divided by the perpendicu-

larly through S' with the length α into the sections l_L, l_G; the lever arm of the balance's centre of gravity with a length l_S forms an angle γ with α. In equilibrium, the torqueses are neutralised. With the gravitational accelerations g_L, g_G and g_S, in the three gravitational centres of the masses, the following is valid:

$$\begin{aligned} 0 = {} & g_L m_L \left[l_L \cos\alpha - \alpha \sin\alpha \right] + \\ & g_G m_G \left[l_G \cos(\pi + \alpha) + \alpha \sin(\pi + \alpha) \right] + \\ & g_S m_S l_S \sin(\gamma - \alpha) \end{aligned} \tag{17}$$

In the following it is assumed that $g = g_L = g_G = g_S$. A change in the mass m_L by dm_L causes an inclination of the beam by $d\alpha$; the *sensitivity* of the balance is therefore defined according to E_q. (17) as follows:

$$\begin{aligned} d\alpha / dm_L = {} & (l_L \cos\alpha - \alpha \sin\alpha) / \\ & (m_L \left[l_L \sin\alpha + \alpha \cos\alpha \right] + \\ & m_G \left[l_G \sin(\pi + \alpha) - \alpha \cos(\pi + \alpha) \right] + \\ & m_S l_S \cos(\gamma - \alpha)) \end{aligned} \tag{18}$$

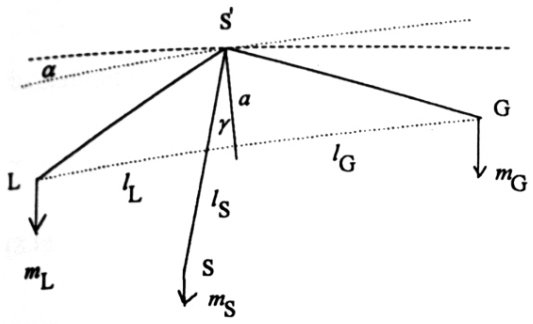

Fig. 4. Beam balance (schematic). S, S' gravitational centre or pivot of the beam; m_S mass of the beam; L, G pivots of the suspensions for the load with a mass m_L and the weights with the mass m_G; a distance between S' and the connecting line LG: l_L, l_G lever lengths of the load and weight arms projected on to LG; l_S lever length of the balance's centre of gravity; α angle of beam's inclination; γ angle between l_S and α.

According to Eq. (18) the balance's sensitivity depends generally on all the parameters.

Case I: $\alpha = 0$ (horizontal position)

$$0 = m_L l_L - m_G l_G + m_S l_S \sin\gamma \tag{19}$$

or:

$$0 = \frac{m_L}{m_G}\frac{l_L}{l_G} - 1 + \frac{m_S}{m_G}\frac{l_S}{l_G}\sin\gamma \tag{20}$$

and

$$\frac{d\alpha}{dm_L} = \frac{l_L}{(m_L + m_G)\alpha + m_S l_S \cos\gamma} \tag{21}$$

From Eq. (20) it is apparent that a change in the arm length ratios l_L/l_G is inversely proportional to the mass ratios m_L/ m_G.

Case II: $\alpha = 0$ and $l = l_L = l_G$ (equal arm lengths):

$$0 = (m_L - m_G) / l + m_S l_S \sin\gamma \tag{22}$$

$$\frac{d\alpha}{dm_L} = \frac{1}{(m_L + m_G)\alpha + m_S l_S \cos\gamma} \tag{23}$$

The sensitivity now depends only on the load $m_L + m_G$ and one the angle γ of the position of the level arm's centre of gravity.

Case III: $\alpha = 0$, $l_L = l_G - l$; and $\gamma = 0$ (symmetrical balance)

$$m_L = m_G = m \tag{24}$$

$$\frac{d\alpha}{dm_L} = \frac{1}{2m\alpha + m_S l_S} \tag{25}$$

The beam of a symmetrical balance is horizontal only if masses m_L and m_G are equal. If the shape of the beam is also symmetrical the centre knife-edge and the two suspensions mounted on the side knife-edges are the same in form and mass, the balance is not sensitive to changes in air pressure and the relative air moisture. However, the sensitivity still depends on the mass m of the load body (see Eq. (25)). This means that if the side knife-edges are lower than the centre one ($\alpha > 0$), the sensitivity decreases with increasing load; if they are higher ($\alpha > 0$), and then the sensitivity increases with the load up to an α where the balance becomes unstable, that is when $2ma + m_S l_S \leq 0$.

Case IV: $\alpha = 0$, $l = l_L = l_G$, $\gamma = 0$ and $\alpha = 0$ (pivots on one level);

$$\frac{d\alpha}{dm_L} = \frac{1}{m_S l_S} \tag{26}$$

In this case the sensitivity is independent of load, depending only on the mass and the position of the centre of gravity.

3. CONCLUSION

The results achieved by National Agency of Metrology are quite acceptable as national standard. Drift and error values are well within requirements for E1 class. The equipment and procedures used by the laboratory allow most accurate and perfectly traceable measurements. Most customers only need F2 or M1. However, some of them require calibration of E1 weights (for example, pharmaceutical industry). The laboratory can satisfy all their needs, at the same time remaining small and effective organisation. This is very important for such a small country like Latvia.

At present, all standards used by the laboratory are being sent for calibration to other laboratories such as DFM

(see Fig. 1). In theory, it is possible to have direct traceability to international mass standard. Directly traceable laboratory could provide metrological services to the most demanding customers such as national metrology organizations of other countries and research institutions. However, further improvement is needed to become international laboratory like this. From purely technical point of view, overall design of the building and location of the laboratory must be reconsidered. In urban areas, moving masses (trucks etc.) and ground vibrations may influence results of highly accurate mass measurements. The laboratory should be moved outside the city. The building must be designed with maximum stability in mind.

REFERENCES

1. **Kochsiek M., Gläser M.** (1984), Comprehensive Mass metrology, Mass Comparators, Physikalisch-Technische Bundesanstalt, Braunschweig, Germany.
2. International Recommendation OIML R 111-1 Edition 2004 (E), Weights of Classes E1, E2, F1, F2, M1, M1-2, M2, M2-3 and M3, Part 1: Metrological and technical requirements, International Organization of Legal Metrology, Paris, 2004.
3. Premium Accuracy for Weighing and Mass Comparison, Publication W—1064-e04116, Sartorius mechatronics, http://www.dataweigh.com/.
4. The Latvian law “On uniformity of measurements” ("Par mērījumu vienotību"), initial edition 27 February 1997, current edition 21 July 2006.
5. Traceability of Measurements, ILAC–G2:1994, International Laboratory Accreditation Cooperation (ILAC), 1996.

APPLICABILITY ESTIMATION OF A LOW-COST HAPTIC DEVICE FOR THE PURPOSE OF STEERING THE MOBILE PLATFORM

Roman Z. KACPRZAK*

*Institute of Automatic Control, Technical University of Lodz, ul. Stefanowskiego 18/22, 90-924 Łódź, Poland

rzkacp@wpk.p.lodz.pl

Abstract: In this paper a concept of using an easily accessible (i.e. commercially available for common home user) model of enhanced user interface – Haptic Device – for purpose of steering a mobile platform is presented. The functional requirements for the investigated device are specified based upon literature sources and verified empirically by author by performing real-time experiments in Matlab\Simulink.

1. INTRODUCTION

Haptic User Interfaces stand for a group of devices that opposed to standard user interfaces, take advantage of the human body's sensation of touch by means of mechanical signal generation. Depending on the type of receptors, which are sensory elements, one differentiates tactile and kinesthetic sensations. The tactile sensations refer to receptors located in the skin and they can be recorded with pressure or vibration functions. The kinesthetic sensations that are often described as force sensations can be felt with muscles and tendons. The main control issue that arises in this context is a sensorimotor control comprising the frequency with which the stimuli are sensed and the rapidity with which humans can respond. This paper will focus mainly on applicability of an example of a low-cost haptic device for the purpose of steering the mobile robot. Due to cost reduction, such of-the-shelf device possesses the limited mechanical and computing capacity of force stimulation that effects generation of solely kinesthetic stimuli. Hence, the presented low-cost haptic device is often also called a force-feedback device.

The main feature of haptic devices that distinguishes them from the standard user interfaces is utilization of an active and bidirectional information channel. It enables a force-feedback loop implementation (see Fig. 1) where the signals of motion commands flow from the user in the remote slave plant direction (light arrows) and simultaneously the force signals acting on the remote robot are transferred back to the user (dark arrows). In this approach the perception block of sensory-motor control is extended in addition to the vision element over the kinesthesia and tactility. The force-feedback loop adaptation changes the information exchange process into a live and intensive interactive workflow.

In this paper, first the Mobile Platform Haptic System and its major subsystems are presented. Next, several functional requirements for selected model of Haptic Device are specified based upon literature sources and verified empirically by performing experiments in Matlab\Simulink. This programming environment, which is rich in many powerful tools, enables the user to run simulation application in real-time in common Windows OS. It facilitates as well communication with peripheral equipment with the aid of a Simulink block which relieves the user from burden of device driver programming. The assumption about an application execution in real-time is critical in reference to control the Mobile Platform Haptic System according to automatic control theory engineering. Finally, the experiment results are compared with the previously outlined functional requirements and conclusions are drawn.

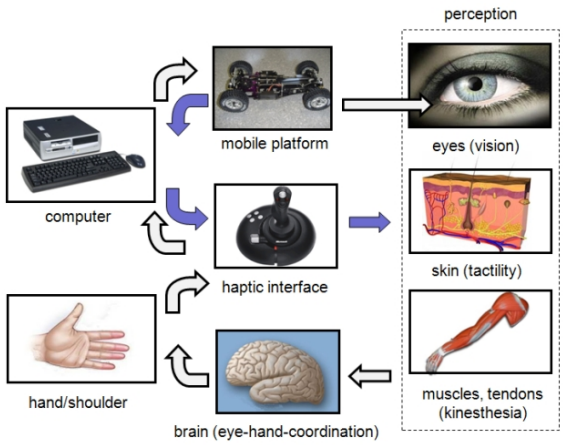

Fig. 1. The extended (over tactility and kinesthesia) sensory-motor control loop with an adapted haptic device, computer and mobile platform (the dark arrows stand for force signals that are fed back to operator perception block)

As subject of this article refers mainly to low-cost haptic device all references to or all sentences containing phrases haptic device, haptic user interface or low-cost haptic device will be used next, except as otherwise stated, in the sense of the low-cost force-feedback (kinesthetic) joystick. In this article only general information referring differences between distinct models of haptic user interfaces are mentioned. In case of additional interest it will be

asked the reader to consult the previous author's documents (Kacprzak and Bartoszewicz, 2007; 2005) where in the introductory part a comprehensive information concerning the history, the structure and the principles of operation of haptic user interfaces are presented.

2. MOBILE PLATFORM HAPTIC SYSTEM (MPHS)

The MPHS frame, in general, is composed of three main hardware subsystems: the low-cost haptic user interface, the mobile platform and desktop computer. The simplistic control architecture of the MPHS is presented in Fig. 2. The blocks placed on the dimmed background are controllable (outward-positioned arrowhead) or readable (inward positioned arrowhead) elements. The two blocks marked with bold frame are the controller which will be mentioned in later sections. The control blocks are user accessible which means that they can be freely programmed.

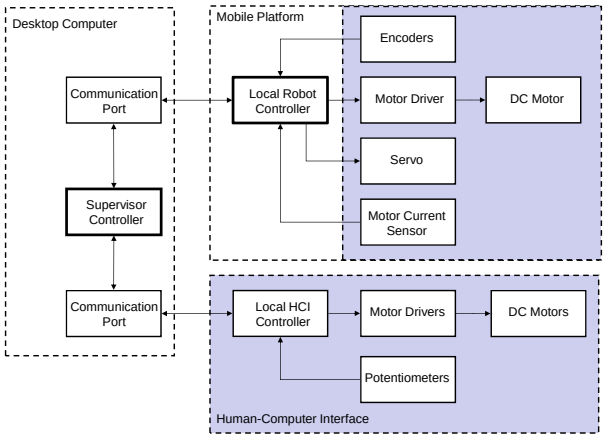

Fig. 2. Generic control system architecture

3. MOBILE PLATFORM (MP)

For the mobile robot construction partially ready-made elements were used placing more attention to electronic architecture set-up and hardware programming issues than to robot mechanics. For the mobile platform base a gear-belt and electric-drive car-like chassis (scale 1:10) were adapted with a few modifications related to chassis equipment (e.g. encoders attached, front axle mechanism modification, etc.). The main component of the mobile platform is the MB-128-MAX module with an embedded 8-bit Atmega128 microcontroller clocked with a 16 MHz crystal oscillator. This mini-module serves as the central processing unit and due to the real-time triggered interrupts can be used for Local Robot Controller (LRC) implementation. Currently, simple proportional controller is in operation. Given that more complex control unit should be applied as the LRC and the restricted sampling rate is kept, a need arises to add an upper hardware layer (e.g. an additional motherboard with embedded processor) where the controller will be located. The peripheral features (e.g. USART, TWI, external RAM interface) of MB-128-MAX build-in microcontroller enable control loop realization with data reading from encoders and motor current sensor, and command writing to a motor driver and a front axle servo. The local control loop is utilized with a sample rate of 100Hz. This sampling rate was assigned empirically with regard to hardware capability without signal parameters identification in compliance with the Nyquist–Shannon–Kotelnikov theorem. Therefore, some further investigation may be necessary to avoid aliasing and for perfect signal reconstruction (e.g. applying digital or analog anti-aliasing filter). Nevertheless, a sample rate of 100Hz was estimated as multiplicity of the value of joystick (10-30Hz) and kinesthetic system (20-30Hz) bandwidth.

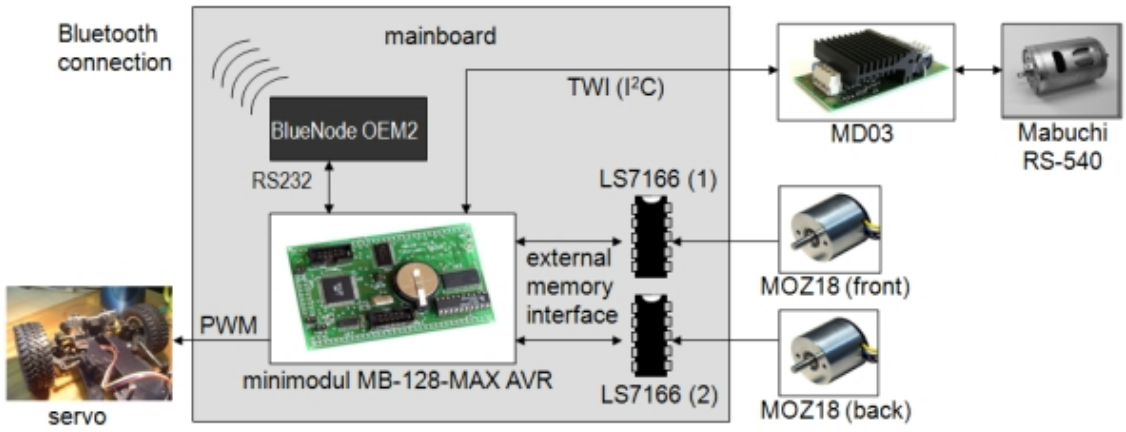

Fig. 3. The electronic architecture of the mobile platform

The electronic architecture of the mobile platform is illustrated in Fig. 3 and it consists of the following modules:

- credit card-sized circuit board – MB-128-MAX AVR module;
- DC motor driver MD03 for cart speed control;
- DC motor Mabuchi RS-540;
- servo-steering mechanism Hitec HS-475HB;
- Bluetooth module BlueNode OEM2 for wireless data link;
- two incremental encoders MOZ18 with dedicated LS7166 integrated circuits.

The MD03 motor driver enables both writing the desired velocity value and reading the ongoing electric current value from the memory registers. The computation of the covered distance is performed indirectly using the LS7166 counters that count the falling and rising signal edges from encoders output channels. The direction of motion of the mobile robot can be determined by means of a servo-steering mechanism Hitec HS-475HB. It is mounted on the front of the robot and connected through special links to the front axle with the purpose of adjusting the steering angle. The 8-bit inner counter of the Atmega128 microcontroller generating PWM signal is used to control the Hitec servo.

4. HAPTIC USER INTERFACE (HUI)

For the mobile platform motion control a low-cost haptic device was chosen (see Fig. 4). Such devices are commonly used with computer games or just as input devices to interact with operation system. In order to set the velocity, turn and direction commands a common force-feedback joystick can be utilized. This example of user interface has two force degrees of freedom that means its actuators (DC motors) are able to provide force sensations in two directions. The low cost of force-feedback joysticks introduces some constraints in the mechanics and computing power that refer mainly to frequency and value of generated forces as well as to the resolution of the position determination. On the other hand, some design constraints could be established for the system given the limits of performance of the human cutaneous sensory system.

In order to assess the efficiency of a low-cost force-feedback joystick in presenting force stimulation to the human wrist, several functional requirements for the device will be defined, then common features of an arbitrary force-feedback device taken from technical literature will be conveyed. Thereafter, selected model the SideWinder 2 Force Feedback Joystick from Microsoft will be evaluated during tests in Matlab/Simulink environment. After all, the test results will be compared with the previously outlined fun-ctional requirements.

Fig. 4. Examples of low-cost hapitc devices: the Microsoft SideWinder and Logitech Wingman force-feedback joysticks (from the left) and the internal view on electric actuators

5. DESKTOP COMPUTER

The idea of using a desktop computer as a hardware platform and Windows OS for a supervisory controller was imposed by programming requirement of the force-feedback joystick and partially by benefits of using the Matlab/Simulink tools in analysis and evaluation process. The Real-Time Workshop with an additional toolbox the Real-Time Windows Target enables through the use of two Simulink blocks: the Analog Input Block and the Analog Output Block in external mode, the user-friendly programming of force-feedback joysticks and ensures communication with them in real-time.

6. THE HUMAN CUTANEOUS SENSORY SYSTEM

In the beginning, it is reasonable to point out which joints of the human arm take part in actuation of a joystick handgrip (see Fig. 5). For simplicity, it can be assumed that only forearm and wrist are affected provided that forearm is at standstill. In general, the cutaneous senses are served by the somatosensory system, which includes tactile perception which is caused by mechanical displacement of the skin, proprioception, the sense of position of the limbs and kinesthesis, the sense of movement of the limbs. In the case of a low-cost force feedback joystick only a few sensations connected with the somatosensory system are significant due to device limitations.

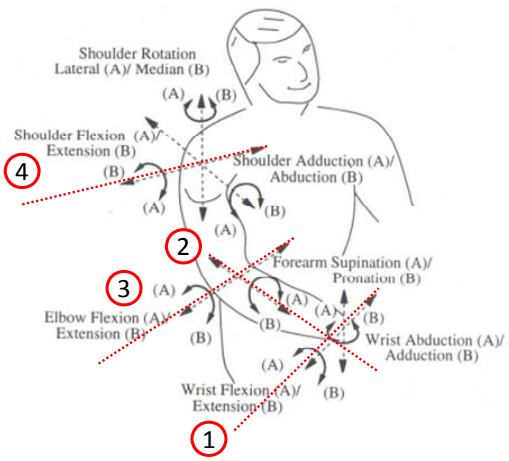

Fig. 5. Human arm degrees of freedom with joints marked that take part in joystick handgrip movements: 1–wrist flexion/extension, 2–forearm supination/pronation, 3–elbow flexion/extension, 4–shoulder flexion/extension (Caldwell et al., 1995).

Among several types of touch receptors located in the skin (see Fig. 6) the Ruffini's endings can be constrained. The receptor endings and nerve fibers associated with them define the type of stimulation to which they respond. The Ruffini cylinder's fibers are slow-adapting (SAII) nerve fibers which means they produce a regular discharge rate for a steady load (they continue responding as long as the stimulus continues). Psychophysically, the Ruffini's endings respond to frequencies ranging from 0-10 Hz after (Burdea and Coiffet, 2003) and less than 8 Hz after (Wall and Harwin, 2001)) and their stimulation results in the perception of stretch (detect stretching of skin or movements of joints and corresponds to static force function).

Regarding proprioception and kinesthesia, the state of muscles and joints and position of the limbs is monitored by two major kinds of receptors (apart from receptors located at skeletal articulations): muscle spindles, which lie in parallel with the muscle fibers, and Golgi tendon organs, which lie in series with muscles where one end is attached to tendon and the other to muscle, presented in Fig. 7a. The muscle receptors activity referring to their excitation is shown in Fig. 7b,c,d corresponding to the states of: muscle relaxed, muscle stretched and muscle contracted, respectively. The muscle stretching activates special muscle spindles and transiently Golgi tendon organs whereas the muscle shortening during contraction activates tendon organs.

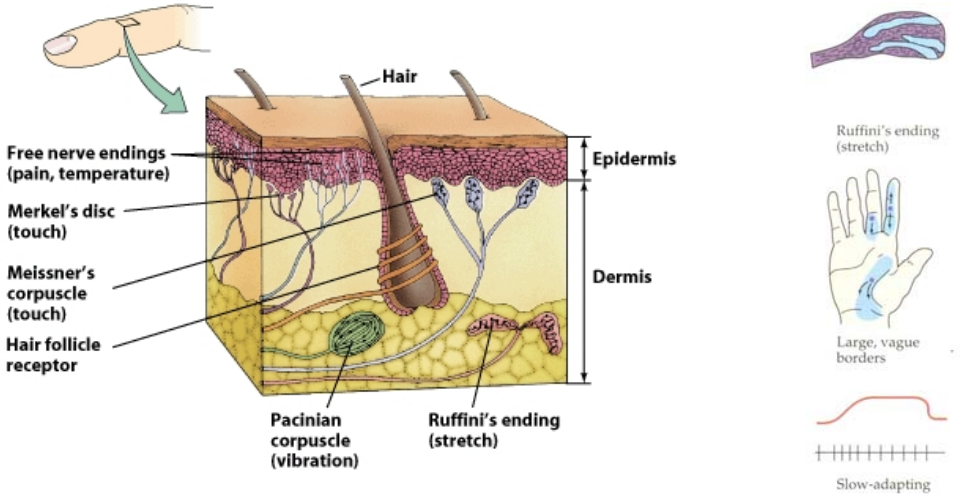

Fig. 6. A cross section of the skin, showing the location of receptors (left) and Ruffini's cylinders in the palm as skin receptors detect skin stretching or joint movement (right) (Rosenzweig et al., 2002)

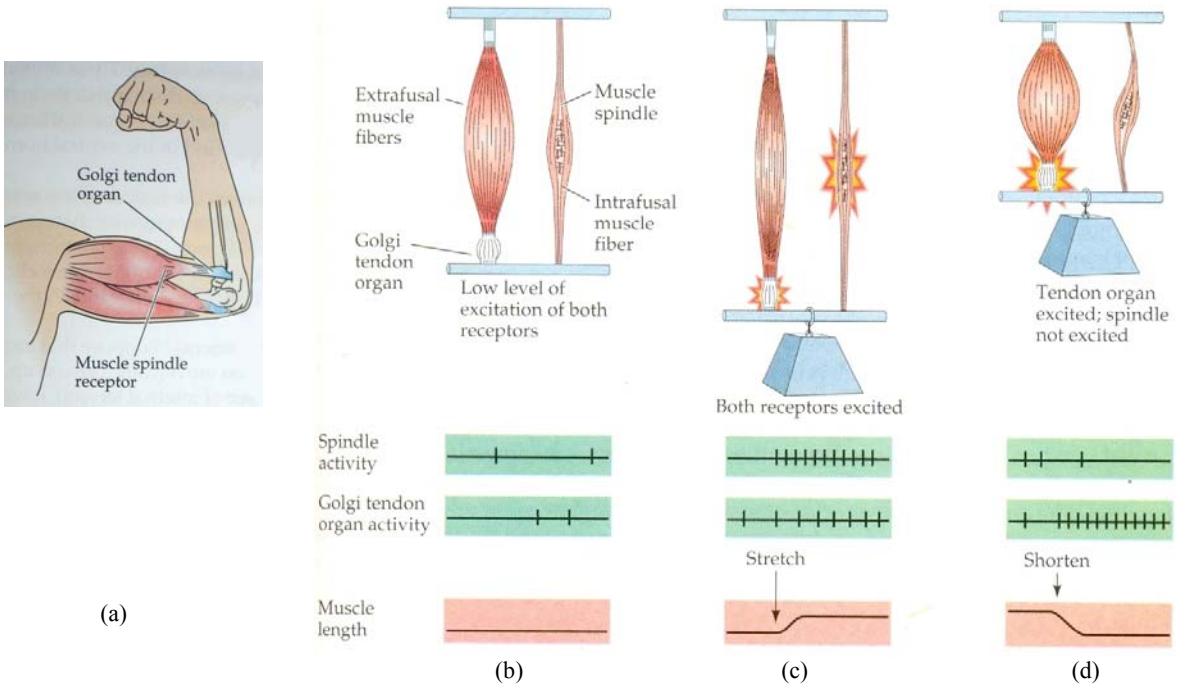

Fig. 7. Muscle Receptors: a) muscle spindles and Golgi tendon organs, b) muscle relaxed, c) muscle stretched, d) muscle contracted (Rosenzweig et al., 2002)

7. FUNCTIONAL REQUIREMENTS

Concluding the above information regarding the cuta-neous sensory system, the first important functional features *the sensory and motor bandwidths* of an investigated device can be noted. The bandwidths of sensory-motor control loop are: *the sensing bandwidth* that refers to the frequency with which stimuli are sensed and *the control bandwidth* that refers to rapidity of human responses. Both bandwidths are asymmetric as humans sense stimuli much faster than can respond to them (see Fig. 8 left). A typical maximum frequency with which a human hand can move a grasped joystick hand grip is 5-10 Hz whereas reliable force signals have to be submitted backward with frequencies not less than 20-30 Hz. The bandwidth requirements depend upon the nature of the task and can be selected upon the scale in Fig. 8 right.

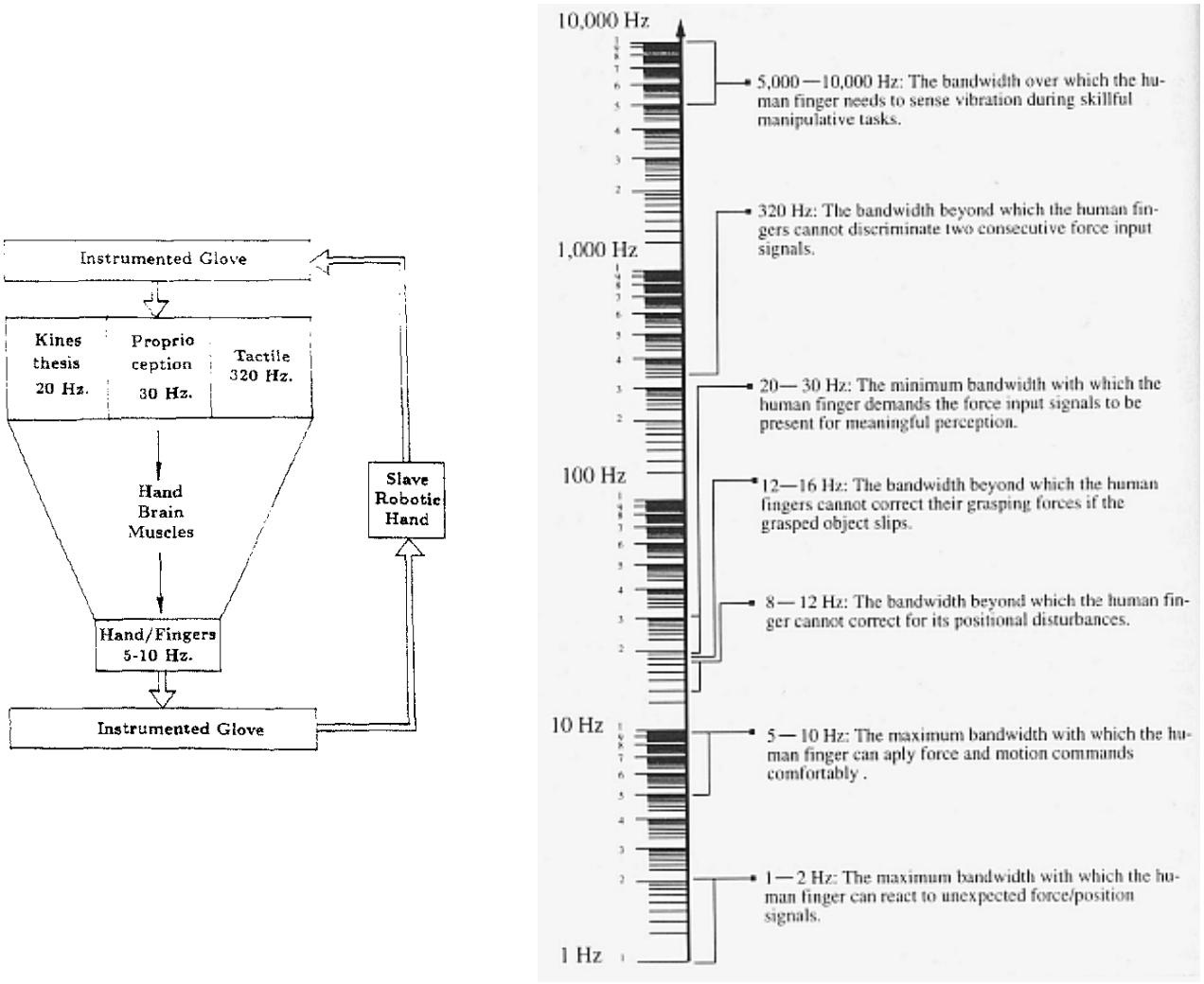

Fig. 8. The asymmetric capabilities of sensory-motor control loop of the human hand (left) and the range of bandwidths for different tasks (right) (Shimoga, 1993)

Continuing the consideration of functional requirements of simple force-feedback devices the issues regarding interaction forces exerted on the human arm will be addressed. In this context, the critical factors are *the maximum magnitude of force stimuli* and *their resolution*. The human arm should be able to sustain the exerted forces as well as to discriminate between significantly different stimuli.

Taking into account the problem of maximum force exertion the results of previous works found in An et al., (1986) can be adapted. The maximum power grasping force for males equals to 400 N and for females equals to 228 N. These results are not relevant assuming that human can apply the maximum force only for short period of time due to muscle fatigue. Looking on the Table 1 the difference in sustained opposite to maximum force magnitude can be seen. After the result of much research (Wiker at al., 1989) it has been discovered that the value of controllable force sensation belongs to the range of 15-25% of the maximum exerted force. Hence, for the purpose of a low-cost force-feedback joystick it can be assumed that the magnitude of forces for wrist joint should be in order of 7.5-12N.

In order to quantify the intensity of kinesthetic sensation several factors defined in the literature can be used for. The first is so-called *absolute threshold*, where the term absolute threshold stand for the minimal energy of touch that can be recorded by body receptors. Second one corresponds

to spatiotemporal resolution where the size of receptive fields are assumed. Next one is called *Weber ratio* or *the differential limen* (DL) or *the just-noticeable-difference* (JND), defined as the quotient of the just-detectable intensity increment or decrement over a baseline intensity that already exists.

Tab. 1. Average Maximum Controllable Force in the Arm (data from An et al., 1986)

Joint	Subjects		
	Female	Male #1	Male #2
Wrist	35.5 N	64.3 N	55.5 N
Elbow	49.1 N	98.4 N	78.0 N
Shoulder (side)	68.7 N	101.5 N	102.3 N
Shoulder (front)	87.2 N	101.6 N	101.7 N

The last one of presented here after mpb-technologies.ca/mpbt/haptics/hand_controllers/freedom/resources/Human%20Factors.pdf, as well-defined one, will be used next for haptic device evaluation. It defines the ability to distinguish a difference in force and is called the force resolution. Its value is around 10% of the reference force depending on task nature. Hence, for mobile robot executing task where 5N of force is needed (due to constrained output of the mobile robot), the operator should be able to detect 0.5N difference in force. This requirement is defined in reference to inner friction forces of the haptic device itself, that should be imperceptible for a human operator. In case the friction forces of joystick handle are higher than the force resolution ratio, the user will not be able to distinguish the desired force from the friction.

The ability to detect a change in position differs in each joint: the wrist and elbow can detect 2º and shoulder 0.8º (Tan et al., 1994). Assuming a palm length (clenched on the joystick handgrip) of 10 cm and , the position resolution of the hand controller needs an accuracy of (100*mm*) x tan(1°) = 1.75 *mm*.

8. THE HARDWARE FEATURES

After the constraints of human perception system have been shown, in this section attention will be focused on the hardware features with their limitations referring to generation of force stimuli.

Let us then start with the bandwidth of the sensory-motor control loop. The main issue in this aspect is the answer to the questions: how often can the force data be written to and the position data be read from the device and how fast can the device process force data itself? To solve the problem the hardware and software issues are considered.

First, we will look at hardware structure and more particularly at the mechanical assembly of a low-cost force-feedback joystick (see Fig. 9). Its main principle of operation is based on the usage of two separate DC-motors (numbers 1 for x and 2 for y axis respectively) for each axis that are coupled to the joystick control handle via various mechanisms. This enables the motors to provide the desired forces to joystick handle by means of producing on the motor shaft proportional torques. Simultaneously, the position of the joystick handgrip is determined by electro-mechanical or optical position sensors placed along a motion axes X and Y and coupled to drive shafts.

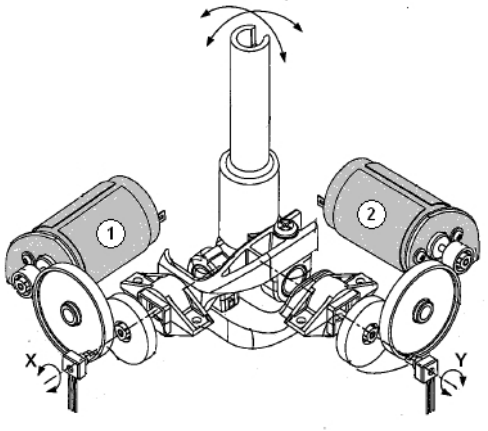

Fig. 9. The isometric view of a motorized quarter-gimbal mechanism that is used in a haptic feedback joystick (Patent International Publication Number: WO 01/65328 A1)

An important invention of force-feedback input/output devices of the prior is the usage of a separate microprocessor local to the interface device that is separate from the one of host computer system. The additional microprocessor implements a local force-feedback loop containing low-level commands (i.e. the force commands to actuators determined in accordance with local microprocessor force routine, sensor data and high-level host commands) independently from host computer microprocessor updating software application, e.g. game or simulation software. It relieves the host system of computational burden; conserves significant processing time of the host processor; provides an optimal utilization of the relatively low-bandwidth interface due to the fact that only the high-level force commands (i.e. general information referring force effect) and sensor data are transmitted over it. This finally allows more realistic and accurate force sensation to be provided to the control handle of force feedback device and be perceived by human arm.

The performance of sensory-motor control or simply a haptic loop depends strongly on software, particularly on the software application running in a particular operating system as on the operating system structure itself. The software running on microprocessor local to the haptic device generally has a significant impact on whole haptic loop. In the case of high fidelity haptic devices (specialized and expensive devices not just simple kinesthetic devices, that provide full haptic sensation) this part of a sensory-motor control loop would be considered separately. Nevertheless, low-cost haptic devices are provided of-the-shelf with an embedded microprocessor that runs quasi real-time software. Sometimes the vendors provide the ability to program haptic devices but it is often limited to upload some force effects that has no effect on the control issues of the haptic loop. As the local to interface device haptic loop cannot be affected by the user it will not be discussed in this paper.

For further considerations it will be assumed that the force-feedback joystick runs under Windows XP OS and the API (application programming interface) functions of DirectX libraries are used for wrapping of low-level driver commands.

As Windows XP OS is not any kind of real-time operating system (either soft or hard RTOS) the joystick input/output operation times may vary with the OS load. Therefore, in order to assure all operations are most likely time-invariant (i.e. they are independent on operating system response time and occurring time lags in processor allocation) the investigation of software characteristics and identification of haptic loop parameters was performed in a Matlab\Simulink programming environment. Two toolboxes were selected: the Real-Time Workshop and the Real-Time Windows Target. They appear to be the most useful as they match the criteria of running the simulation in real time under arbitrary Windows OS.

In addition, it is proper to assume, that the Windows OS is running on hardware that is optimal for Matlab\Simulink environment, i.e. the hardware does not impose any additional constraints on system performance. Then, if most system resources are available, i.e. no additional background work is performed, the programming environment of Matlab\Simulink can constrain the communication rate with haptic device exclusively, which will be explained further. In the case that enormous system load is present the communication loop is affected and the communication bandwidth will be constrained in addition.

9. EXPERIMENTS

To fulfill all of the mentioned above requirements a desktop PC was prepared with the intension to install only a pure Windows XP operating system with Matlab\ Simulink software exclusively.

As one can read in the Matlab tutorial in the chapter 'RTWT\Features\Real-Time Kernel' the standard Win32 API calls are incompatible with the RTW kernel. It is generally true but joystick and mouse drivers are exceptions that use special mechanisms which allows them to pass data from the Win32 layer to the kernel without breaking the real-time constraints. The communication between kernel and joystick is done asynchronously to the sampling rate of Simulink model, using a separate Win32 thread. This thread awakes periodically and sends the joystick coordinates to the kernel, while at the same time it retrieves force-feedback values from the kernel. This is entirely independent of any sampling period the kernel processes may run at. The sampling rate of the joystick communication is dependent on the particular joystick model. The software producer of the RTWT the Humusoft company states that it is usually in the range up to 100Hz. The Simulink model sampling rate can be significantly higher, up to 1kHz.

The approach the RTWT kernel uses for I/O joystick operations is possible only with human interface devices as no human being is able to react in the order of milliseconds. Due to this assumption the software producer concludes that the millisecond delays caused by the Win32 thread do not have any effect. This approach is intended for joysticks and mouse explicitly and is not useful with data acquisition boards which drivers have a true real-time code that accesses their devices directly from kernel.

The Win32 thread communicates with joystick by means of DirextX interface. As this programming interface is not real-time by design the Real-Time Windows Target does the data exchange process in such a way that the Win32 thread does not slow down the real-time operation of the RTWT kernel. This means that the RTWT kernel places a request to DirectX but does not wait for the request to be completed and similarly, it asks DirectX for the joystick position data but if DirectX does not respond in time, the data is taken in next sample. The Simulink model uses only the last joystick position value that the Win32 thread returns, and only the last force-feedback value passed on to the Win32 thread is applied, so no joystick commands are lost.

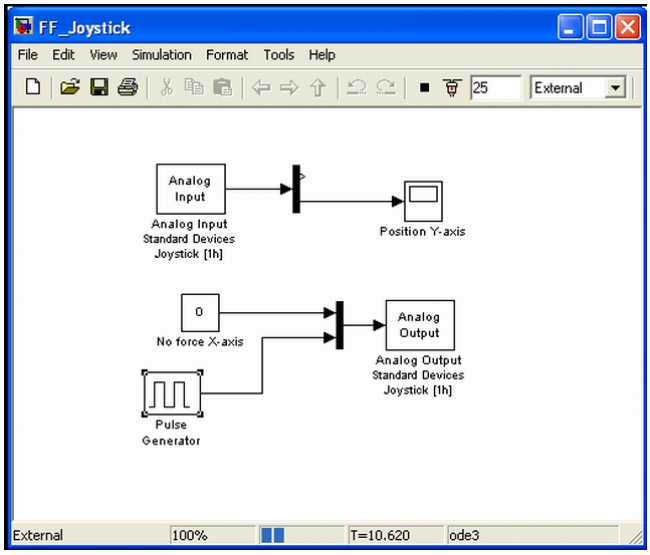

Fig. 10. The Simulink model with the Real-Time Windows Target blocks

The research methods used during tests:

1. An extension of capabilities of Simulink and Matlab: The Real-Time Workshop was used. In addition, for compilation of Simulink model the Real-Time Windows Target was chosen as option in 'Real-Time Workshop\System Target File' section of 'Simulation\ Configuration Parameters' (rtwin.tlc). In 'Solver Options' section following values was typed: 'Fixed-step' in Type field and 0.01 in 'Fixed-step size' field. The Simulink model consists mainly of two following blocks (see Fig. 10): 'Analog Input' and 'Analog Output' with 'Standard Devices Joystick [1h]' as current board, a value 0.01 in 'Sample Time' field, a vector '[1 2]' in Input Channels field and '-1 to 1 V' in 'Input\Output Range' field what limits the joystick input\output signals values to the range [-1,1]. In consequence, to run the created model the external mode in main model menu was selected.
2. For the purpose of determination of a single position (along one axis) sample time the test was performed where the human operator was trying to move the joystick handle as fast as possible.

3. For the purpose of determination of a position resolution (along one axis) the test was performed where the human operator was asked to move the joystick handle as precisely as possible. At the beginning, the maximal deflection of joystick handgrip in both direction along one axis was measured with a ruler for further calibration and determination of the magnitude of position threshold in millimeters.
4. For the purpose of determination of a maximal force that can be generated by joystick actuator along one axis the digital force measurement device CNR ST 100 (see Fig. 11) which can measure the forces up to 100N with resolution of 0.01N was used.
5. For the purpose of determination of a force resolution of force stimuli generated by joystick actuator the test series were performed where a force signal from 'Pulse Generator' Simulink block was provided to the joystick handgrip held by human operator. In subsequent tests the generated force value was increased over 0.25N.

Fig. 11. The digital force measurement device CNR ST 100 from ANDILOG

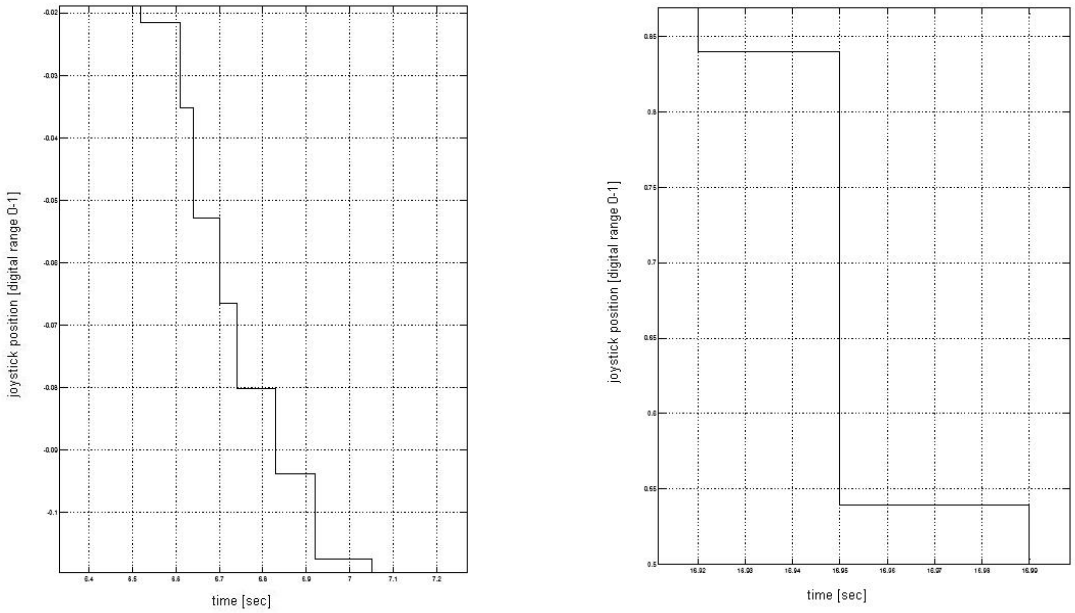

Fig. 12. Determination of joystick parameters regarding position: sampling rate and resolution (performed in Simulink RTWT) during Fast (left) and slow (right) movements of joystick handle with human operator hand

Force resolution was determined during other test separately where 50g weight (and subsequently its multiplication) was attached to unhanded (released) joystick handgrip with the aid of a thin thread rested on the horizontal rod. The weight due to gravity exerts a equivalent force pulling the joystick handgrip upwards.

The test results provided (see also Table 2):

– the time duration for the acquisition of a single position sample ranges between 30ms and 100ms (see time axes on Fig. 12);
– the position resolution of joystick handle equals approximately 0.2mm (see ordinate axes on Fig. 12);
– the maximum force that can be applied by inner motor of the joystick along single axis equals approximately 5N
– the force resolution (the force threshold value) that was found empirically equals 1N.

The arguments for determining the force threshold follow: first, the friction forces of joystick actuator mechanisms were assessed to be in the range of 0-1N. Hence, the desired difference of 0.5N in force is imperceptible for the human arm. Second, even though the force variation of 0.5N can be digitally recorded (see Fig. 13) such small force effects joystick movement that magnitude is less than position resolution (less than 0.2mm). In conclusion, the user is not able to distinguish the kinesthetic stimuli from a friction of joystick actuator mechanisms that are less than 1N.

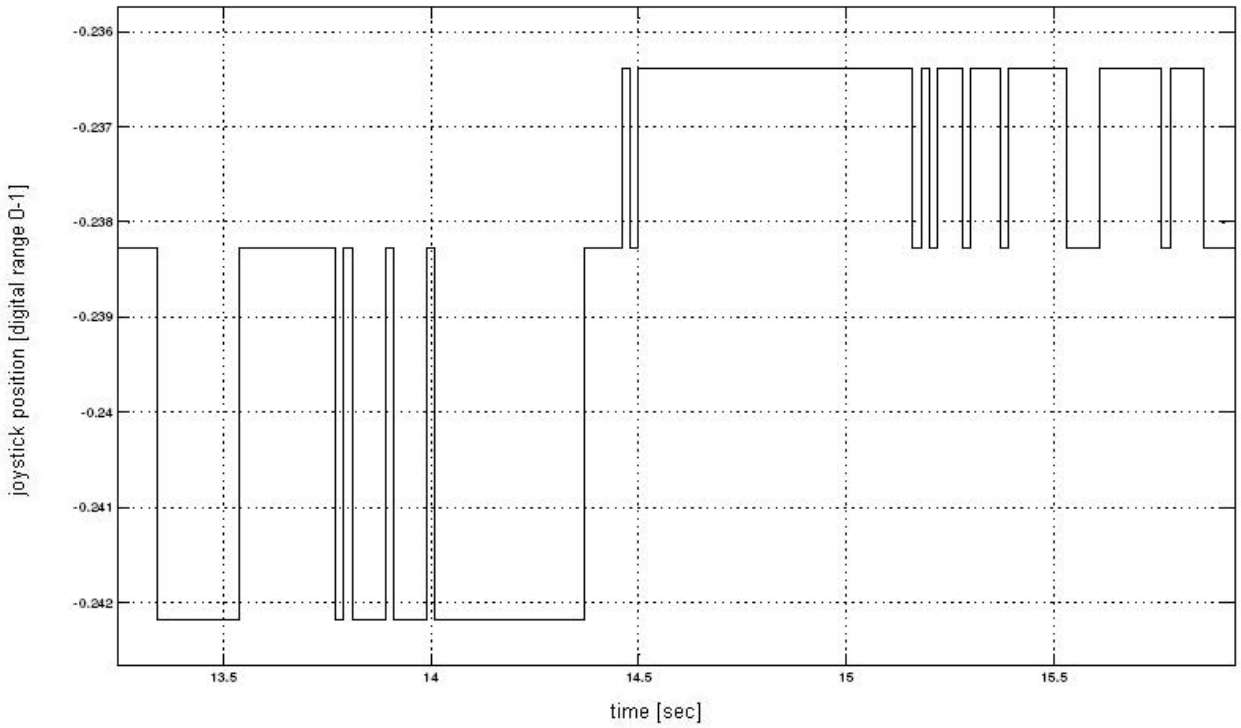

Fig. 13. Freely joystick movements (no human operator hand interference) in arbitrary axis induced by force variations of 0.5N (performer in Simulink RTWT)

Tab. 2. Test results – comparison of the design functional requirements and joystick parameters estimated in experiments in Matlab/Simulink environment

	Functional requirements	Experimental results
bandwidth of sensory-motor control loop	20-30Hz (sensory) 5Hz (motor)	10-30Hz (for both)
max. magnitude of force stimuli	7.5-12N	5N
force threshold	10% of the reference force	1N
position resolution	1.75mm	0.2mm

10. SUMMARY

The main goal of joystick parameters assessment and their comparison with the desired (that were described as functional requirements) was the estimation of applicability of low-cost force-feedback joystick for the purpose of steering the mobile platform in real-time without significant time delays. As it was explained at the beginning, due to the cost reduction such devices were addressed mainly to the undiscriminating home user that utilize force-feedback devices in computer games. Beyond the doubt, the joysticks have been designed properly to meet the conditions of force stimuli generation required to truly simulate the game activities. This assumption is still weak and insufficient in order to state about reasonableness of using the low-cost haptic device for mobile robot steering. As the manufacturers provide only general information referring device specification and no comprehensive information concerning psychophysical features and physiology of touch is public available, the author decided to perform self-designed test of particular low-cost force-feedback joystick. As the references the functional requirements defined well in literature were assigned.

Finally, the test results are combined with the functional requirements specified previously. The estimated parameters of the joystick device are (as it can be seen in Table 2) close to reference values. Two of them, the magnitude of motor control bandwidth and the accuracy of position resolution match the target value where the latter even exceed it greatly. The Joystick parameters considering the force stimuli differ from the reference. The maximum force that can be provided to the human wrist is a half of the for wrist desired value (5N instead of average 10N), the same as the small perceptible difference in force (1 instead of 0.5N) that corresponds to the maximum magnitude of 5N reference force i.e. the force value needed to accomplish some task in environment of the mobile robot. If we assume that the maximum reference force is 10N then the desired force resolution calculated as 10% of reference force will be 1N. This magnitude matches functional requirements and experimental results and hence, it is acceptable to an operator of the mobile robot. The assumption allows the user to feel stimuli with low sufficient difference of 1N in force but simultaneously constrains the ability of perception to upper value of 5N. That means the user will be not able to feel all forces larger than 5N acting in remote environment of the mobile robot.

Joystick parameters according to performance of the motor-control loop were assessed using a Matlab\Simulink programming environment, here there is a need for coupling both subsystems of the MPHS i.e. the Mobile Platform and Haptic User Interface together. The former approach (Wiker et al., 1989) achieved by the author

without com-pliance of real-time aspects provided much information about system nature but didn't meet demands according automatic control engineering. Therefore, further test of the MPHS in Matlab\Simulink utilizing the Real-Time Windows Target toolbox are going to be performed.

REFERENCES

1. **An K. N., Askew L., Chao E.** (1986), Trends in Ergonomics/Human Factors III, *Biomechanics and Functional Assessment of Upper Extremities*, Elsevier, 573-580.
2. **Burdea G. C., Coiffet P.** (2003), *Virtual reality technology* – 2nd ed., A Wiley-Interscience publication, U.S., 94.
3. **Caldwell, D. G. et al.** (1995), Control of pneumatic muscle actuators, *Control Systems Magazine*, IEEE, Vol. 15, Issue 1, 40-48.
4. **Kacprzak R. Z., Bartoszewicz A.** (2005), Interfejsy haptyczne – wzbogacona forma komunikacji człowieka z komputerem, *Proceedings of XIII Conference on Networks and Computer Systems*, 653-662.
5. **Kacprzak R. Z., Bartoszewicz A.** (2007), Mobile Platform Control with Haptic Interface – Hardware and Software Issues, *Computer Applications in Electrical Engineering*, Electrical Engineering Committee of PAN, Poznań University of Technology.
6. **Rosenzweig M. R. et al.** (2002), *Biological Psychology*, 3rd ed., Sinauer Associates, Inc.
7. **Shimoga K. B.** (1993), A Survey of Perceptual Feedback Issues in Dexterous Telemanipulation: Part I. Finger Force Feedback, *Virtual Reality Annual International Symposium*, IEEE, 263-270.
8. **Tan H. et al.** (1994), *Proceedings of ASME WAM*, DSC-Vol. 55-1, ASME, New York, 353-360.
9. **Wall S. A., Harwin W.** (2001), A high badwidth interface for haptic human computer interaction, *Mechatronics*, Vol. 11, 371-387.
10. **Wiker S., Hershkowitz E., Zik J.** (1989), *Proceedings of NASA Conf. on Space Telerobotics*, Vol. 1, 99-107.
11. Patent International Publication Number: WO 01/65328 A1, International Publication Date: 07.09.2001, Applicant: Microsoft Corporation, Patent Title: Haptic Feedback Joystick.
12. mpb-technologies.ca/mpbt/haptics/hand_controllers/freedom/resources/Human%20Factors.pdf

The author is a grant holder of "Mechanizm WIDDOK" project supported by European Social Fund and Polish State (contract number Z/2.10/II/2.6/04/05/U/2/06).

COMPUTER MODELING OF THE CHARACTERISTICS AND MAGNETIC FIELD OF SINGLE - PHASE COMMUTATOR MOTOR

Bronius KARALIUNAS*

*Department of Automation, Vilnius Gediminas Technical University, Naugarduko str. 41, Vilnius LT-03227, Lithuania

Bronius.karaliunas@el.vgtu.lt

Abstract: The article presents some calculation results of dynamic characteristics of the single – phase series – excited commutator motors and magnetic field analysis.
Single – phase commutator motors in up – to – date literature are called universal motors, because they can be used in both alternating current (AC) and direct current (DC) systems. The single – phase AC small power commutator motors are widely used in different vacuum cleaners, electric tools, drives of household, electrical, medical and hygienic equipments and portable electrical hand tools. However, the principal defect of those motors is worse commutation with sparkling between brushes and the collector, and high enough level of radio interferences on wide frequency range.
In this article obtained expressions compounds the mathematical model of the single – phase series – excited commutator motor. The model of the dynamic processes of the motor and its block diagram are compiled according to the differential equations which were derived from the equations of voltage balance. The software of Matlab/Simulink is applied here which has integrated the methods of the solution of differential equations for the motor.
For modeling the magnetic field of a AC series – excited commutator motor there was used the software JMAG. The program is complied by means of finite elements, by attaching on the computer separate geometric figures their titles and character-ristics. Since the magnetic field in the air gap between the salient poles and armature is not homogeneous, so the density
of the grid has to be the highest. The obtained results of modeling describe a very complicated structure of a magnetic field of a commutator motor for the analysis of which are required new and comparatively accurate mathematical models.

1. INTRODUCTION

In manually operated devices, where high velocities of (20 – 40) thousands r/min and a comparatively small masses are required, there are applied universal commutator motors. These motors are mostly applied as single – phase alternating current (AC) in series – excited motors. However, motors themselves as well as manual tools and devices with commutator drives not always comply with modern requirements in the field of electromagnetic compatibility, environmental protection and radio interferences reduction. Moreover, there are problems in relation with the application of electronic digital control systems, application of control and braking systems for commutator drives. From that point of view, the investigation of the following issues, namely the magnetic field of commutator motors, calculation of their characteristics, optimization of the design as well as reduction of radio interferences are considered to be very relevant issues for analysis.

Recently, there have appear scientific works dealing with the analysis of the problems concerning the theory of commutator type electric motors and their practical application. In the author's presented list of literature (Puternicki, 2000, based on the achievements of modern technologies, there have been solved very significant problems of automatized designing, structure optimization and synthesis as well as search for an optimal version of low capacity commutator motors. The long – lasting experience of the author is summoned here concerning the designing, manufacturing, experimental research of such motors.

In article (Karaliunas, 2005) there are presented the findings on the magnetic field of single – phase commutator motors in order to achieve the reduction of the intensity of radio interferences caused by such motors. The methodo-logy for calculating the characteristics of alternating current (AC) commutator motors is submitted in article A group
of authors in their report (Jack et al., 2000) analyse the magnetic system of a salient pole stator of universal motor, in which the poles tips is manufactured from a special material – Somaloy 550. The authors state that in this case the manufacture of the magnetic circuits of the motor is simpler and cheaper. In article (Tuncay et al., 2001) there are presented the results of modelling characteristics of universal motors with different capacities. The authors presents the patterns of distribution of the magnetic flux lines in the magnetic system of the motor and the diagrams of dynamic characteristics. It is not possible to install the usual measures of commutation improvement such as additional poles and the windings of compensation in the low capacity commutator motors due to space shortage. That is why the decisive influence on the commutation processes of the current, the intensity of sparking and the intensity of radio interferences in such motors make the specific type of disturbance appearing in the air gap of the magnetic

field. The mentioned above issues have not received the required attention in the scientific literature so far. That is why the purpose of the work is to investigate the magnetic field
of the single – phase series excited commutator motors and to analyze their dynamic characteristics.

2. THE MAIN EQUATIONS AND THE BLOCK DIAGRAM

When simulating, there are applied the differential equations of the exciting circuit and armature circuit, derived from the equations of voltage balance. In the mentioned above equations there are evaluated the mutual inductance of both the circuits and the excitation currents as well as the change of armature current at the moment of starting the motor. For the excitation circuit it is possible to write the following:

$$u_e = i_e r_e + L_e \frac{di_e}{dt} + M_{ea} \frac{di_a}{dt}; \quad (1)$$

where u_e, i_e, r_e – is the voltage of the series excitation winding, the current and active resistance; L_e– is the self – inductance of series excitation winding; M_{ea}– is the mutual inductance of series excitation winding and armature winding; i_a– is the armature winding current.

The following equation is received for the armature circuit:

$$u_a = i_a r_a - \omega i_a L_{a1} + L_{a2} \frac{di_a}{dt} + \omega i_e M_{ea1} + M_{ea2} \frac{di_e}{dt}; \quad (2)$$

where u_a, r_a– is the voltage of armature winding and active resistance; ω – is the angular velocity of armature rotation; L_{a1} and L_{a2} – are self – inductances of parallel branches of armature winding.

The equations (1) and (2) are modelled together with the main equation of motion of commutator drive:

$$J \frac{d\omega}{dt} = T_e - \varepsilon\omega - T_l; \quad (3)$$

where J – is the torque of armature inertion; T_e– is electromagnetic torque of the motor; εω εω – is the component of the resistance torque due to the friction in the bearings and in the commutator brushes sliding contacts; T_l – is the load torque of the motor.

Electromagnetic torque of the single – phase commutator motor is proportional to the instantaneous power and could be calculated in the following way:

$$T_e = \frac{e_a(t) \times i(t)}{\omega}; \quad (4)$$

where $e_a(t)$ – is the instantaneous value of electromotive force induced in the armature winding.

Expression (4) indicates that the torque of the motor is generated not only by the rotational, but by the transformer armature electromotive force. Then after determining the expressions of electromotive forces and inserting them into (4), we derive that the electromagnetic torque consists of four components:

$$T_e = T_{rv} + T_{trv} + T_{rk} + T_{trk}; \quad (5)$$

where T_{rv} and T_{trv} – is the average components of the torque caused by the rotational and transformer electromotive forces; T_{rk} and T_{trk}– is the alternating components of the torque, which varies with double frequency of the network.

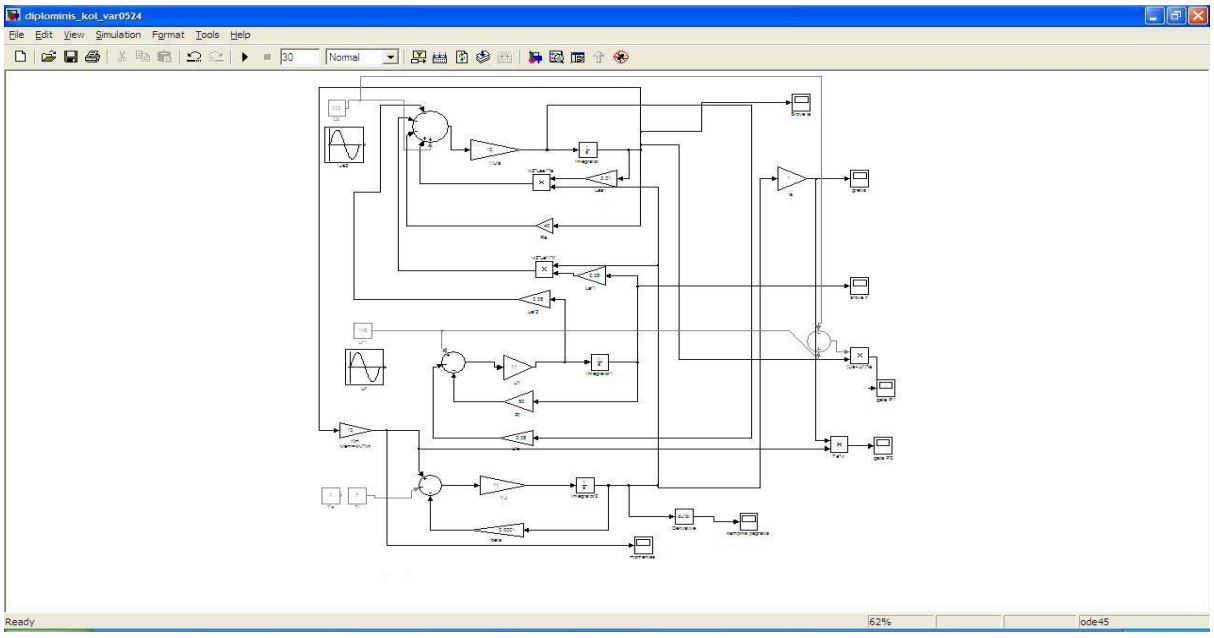

Fig. 1. Matlab/Simulink model of a single – phase commutator motor

For calculating the several components of the torque the following expressions were obtained:

$$T_{rv} = \frac{pN}{4\pi a}\Phi_m I_m \cos\gamma\cos\beta\,; \tag{6}$$

$$T_{trv} = \frac{w_a \omega_1}{2\pi\omega}\Phi_m I_m \sin\gamma\sin\beta\,; \tag{7}$$

$$T_{rk} = \frac{pN}{4\pi a}\Phi_m I_m \cos\gamma\cos(2\omega_1 t-\beta)\,; \tag{8}$$

$$T_{trk} = \frac{w_a \omega_1}{2\pi\omega}\Phi_m I_m \sin\gamma\sin(2\omega_1 t-\beta)\,; \tag{9}$$

where p – is the number of pairs poles of the motor; N – is the number of the armature conductors; a and w_a– are the numbers of parallel branches and coils of armature winding; I_m and Φ_m– is the amplitudes of excitation current and magnetic flux; γ – is the angle of bend of brushes sliding from the geometric neutrality; β – is the angle of motor losses; $\omega_1=2\pi f_1$ – is the angular frequency of excitation current.

Having the equations (1) – (3) and the expressions of torque (6) – (9) it is possible to get all the transver functions required for compiling the computer model. The software Matlab/Simulink is used, where the methods of differential equations solution are integrated there. Then in the Simulink desktop there are connected separate subsystems to form block diagram of which is presented in Fig. 1.

3. MAGNETIC FIELD MODELING

For modelling the magnetic field of a commutator motor there was applied the software JMAG. The software for modelling was compiled by the method of finite elements, when in the computer to the separate sectors of the magnetic system, there were attached their titles, characteristics and other parameters.

In Fig. 2 there is presented the finite element model of the magnetic circuit of the motor together with the inductor and the scheme for connecting both the armature windings and commutator.

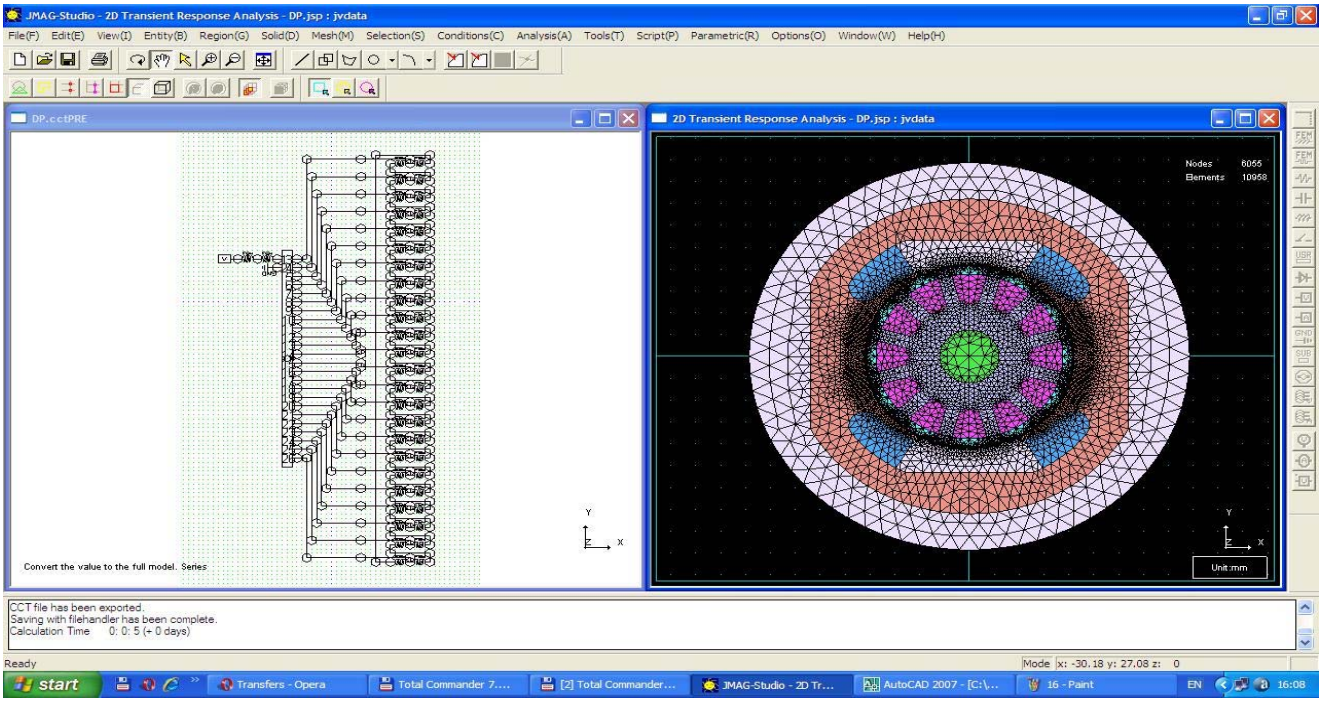

Fig. 2. The model of the magnetic system of commutator motor with the logical scheme of windings connecting

4. RESULTS OF MODELING

By using Matlab/Simulink model presented in Fig. 1, there were obtained the patterns of the velocity, acceleration, electromagnetic torque, currents and dynamic characteristics. The variation of the electromagnetic torque in time is presented in Fig. 3. Distribution of magnetic induction in the motor is presented in Fig. 4.

The results of modelling indicate, that the character of transitional processes of high speed single – phase commutator motors is similar to the transitional processes of the practically tested motors. Judging from the results presented in Fig. 4 the conclusion is derived stating that in the operating motor there appear the demagnetization effect of the reactions of an armature. Due to that the highest density of the magnetic flux is observed not at the poles of the excitation, but they are shifted by a certain angle from the longitudinal axis of the motor. That is why in non – reverse commutator motors the brushes have to be turned from the geometric neutrality by the same angle, namely from the cross – sectional axis of the motor. This measure allows increasing the coefficient of efficiency of a motor, to reduce the sparkling and the intensity of radio interferences.

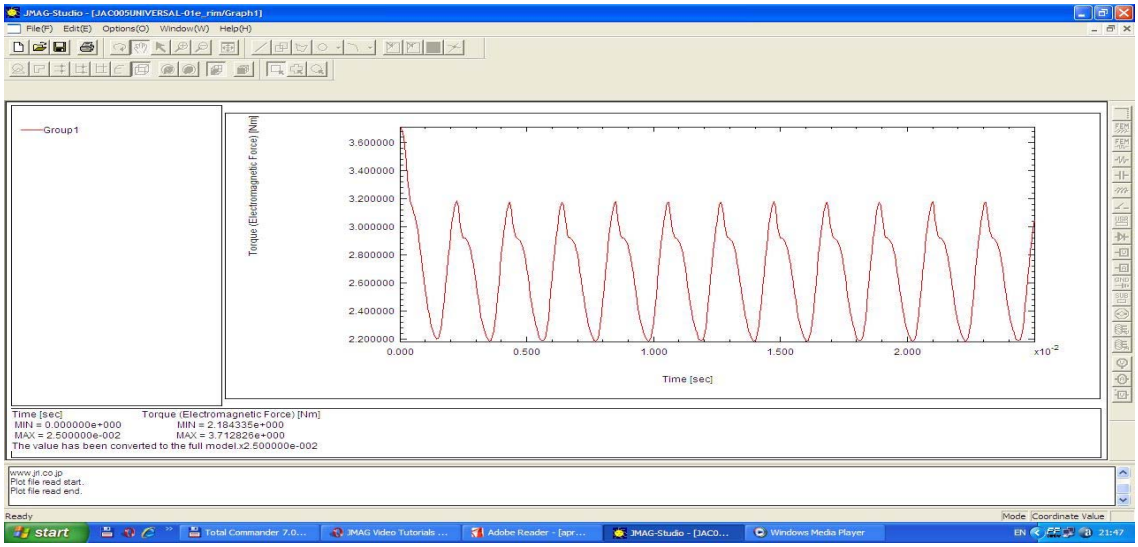

Fig. 3. Variation of electromagnetic torque in time

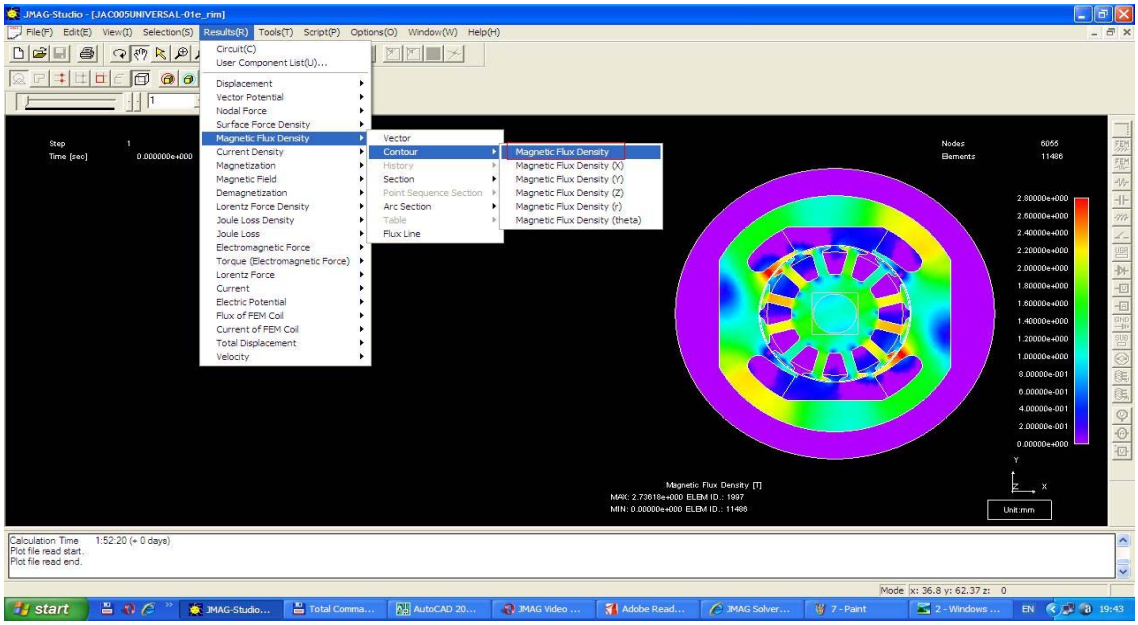

Fig. 4. Distribution of magnetic induction in a commutator motor

5. CONCLUSIONS

The new simulation model of transitional processes and dynamic characteristics is derived for a alternating current single – phase series excitation commutator motor.

The results of modeling indicate that the type of transitional processes of velocity, acceleration, torque and currents for low capacity single – phase commutator motors coincide with the results of the experimental research of the practically tested motors.

Modeling and calculation results of dynamic characteristics and magnetic field help to find constructive means which reduce transvese magnetic flux and intensity of the radio interferences. It is recommended to simetrize of magnetic circuit of the small power commutator motors and the elements of interferences reduction must be placed as close as possible to sparkling sources.

REFERENCES

1. **Jack A., Dickinson P., Mecrow B., Janson P., Haltman L.** (2000), **A** Scoping Study of Universal Motors with Soft Magnetic Composite Stators, *Proc. of Int. Conf. on Electrical Machines,* Vol. 2, Helsinki, Finland.
2. **Karaliūnas B.** (2005), Calculation of Characteristics of the Single –Phase Collector Motor, *Proc. of the XV Int. Conf. on Electromagnetic Disturbances, EMD'2005,* Technologija Kaunas – Bialystok.
3. **Puternicki P.** (2000), *Silniki komutatorowe malej mocy. Analiza i optimalna synteza konstrukcji,* Instytut Elektrotechniki, Warszawa.
4. **Tuncay R. N., Yilmaz M., Onculoglu C., Kanca G.** (2001), The Design Methodology to Develop New – Generation Universal – Motors for Vacuum Cleaners, http://www.ieeexplore.ieee.org/iel5.pdf.

THE 2 ½ D ALGORITHM IN ROBOT WORKSPACE ANALYSIS

Gabriel KOST*, Daniel RECLIK*

*Institute of Engineering Processes Automation and Integrated Manufacturing Systems,
Silesian Technical University, Gliwice, POLAND

gabriel.kost@polsl.pl, daniel.reclik@polsl.pl

Abstract: In this paper there is presented the method of 3D manipulator's workspace analysis. The analysis of robot's work-space is necessary for generation the safety movement path. There was 2 ½ D method, which is based on algorithm of following sections defining in robot work area. Those sections are explored by flat analysis, but the results are transposed into graph form. This graph is the record of all possible movements, so to get the optimum movement there must be used Floyd's algorithm. This, shortest trace is optimized and smoothed by using B-Spline curves.

1. INTRODUCTION

Preparing the production in technological way (1) includes a wide range of very important tasks, which are necessary to start a brand new or to modernize existent technological process. Those tasks refer to overall (general idea) and detailed development of technological process and structural solution (e.g. tools, machines, grips, etc.), as well. In most cases those problems are solved by using techniques of computer-aided the engineering work, which could be e.g. CAx systems (Chlebus, 2000). Generally, CAx systems fulfill all the requirements perfectly. However,
in particular way, the usability of individual subprograms of CAx systems are helpless and, even, useless, e.g. programs from CAD/CAM systems. Possibilities of programming the numerically controlled machine by using CAM systems meet the requirements of technological needs, but, in range of off-line robot programming the possibilities of using such a system are bounded. One of the main reasons, why those systems are helpless, is the necessity of having the correct robot workspace analysis, thanks to it, the production
engineering – programmer can generate the collision-less robot movement in its workspace.

2. PROBLEM OF THE COLLISION – FREE TRAJECTORY PLANNING

Despite the fact that there is a lot of methods which solve the problem, their practical application in this case is small and bounded. The main reason is computational complexity of existent method, which causes serious time-consumption of final solutions. Collision-free robot movement planning is a very complex matter – it consists of many parts, beginning with geometrical analysis of robot workspace and, at the end, collision-free motion steering task based on determined collision-free trajectory (Dulęba, 2001; Kost, 2004; Morecki, Knapczyk, 2001). Additionally, the time-consumption increases the necessity of dynamic modeling the collision-free trajectory with necessary changes of robot movement in its stationary workspace. Those modifications are caused by changes connected with technological activity, e.g. accessibility of selected areas of workspace, connected with necessity or impossibility of tool machine services, warehouse occupancy, grip exchange, etc. The motion planning methodology is shown on the on Fig. 1.

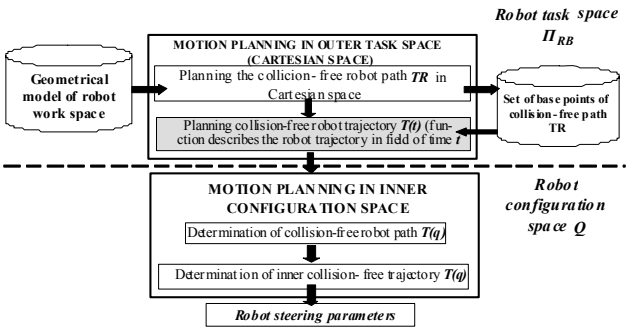

Fig. 1. Task stages of planing the collision-free robot motion: t-time, q – vector natural coordinates of robot

Those problems and difficulties are mainly because of geometrical complexity of robot workspace, which comes from the space configuration of the machines operated by the robot. Determination of collision-free robot movement and workspace analysis are a base, which makes possible the determination of searching collision-free trajectory between initial and final robot position. This subject was't solve enough to use it in off-line programming systems. In connection with it, there is no possibility to compare described method with others – because there is no such one.

1.1. Searching algorithm based on Floyd's method

The collision-free path, which was determined during planning process in robot workspace, is a base for next stage of planning – determining the equation of collision-less path in 3D workspace (collision-free trajectory). Determined collision-less path in 3D workspace defines the set of basis points, which determine the broken line w workspace. According to this broken line the robot should move from initial to final position. It definitely must be broken line equation in workspace, which fulfilled the continuity condition in following basis points and it also must fulfilled the smoothness conditions in geometrical sense. Those conditions fulfilled second degree curves; it means C2 curves with continuity acceleration. The curves can be determined by the method of interpolation the basis points set – third degree polynomials. Polynomials, which can be used in steering task, are (Demaine, 2002; Kozłowski, 2003; Fortuna, 1999): Bestsein-Bézier's polynomials, NURBS and B-Spline. The main problem in defining C2 curve is getting three-dimensional geometrical model, which comes from three-dimensional robot workspace. The authors propose to use 2 ½ D geometrical model, thanks to it there is possible to simplify basis points settling in planning task.

2. THE 2 ½ D METHOD FOUNDATION

In this paper the authors take the following foundation:

- Analyzed robot workspace is static and ordered, which is the main foundation in manipulators motions planning (Majchrzak,2004; Latombe, 1993),
- Data comes from geometrical analysis of robot scene by using octal analysis. The collision-free robot path is determined from the set, which is free from roadblocks,
- Dimensions of octants, which compose the path, are dynamically defined by using the dimensions of manipulating object (Kost, 2004; Dulęba, 2001; Latombe, 1993).

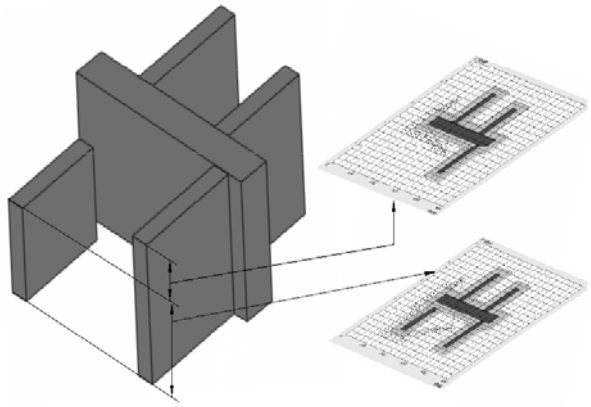

Fig. 2. Robot workspace with determined sections (after planar collision-less movement planning process)

In order to simplify the computational complexity of determining the collision-free robot path in three-dimensional space there was used 2 ½ D interpolating mechanism. In presented issue the 2½D method causes the implementation of 2D method with proper algorithm which controls the location of the analyzed plane in three-dimensional space (the place of making the proper section). Thanks to that simplification there is possible to use the mechanism of generating others sections in robot workspace, which together make a spatial shape of analyzed task. When one considers separately the received three-dimensional section planes, there is possible to analyze the collision-free path as 2D task. However, this could be possible, if one fulfills some conditions. The necessary condition is to model the machines which cooperate with robot. It is so important because those machines can cause the collision. Those machines must be model as a rectangular prism base of a square or, at least, rectangle. The most important thing in motion trajectory planning application is proper selection of following plane sections. It's worth seeing that over-richness of section number increases number of calculations. To provide the possibility of received robot path (optimal in its length) there is necessary to take into consideration all of the sections, which vary in number of crossed machines. Because, theoretically those machines have their own height, the simplest way of passing them by is to go up all those machines and pass them by in straight line. Sometimes it is impossible to go the robot bunch up on the proper height, that's way there must be fulfilled another condition – boundary condition of maximal height of robot bunch. Generating following scene sections for correct height range is accepted as a correct solution. To provide the motion safety there was necessary to define the protection area (Kost, 2004) round every machine in order to guarantee passing the roadblocks by in proper and safety way. The height sharing are made in turn from the back, it means the first range enclose the height from zero (plane of robot base) to the shortest machine tool (or its component), enlarged on the protection area. The next range encloses bigger height – from the shortest machine to another, bigger one, which is also enlarged on the protection area. Fol-lowing parts of the rest range are made in the same way (till the final height – the maximal motion height of robot bunch). Because all of the sections of robot scene are determined in the same way, the calculation complexity, presented in this method, depends on height diversification of the machine tools and the final height of robot bunch. Because the motion collision-free trajectory planning application determines the optimal basis points of movement length (it means the shortest way), therefore there must be the same motion path at a given range of height. Therefore the received information about safety path on the proper height (coordinates x, y, z of basis points) requires transformation of the standard points determined in sections. On Fig. 2 there is shown the principle of subprogram operation which generates the sections. In this example (Fig. 2), the analysis of robot scene topography with the condition of maximal height of robot bunch, shows the occurrence of two different height of machines, therefore as a result of method working there was received two sections

of robot scene (as it is shown on Fig. 2) with marked initial and final points of movement with x and y coordinates.

3. DIAGRAM OF COLLISION-FREE PATHWAY IN ROBOT WORKSPACE

To make possible the 2½D method application with the mechanism of section generating for determining three-dimensional curves of robot motion in its workspace there is necessary to generate a collision-free pathway diagram. This diagram consists of basis points of collision-less path, which are the input data in presented method. In the coordinates there is modified the Z value so that it allows having all basis points of the path placed in analyzed section on defined parting plane. The most important thing of the diagram creating stage is having the correct section for initial and final motion point. Obviously, those points can lay down on different heights; moreover, their height can be in different section range. Received, in this way, basis points can by linked as collision-free path diagram. In order to improve the complexity of taken analysis, additionally, there was decided to fulfill the diagram with additional basis points received on the way of following robot scene sections. It allows having more numerous set of basis points, thanks to what it was possible to lead the pathway optimization by the diagram from the point of the smoothness robot motion, the shortest way and the fastest robot movement from initial to final position. On the fig. 3 there is shown the generated diagram of collision-free pathway. It's worth seeing that the diagram tops are creating a middle of half-tone screen, which were used to generate the collision-free robot path (Kost, 2004; Morecki, 2001). On Fig. 3 there are marked points generated by made sections in blue color and additional points marked in red. Moreover, on the right there are presented results of working the 2D motion trajectory planning application for each section. Such prepared data cause that in the next stage there is pathway optimization by the diagram with using Floyd's method (Demaine, 2002; Rosen, 1991).

3.1. Searching algorithm based on Floyd's method

The algorithm, which was used to solve the problem of determining the optimal robot pathway in its workspace, calculates the importance edge sum which link directly or indirectly all of the diagram top pairs. To receive and remember, during calculations, the results there was necessary to create a matrix in n x n size (n means the number of diagram tops). The adjacency matrix (Demaine, 2002; Rosen, 1991) is a two-dimensional chart in n^2 size. Following rows and columns in this matrix are representing the diagram tops; however the value of crossing the i-row and j-column in adjacency matrix is an importance of edge linking the tops (Majchrzak, 2004).

To save the original value of edge importance there is necessary to define the second chart in the same size. It would be a working chart, where after finishing the calculations, one can find the final results. To make possible the replacement of following top sequences creating the pathway between tops, there is necessary to create one more chart - a predecessor matrix. This matrix is used to defining the possibilities of collision-free robot movement between particular points of pathway diagram. Such solution allows sorting analyzed basis points automatically. As an importance there is used true distance between points as follows:

$$K_{i,j} = \sqrt{\left(x_i - x_j\right)^2 + \left(y_i - y_j\right)^2 + \left(z_i - z_j\right)^2}, \quad (1)$$

where: x, y, z – are the following coordinates of trajectory basis points in pathway diagram.

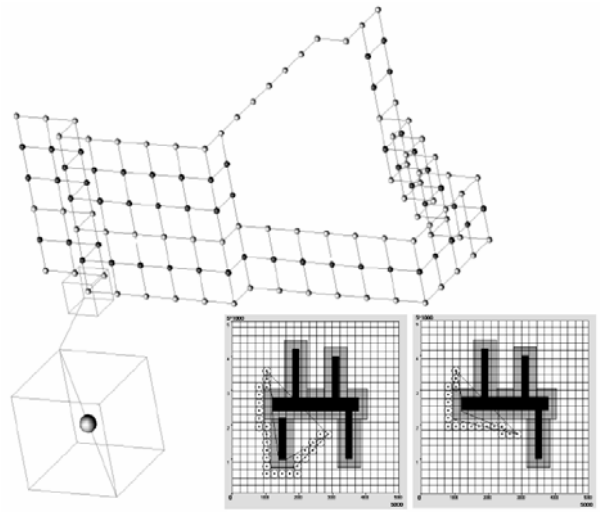

Fig. 3. Result of the section searching algorithm's working – safe trajectories movement graph

Floyd's algorithm operations in presented task one can define as it follows:

```
for k equal from 0 to n-1 do:
  {
  for i equal from 0 to n-1 do
    {
    for j equal from 0 to n-1 do
      {
      if there is a path between i and k and k and j do:
        {
        if there is not a path between i and j then take the movement
        length between I and j as a  path sum from I to k and k to j  if
        there is a path from I to j then take the movement length between
        I and j as path  minimal from I to k plus k to j or I to j
        update the pathway matrix – mark path from i to j as a path
        possible to overcome
        }
      }
    }
  }
```

The result of the algorithm working (Fig. 4) is determining the minimal length between each pair of diagram tops. Because above there was included the additional matrix, besides the value of the shortest movement length, one can find the pathway sequence of following diagram tops.

4. SOLUTION OPTIMIZATION OF PATHWAY DIAGRAM IN THREE-DIMENSIONAL SPACE

The applied method has to mineralize the calculation complexity, which is required to generate three-dimensional collision-free robot movement. There was necessary
to develop a suitable module which can change the number of received basis points made from pathway diagram. The assumption was that the final trajectory must be smooth in geometrical way, and also, there must be fulfilled the continuity condition of second derivative of the path function (C2 class). The authors used for realization the presented task (for interpolation the 2-and 3- dimensional curves) mainly B-spline and NURBS.

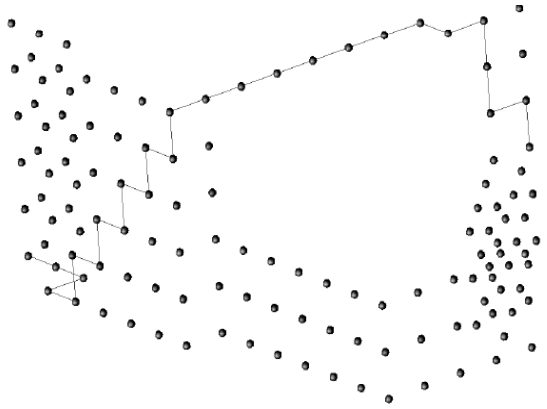

Fig. 4. Results of working the Floyd's algorithm

4.1. The algorithm of generation the interpolated curves

Interpolated curves, based on Berstein-Bézier polynomials, NURBS curves and B-spline, are composite functions. The base of generating those curves is basis function, which gives the proper shape of 3-dimentional curve with set parameters when it is suitable linking up. Because basic functions are defined by the time, therefore, one can found that, the curve, which comes from the junction, is also indirectly defined by the time. Therefore, to determine the interpolated curve of robot movement on collision-free trajectory, at first, there must be provided the total time of movement duration. This time (of movement duration) is indicate as base unit, it means that the movement lasts from 0 to 1 in time interval, that is from 0 to 100% of real time. Because the NURBS mathematical algorithm is very universal, therefore there is described the procedure of realization that algorithm (Dulęba, 2001; Majchrzak, 2004). It is necessary to determine the kinematic pair at first during creating the polynomial of flexible interpolated function. Because the movement on curve must last from 0 to 1, therefore the interval time from that range is interpolated kinematic pair. To accept the right number
of interpolated kinematic pair, there must be defined the degree of interpolated polynomial *n* and number of ordinary points of interpolation *Li*. Kinematic pair set can be passed mathematically in following way:

$$T = \{t_0, t_1, t_2, t_3, t_4, t_5, \ldots, t_k\}, \tag{2}$$

However, the number of kinematic pair *ti* must be equal to:

$$U = Li + n + 1, \tag{3}$$

To assign the right value of time from 0 to 1 there must be used the following procedure: the first *n*+1 of kinematic pair must be fulfilled by 0 and the last *n*+1 must be fulfilled by 1, however the remaining kinemaic pairs must be fulfilled proportionally by ascending time values. The set of interpolated kinematic pairs for curve of third degree and for seven basis points has been shown below:

$$T = \{\, 0, 0, 0, 0, 0.25, 0.5, 0.75, 1, 1, 1, 1 \,\}, \tag{4}$$

Having defined the kinematic pairs of interpolation (*T* points on time axis), it is possible to determine the basic function component of rational B-spline polynomial (NURBS). Defining the basic functions must be done iterative, because if one want to have determine the basic function of any degree, at first one must defined the basic function of lower degree. That's why; the whole process of defining the basic functions starts from determining the basic function of 0 degree, which is defining as follows: for set time interval are 1, while for others time interval are 0 as it shown below (Majchrzak, 2004):

$$Ni,0 = \begin{cases} 1 & \text{for moment t which belong to time interval among } t_i \text{ and } t_{i+1}, \\ 0 & \text{for other time } t \end{cases} \tag{5}$$

Having computed values of basic functions, there can be determined the points' coordinates of interpolated polynomial *X(t), Y(t), Z(t)* as superposition of values of particular cartesian coordinate system. In case of conventional B-spline polynomial, the values of coordinates are determined as product sum of basic functions and coordinate values of basis points P, in a way as it is shown on the next page in eq.6 (Dulęba, 2001; Fortuna, 1999).

$$\begin{aligned} X(t) &= \sum_j N_{j,m}(t) * Px_j \\ Y(t) &= \sum_j N_{j,m}(t) * Py_j \\ Z(t) &= \sum_j N_{j,m}(t) * Pz_j \end{aligned} \tag{6}$$

For determine the rational B-spline polynomial (NURBS) one must take into consideration the importance of the basic points *P*, which are indicate as *w*. Knowing the importance of basic points one can determine particular coordinates of interpolated polynomial by using below formulas (Majchrzak, 2004):

$$X(t)=\frac{\sum_j N_{j,m}(t)*Px_j*w_j}{\sum_j N_{j,m}(t)*w_j}$$

$$Y(t)=\frac{\sum_j N_{j,m}(t)*Py_j*w_j}{\sum_j N_{j,m}(t)*w_j}, \quad (7)$$

$$Z(t)=\frac{\sum_j N_{j,m}(t)*Pz_j*w_j}{\sum_j N_{j,m}(t)*w_j}$$

Enlarging the degree of the polynomial causes decreesing curve inflexion, what, in result, causes that the curve has softer rounding. For particular positions – base points P_i, which determine the robot planning trajectory related to its configuration space Q the simple and reverse cinematic task is solving in following stage (e.g. Moore-Penrose' method or weighted pseudo-inversion). For instance, using Moore-Penrose' method, you can verify, based on reverse robot cinematic model, the internal vector q_i for each base point P_i of collision-free planning robot trajectory. The most important requirement, which must be fulfilled is (Koch, 1996):

$$\dot{q}_i = J^{\#}(q_i)\cdot \dot{d}_i \,, \quad (8)$$

where: $J^{\#}(q_i)=J^{T_Q}(q_i)\cdot\left[J(q_i)\cdot J^{T_Q}(q_i)\right]^{-1}$ is a Moore-Penrose' pseudo-inversion, $J(q_i)$ - Jacobian defined for Pi robot position in robot space expressed by q_i, $J^{T_Q}(q_i)$ - transposed Jacobian J in Q robot space, d_i -vector of position defined for P_i, $\dot{d}_i$ - time derivative of robot movement for P_i, $\dot{q}_i$ time derivative of q_i vector defined for P_i. Additionally, there must be fulfilled another condition, that the matrix of simple transformation T the kinematics of robot, transpose the robot configuration from tack space to inner space condition:

$$T_Q^{-1}: d_i(s) \rightarrow q_i = T_Q^{-1}(d_i), \quad (9)$$

$$d_i(s_i) \in \Pi_{RB}, \quad (10)$$

where: T_Q^{-1} - the matrix of cinematic reverse task transposition, Π_{RB} - The outer robot configuration space

5. RESULTS OF ALGORITHM WORKING

Because the optimization process of the spatial trajectory (for following reasons: used tools and worked out algorithms) has enormous computational complexity, it can be used for off-line robot programming. Findings are in NURBS curve shape, which can be digitize (it means that we can establish the number of generated points of the function). Likewise on the plane, the smooth process goes in iterative way with checking the calculation correctness (collision-free movement). Fig. 5 shows how the trajectory changes during calculations. Fig. 6 show generated and optimized robot trajectory in its workspace. There was marked safety area in half-transparent block. The dimensions of robot roadblocks (machines) are marked in blue color, while in red there was marked the collision-free robot path.

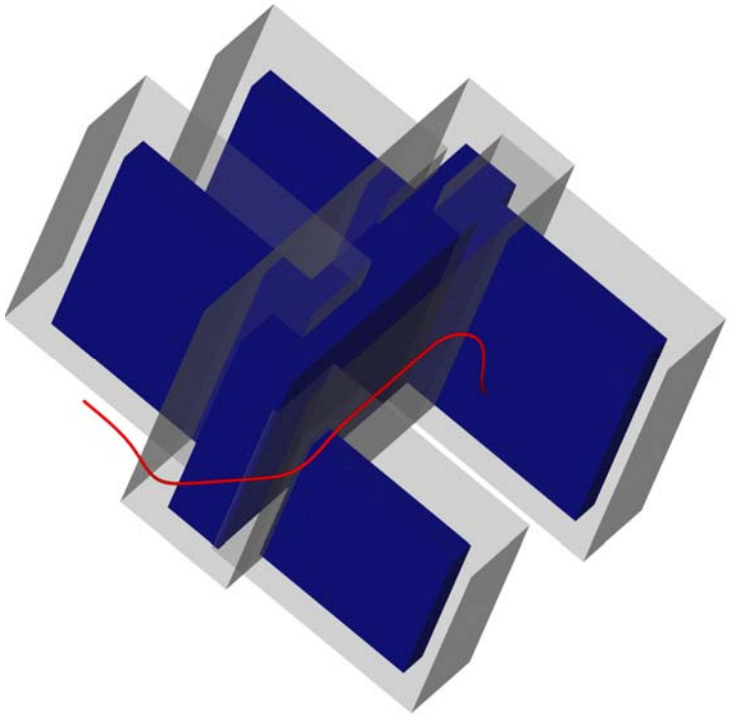

Fig. 6. View of robot scene with generated collision-free motion path with C2 smoothness

6. SUMMARY

Thanks to presented algorithmical solutions, there was received fully satisfactory spatial robot path, although the calculations were made as a two-dimensional problem, represented by the revert diagram. The system of searching collision-free robot trajectories, which is presented in this paper, has not been fully finished yet. This system is constantly developed; especially the authors are working on mechanism of 3D optimal searching the equation of robot's movement in its work space. In effect, the authors will prepare the fully functional system, based on B-spline, which can be added to one of off-line programming system of robot. Developed solution and its simplification by using 2½D algorithm allows to simplify and bound the number of calculations, which are needed to generating the equation of robot trajectory.

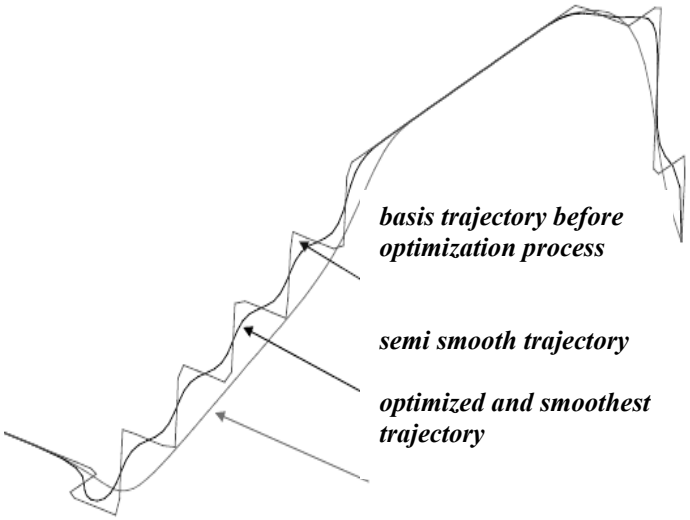

Fig. 5. View of following stages of motion smoothing in three-dimensional workspace

REFERENCES

1. **Chlebus E.** (2000): *Techniki komputerowe CAx w inżynierii produkcji,* WNT, Warszawa.
2. **Demaine E., Gweightwasser S.** (2002): *Introduction to Algorithms,* MIT.
3. **Dulęba I.** (2001): *Metody i algorytmu planowania ruchu robotów mobilnych i manipulacyjnych,* Akademicka Oficyna Wydawnicza EXIT, Warszawa.
4. **Fortuna Z., Macukow, B, Wąsowski J.** (1999): *Metody numeryczne. Podręczniki Akademickie. Elektronika. Informatyka. Telekomunikacja,* PWN, Warszawa.
5. **Koch T.** (1996): *Programowanie redundantnych robotów przemysłowych*. Prace Naukowe Instytutu Technologii Maszyn i Automatyzacji Politechniki Wrocławskiej, Oficyna Wydawnicza Politechniki Wrocławskiej, Wrocław.
6. **Kost G. G.** (2004): *Planowanie bezkolizyjnych ścieżek manipulacyjnych i stacjonarnych robotów przemysłowych oparte na procesach decyzyjnych Markowa i funkcji ocen*, Wydawnictwo Politechniki Śląskiej, Gliwice 2004.
7. **Kozłowski K, Dutkiewicz P., Wróblewski W.** (2003): *Modelowanie i sterowanie robotów,* PWN, Warszawa.
8. **Latombe J.C.** (1993): *Robot motion planning,* Kluwer Academic Publishers, Boston/London.
9. **Majchrzak E.,Mochnacki B.** (2004): *Metody numeryczne. Podstawy teoretyczne, aspekty praktyczne i algorytmy*, Wydawnictwo Politechniki Śląskiej, Gliwice.
10. **Morecki A., Knapczyk J.** (2001): *Podstawy robotyki. Teoria i elementy manipulatorów i robotów,* WNT, Warszawa.
11. **Rosen K.H.** (1991): *Discrete Mathematics and Its Applications, 2nd edition,* McGraw-Hill Publishing, New Yersey.

DESIGN, PROTOTYPE AND EXPERIMENTAL EVALUATION OF A WHEELCHAIR TREADMILL

Mustafa Kurt[*], Hasan Geyik[*], Bilçen Mutlu[*], Yaşar Tatar[**], Ergun Nart[***]

[*] Marmara University, Technical Education Faculty, Mechanical Education Department, 34722 Kadıköy, Istanbul, Turkey
[**] Marmara University, Prosthetics and Orthotics Centre,34722 Kadıköy, Istanbul, Turkey
[***] Sakarya University, Technical Education Faculty, Mechanical Education Department, 54187 Adapazarı, Turkey

mkurt@marmara.edu.tr, hasan_geyik@yahoo.com, bmutlu@marmara.edu.tr, ytatar@marmara.edu.tr, enart@sakarya.edu.tr

Abstract: Generally, wheelchair users cannot move easily within buildings since living areas in architectural structures are not suitable for them to maintain or to improve their physical capabilities. Because living area restrictions affect the physical performance of the users outside during the day, the reduced mobility causes several health problems. These problems become more intense by the time. Especially heart and lung related illnesses are common among the wheelchair users since the immobility decreases respiration capacity. The aim of this research is to design and prototype a wheelchair treadmill to help wheelchair users improve their upper extremity system. In this study, CAD was employed for the design of wheelchair treadmill. Then finite element analysis (FEA) was carried out for the parts of the wheelchair treadmill and the prototype was manufactured based on the results. The prototype was tested under the conditions the product was originally intended to function. In the experiments, the speeds of wheelchair and wheelchair treadmill were measured. The distances taken by users were also recorded, and the results were evaluated with respect to road surface conditions.

1. INTRODUCTION

Sports are just as important to persons with disabilities as to "able-bodied" people, if not more so (Yim at al., 1993). Sports help maintaining an individual's fitness while improving feelings of self-worth. Lack of physical fitness can cause obesity and cardio respiratory ailments to which manual wheelchair users (MWCU) are particularly prone (Robinson et. al., 1988).

The functional consequences of lower-limb disability result diminished independence, fitness, work capacity and recreational/employment opportunities. Particularly, the upper-limb pain resulting from overuse injury affects the physical performance and the quality of life for MWCU. Chronic conditions such as carpal tunnel syndrome, rotator cuff injuries, elbow/shoulder tendonitis, and osteoarthritis have also been associated with long-term manual wheelchair use. Shoulder or wrist joint pain has been reported in 64-73 % of those who use manual wheelchairs with spinal cord injuries. In the previous studies, 67 % of MWCU had upper-limb mononeuropathies defined by strict electro diagnostic criteria. In addition, ineffective biomechanics can decrease the economy of wheelchair operation and lead to excessive metabolic and cardiopulmonary demand. Investigators have identified several possible contributors to overuse injuries in MWCU, including duration of manual wheelchair use, frequency of arm use, and propulsion style kinematics (Brubaker, 1990). On the other hand, several researchers have proposed that Chronic wheelchair-use creates imbalances in propulsion agonists and antagonists, and training of the antagonists may correct these imbalances, reduces the potential for associated upper-limb pain (Koontz, 2002), and improve the blood circulation in the lower body that is not in motion at all the times (Devillard et. Al., 2001). Therefore, training and related equipment for wheelchair-users offer an area of research that may result increased physical performance, and decreased health care costs for the users (Koontz, 2002).

This device also gives an important adaptation platform for beginners, prevents the possible injuries in user's arms and wrists in daily usages, and introduces a training platform for the people make wheelchair sports. Therefore, the aim of this study is to design and prototype an optimum wheelchair treadmill, which strengthens the upper extremity (shoulder, arm and wrist), and measures performance of the users. According to the extracted design parameters, a prototype was designed using CAD software in detail, and then finite element analyses were performed for the designed parts respectively. Then, the prototype was manufactured according to the results provided by FEA.

2. MECHANICAL SYSTEM DESCRIPTION

A solid model of wheelchair treadmill is shown in Fig. 1. As shown in Fig. 1, Wheelchair treadmill is an entirely user independent system. The system consist of five main components: the roller (1), the frame (2), the ramp (3), the magnetic unit (4), and enter/exit unit (5).

1. Rollers: It is the most critical module of the product. If the rollers are not functional or any problems which affect their functionality are not prevented, the product is essentially useless. Therefore, the core of the roller assembly has to be made of a hardened steel shaft that runs through the length of the roller. This ensures that the ends of the roller assembly be collinear and help with alignment.

The shaft diameter was determined as 17 mm. The DIN 115 Cr V3 shaft material was selected which meets requirements for strength and cost effectiveness. ORS brand high quality roller bearings have been used, rated for an angular velocity of 1700 rpm with a load capacity of 9,55 kN.

2. Frame: Designing the frame is an integral process for several reasons. First, the frame has to be designed to accommodate the motion of the rollers, so the integration between these two parts is crucial. Second, the frame needs to be able to bear the load applied by the user and wheelchair, as well as fit for various different wheelchair sizes. For this reason, the base consists of a flat rectangle made from profile of 60x40 mm. Rectangular comer braces and a center strip are welded to the frame to ensure accurate alignment for the base rollers. Supports are added to hold the shafts for the rollers and the platform.

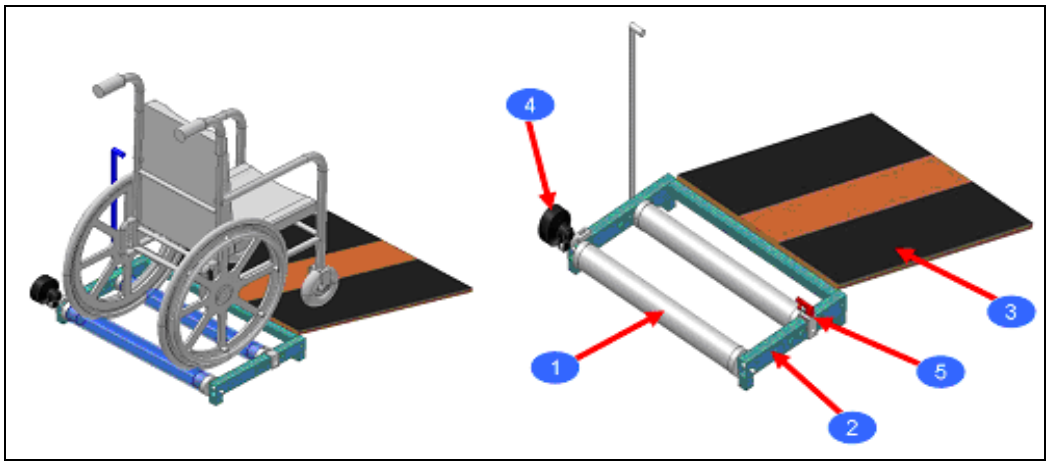

Fig. 1. A Solid Model of Wheelchair Treadmill

3. Ramp: The ramp, though seemingly a small part of the entire design, is important because it supplies what is desired for the overall comfort levels of the users. If the user cannot easily set him or her up on the machine, surely customers won't be happy to use it. Therefore, the ramp and the platform are constructed from 18 mm plywood. The platform is designed for a height of 100 mm. This low profile allows for a short (381 mm) ramp with a practical l/10 ratio. The large platform (1000 x 900 mm) allows the user to train using standard wheelchairs, as well as long racing wheelchairs.

4. Magnetic Device: A commercial magnetic device was attached to the Wheelchair Treadmill mechanism. The device supplies resistance to the rear roller through a belt and pulley system. A mounting block is welded to the frame to support the magnetic resistance device. Two rollers are used with deflection devices that eliminate the need for a clamping mechanism. Essentially, the magnetic unit is coupled to the back roller to allow seven levels of workouts corresponding to various levels of user abilities, and it can be disconnected to perform hand stroke analyses.

5. Enter/Exit Brake: A brake system was designed in order to lock the front roller into the frame. By locking the front roller, the mechanism between rollers and wheelchair is transformed to a static structure. So wheelchair users can safely enter and exit the equipment.

In the model the followings are assumed:

- Wheelchair users do not change posture,
- The weight of wheelchair users is 100 kg,
- The weight of wheelchair is 20 kg,
- Wheelchair has a 40 cm wheelbase,

The way to estimate center of mass (COM) described by Tomlinson (2000)

Fig. 2 shows weight distribution for a typical wheelchair.

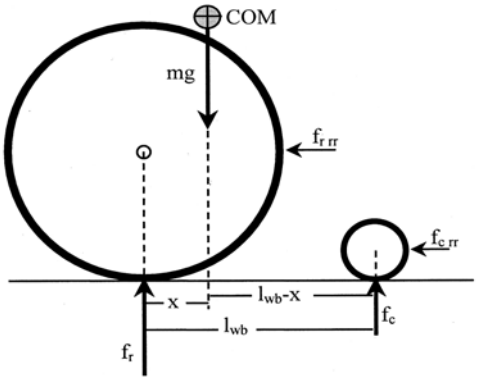

Fig. 2. Wheelchair weight distribution

Equations used:
Weight distribution

$$r_{wd} = \frac{f_r}{mg} = \frac{l_{wb} - x}{l_{wb}} \quad , \quad c_{wd} = \frac{f_c}{mg} = \frac{x}{l_{wb}} \tag{1}$$

Using this Equation (1), weight on caster (f_c) and weight on rear wheels (f_γ) can be calculated.

$$f_c = m.g.c_{wd} \tag{2}$$

$$f_r = m.g.r_{wd} \tag{3}$$

Results: $f_c = 294$ N, $f_r = 883$ N

Two major geometrical factors can affect the radial load applied at each bearing. These are "Roller Distance", the horizontal distance between each roller, and "Roller Size", the diameter of the roller. Fig. 3 shows cross-sectional view of a wheelchair wheel in contact with a set of rollers. The Figure simply includes the wheelchair and two rollers represented by a large circle and two small circles respectively, and a number of different forces exerted on the bodies.

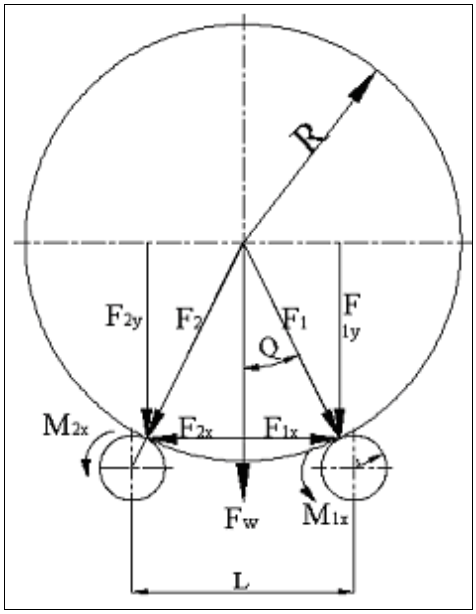

Fig. 2. Forces and force components exerted on rollers due to wheelchair load

As shown in Fig. 3, L, R, and r represent the distance between roller axes, the radius of the wheelchair wheel, and the radius of the roller respectively. The force due to weight of the wheelchair and person is defined as F_w, and F_1 is used to define the radial force on the rollers. "½ F_w" simply corresponds to a component of the radial force, and Q stands for the angle between the radial force and force due to the weight of the wheelchair.

$$\theta = \sin^{-1}\frac{L}{2(R+r)} \tag{4}$$

$$F_N = \frac{1}{Cos\theta} * (\frac{1}{2} F_w) \tag{5}$$

Using the equations (4) and (5), the relationship between roller distance and radial load can be calculated, as shown in Tab. 1.

Tab. 1. Radial load on rollers

L [mm]	200	250	300	350
F_x [N]	64,9	81,7	97,5	113,7
F_y [N]	211,0	205,1	198,1	189,2
M [N.m]	19,2	24,1	28,8	33,6

3. DESIGN ANALYSIS

The roller, which is the major component of the wheelchair treadmill, is the most critical part of the device. It supports all of the weight of a person and a wheelchair. In this study, a computer model of the wheelchair treadmill was produced using a CAD software, and then, each part in the model was transferred to ANSYS Workbench 10.0 FEA software. The frame and the rollers were assembled for the analysis. Then, aluminum 6063-T6-pipe roller material has been chosen because of its strength and affordability. Next, interactions have been defined by introducing the contact pairs between the related surfaces of the parts in the assembled model. In addition, loads and boundary conditions have been assigned (Fig. 4) and a suitable mesh was generated for each part. At the end, a general static geometrically nonlinear analysis was submitted to FEA software.

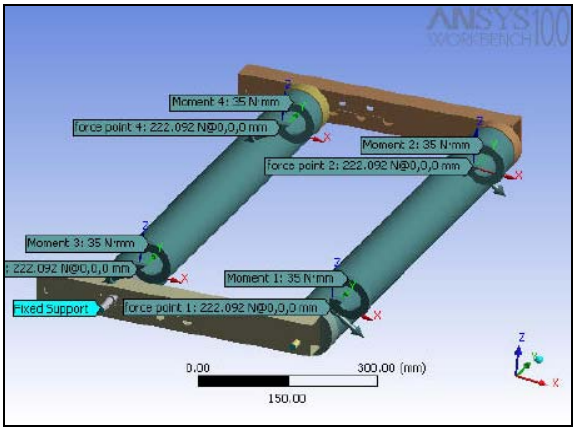

Fig. 3. Load Distribution of the Rollers

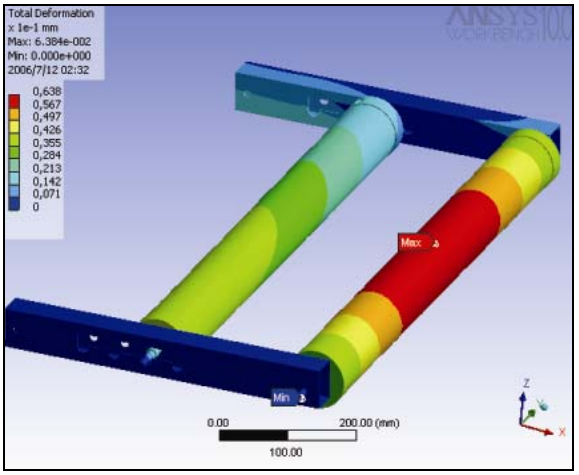

Fig. 4. Deformation on the roller

Having completed the analysis, the results have been obtained as shown in Fig. 5 and Fig. 6. Fig. 5 reveals that the critical point on the roller is located at the middle of the first roller where the deflection and the moment are the highest. Similarly, by looking the results, the stresses have been controlled to make sure that no place in the model has exceeded the mechanical limits.

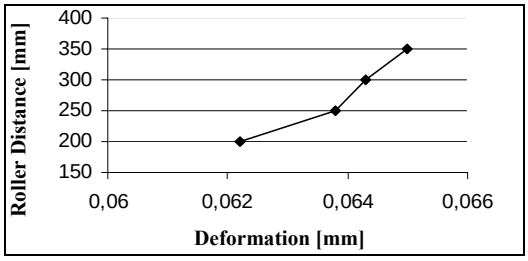

Fig. 5. The relationship between roller distance and deformation

4. TESTING AND EXPERIMENTAL RESULTS

After manufacturing the designed prototype (Fig. 7), several experiments have been planned and conducted. To choose suitable users for the experiment, the weight and age of the wheelchair users and the time of the wheelchair's usage have been considered carefully. In the first experiment, velocities of several wheelchair users on the road conditions such as the flat asphalt and the ceramic tile coated surfaces in buildings have been measured and the average velocity, maximum velocity, and the distance covered by the users have been recorded. In the second experiment, similar parameters have been observed. However, during this experiment, the resistance level of magnetic brake located on the wheelchair treadmill has been increased step by step from 0 to 7, and for each level, the average velocity, the maximum velocity, which the wheelchair user is able to reach, and the equivalent distance have been measured with a digital speedometer mounted on the wheelchair. The duration of experiment at each resistance level has been determined for at least one minute to fulfill the requirements. Finally, the velocity of the subjects in wheelchair treadmill has been shown in Fig. 8.

Fig. 6. Schematics of experimental prototype

Table 2. Velocities of users

	1.Subject		2.Subject		3.Subject		4.Subject	
	Asphalt	Parquet	Asphalt	Parquet	Asphalt	Parquet	Asphalt	Parquet
Average Velocity [km/h]	1,275	1,336	1,333	1,575	1,116	1,183	1,216	1,366
Maximum Velocity [km/h]	1,422	1,475	1,605	1,672	1,422	1,475	1,416	1,733
Trip Distance [m/min]	77	80	80	95	67	71	73	82

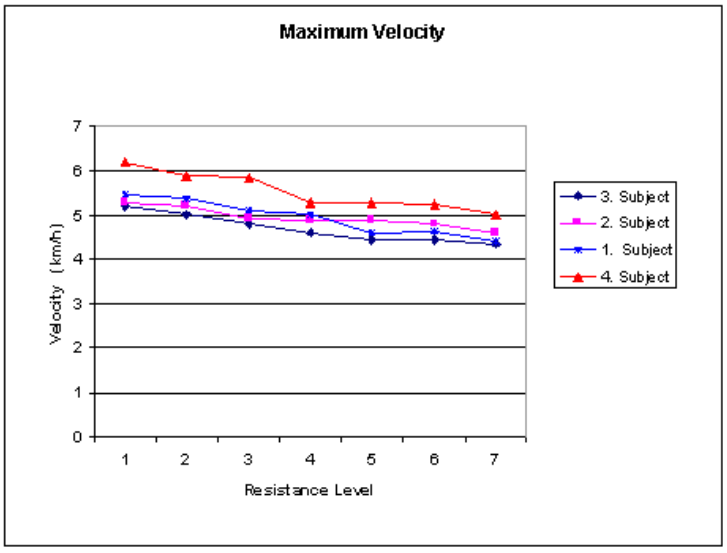

Fig. 8. Subjects velocity in the wheelchair treadmill

5. CONCLUSIONS

In this study, a wheelchair treadmill mechanism has been designed, and a prototype of it has been manufactured. The mechanism has been tested both for disabled and normal people. The average, maximum speed and the distance covered have been measured on asphalt road, parquet surface as well as on the produced wheelchair treadmill. These measurements have been performed taking the values from a digital speedometer for one minute period. The experiments have been conducted in the rehabilitation center of Marmara University

The average speed while increasing the magnetic resistance level of the wheelchair treadmill for different subjects is shown in Fig.7. In order to achieve the speed on the normal ground, wheelchair users should simply adjust the resistance to level 2. Similarly, the users can increase the resistance level to maximum for claiming a ramp. For these proposes, the system has been constructed in such a way that the different resistance levels are achieved by adjusting the distance between rollers. This functionality provides users with a useful tool to make their daily activities even in small living areas.

On the other hand, it has been observed that various factors associated with manual wheelchair driving force have strong effect on the results of experiments performed on the wheelchair treadmill. These factors are (a) wheelchair design and quality of the components, (b) environment in which the wheelchair is used, (c) the extent of person's disability, (d) person's level of physical fitness, and (e) person's skill and experience in using a wheelchair.

REFERNCES

1. **Brubaker C. E.** (1986), Wheelchair Prescription: An Analysis of Factors That Affect Mobility and Performance, *J. Rehab. Res. Dev.*, Vol. 23, Issue: 4, 19-26.
2. **Brubaker C. E.** (1990), Ergonomic Considerations, J*ournal of Rehabilitation Research and Development*, Clinical supplement, Issue 2, 37-48.
3. **Devillard X., Calmels P., Sauvignet B., Belli A., Denis C. Simard C., Gautheron V.** (2001), Validation of a New Ergometer Adapted to All Types Of Manual Wheelchair, E*uropean Journal of Applied Physiology*, Vol. 85, No.5, 479-485.
4. **Koontz A.** (2002), Manual Wheelchair Use and Upper Extremity Pain and Injury, *Human Engineering Research Laboratories*, Pittsburgh.
5. **Kulig K., Newsam C. J., Mulroy S. J., Rao S., Gronley J. K., Bontrager E. L., Perry J.** (2001), The Effect of Level of Spinal Cord Injury on Shoulder Joint Kinetics During Manual Wheelchair Propulsion, *Clinical Biomechanics*, Vol. 16, Issue 9, 744-751.
6. **Langbein W. E., Robinson C. J., Kynast L., Fehr L.** (1993), Calibration of a New Wheelchair Ergometer: The Wheelchair Aerobic Fitness Trainer, *IEEE Transactions on Rehabilitation Engineering*, Vol. 1, No. 1, 49-58.
7. **Robinson C. J., Langbein W. E., Kampschoer C. J., Kynast L.T.** (1998), Interface Considerations for the Wheelchair Aerobic Fitness Trainer, *Engineering in Medicine and Biology Society*, Proceedings of the Annual International Conference of the IEEE.
8. **Tomlinson J. D.** (2000), Managing Maneuverability and Rear Stability of Adjustable Manual Wheelchairs: An Update, Physical *Therapy*, Vol. 80 . No. 9.
9. **Yim S. Y., Cho K. J., Park C. I., Yoon T. S., Han D. Y., Kim S. K., Lee H. L.** (1993), Effect of Wheelchair Ergometer Training on Spinal Cord-Injured Paraplegics, *Yonsei Med J.*, Vol. 34, No. 3, 278-86.

HIGH FREQUENCY VIBRATION MONITORING AND DIAGNOSTICS OF HIGH-SPEED PUMP ROLLING BEARINGS

Dmitry LITVINOV[*], Janis RUDZITIS[*]

[*]Riga Technical University, 1 Kalku Street, Riga, PDP, LV-1658, Latvia

arminius@inbox.lv, arai@acad.latnet.lv

Abstract: Evolution of modern industry makes great demands to reliable work of pump equipment with large revolutions number of rotating parts. Under special supervision must be the centrifugal high-speed pumps. One of the major and hardly loaded units of high-speed pump equipment are rolling bearings, therefore it is very important to conduct monitoring and early diagnostics works to find out defects in them. For the high-frequency vibration detection and analysis it is possible to use both stationary and portable systems of monitoring and diagnostics. This diagnostics advantage is early detection of aberration from normal operation of rolling bearings and transition from equipment service and repair on-schedule to real situation service and repair, which is determined on periodic diagnostics results.

1. INTRODUCTION

Pumping equipment of various enterprises as well as any other equipment is subject of disrepairs and failures, which result in a substantial economic loss. From the large variety of technological equipment, pumps are taking a one of
lea-ding places. All of pumping equipment requires the permanent supervising after its work. But under the special supervision there must be centrifugal pumps (Fig. 1) with the high-speed coefficient $n_s \geq 150$, which is determined by:

$$n_s = 3,65 \cdot n \cdot \sqrt{\frac{Q}{H^{\frac{3}{4}}}} \; ; (1)$$

where: Q - complete pressure (m^3/h); H - feed of pump (m); n - revolutions amount of working shaft (rpm).

From a formula (Eq.1) evidently, that the impeller of centrifugal pump, intended for work with defined Q and H, possesses the greater high-speed, than anymore its rotation frequency. Large rotation frequencies set conditions for small sizes and mass of pumps and drive engines at high output of aggregates. Therefore application of working impellers with high n_s (Fig.1 pos. 1; 2; 3) economically feasible.

At the determined rotation frequency high-speed the higher, than anymore feed and less pressure, developed by working impeller. Therefore centrifugal pumps having working impellers with the high coefficient of high-speed have a low-pressure and give a large feed (Черкасский, 1984).

Consequently, to provide this type pumping equipment reliable and trouble-free work, it is necessary, that this equipment constantly be under control.

The most important and high-loaded units of high-speed pumps are rolling bearings; therefore it is very important to conduct works for monitoring and early diagnostics to find out defects in it already on the early stage.

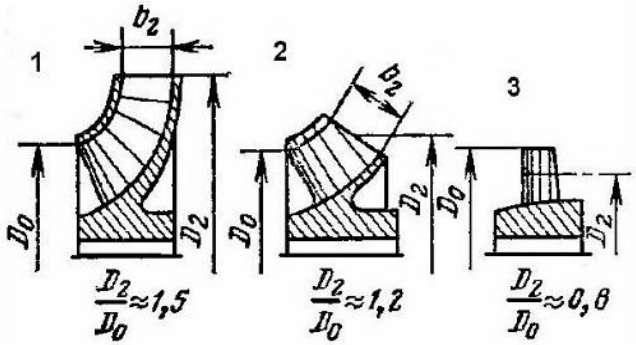

Fig. 1. Types of high-speed pump working impellers: 1 - High-speed impeller, $n_s = 150 \div 300$; 2 - diagonal impeller, $n_s = 300 \div 600$; 3 - axial impeller, $n_s = 600 \div 1200$

One of bearing incipient wear signals is a high-frequency vibration. It is the vibration in frequency range from above 20 kHz. Difficulties during the diagnostic information selection from low frequency and middle frequency vibrations, possible its distortions and complications of defect's localization it is all defined the promoted interest to the high-frequency vibration. Advantage of this diagnostics is an early acquisition of deviations from rolling bearings normal work and transition from equipment's maintenance and repair on regulation to maintenance and repair on the actual state.

The basic high-frequency vibration discovery and analysis method is a narrow band spectral analysis of signals, got from bearings, with large permission on frequency. This analysis is carried out by Fourier discrete transformation.

In the transformation the probed function is periodic, has an eventual period of repetition, and is discrete and actually allows presenting a discrete function as an eventual number of frequencies with the defined values of amplitude and phasing (lays out a function in its spectrum).

$$\mathrm{Re}\, X[k] = \sum_{i=0}^{N-1} x[i] \cos\left(\frac{2\pi \cdot k \cdot i}{N}\right); \quad (2)$$

$$\mathrm{Im}\ X[k] = -\sum_{i=0}^{N-1} x[\ ] \sin\left(\frac{2\pi \cdot k \cdot i}{N}\right) \quad (3)$$

Where: ReX[x] - an array, containing cos values; Im X[x] - an arrayy, containing sin values.

By another words it is possible to say that this transformation is laid out by the probed signal on the base functions of sine (Eq.2) and cosine (Eq.3). They are analogues of two mutually perpendicular vibrations, because on a phase displaced in relation to each other on 90 degrees (http://shackmaster.narod.ru/fourier.htm)

2. NATURE OF ROLLING BEARING'S VIBRATION

Rolling bearing's work in high-speed pump composition and at presence faults in it can influence on a vibration and modulating it processes with the followings fundamental frequencies:

- Rotation frequency of movable ring in relation to immobile: $f_{\gamma ot}$;
- Rotation frequency of separator in relation to an outer ring:

$$f_r = \frac{1}{2} \cdot f_{rot} \cdot \left(1 - \frac{d_{sr}}{d_r} \cdot \cos(\alpha)\right); \quad (4)$$

Where: $d_{s\gamma}$ - solid of revolution diameter; $d_\gamma \approx 1/2(d_{out} - d_{in})$ - diameter of separator; d_{out} - diameter of outer ring; d_{in} - diameter of inner ring; αcontact angle of bodies and rolling paths;

- Rolling frequency of sol - id of revolution on an outer ring:

$$f_{out} = \frac{1}{2} \cdot f_{rot}\left(1 - \frac{d_{sr}}{d_r} \cdot \cos(\alpha)\right) \cdot z = f_r \cdot z; \quad (5)$$

Where: z - solid of revolution number;

- Rolling frequency of solid of revolution on an inner ring:

$$f_{in} = \frac{1}{2} \cdot f_{rot}\left(1 + \frac{d_{sr}}{d_r} \cdot \cos(\alpha)\right) \cdot z = (f_{rot} - f_r) \cdot z; \quad (6)$$

- Rolling frequency of solid of revolution in relation to the surface of rings:

$$f_{sr} = \frac{1}{2} \cdot f_{rot} \cdot \frac{d_r}{d_{sr}}\left(1 - \frac{d_{sr}^2}{d_r^2} \cdot \cos^2(\alpha)\right); \quad (7)$$

Expressions (Eq. 4, Eq. 5, Eq. 6, and Eq. 7) are evaluating only basic harmonics frequencies in the vibration spectrums and envelope of its high-frequency components at the different types of defects (Барков et al., 2000)

3. METHODS OF MONITORING AND DIAGNOSTICS

Among the monitoring and diagnostics different methods of the high-speed pump's rolling bearings state it is possible to select two basic:

3.1. High-frequency vibration form analysis, excited short shock impulses

This method is sensible to microshocks appearance at the friction elements contact in rolling bearings. It got the name «Method of shock impulses». For such type of high-frequency vibration analysis implementation the specialized measuring devices were created.

To illustrate this method, on Fig. 2 the rolling bearing's high-frequency vibration signals are resulted without defects (Fig. 2a), with the friction surface wear (Fig. 2b), and with a shell on the friction surface (Fig. 2c). Shock impulses arise up in third case, at the rotation of bearing with a shell on any of rolling friction surface. They are revealed by the size of signal maximal value relation to its RMS value. This relation is named by pick factor and at rare shock impulses appearance can exceed a value ten. In default of shock impulses it, as a rule below to five.

Utilizing this method it is possible to find out the engendered microscopic greasing defects at which the oil tape breaks take a place rarely and irregularly, and also mechanical micro faults of bearings, on unstable rotation frequencies, for short time (for 2-3 turns). Thus, in practical diagnostics, method of shock impulses not using separately, in the aggregate with the *high frequency vibration power checkout* only (Maurice and Adams, 2001).

3.2. High-frequency vibration power oscillations spectral analysis

This method possesses more high possibilities on control after the rolling bearing's state of high-speed pumps on the high-frequency occasional vibration envelope spectra, excited by friction forces in oil tape of bearing, and also by shock impulses at its breaks.

Occasional signal envelope spectra gives information about periodic changes of high-frequency vibration power in the frequency range, which is preliminary selected from the vibration signal by one third octave band filter (narrow band filter).

In the Fig. 3 the vibration spectrum of bearing unit is resulted in a range from 10 kHz to 25.6 kHz, where is

shown the frequencies range of filter, utilized for a high-frequency casual component selection with the envelope consequent forming.

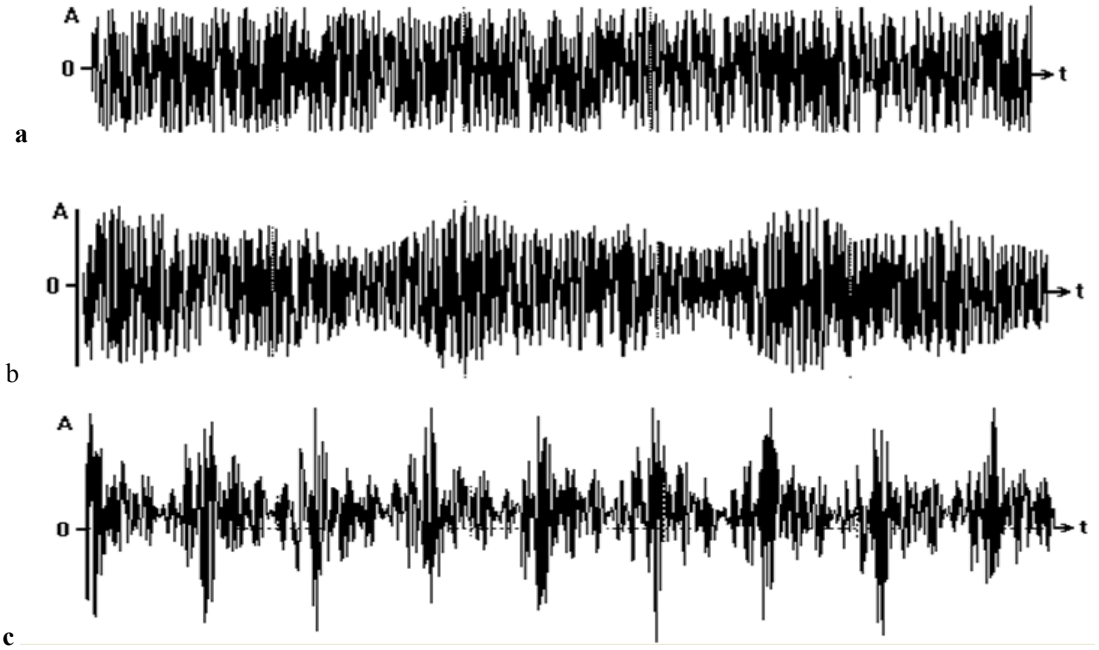

Fig. 2. High-frequency vibration of rolling bearings: a – without defects; b – with the friction surface wear; c – with a shell on a friction surface

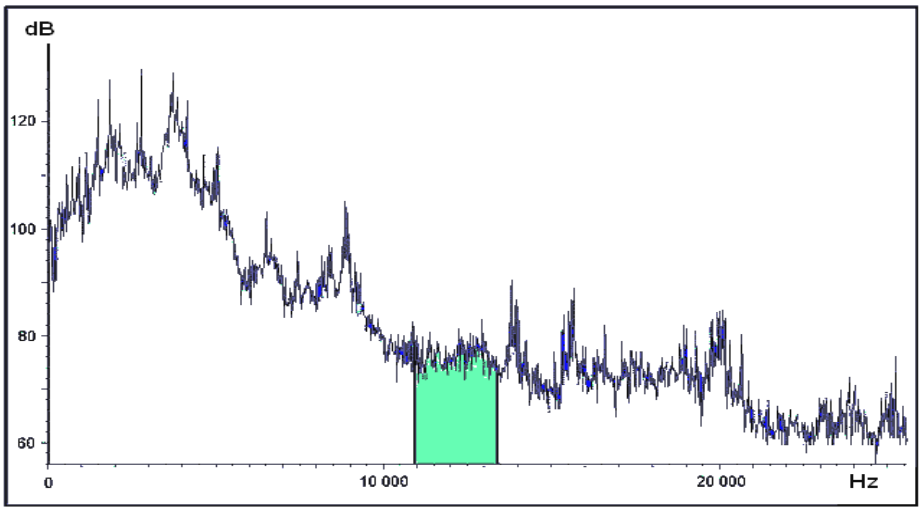

Fig. 3. Rolling bearing's vibration spectrum of high-speed pump with selected of one third octaves frequency band

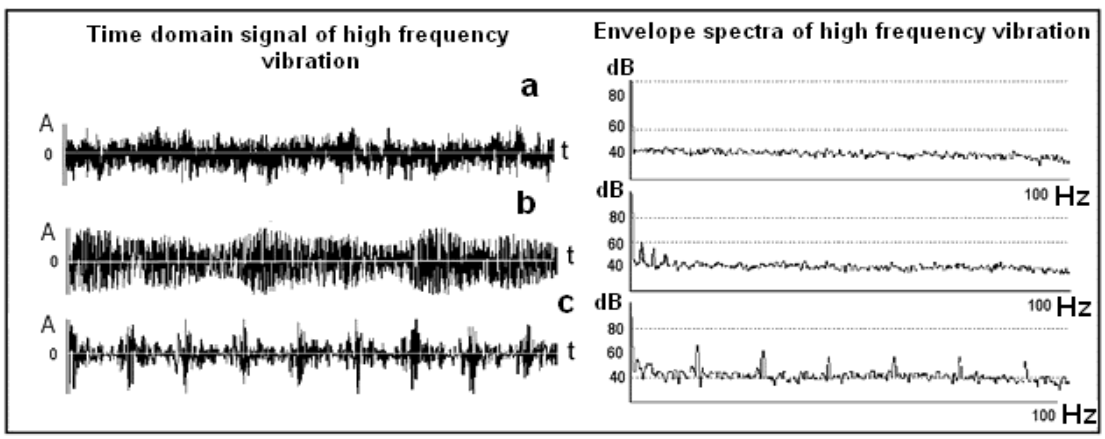

Fig. 4. Forms of the high-frequency vibration and its envelope spectrums are for three identical bearings, accordingly, without faults (a); with the fault of separator (b); with a shell on an outer ring (c)

The method gives positive results only when harmonic constituents of vibration do not get in the frequency band of filter, by power exceeding an occasional vibration. Otherwise the power oscillations sum of harmonic and occasional constituents decreases and an envelope spectrum giving the distorted information about bearing's state (Баркова, 2003).

In spite of certain complication of high-frequency casual vibration envelope spectra measuring as compared to mea-suring, executable by the «shock impulses» method, all possibilities of envelope method's realization allows to solve many important problems of high-speed pump rolling bearing's diagnostics.

4. EQUIPMENT FOR MONITORING AND DIAGNOSTICS

In technical maintenance of high-speed centrifugal pumps, the vibration monitoring and diagnostics fill the special place because of the possibilities to find out the changes in the condition long before emergency situation.

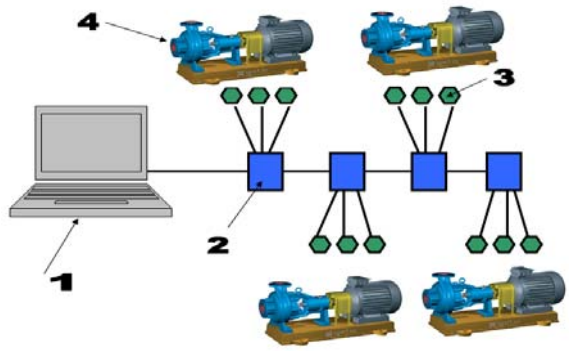

Fig. 5. The monitoring and diagnostics stationary system structure (1 - computer with special software; 2 – boards of transformation signals from sensors in digital form; 3 – sensors of vibration; 4 – centrifugal pumps)

Fig. 6. The monitoring and diagnostics portable system structure (1 – Laptop with special software; 2 – data collector-analyzer; 3 – the sensor of shaft revolutions; 4 – vibration sensor)

The modern systems of looking after pumping equipment unite in it both monitoring and diagnostics functions. These systems can be both stationary and portable.

It is expedient to apply the monitoring and diagnostics stationary systems at supervising pumps large amount presence. The generalized structure of the stationary system is shown on Fig. 5.

For necessary mobility and realization monitoring and diagnostics works providing in different situations, utilize the portable systems (Fig. 6).

Utilizing experience of both stationary and portable systems shows that a most economic effect is obtained at presence on an enterprise simultaneously both stationary and portable system.

5. SUMMARY

It is possible to draw a conclusion from all of above-stated, that high-speed centrifugal pumps equally with other rotating machinery require permanent control after their technical state. It is very important to find out defects in rolling bearings on the occurrence early stage. That is possible due to the vibration control in high-frequency range (in frequency range from above 20 kHz). Only in this range possible to find out the engendered defects of rolling bearings. All these actions are necessary for a transition from the planned repairs of equipment to repairs on the actual state.

REFERENCES

1. **Maurice L. Adams, Jr**. (2001), *Rotating Machinery Vibration. From Analysis to Troubleshooting*, Routledge, New York.
2. **Барков А.В., Баркова Н.А., Азовцев А.Ю.** (2000), Мониторинг и диагностика роторных машин по вибрации, Санкт Петербург: Изд. Центр СПбГМТУ, 2000.
3. **Баркова Н.А.** (2003), Оптимизация методов диагностики подшипников качения по высокочастотоной вибрации // Сборник методических материалов семинара, 50-60.
4. Применение преобразования Фурье в цифровой обработке звука, http://shackmaster.narod.ru/fourier.htm
5. **Черкасский В.М.** (1984), Насосы, вентиляторы, компрессоры, Москва: Энергоатомиздат, 416.

A FAULT-TOLERANT CONTROL SYSTEM FOR A HEXAPOD MOBILE ROBOT

Cristina PANA*, Viorel STOIAN*

*CCMR Craiova-University of Craiova, Mechatronics Department, 107, Decebal Street, 200440, Craiova, ROMANIA

cristina@robotics.ucv.ro, stoian@robotics.ucv.ro

Abstract: This paper presents a fault-tolerant control system for a hexapod mobile robot. First, a description of the dynamic model of the hexapod mobile robot by a system of differential equations is made and after that, a representation of the system in state variable space is obtained. A fault detection and identification algorithm is proposed. The modality used here is an analytical redundant process, which supposes that the processing of the information is made at a superior level for the identification of the changes due to the faults. By this method, the actualized model obtained by the on-line identification of the system, is permanent compared with nominal model (without faults). The adaptive control system for uncertain non-linear systems proposed here has two main blocks: adaptation mechanism block which implements the mathematical model of the adaptation error and control law accommodation block which changes the characteristics of the control law. Finally, the authors propose the hexapod mobile robot which is open to fault events, to be a variable structure system and analyze a specific control method.

1. INTRODUCTION

The desire to develop a legged robot has existed for hundreds of years; however, it has only been in the last half century with the advances of technology that dream has become achievable. A large number of legged robots have been built to date.

The motion of walking machines is not a continuous motion like a wheel motion. With sufficient technology development walking robots has the potential to traverse much more rugged terrain than current wheeled or tracked platforms since they do not need a continuous support surface (Manko, 1992). Previous studies addressed mainly the robot control, at the leg level, or the leg coordination, adopting strategies such as neural networks (Tsai and Lee, 1997), fuzzy logic (Tsai et al., 1997), hybrid force/position control (Song et al., 1997), subsumption architecture (Brooks, 1989) and insect-like scheme (Ferell, 1995).

The mechanical systems are generally subjected to different faults as caused by unexpected internal parameter alterations or by actuators or sensors problems (malfun-ctions).

Topics like fault detection, fault diagnosis and fault tolerant control (FTC) have been principal subjects of considerable study in the past years. The design of fault-tolerant systems is an important research field (Blanke et al., 2003; Zhang and Jiang, 2003).

When faults exist, it is very important for a hexapod mobile robot to be kept stable with acceptable performances and to have a safe and reliable function for a minimum required period. The problem of stability can be solved by keeping the center of the mass of the machine within the polygon of support formed by the supporting feet.

In Patton, 1997; Blanke et al., 2000; Wang and Wang, 2001; Iichman, 1993; Kabore and Wang, 2001; Polycarpou, 2001; Loose et al., 1985; Veillette et al., 1990, Wallacc and Vander, 1984 and Veillette, 1995 a lot of algorithms and methods have been designed and applied successfully to different practical systems. In Zhihua et al. (2003), a robust fault-tolerant control method is presented for uncertain non-linear systems which are based on a robust measure of failures and which can switch between one robust control algorithm developed under a normal operating conditions and another, developed under a faulty operating conditions. Structural analysis has been used for large-scale system decomposition (Steward, 1962), observability and controllability (Lin, 2001; Murota, 1987), control and diagnostic design, including sensor placing (Meyer et al., 1994).

2. DYNAMIC MODEL OF THE HEXAPOD MOBILE ROBOT

Fig. 1. The hexapod mobile robot (a); The variables of the leg i (b)

In Fig. 1 the structure of a hexapod mobile robot and the variables of the leg i are represented. In relation (4) we can see all components of the internal variables' vector of the hexapod robot system where:

$$\mathbf{w}_B = [x_B \; y_B \; z_B]^T \quad (1)$$

– by reason of translation motion of the hexapod body

$$\boldsymbol{\theta}_B = [\theta_{Bx} \; \theta_{By} \; \theta_{Bz}]^T \quad (2)$$

– by reason of rotation motion of the hexapod body

$$\boldsymbol{\theta}_i = [\theta_{i1}\ \theta_{i2}\ \theta_{i3}]^T,\ i = 1, 2, \ldots.6 \tag{3}$$

– the variables of the six legs

$$q = \left[w_B^T \quad \theta_B^T \quad \theta_1^T \quad \theta_2^T \quad \theta_3^T \quad \theta_4^T \quad \theta_5^T \quad \theta_6^T \right]^T \tag{4}$$

T – transpose

In Pana et al. (2008) the dynamical model of the hexapod robot is obtained. Its vector form is:

$$M(q)\,\ddot{q} + C(q, \dot{q})\,\dot{q} + G(q) = \tau \tag{5}$$

M(q) is the inertia matrix and its structure is (Pana et al., 2008):

$$M(q) = \tag{6}$$

$$\begin{bmatrix}
m_{w_B} & m_{w_B\theta_B}^T & m_{w_B\theta_1}^T & m_{w_B\theta_2}^T & m_{w_B\theta_3}^T & m_{w_B\theta_4}^T & m_{w_B\theta_5}^T & m_{w_B\theta_6}^T \\
m_{w_B\theta_B} & m_{\theta_B} & m_{\theta_B\theta_1}^T & m_{\theta_B\theta_2}^T & m_{\theta_B\theta_3}^T & m_{\theta_B\theta_4}^T & m_{\theta_B\theta_5}^T & m_{\theta_B\theta_6}^T \\
m_{w_B\theta_1} & m_{\theta_B\theta_1} & m_{\theta_1} & 0 & 0 & 0 & 0 & 0 \\
m_{w_B\theta_2} & m_{\theta_B\theta_2} & 0 & m_{\theta_2} & 0 & 0 & 0 & 0 \\
m_{w_B\theta_3} & m_{\theta_B\theta_3} & 0 & 0 & m_{\theta_3} & 0 & 0 & 0 \\
m_{w_B\theta_4} & m_{\theta_B\theta_4} & 0 & 0 & 0 & m_{\theta_4} & 0 & 0 \\
m_{w_B\theta_5} & m_{\theta_B\theta_5} & 0 & 0 & 0 & 0 & m_{\theta_5} & 0 \\
m_{w_B\theta_6} & m_{\theta_B\theta_6} & 0 & 0 & 0 & 0 & 0 & m_{\theta_6}
\end{bmatrix}$$

where all its components are submatrices of size 3x3 and contain mass components, inertia moments, jacobian matrices and transformation matrices between different frames. They are defined in Pana et al. (2008). M(q) is symmetric, positive definite and both M(q) and $M^{-1}(q)$ are uniformly bounded as function of $q \in R^n$.

$C(q, \dot{q})\,\dot{q}$ is a vector which contains centrifugal forces (terms of type $\dot{q}_k^2$) and Coriolis forces (terms of type $\dot{q}_i\dot{q}_j$; $i \neq j$) and its expression is:

$$C(q, \dot{q})\,\dot{q} = \dot{M}(q)\,\dot{q} - \frac{1}{2}\frac{\partial}{\partial q}\left(\dot{q}^T M(q)\,\dot{q}\right) \tag{7}$$

The matrix $N(q,\dot{q}) = \dot{M}(q) - 2\,C(q,\dot{q})$ is screw symmetric, where C is defined using Christoffel symbols. The vector G(q) is the vector of the gravitational forces:

$$G(q) = \frac{\partial E_P}{\partial q} \quad (E_P \text{ is potential energy}) \tag{8}$$

Using the properties of the inertia matrix M(q), the relation (10) can be written:

$$\ddot{q}_i = f_i(q_1,\ldots q_n,\dot{q}_1,\ldots\dot{q}_n) + B_i(q_1,\ldots q_n,\dot{q}_1,\ldots\dot{q}_n)\begin{bmatrix}\tau_1\\ L\\ \tau_n\end{bmatrix} \tag{9}$$

The expression (11) separates the terms which define internal evolutions of the robot of the terms with external variables (control variables τ_i). The new coefficients are:

$$f(q, \dot{q}) = -M^{-1}(q)\left[C(q, \dot{q})\,\dot{q} + G(q)\right]$$

$$B(q, \dot{q}) = M^{-1}(q)\ \ I \tag{10}$$

The outputs of a general mechanical system are:

$$y_k = C_k(q_1,\ldots q_n,\dot{q}_1,\ldots\dot{q}_n) + D_k(q_1,\ldots q_n,\dot{q}_1,\ldots\dot{q}_n)\begin{bmatrix}\tau_1\\ L\\ \tau_n\end{bmatrix}; \tag{11}$$

k = 1, 2, … m

Generally, the outputs of a robot system directly depend not on input variables, so we can write:

$$y_k = C_k(q_1,\ldots q_n,\dot{q}_1,\ldots\dot{q}_n); \tag{12}$$

k = 1, 2, … m

For a representation in state variable space, we built the vector of the state variables:

$$x = \begin{bmatrix}x_1\\ x_2\\ L\\ x_{2n}\end{bmatrix} \tag{13}$$

$x_i(t) = q_i(t)$, i = 1, 2, … n

$$x_{i+n}(t) = \dot{q}_i(t),\ i = 1, 2, \ldots n \tag{14}$$

With these notations, the equations (9) – (12) become (15) and (16):

$$\begin{bmatrix}\dot{x}_1\\ \dot{x}_2\\ L\\ \dot{x}_n\\ \dot{x}_{n+1}\\ \dot{x}_{n+2}\\ L\\ \dot{x}_{2n}\end{bmatrix} = \begin{bmatrix}x_{n+1}\\ x_{n+2}\\ L\\ x_{2n}\\ f_1(x)\\ f_2(x)\\ L\\ f_n(x)\end{bmatrix} + \begin{bmatrix}0\\ 0\\ L\\ 0\\ B_1(x)\\ B_2(x)\\ L\\ B_n(x)\end{bmatrix} \times \begin{bmatrix}\tau_1\\ \tau_2\\ L\\ \tau_n\end{bmatrix} \tag{15}$$

$$\begin{bmatrix}y_1\\ y_2\\ L\\ y_m\end{bmatrix} = \begin{bmatrix}C_1(x)\\ C_2(x)\\ L\\ C_m(x)\end{bmatrix} \tag{16}$$

We establish the notations:

$$A^*(x) = \begin{bmatrix} x_{n+1} \\ L \\ x_{2n} \\ f_1(x) \\ L \\ f_n(x) \end{bmatrix}; B(x) = \begin{bmatrix} 0 \\ L \\ 0 \\ B_1(x) \\ L \\ B_n(x) \end{bmatrix}; \quad (17)$$

$$C(x) = \begin{bmatrix} C_1(x) \\ C_2(x) \\ L \\ C_m(x) \end{bmatrix}; u = \begin{bmatrix} \tau_1 \\ \tau_2 \\ L \\ \tau_n \end{bmatrix}$$

where A, B, C and u have the dimensions: [2n x 1], [2n x n], [m x 1] and [n x 1].

In this case, the relations (15) and (16) become (18) and (21) and hereafter, (20) and (22).

$$\dot{x}=A^*(x)+B(x)\times u \quad (18)$$

From relations (17) we can see that $A^*(x)$ can be written:

$$A^*(x) = A(x) \cdot x \quad (19)$$

where A(x) is a [2n x 2n] matrix. The relation (18) becomes

$$\dot{x}=A(x)\times x+B(x)\times u \quad (20)$$

$$y = C(x) \quad (21)$$

Because output hexapod variables are represented by internal coordinates $q_i(t)$, (21) becomes:

$$y(t) = C\cdot x(t) \quad (22)$$

The relations (20) and (22) define the input-state-output relations of the hexapod mobile robot.

3. FAULT DETECTION AND IDENTIFICATION (FDI) PROCESS TO THE HEXAPOD ROBOT

The FDI concept is a very important element in automat control theory. Its implementation in practical applications is made in two modalities: physical redundant processes, where control structures with parallel processing of the information and analytical redundant processes are realized, which supposes that the processing of the information is made at a superior level for identifying the changes due to the faults.

The main requirements imposed to a FDI algorithm are: fast response when a fault arises, robustness with regard to model errors and system noises, reduced risk for the generation of false alarms, smaller computation effort.

Here we will use the second modality and for that the dynamic model of the hexapod robot is very important. By this method, the actualized model M_A (obtained by the on-line identification of the system) is permanent compared with nominal model M_N (without faults). This algorithm with two phases is presented in Fig. 2.

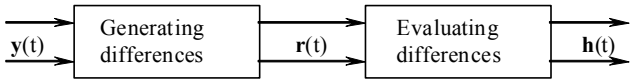

Fig. 2. The two phases of the FDI algorithm

where y(t) is the vector of the experimental information (measured parameters), r(t) is the residual vector (contains the differences related to ideal parameters) and h(t) is the vector of the decision and evaluating signals.

In Fig. 3 the external variables of the hexapod robot system are presented:

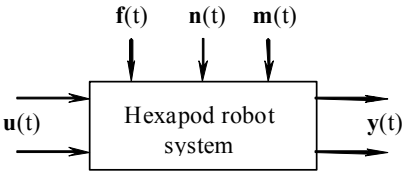

Fig. 3. The external variables of the hexapod robot system

x(t), u(t) and y(t) are state, input and output vectors, f(t) is the error vector, n(t) is the vector of the external perturbations, m(t) is the vector of the errors of the robot model.

The elements of the hexapod robotic system exposed to faults are: the actuator system, the mechanical structure of the robot and the sensorial system (Fig. 4).

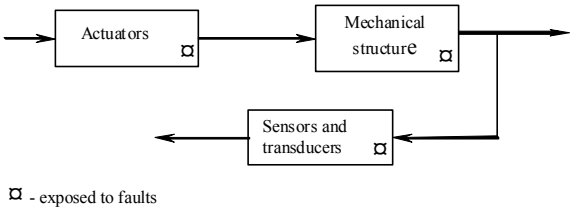

Fig. 4. Elements of the robotic system exposed to faults

With this information the model (20), (22) becomes:

$$\dot{\mathbf{x}}(t) = Ax(t) + Bu(t) + E_x f(t) + F_x n(t) + G_x m(t)$$
$$y(t) = Cx(t) + E_y f(t) + F_y n(t) + G_y m(t) \quad (23)$$

Analytical redundancy concept which is based on etalon models has two design methods: state estimation and parameter identification. We use here the second method which is represented in Fig. 5 where: RS – real system (hexapod robot), PIB – parameter identification block, M_A and M_N - actualized and nominal model of the hexapod mobile robot, ΔM – block which generates the parameter differences (residuals r(t)), DEB – decision and evaluating block, CS – control system.

Supposing the system structure is known, we can make the dynamic nominal model of the robot:

$$M_N:\begin{cases}\dot{x}_n(t)=f\left[x_n(t),\, u(t),\, p_n,\, t\right]\\ y_n(t)=g\left[x_n(t),\, u(t),\, p_n,\, t\right]\end{cases} \tag{24}$$

where p_n is the vector of the real parameters and it has m components:

$$p_n = [p_{n1},\, p_{n2},\, \dots\, p_{nm}]^T \tag{25}$$

$$M_A:\begin{cases}\dot{x}_e(t)=f\left[x_e(t),\, u(t),\, p_e,\, t\right]\\ y_e(t)=g\left[x_e(t),\, u(t),\, p_e n(t),\, t\right]\end{cases} \tag{26}$$

where n(t) is added noise and p_e is the vector of the estimated parameters:

$$p_e = [p_{e1},\, p_{e2},\, \dots\, p_{em}]^T \tag{27}$$

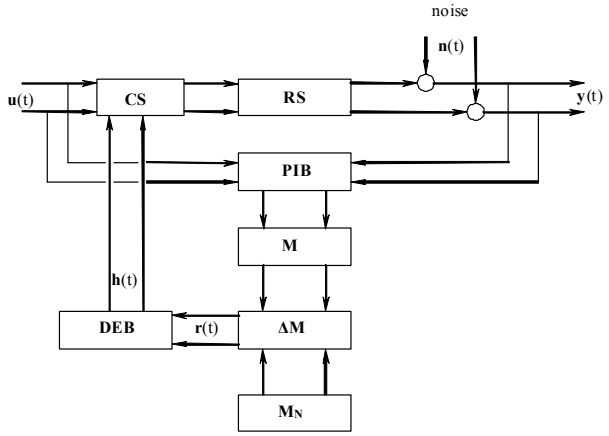

Fig. 5. FDI by parameter identification

For detection and identification of the faults, the parameter vector of real system is permanently evaluated, but indirectly, by the vector of the estimated parameters p_e. For that, the error criterion is minimized:

$$E=\int_{t}^{t+T_0}[y(\tau)-y_e(\tau,p_e)]^T[y(\tau)-y_e(\tau,p_e)]d\tau \tag{28}$$

In (28) $y(\tau)$ is output vector of RS and $y_e(\tau, p_e)$ are outputs of the estimated system. We impose:

$$\frac{\partial E}{\partial p_i}=0,\quad \forall i=\overline{1,m} \tag{29}$$

Solving the system (29) which has m equations with m unknown variables we obtain explicit mathematical relations and determine the vector p^*_e:

$$p^*_e=\left[p^*_{e1},\, p^*_{e2},\, ...,\, p^*_{em}\right]^T \tag{30}$$

E has a minimal extreme point if it verifies the following need:

$$\frac{\partial^2 E}{\partial p_{ei}^2}>0,\quad \text{for } p_{ei}=p^*_{ei},\ \forall i=\overline{1,m} \tag{31}$$

With the vectors p_n and p^*_e we can determine the difference ΔM:

$$\Delta M:\ r(t)=p_n-p^*_e=[p_{ni}-p^*_{ei}]_{i=1,2,\dots m} \tag{32}$$

4. ADAPTIVE CONTROL SYSTEM

We consider the control system from Fig. 5 (**CS**) to be an adaptive control system (Fig. 6) and we consider for that the dynamic model of the robot (20) and (22).

The actualized reference model is:

$$\dot{x}_m=A_m x_m+B_m u,\ y_m=C_m x_m \tag{33}$$

where A_m, B_m and $\mathbf{C}_m$ are constant matrices which have the dimensions: [2nx2n], [2nxn], [mx2n].

The adaptive system task is to determine the parameter changes of the control system so that the state vector of the robot tends to state vector of the model. We consider the matrices Γ and **Δ** with dimensions: [2nx2n] and [2nxn]. Their coefficients $\gamma_{ij}(t)$, $\delta_{ij}(t)$ help us to design the adaptation law.

$$\Gamma=A_m-A(x),\ \Delta=B_m-B(x) \tag{34}$$

$$\gamma_{ij}(t)=a_{mij}-a_{ij}(\mathbf{x}(t),t)\ \ i,j=1,2,\dots 2n$$

$$\delta_{ij}(t)=b_{mij}-b_{ij}(\mathbf{x}(t),t)\ \ i=1,2,\dots 2n,\ j=1,2,\dots n \tag{35}$$

Initially, a_{ij} and b_{ij} are the coefficients of the model (20), afterwards they have a role helping the error to converge to zero. The adaptation mechanism establishes their temporal evolution. So, we define the adaptation error and error derivative:

$$e=x_m-x,\ \dot{e}=\dot{x}_m-\dot{x} \tag{36}$$

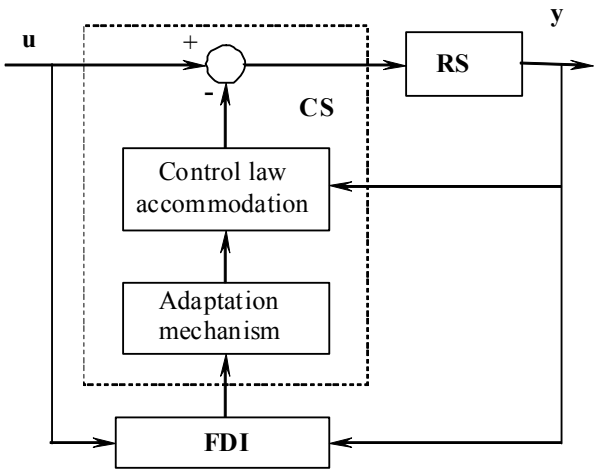

Fig. 6. Adaptive control system of the hexapod

If we use the expressions of x_m and x from (20) and (33), we obtain:

$$\dot{\mathbf{e}}=A_m x_m-A(x)x+(B_m-B(x))u \tag{37}$$

If we use the definition of the error (36), we have:

$$\dot{\mathbf{e}}=A_m e+(A_m-A(x))x+(B_m-B(x))u \tag{38}$$

The relation (38) depicts the mathematical model of the error and it defines the adaptation system. This mechanism works correctly when:

$$\lim_{t\to\infty} e(t)=0 \tag{39}$$

To analyze the stability conditions of the relation (38) we can use the second Lyapunov method like in Ivanescu (1994). So, there is a positive definite and symmetric matrix P which is a solution for the matrix relation:

$$A_m^T P + P A_m = -Q \tag{40}$$

where Q is, likewise, a positive definite matrix. In Ivanescu (1994) the stability conditions are obtained:

$$\mu_{ij}\dot{\gamma}_{ij} + x_j e^T p_i = 0$$

$$\nu_{ij}\dot{\delta}_{ij} + u_j e^T p_i = 0 \tag{41}$$

where μ_{ij} and υ_{ij} are positive and constant parameters, p_i is the column i from matrix P, x_j and u_j are the elements ji from the vectors x and u, respectively. The relations (41) depict the adaptation mechanism. By a integration process we can obtain the matrix coefficients $\gamma_{ij}(t)$ and $\delta_{ij}(t)$ which allow the calculus of the adapted matrices A and B from relations (34) according to variables x_j, u_j and the error e. The vectors p_i can be established off-line depending on the reference chosen model.

5. VARIABLE STRUCTURE CONTROL

In this chapter we consider the situations when the faults are produced by blocking of some links of the legs. For describing these events we establish a data base with mathematical models (filters), one model (filter) for every possible situation (Fig. 7). One of the filters is the healthy state. The outputs of the real system are permanently compared with the outputs of the filters and a testing and control block (TCB) analyzes the comparison result and establishes one action assumption. According to the implemented algorithm in TCB, an action assumption (hypothesis) has the best probability to be true if the residual vector concordant with that hypothesis is most contiguous to zero (Iancu and Vinatoru, 2003; Willsky, 1976).

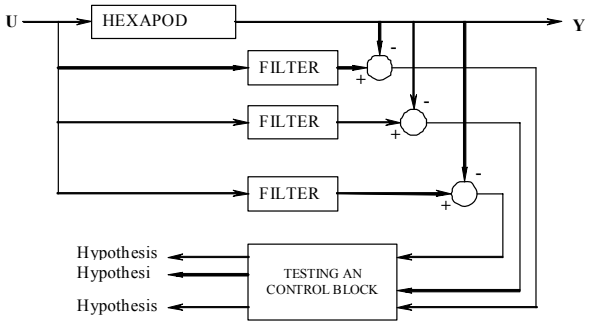

Fig. 7. FDI by multiple filters method

We consider the hexapod mobile robot system, when it is possible to block one or more links and when we use the multiple filters method, a variable structure system because the control system can change control parameters according to the changes of the system structure.

6. CONCLUSIONS

This paper presents a fault-tolerant control system for a hexapod mobile robot. First, a description of the dynamic model of the hexapod mobile robot by a system of differential equations is made and after that, a representation of the system in state variable space is obtained. A fault detection and identification (FDI) algorithm is proposed. The FDI concept is a very important element in automat control theory. Its implementation in practical applications is made in two modalities: physical redundant processes, where the control structures with parallel processing of the information and analytical redundant processes are realized, which suppose that the processing of the information is made at a superior level for identifying the changes due to faults. The modality used here is the second process. By this method, the actualized model obtained by the on-line identification of the system, is permanent compared with nominal model (without faults). The adaptive control system for uncertain non-linear systems proposed here has two main blocks: adaptation mechanism block which implements the mathematical model of the adaptation error and control law accommodation block which changes the characteristics of the control law. Finally, the authors propose the hexapod mobile robot which is open to fault events to be a variable structure system and analyze a specific control method. The future work will be focused on topics like collaborative system, hierarchical control and robust controller. The system discussed here, a hexapod mobile robot, is a multi-chain robotic system and it is a collaborative system because it is composed by a number of co-operant subsystems: the body and six legs. The control system is a hierarchical control system with two levels. The upper level coordinator gathers all the necessary information to resolve the force distribution. Then, the lower-level local control problem is treated as an open-chain manipulator control problem. A control system can switch itself between one robust control strategy designed under normal operating conditions and other control strategies under the fault conditions. For some simple systems, a robust controller is sufficient to achieve a fault tolerance. The changes in system parameters caused by faults can have a significant effect on the global stability of the hexapod mobile robot motion and it may be impossible to stabilize this system by only a robust controller. Some simulations results will be presented and discussed.

REFERENCES

1. **Manko D. J.** (1992), *A General Model of Legged Locomotion on Natural Terrain*, Kluwer Academic Publishers, Westinghgouse Electric Corporation.
2. **Tsai C. R., Lee T. T.** (1998), A Study of Fuzzy-Neural Force Control for a Quadrupedal Walking Machine, *Journal of Dynamic Systems, Measurement and Control*, 120, 124-133.
3. **Tsai C. R., Lee T. T., Song S.M.** (1997), Fuzzy Logic Control of a Planetary Gear Type Walking Machine Leg, *Robotica Journal*, 15, 533-546.

4. **Song J., Low K.H., Guo W.** (1997), A Simplified Hybrid Force/Position Controller Method for the Walking Robots, *Robotica Journal*, 175, 583-589.
5. **Brooks R.A.** (1989), *A Robot that Walks*; Emergent Behaviors from a Carefully Evolved Network, A.I. Memo 1091, Artificial Intelligence Laboratory, MIT.
6. **Ferrell C.** (1995), A Comparison of Three Insect Inspired Locomotion Controllers, *Robotics and Autonomous Systems Journal*, 16, 135-159.
7. **Blanke M., Kinnaert M., Lunze J., Staroswiecki M.** (2003), *Diagnosis and Fault Tolerant Control*, Springer-Verlag, Berlin-Heidelberg, Germany.
8. **Zhang Y. M., Jiang J.** (2003), Bibliographical Review on Reconfigurable Fault-Tolerant Control Systems, *Proc. of IFAC Symp. SAFEPROCESS'03*, Washington, DC, 265-276.
9. **Patton R. J.** (1997), Fault tolerant control: the 1997 situation, P*roceedings of IFAC Symposium on Fault detection, supervision and safety for technical processes*, Hull, UK, 1033-1055.
10. **Blanke M., Frei C., Kraus F., Patton R. J., Staroswiecki M.** (2000), What is fault tolerant control?, *Proceedings of the 4th IFAC Symposium on Fault detection, supervision and safety for the technical process*, Budapest, Hungary, 40-51.
11. **Wang H., Wang Y.** (2001), Neural-network-based fault-tolerant control of unknown nonlinear systems, *IEE Proc. Control Theory Appl.*, 146 (5), 389-398.
12. **Iichman H.** (1993), Non-identifier-based high-gain adaptive control, Chapter 5, Springer-Verlag, London.
13. **Kabore P., Wang H.** (2001), Design of faults diagnosis filters and fault tolerant control for a class of non-linear systems, IEEE Trans. Autom. Control, 46(11), 1805-1809.
14. **Polycarpou M. M.** (2001), Fault accommodation of a class of multivariable nonlinear dynamical systems using a learning approach, *IEEE Trans. Autom. Control*, 46(11), 736-742.
15. **Loose D. P., Weise J. L., Eterno J. S., Barrett N. M.** (1985), An automatic redesign approach for reconstructable control systems, *IEEE Control System Mgmt*, 5(2), 16-21.
16. **Veillette R. J., Medanic J. B., Perkins W. R.** (1990), On the design of reliable control systems, *Proceedings of the 1990 American Control Conference*, 3030-3035.
17. **Wallacc R. J.,Vander V.** (1984), Control system reconfiguration, *Proceedings of American Control Conference*, 1741–1745.
18. **Veillette R. J.** (1995), Reliable linear-quadratic state-feedback control, *Automatica Journal*, 31(1), 137-143.
19. **Zhihua Q., Ihlefeld C., Yufang M. J., Apiwat A. S.** (2003), Robust fault-tolerant self-recovering control of nonlinear uncertain systems, *Automatica Journal*, 39(10), 1763-1771.
20. **Steward D. V.** (1962), On an approach to techniques for the analysis of the structure of large systems of equations, *SIAM Revue*, 4, 321-342.
21. **Lin C. T.** (2001), Structural controllability, *IEEE Trans. Autom. Cont.*, AC-19(3), 201-208.
22. **Murota K.** (1987), *Systems analysis by graphs and matroids. Structural solvability and controllability*, Springer-Verlag, Berlin.
23. **Meyer M., Le Lann J.-M., Koehret B., Enjalbert M.** (1994), Optimal selection of sensor location on a complex plant using a graph oriented approach, *Computer Chemistry Engineering*, 18, S535-S540.
24. **Pana C. F., Stoian V., Pana D. M.** (2008), Dynamic Model of n-legged Robot, *Proceedings of the 3rd International Conference on Optimization of the Robots and Manipulators"-OPTIROB*, Predeal, Romania.
25. **Ivanescu M.** (1994), *Industrial Robots*, Ed. Universitaria, Craiova, Romania.
26. **Iancu E., Vinatoru M.** (2003), Analitical Methods for Fault Detection and Identification. Chapter 2, *Control Ingineering Series*, Ed. Universitaria, Craiova.
27. **Willsky A.S.** (1976), A Survey of Design Methods for Failure Detection in Dynamic Systems, *Automatica Journal*, (1976), Vol. 12, 601-611.

DEVELOPING AN EDUCATIONAL SOFTWARE CONTROLLING DATA TRANSFER OF SERIAL AND PARALLEL PORTS

İlhan TARIMER[*], Serkan ÖRÜCÜ[**], Rıza GÜRBÜZ[**]

[*]Technical Education Faculty, Department of Electronics and Computer Education, Kotekli Campus, 48000, Mugla,Turkey
[**]Çankırı Karatekin University, Technical and Business College, Turkey

itarimer@mu.edu.tr, ser_khanor@hotmail.com, gurbuz@cmyo.ankara.edu.tr

Abstract: In this study, it has been examined whether computer-based teaching software is applicable in today's electronic and computer teaching. By the improvement of today's computer teaching, people are able to reach information easily. Both indoor and outdoor of classroom works, teaching software, which supports learning, has been aimed to help both teachers and students. The educational software prepared in this study that can be used in the area of controls with parallel and serial computer ports. In this study, basic properties of parallel-serial ports, to use them in mechatronics and their using facilities have been explained. How to program these ports together with their connections have been embedded into the educational teaching software. Thus, according to its algorithm and frame, this educational software interface developed can be used for general mechatronics training.

1. CAT SOFTWARE

CAT software change according to the area which they are used and according to specifications of the users. For instance, specifications of a lesson software which is prepared for the usage of one's his/her own working style and for himself herself is obviously different from the specifications of a lesson software which will be applied in a lesson time, in the laboratory under the under the control of a teacher (www.aof.edu.tr/kitap/IOLTP/2276/unite10.pdf 2006).

Computer which operates the software leads among the sectors which have an interrelation with teaching softwares. The first student is the person which communicates with software that can be found frequently. There is not an exception; software is controlled by the first user. The second student is the other student who is also going to use the computer. In the simultaneous applications, the software can be used by students or teachers, or by a group. Teacher is also the director of the software in a laboratory environment (www.aof.edu.tr/kitap/IOLTP/2276/unite10.pdf, 2006; www.ceit.metu.edu.tr/~yuksel/cai-1.doc, 2006).

The first part of program which called "What is parallel port", trains students about parallel port basics, and signal types. The code snippet supports learners to understand parallel port fundamentals with several animations as code based and sound records. While reading these explanations and code based animations with sound records, powerful learning effects would occur. The code based animations initially shows how to send data via parallel ports. The results which got from experiment kits and screen definitely seem to be obtained at the same time. Once the lessons completed, learners can use testing part of program to define its learning level. The second part of program which called "What is serial port" has been prepared as similar as to the program of "What is parallel port", but it includes only serial port lessons.

2. CONTROL OF PORT

Electronic ways which are used for getting and sending data are called as communication points (http://www.cs.itu.edu.tr/~gunduz/courses_2005/mikroisl/slides/d8.pdf, 2006). They are known as "ports" as well. These pins are used for programming hardware or sending data to the computer over the motherboard. The ports of a computer are introduced in below lines.

2.1. Parallel communication and parallel port

If a separated line is used for each bit of the data while transporting a datum, such kind of a communication is called as parallel communication. In the Fig. 1, two units are connected each other by using the technique of parallel communication.

On DB-25 pins, there are 3 ports named, data, status and control (Fig. 2). All of these pins are the exit pins at the level of TTL. The exit of parallel port is at the level of TTL Logic. Even though it changes one computer to another that the capacity of port's current absorbing and carrying; it is limited to a few miliamperes their level of current which will be absorbed and carried. In the figure-2 Port of data, status and control are given with their pin numbers.

It has been thought to use Visual Studio.NET 2005 platform (Tuğay, 2005; Yanik, 2004) for preparing the program on controlling the ports in this study. But Visual Studio.NET 2005 platform doesn't include any component for the control of parallel port, so, only way to reach the addresses of parallel ports is installing an external component. Mostly, inpout 32 DLL is preferred which is mostly known. Also this DLL is used for its blocking the operating systems to reach to ports in the systems which are Windows NT based. Inpout 32 DLL's description in the programming table of C# [1, 2] is like that; firstly that code is added to the form. Inpout 32 DLL basically includes two functions:

using System.Runtime.InteropServices;

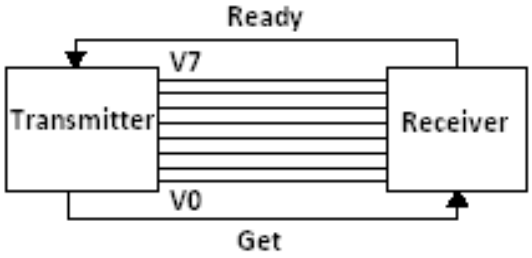

Fig. 1. Two connected nodes for parallel communication

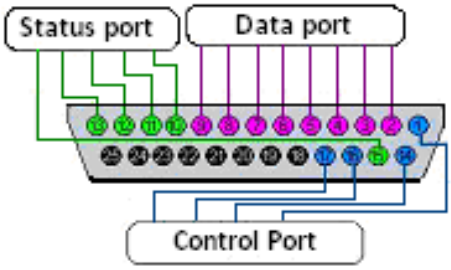

Fig. 2. Data, Status and Control ports

These are Inp32 and Out32. Inp32 is used to read the data which come from pointed addresses, and on the others hand addresses which will be read are defined with variables from the genre of integer. Out32, similar to Inp32, is defined with variables from the genre of integer which includes the values of data which will be written to that address and the address to write the data (http://www.codeproject.com/csharp/csppleds.asp, 2006; http://msdn2.microsoft.com/enus/library/system.io.ports.serialport(VS.80).aspx2006).

```
public class read_port
{[DllImport("Inpout32.dll")]
public static extern short Inp32(int address);}
public class write_port
{[DllImport("inpout32.dll")]
public static extern void  Out32(int adress, int value);}
```

To write data onto the parallel port after the definitions of DLL and function, following code pattern is used (http://www.csharpnedir.com/makalegoster.asp?MId=576, 2006; Axelson, 1998).

```
private int baseadres = 0x378;
private void timer1_Tick(object sender, System.EventArgs
e)
scan_status_port(baseadres);}
public static int Read_status_port(int base_address)
{int veri =read_port.Inp32(base_address+1);
data= data & 120; return (data >> 3);}
```

By the help of a timer which is integrated into the form, if a code is written as "read_status port" to scan the ports in a specific time, the data which come from port are scanned automatically in a specific time. Reading data by using data port of parallel port is easier and done as shown below;

```
write_port.Out32(888, x);
```

2.2. Serial Communication and Serial Port

In version 2005 of C# programming language which is the one among Visual Studio.NET platforms, for port accesses, one of the components of this software is defined for only serial port (Karagülle, 2004). To be able to use serial port, firstly the component of serial port is added to the form in figure 3.

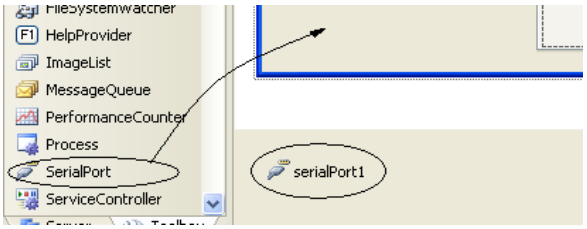

Fig. 3. Adding serial port component

The way to add the component of serial port is shown in the figure 3. This library supplement enables all of the functions related with the serial port to use altogether. Furthermore, an example to form some functions can be defined and can be given as like below lines (http://www.dotnetmagzin.de/itr/online_artikel/psecom,id,397,nodeid,31.html, 2006).

```
private void Form1_Load(object sender, EventArgs e)
{serialPort1.StopBits= StopBits.One;
serialPort1.DataBits = 8;
serialPort1.Parity= Parity.None;
serialPort1.BaudRate = 9600;
serialPort1.PortName = "COM1";
serialPort1.Open();}
```

When data transfer from serial port was being examined, the device developed for experiments must be installed. Thus, a code pattern is obtained to read and to write like
as one in the below lines;

```
string data_write = textBox1.Text;
serialPort1.WriteLine(data_write);
```

```
string data_read;
data_read = serialPort1.ReadLine();
```

Instead of this way, a delegate might be used for opening data process channel (Tuğay, 2005; Gümüşkaya, 2004). In this case, a code pattern is occurred like as ones in the below lines;

```
private delegate void run(string value);
private run serial_port_thread;
private void Form2_Load(object sender, EventArgs e)
{serialPort1.StopBits = StopBits.One;
serialPort1.DataBits = 8;
serialPort1.Parity = Parity.None;
serialPort1.BaudRate = 9600;
serialPort1.PortName = "COM1";
serialPort1.Open();
seri_port_thread=new run (port_listen);}
private void button1_Click(object sender, EventArgs e)
{string a = textBox1.Text; serialPort1.WriteLine(a);}
private void get_data(object
sender,System.IO.Ports.SerialDataReceivedEventArgs e)
{string data = serialPort1.ReadExisting();
this.Invoke(this.serial_port_thread, new object[] {data });}
```

The educational software program has been designed as two separated parts. One of them is for the kits and the other is for the experimental devices. They could be combined constructional controlling of this computer and the software according to port types which people need. A sample has been given in figure 4. It shows the animation of data transfer which is used in the part of "what is parallel port?" which is one of P-Kod software. The other sample software has been given in the figure 5 which shows transferring data from/to the addresses of parallel ports according to the boxes which are clicked.

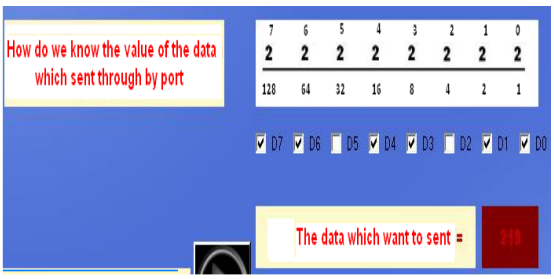

Fig. 4. An animation written with codes

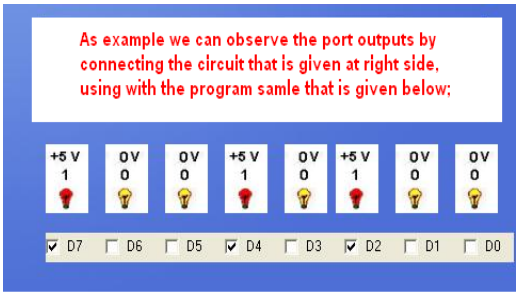

Fig. 5. A sample software usage panel

By the time first installation, the form view of "what is parallel port" program which is the first part of P-Kod software is shown as in the figure 6. When it is clicked to the parallel port button, the screen view transforms its form into the figure below (Fig. 7). The first part of the software appears to the form that concerns with the teaching of the lecture topic. At this part, the basic functions of parallel ports could be examined as audio–visual. However an audio and video playback dll which is one of the dll of Direct X has been used in this coding section of the program.

Fig. 6. P-KOD software main page

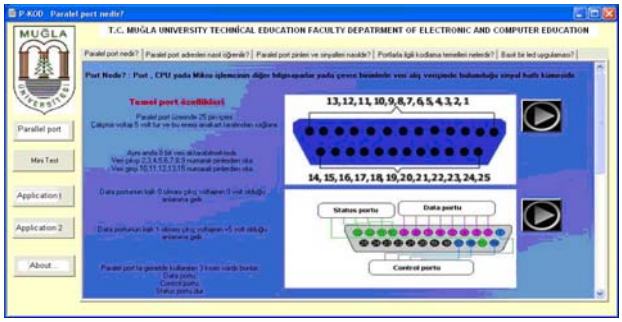

Fig. 7. P-KOD software teaching part

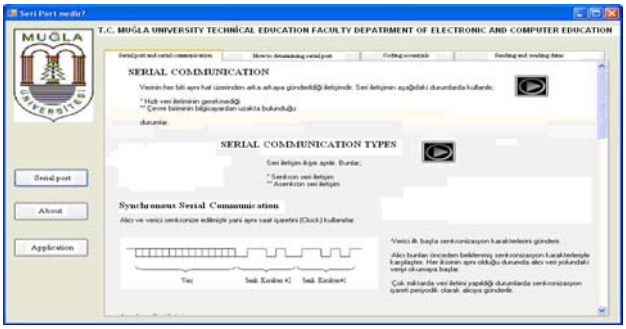

Fig. 8. The software tutoring part

"What is serial port", which is the second part of P-Kod software is similar to the view of the first installation section of "what is parallel port". When clicked the button "serial port", it transforms its screen view into the view as it seen in figure 8. The view of mini experiment kits are given in the figure 9 which was prepared for P-Kod. The circle of data reading contains 4 units of buttons and resistances, and the circle of data writing contains 8 units of LEDs and 8 resistances.

Fig. 9. Mini experiment kits

3. USING THE SOFTWARE INTERFACE AND COMPARISONS

Once clicked on to the button of parallel port, the initial section of the software application related with teaching lesson appears to our face. In this section, features of parallel port can be examined as audio visually. After that it has been stated pin numbers and basic features of data, control and status ports (Fig. 10). At the next steps of this software interface, there is a sample workable application using with together an experiment kit. To be able to have the sample software interface to connect the experiment kit numbered 1 with the cable belonging to that one, they must connect to each others via normal apparatus (Fig. 9). The first section of serial port tutoring is being related with serial communication. Then general specifications of serial port have been prepared to be taught to learners in a form of charts as audio visual (Fig. 11).

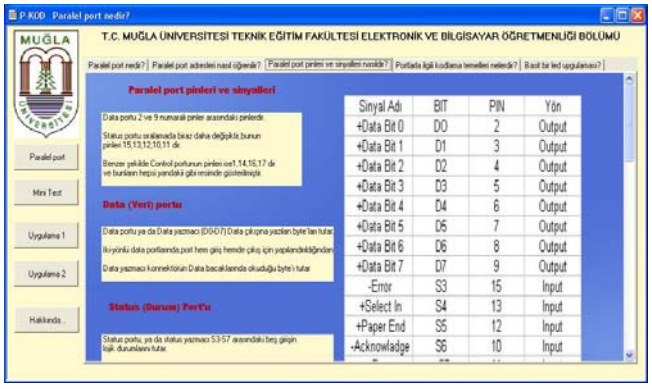

Fig. 10. Pin numbers and basic features

When clicked on to the button of application, a new segment is opened. This segment is the last section of the software interface and it makes the two computers to communicate together (Fig. 12). In both sections there have been several tests in which learning levels can be evaluated. Therefore this software includes open source codes as well and it steers learners to benefit from these codes for ascending their personal experiences (Fig. 13).

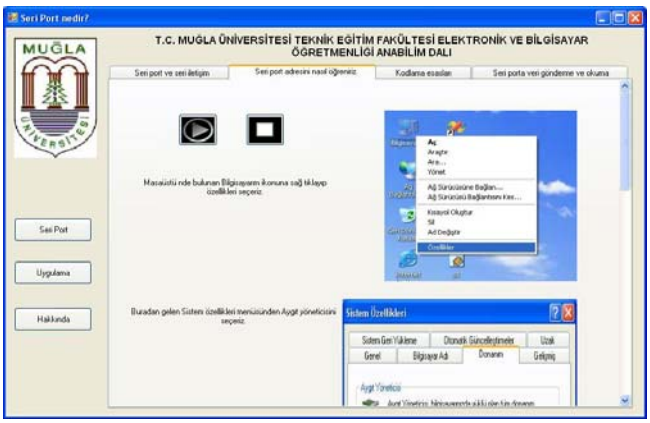

Fig. 11. Experiment kit

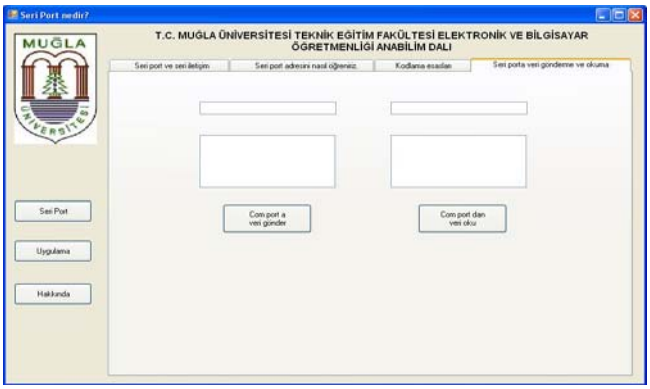

Fig. 12. Application window of the software interface

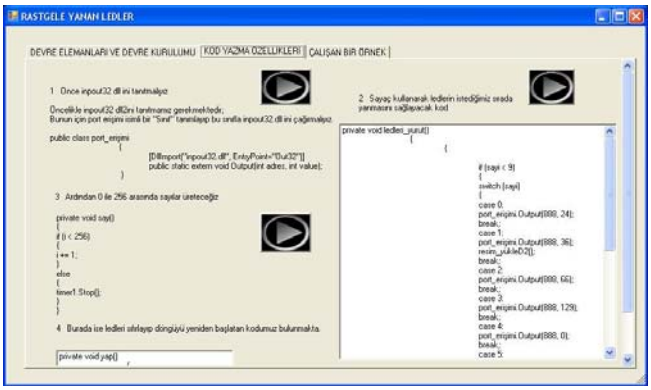

Fig. 13. Open source codes

These codes in which any learners interested in using of them have been designed and written according to the system of chart. So, students and learners have got a re-playing chance. Thus, this software interface forms the learning and teaching process more rapid, more retentive and absolutely independent from an experimental environment.

4. CONCLUSIONS

In this study, it has been examined an educational software for teaching of parallel and serial ports in electronics, computer and mechatronics. To do this, a computer based teaching programs have been developed by using C# pro-

gramming language which is one of the Visual Studio.NET 2005 platform programs. The software developed provides the users to learn port control theories both on their own and under control of a teacher. Although the port addresses used in this application are stationary, the user can also choose other addresses that he wants to write. The entire program modules were powered by a graphic user interface. It has been examined within the program, how audio sources support learners besides the visual sources. From this aspect, the results obtained would be a pioneer amongst port control teaching programs. With this technique, both theory and applications in area of electronics, computer and mechatronics would be applied together and there might be no need for installing and running additional hardware equipments.

REFERENCES

1. **Karagülle İ.** (2004), *Visual C#.Net Introduction Guide*, Türkmen Pub. House, Istanbul.
2. **Yanık M.** (2004), *Microsoft Visual C#.Net*, Seckin Publishings.
3. **Tuğay G.** (2005), *Electronics Hobby*, ALFA Publications, Istanbul.
4. **Axelson J.** (1998), *Parallel Port Complete*, Lakeview Research, USA.
5. **Gümüşkaya H.** (2004), *Microprocessors and Computers*, ALFA Publications, Istanbul.
6. Anadolu University, Open Learning Faculty Lecture Notes, M. Emin Mutlu, www.aof.edu.tr/kitap/IOLTP/2276/unite10.pdf, (Access: January 2006).
7. ITU, Lecture Notes, Şule Öğüdücü, http://www.cs.itu.edu.tr/~gunduz/courses_2005/mikroisl/slides/d8.pdf (Access: January 2006).
8. Levent Saltuklaroğlu, http://www.codeproject.com/csharp/csppleds.asp, (Access: Feb. 2006).
9. METU, Lecture Notes, Yüksel Göktaş, www.ceit.metu.edu.tr/~yuksel/cai-1.doc, (Access: January 2006).
10. http://msdn2.microsoft.com/enus/library/system.io.ports.serialport(VS.80).aspx, (March 2006)
11. http://www.csharpnedir.com/makalegoster.asp?MId=576, Fevzi Özgül, (Access: April 2006).
12. http://www.dotnet-magazin.de/itr/online_artikel/psecom,id,397,nodeid,31.html Markus Palme, (Access: January 2006).

ISMAIL AL JAZARI MACHINES AND NEW TECHNOLOGIES

Abdullah UZUN[*], Fahri VATANSEVER[**]

[*]Sakarya University, Sakarya Vocational School, Computer Programming, İzmit cad. Kapali spor salonu yani, 54187, Sakarya, Turkey
[**]Sakarya University, Technical Education Faculty, Teknik Eğitim Fakültesi, kampus, Sakarya, Turkey

auzun@sakarya.edu.tr, fahriv@sakarya.edu.tr

Abstract: Al-Jazari was a 12th Century Turkish Scientist, Engineer and writer. His full name was Badi Al-Zaman AbulI-Izz Ibn Ismail Ibn Al-Razzaz Al-Jazari. He lived in Diyarbakir region in Turkey (1206 AD). As his town name is Cizre, the modern Turkish scripting of Jizra , his last name is known as Jazari (Uzun, 1997). Badi Al Zaman means "prodigy of the Age" and was applied to other well-known men (Hill, 1974). He served the Artuks a Seljuks dynasty in Diyarbakir, as a chief engineer – as did his father before him. He invented the crankshaft and some of the first mechanical clocks, driven by water and weights- used water power. He authored and drawed 60 inventions in his book "Al-Jami Bain Al-Ilm Wal-Amal Al-Nafi Fi Sinat'at Al-Hiyal" (The Book of Know-ledge of Ingenious Mechanical Devices). Kitab al-Hiyal is an interesting work on automatic control mechanism, fountains, devices, pipes, valves and siphons. The importance and originality of Kitab al-Hiyal is due to its being an earlier example of the automatic control studies in the history. There are a number of manuscripts of Jazari's work in Oxford, Leiden, Paris, Dublin and İstanbul. Equally cranks may have first been documented by Al Jazari – 300 years before western engineers achieved this (Francesco di Giorgio Martini and Leonardo Da Vinci). He used some kind of symbols for understanding of his drawings like using of electronic circuits. We found that his machine drawings and manufacturings quite qualified understanding (http://orionrobots.co.uk/tiki-index.php?page=Al+Jazari). The aim of this study is to review and examine Al Jazari's drawings and then, to compare and examine with the new technology period.

1. INTRODUCTION

Abu Al Izz Ismail al Jazari lived in Amid, that is called now Diyarbakir in South-east of Anatolia in Turkey, (12th century) during Artuk Seljuqs period. He had spent twenty-five years in service of Seljuqs Sultans (Nasiruddin Abul Fath Muhammed bin Karaaslan and his father).

The Artuks were a Turcoman dynasty descended from Artuk, a general who served Malik Shah, the Seljuq Sultan, at the end of the 5th/11th century. They were divided into two main branches, descended from two sons of Artuk-Ilghazi and Sukman. Al Jazari's masters belonged to the Sukman branch of family (Hill, 1974).

We know from his book that Al-Jazari wrote that book, which finished (16th jan . 1206), on the request of Sultan Nasiral-Din Mahmud bin Karaaslan after spending twenty five years in his service (1198). Al-Jazari wrote his book in Arabic alphabet that was dynasty palace's language at that time.

He frankly acknowledged that he got some knowledge from the formers such as Archimedes. "I have studied the books of the earlier (scholars) and the works of the later [craftsmen]-masters of ingenious devices with movements like pneumatic (movements), and water machines for the constnat and solar hours, and the transfer by bodies of bodies from their natural positisons.I have contemplated in isolation and in company the implications of proofs. I considered the treatment of this craft for a period of time and I progressed, by practising it, from the stage of book learning to that of witnessing and I have taken the view on this matter of some of the ancients and those more recent (scholars). I was fervently attached to the pursuit of this subtle science and persisted in the endeavour to arrive at the truth. The eyes of opinion looked to me distinguish myself in this beloved science. Types of (machines) of great importance came to my notice, offering possibilities for types of marvellous control.

His book showed a deep understanding, and is still analyzed today by the world's top engineers. Prof. Lynn White Jr. writes: "Segmental gears first clearly appear in Al-Jazari, in the West they emerge in Giovanni de Dondi's astronomical clock finished in 1364, and only with the great Sienese engineer Francesco di Giorgio (1501) did they enter the general vocabulary of European machine design" (http://en.wikipedia.org/wiki/Al-Jazari).

I assembled that in a book (lit. Introduction Mugaddima) comprising fifty specimens and it is divided into six categories. I have been thorough in description and in particulars. In what I have written I have used foreign names passed on by earlier people and adherence to these has continued until to today; and other expressions made necessary by time. For the people of every epoch have [their own] language and every group of scholars have technical terms understood among themselves, and convertions familiar to them. For every specimen (shakl) I have drawn a picture, and have marked it with letters for guidance and have (also) put altenatives for these letters.

Catergory I. On the construction of clocks from which can be told the passage of the constant and solar hours-10 Charpters (it.specimens-ashkal).

Catergory II. On the construction of of vessels and figures suitable for driking sessions-10 Charpters.

Catergory III.On the construction of pitchers and basins for phlebotomy and ritual washing-10 Charpters.
Catergory IV. On the construction in pools of fountains which change their shape and of machines for the perpetual flute -10 Charpters.
Catergory V. On the construction of machines for raising water from standing water which is not deep and from a running river-5 Charpters.
Catergory VI. On the construction of different, dissimlar things -5 Charpters" (Uzun, 2003).

But according to Al-Jazari, some of these knowledge are correct some are not. Al-Jazari described approximately fifty mechanical devices in six different categories, including water clocks (one of his famous clocks was reconstructed successfully at the London Science Museum in 1976 and Istanbul Technical Universty in 1982), automata, combination locks, hand washing device (Wudhu machine) , machines for raising water, double acting pumps with suction pipes and the use of a crank shaft in a machine, accurate calibration of orifices, lamination of timber to reduce warping, static balancing of wheels, use of paper models to establish a design, casting of metals in closed mould boxes with green sand, and more. He is also regarded as one of the first recorded designers of a humanoid robot (cybernetics).

First his work was machine of Wudhu (preparing top ray, washing hands and face etc. before salah) for Sultan. Sultan admired his machine and asked him to write a book. That was claimed the first of his manuscript. There are a number of manuscripts of Al Jazari's work, which are available in İstanbul, London, Paris, Dublin, Leiden etc.

Ibn Ismail Ibn al-Razzaz Al-Jazari (1206 AD) was one of history's greatest engineers. He invented many automata and some of the first mechanical clocks, driven by water and weights. He was called Al-Jazari after the area where he was born. Since the pre-Islamic times, al-Jazira has been an economically prosperous region with various agricultural (fruit and cereal) products, as well as a prolific manufacturing (food processing and cloth weaving) system. Al-Jazira, which is the traditional Arabic name for northern Mesopotamia or Jazira is a town in the south-east Anatolia in Turkey (near Diyarbakir). His tomb is in that town. Al-Jazari draws on the works of its predecessors both from the Greeks (Philon, Heron and Archimedes) and Islamic scholars and engineers (Banu Musa brothers, Al-Khuwarizmi and Ridwan). His contribution was very important for the diffusion of knowledge in the Arabic world and after in Europe due to the translations of his books like "The Book of Knowledge of Ingenious Mechanical Devices" which contains more than 150 automata and mechanical devices.

Eilhard Wiedemann was the first most important researcher studied on Al Jazari's works. He (1852-1928) studied on Islamic science, medicine, mathematics and technology his life's work, and in these fields his writings are of great importance. His many articles are scattered among a number of learned German Periodicals. He was worked with Fritz Hauser, a German engineer. Al Jazari's works were examined by Wiedemann and Hauser in seven articles in various periodicals. These articles have several merits, and in particular they give a fairly clear understanding, to anyone with some measure of technical knowledge, of the design, construction, and operation of each of devices (Hill, 1974).

In 1974 Donald R. Hill translated and annotated Al Jazari's book in Boston –USA. His manuscripts were translated, and drawings additionally guieded to understanding. That book name is "The Book of Knowledge of Ingenious Mechanical Devices".

In 1951, Ibrahim Hakki Konyali for the first time mentioned about that manuscript in a magazine in Turkey. Dr. Ayhan Songar, Dr. Toygar Akman wrote about Al Jazari's work. Prof. Dr. Kazim Çeçen made one of Al jazari's machines (Water Clock) in Istanbul Technical Universty in 1980's. Prof. Dr. Atilla Bir wrote some article about his life and Works. 1997 first book was puplished in Konya about Al Jazari's life and his Works by Abdullah Uzun then 2004 his manuscripts full translated in Turkish.

2. HIS MACHINES IN COMPARISON TO SOME NEW TECHNOLOGIES

The first water clocks in their simplest form were used by the ancient civilizations of Babylonia and Egypt (Hill, 1974). After and before Al Jazari, a lot of water clocks and ingenious devices made in Asia Minor, Philon of Byzantium and Arabs. Some of those technologies was transferred to Spain and to Maghrib (Andalusia).

Al-Jazari's book delt with completely devices and automatas for multiple functions. What they have in common is the considerable degree of engineering skill required for their manufacture, and the use of delicate mechanisms and sensitive control systems. Many of the ideas employed in the construction of ingenious devices were useful in the later development of mechanical technology. Al-Jazari inherited the knowledge of his predecessors, but he improved on their designs and added devices of his own invention (http://www.history-science-technology.com/Articles/articles%206.htm).

Al-Jazari use some symbols like electronics works in his manuscript. He wrote and designed his machine very carefully. Pictures are nice and colours are not pale that are of great artistic merit. Some historians of art acknowledges that his manuscripts were illustrated in marvelous form and conditions.

Being honest and humble, he always expressed that he had got some technical principle from Archimedes and other previous scientists.

In 1206, Al-Jazari presented his "Book of Knowledge of Ingenious Mechanical Devices", devised for both educational and entertanment purposes, to the Sultan. In this singularly important work, he described contemporary labor-saving devices and unusual clocks, including some of his own designs. Even though the book does not contain descriptions of the astrolabe or balance, for which Arab scientists were famous, it plainly displays stronger and weaker aspects of Arabic engineering.

Most of the machines, with varying degrees of utility, used age-old principles of mechanics, including systems of weights, pulleys, gears, cams, and levers. The crankshaft was first described Al-Jazari, though it is not clear whether

or not it has been invented by him. In fact, some scientists say that he invented the crankshaft and some of the first mechanical clocks, driven by water and weights (http://en.wikipedia.org/wiki/Al-Jazira%2C_Mesopotamia Minor).

Fig. 1. Mechanical pump by Jazari

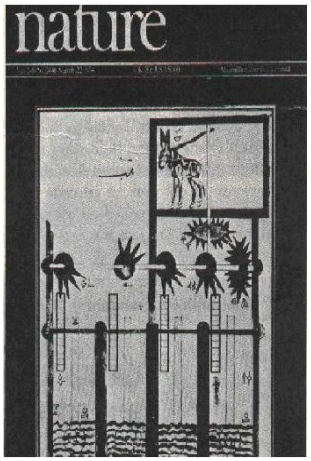

Fig. 2 Al-Jazari in the Nature magazine

Prof. Lynn White Jr. writes: "Segmental gears first clearly appear in Al-Jazari, in the West they emerge in Giovanni de Dondi's astronomical clock finished in 1364, and only with the great Sienese engineer Francesco di Giorgio (1501) did they enter the general vocabulary of European machine design".

Equally cranks may have first been documented by Al Jazari 300 years before Western Engineers achieved this (Francesco di Giorgio Martini and Leonardo Da Vinci) (http://en.wikipedia.org/wiki/Al-Jazira%2C_Mesopotamia_Minor).

Al-Jazari noted a number of practical joke devices in his text. Some were trick drinking vessels that appeared to contain water but could not be emptied. Others looked empty but produced water when tipped over.

In producing these not-so-useful inventions, Al-Jazari was typical of his age. The engineers of that time had a reputation for frivolous machines that dated back to the writings of the ancient Greeks. Had he lived in a different society, Al-Jazari might have put his ingenuity to a different purpose.

In Fig. 1, there is an automata for rotation gearwheels by means of water. Water flows into second section then axle and gearwheel rotates, so it triggers the other gear-wheel and rotation of the vertical axle and then, the rotation of the robot donkey, cupboard turning and rising water at last. This cycle is going as sketched in Fig. 1.

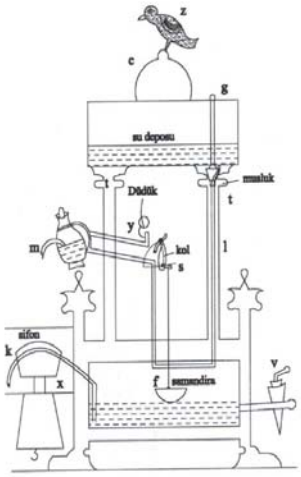

Fig. 3. Automatic Wudhu machine

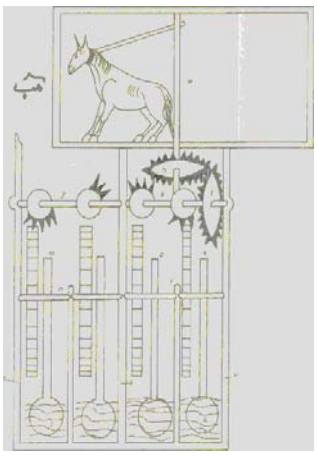

Fig. 4. 4 Effective water rising system (4 stroke cylinder)

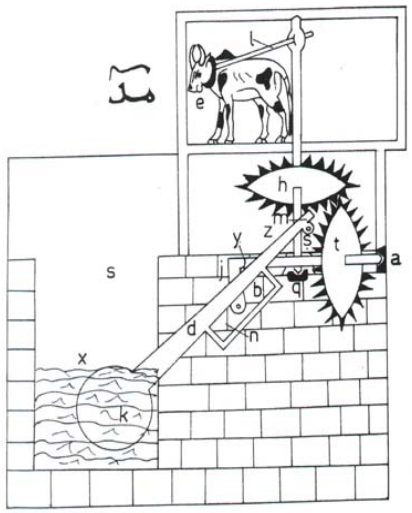

Fig. 5. Crank shaft system water rising machine

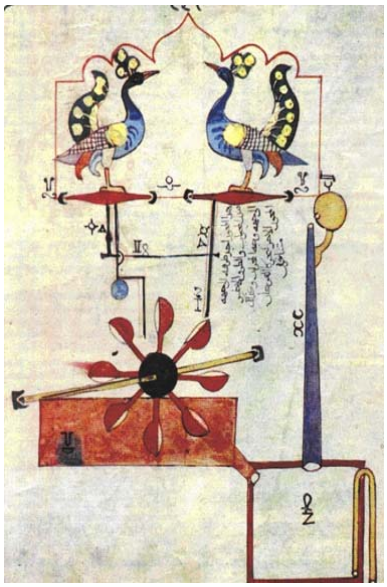

Fig. 6. Water Clock

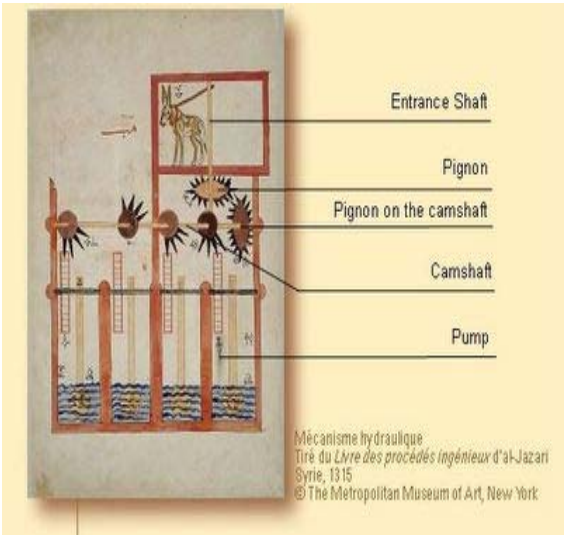

Fig. 7. Four effective water rising system

3. CONCLUSION

Al-Jazari's works and his book occupies an important place in the history of automata, mechanics, mechatrconics, automatic control, robotics and automated musical theaters. His pioneering work is duly acknowledged in most histories.

Al-Jazari was not primarily innovator, but this is not to imply that he made no innovations like this; the perfection of the tipping bucket, the reciprocating pump, measuring basin and some type of water clock. We should also include in his significant innovations his remarks that indicate that he had ideas about application of an escapement to a water-wheel (Hill, 1974).

The life stories of engineers such as Leonardo da Vinci, James Watt and many other scientists including their contributions are quite well known, but it is not very much known about Al Jazari's life. Today there is only Al Jazari's manuscript. As such, none of European scientists do know him nor his works, thus a substabtial attention is needed to be drawn on his possible impacts upon later generations of engineers. Al Jazari's idea and useful machines are in his manuscript but after him no-one has written and followed about him and his works. His drawings are shown with several remarks. He certainly used a technique that is indispensable for all engineering drawing.

Al Jazari, then, gives us the full engineering content of his work. For a given machine he tells us its appearance, purpose and functioning. He describes, step by step, the manufacture of its component parts, setting out, assembly and fitting, joints and connections, and testing. He was a master craftsman, fully conversant with all branches of his trade, consciously proud of his membership of the technical fraternity

REFERENCES

1. **Hill D. R.** (1974), *The Book of Knowledge of Ingenious Mechanical Devices*, Boston, USA.
2. **Uzun A. (**1997), *Cizreli Eb-Ul-İz ve Otomatik Makinaları*, Esra Yayınları Konya.
3. **Uzun A.** (2003), Cizreli Eb-Ul-Iz ve Otomasyon Sistemleri, UMTS, Gazi Üniversitesi, Ankara, Turkey.
4. http://en.wikipedia.org/wiki/Al-Jazari
5. http://en.wikipedia.org/wiki/Al-Jazira%2C_Mesopotamia Minor.
6. http://orionrobots.co.uk/tiki-index.php?page=Al+Jazari
7. http://www.history-science-technology.com/Articles/articles%206.htm

DYNAMICS OF THE AIR BLOWER WITH GYROSCOPIC COUPLE

Marius Vasylius[*], Vytautas K. Augustaitis[**], Vytautas Barzdaitis[***], Marijonas Bogdevicius[****]

[*]Klaipeda University, Mechatronics Science Institute, Bijunu str. 17, LT-91225 Klaipeda, Lithuania
[**]Vilnius Gediminas Technical University, Department of Machine Building, J. Basanaviciaus str. 28, LT-32214,Vilnius, Lithuania
[***]Kaunas University of Technology, Engineering Mechanics Department, A. Mickeviciaus str. 37, LT-44244, Kaunas, Lithuania
[****]Vilnius Gediminas Technical University, Department of Transport Technological Equipment, Plytines St. 27 LT-10105, Vilnius, Lithuania

mvasylius@yahoo.com, pgkatedra@me.vtu.lt, vytautas.barzdaitis@ktu.lt, marius@ti.vgtu.lt

Abstract: To avoid damaging of tilting pad journal bearings, the problem of safety shut down of high speed air blower cantilever rotor becoming important in modern industry. The experimental testing, modeling and simulation of dynamic behavior of rotating system was run to directly evaluate gyroscopic negative effect damaging journal bearings. A dynamic model of air blower rotating system was designed and simulated. A simulation and experimental measurement results of rotating system were used to optimize the shut down regime of machine. Gyroscopic effect influences of rotor bearing stability are confirmed. Results of numerical simulation confirm results of experimental vibration measuring. The theoretical research results are given and conclusions are made. Experimental testing and simulations results was applied to typical air blower rotating systems for elimination of huge negative forces acting on new bearings during shut down of the machine.

1. INTRODUCTION

One of most often problems occurring rotating system exploitations is high vibration displacements of journal in tilting pad bearings. The general causes of these vibrations are unbalance, insufficient dynamic stiffness, mechanical looseness and rotating elements wear, etc. (Bently, 2002)

Rotors of turbines, compressors, fans and etc. carry one or more disks, and these disks besides contributing to a lumped mass at stations where they are located, also introduce a gyroscopic couple. The effect of gyroscopic couple is predominant, if the disk is located at a nodal point or at a free end of the rotor (Rao, 1996) . The effect of gyroscopic couple has been researched in many papers, starting from pioneering works by Smith (1933), Yamamoto (1954), Dimentberg (1961), considering various ways of unfolding the rotor lateral transversal and angular motion. Descriptions of gyroscopic effects, together with more complete lists of references, can be found in publications by Ehrich (1992) and by Vance (1988). An experimental work dealing with parameter identification for the rotor system with large gyroscopic influence was reported by D. Bently et al. (1986) (Muszynska, 2005).

Technological critical machinery is expensive. They cannot be replaced. The stoppage or breakdown of these machines are destructive to all technological process and associated with big economical losses. That is the main reason to estimate the technical condition of the machinery by using technical condition monitoring, protection and failure diagnostics and particular unexpected breakdown preventions systems (Barzdaitis and Činikas, 1998).

The purpose of this paper is to design the mathematical model of air blower rotor's system, which describes the vibrations of the system and to identify the sources of the vibrations: dynamic stiffness of bearing support, the rotor's systems resonance frequency and identify the influence of gyroscopic effect of rotor vibration.

2. ROTATING SYSTEM OF AIR BLOWER MACHINE

The air blower machine SF01-18 comprises high power electric motor EM, gear box GB and blower rotor BR, as shown in Fig. 1. The induction motor (power 5.6 MW) runs at 1500 rpm and rotates an air blower rotor BR through flexible 8 pin type coupling C1, gear box GB and flexible type coupling C2 at high rotational speed at 3119 r/min.

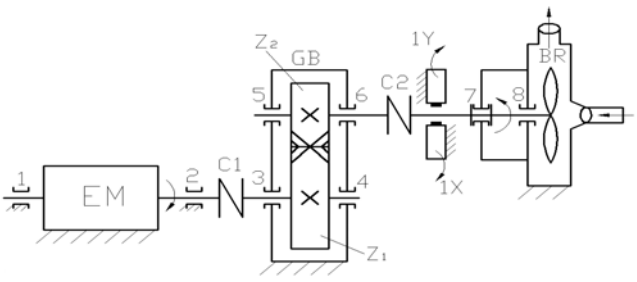

Fig. 1. The air blower and proximity probes location scheme: 1, 2 – journal bearings of EM; 3 - 6 – journal bearings of gearbox (GB) with transmission ratio u = 0.477712, z_2 = 43 of a driven gear and z_1 = 90 of a driving gear; 7, 8 – tilting-pad journal bearings of blower rotor (BR); C1, C2 – flexible couplings; 1X, 1Y – proximity probes fixed at the 7th bearings

For technical condition monitoring and vibration data analyzing has been used diagnostic equipment Dynamic Machine Analyser DMA04 (Epro, Germany, Profess s.r.o., Czech Republic), with software MMS 6850 Database (Adash s.r.o. Czech Republic). The technical condition is evaluated by monitoring of air blower rotor vibration displacement permanently.

In this article we studied dynamics behavior of blower rotor pivoted-pad journal bearings. The objective is to determine the main reason of the journal bearings failure. The blower rotor shaft vibration displacement $s_{p\text{-}p7}$ and s_{max7} values at 7th bearing and maximum vibration displacement s_{max} values of the shaft at the middle location point between 7th and 8th bearings monitored by means of 7X, 7Y proximity probes, contact less measurement induction sensors.

3. RESULTS OF EXPERIMENTAL INVESTIGATION

The experimental testing of the blower rotor vibration made at different running modes: at nominal loading 100 % and 50 % and at free run. The blower rotor resonance speeds measured at run up and coast down regimes. The 7th bearing shaft vibration displacements and orbits at full loading and coast down running mode are presented in Fig. 2a and Fig 2b.

The peak-to-peak vibration displacement values at resonance speed 1436 rpm reached inaccessible values in both *X* and *Y* orthogonal directions as shown in vibration displacements plots and orbit of the shaft, Fig. 2b. These vibration displacements $s_{p\text{-}p}$ values became 6-8 times higher at the resonance in comparison with values at the maximum load at 3119-3132 rpm (Fig. 2a). The blower rotor high vibration displacements at resonance mode damage the journal
bearings. The valuable damages are checked at the upper segment of the 7th bearing and the lower segment of the 8th bearing.

The dynamic forces that damages bearings depend not only by resonance phenomenon but by rotors gyroscopic effect too. The rotors shaft position in the 7th bearings is described by the gap value. When machine runs in coast down mode, the gap between the vertical sensor 7*Y* tip and shaft surface decreases about ~200 μm value reference to nominal position at maximum rotation speed.

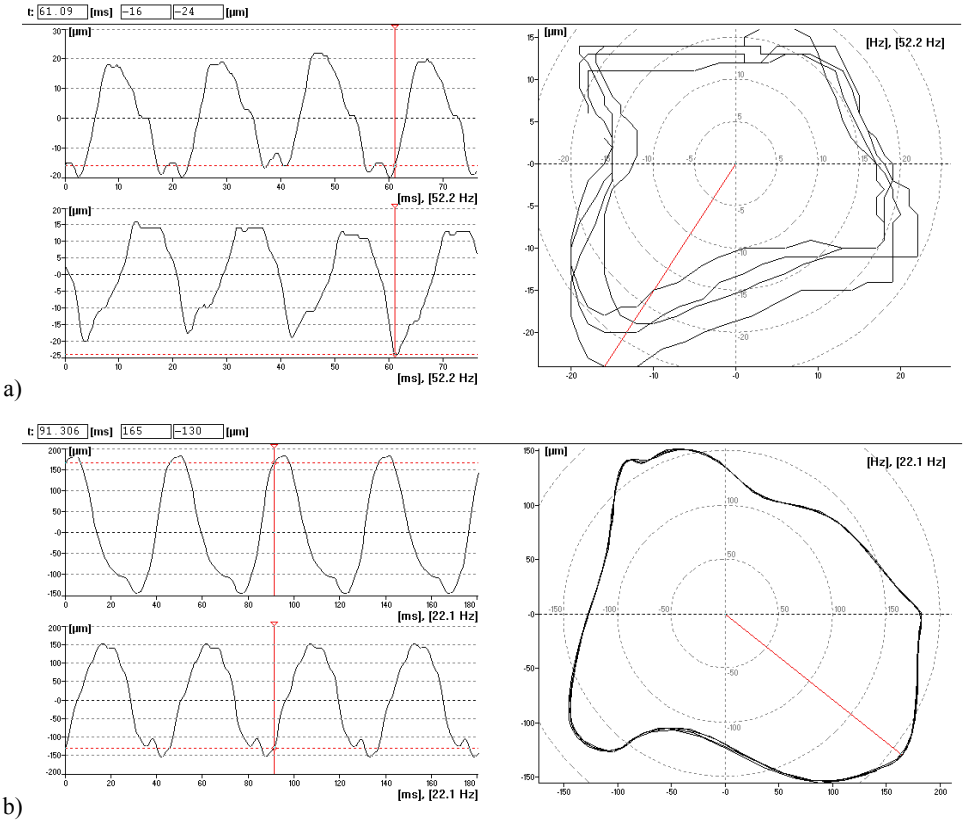

Fig. 2. The vibration displacements plots and orbits of blower rotor measured at bearing 7th at full loading (a): $s_{(o\text{-}p)x}$ = ~22μm, $s_{(o\text{-}p)y}$ = ~20μm and s_{max} = 27μm at 3132 rpm and at coast down, (b): $s_{(o\text{-}p)x}$ = 183μm, $s_{(o\text{-}p)y}$ =155μm and s_{max} = 210μm at 1324rpm

4. MODELING AND SIMULATION OF BLOWER ROTOR

The purpose of the mathematical modeling is to confirm a gyroscopic effect hypothesis and to estimate the influence of dynamics forces to bearings durability. The rotor dynamics is analyzed by the finite-element method, where the finite element consists of two nodes and five degrees (DOF) at each node. The first and the second DOF are displacements along the *y* and *z* axes and the last three DOF are angles around *X*, *Y* and *Z* axes.

The dynamic model of all system in static state is shown in Fig. 3.

There are three coordinate systems of axes to localize rotor position (Fig. 4):

1) Inertia coordinate system *OXYZ*. Point *O* in steady state coinsides with the point where rotor is attached to the blower.
2) In the moving coordinate system $O_1Y_1Z_1$ point O_1 is tightly connected to the rotor. When rotor rotates, geometrical center O_1 moves in plane *OYZ*.
3) Coordinate system $O_CY_CZ_C$ of mass center. Any rotor point P position is defined by vector $\vec{r}_{cp}$.

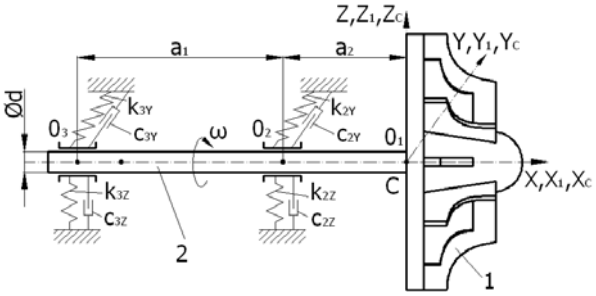

Fig. 3. Dynamic model of the air blower rotor: 1 – air blower, 2 – rotor, d = 0.20m, a_1 = 0.844 m, a_2 = 0.5m

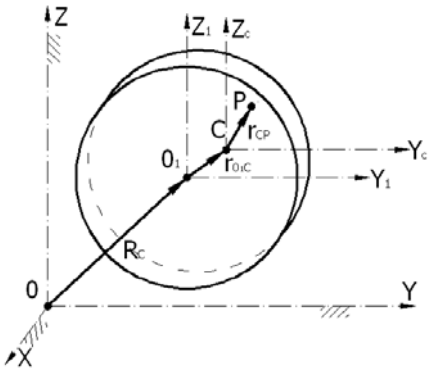

Fig. 4. The scheme of coordinates and vectors deployment which describe the rotor position

Work variation of inertial forces:

$$\delta W = \int_m \{\delta R_p\}^T \{\ddot{R}_p\}\, dm; \qquad (1)$$

Where $\{\delta R_p\}^T$ – variation vector of point P; $\{\ddot{R}_p\}$ – acceleration vector of point P.

The system of equations of blower:

$$[I_b]\{\ddot{\theta}\} = \{F_b(\theta, \dot{\theta}, t)\}; \qquad (2)$$

where

$$I_b = \begin{bmatrix} I_{x1x1} & -I_{x1y1} & -I_{x1z1} \\ -I_{y1x1} & I_{y1y1} & -I_{y1z1} \\ -I_{z1x1} & -I_{z1y1} & I_{z1z1} \end{bmatrix} - \text{mass interia tensor of blower}$$

$\{F_b(\theta, \dot{\theta}, t)\}$ – vector of forces which affecting blower.

Mass inertia tensor of blower:

$$[I_b] = [I_c] + [M_b][\tilde{r}_{01c}]^T [r_{01c}] + [\tilde{r}_{01c}]^T [\tilde{S}] + [\tilde{S}]^T [\tilde{r}_{01c}]; \qquad (3)$$

where $[I_c]$ – mass inertia tensor in respect of mass center. $I_c = \int_V \rho [\tilde{r}_{cp}]^T [\tilde{r}_{cp}] dV$; $[M_b]$ – mass matrix of blower; $[M_b] = diag(m_b, m_b, m_b)$; $[\tilde{r}_{01c}]$ – skew-symmetric matrix associated with vector $\{r_{01c}\}$; $[\tilde{S}]$ – skew-symmetric matrix associated with vector $\{S\} = \int \rho(\{r_{01c}\} + \{r_{cp}\}) dV$; $\{r_{cp}\}$ – vector defined position of either blower point in respect of mass center C.

Vector of forces and moments which affecting blower:

$$\{F_b\}^T = \left[\{F_{bR}\}^T, \{F_{b\theta}\}\right]; \qquad (4)$$

where $\{F_{bR}\}$– vector of forces which affecting blower. It calculable:

$$\{F_{bR}\} = -[\tilde{\omega}][A]\{S\} + [A][\tilde{S}][A]^T [\dot{G}_2]\{\dot{\theta}\}; \qquad (5)$$

where $[\tilde{\omega}]$ – Matrix of angular velocity; [*A*] – transformation matrix between global and local coordinate systems; $[\dot{G}_2]$ – derivate of matrix $[G_2]$ by time in global coordinate system; $\{\dot{\theta}\}$ – vector of derivate of turning angle. $\{F_{b\theta}\}$ – vector of moments which affecting disk. It calculable:

$$\{F_{b\theta}\} = -[\underline{G}_2]^T [\underline{\tilde{\omega}}][I_b]\{\underline{\omega}\} + [\underline{G}_2]^T [I_b][A]^T [\dot{G}_2]\{\dot{\theta}\}; \qquad (6)$$

where $[\tilde{\omega}]$ – skew-symmetric matrix associated with vector of angular velocity in body coordinate system. $\{\underline{\omega}\}$, $[\underline{\tilde{\omega}}] = [A]^T [\tilde{\omega}][A]$; $[\underline{\tilde{\omega}}]$ – skew-symmetric matrix associated with vector of angular velocity in the inertia coordinate system.

Transformations of coordinate:

$$\{R_{01}\} = [B_1]\{q\};$$

where $[B_1]$ – transformations of coordinate.

Angles, first and second derivates of angles vector velocities and accelerations:

$$\{\theta\} = [N_\theta]\{q\}; \quad \{\dot{\theta}\} = [N_\theta]\{\dot{q}\}; \quad \{\ddot{\theta}\} = [N_\theta]\{\ddot{q}\}. \qquad (7)$$

where $[N_\theta]$ – matrix of element form function.

Vector of blower generalized coordinates:

$$\{q_b\} = [B]\{q\}; \qquad (8)$$

The system of equation of blower motion:

$$[B]^T [M_b][B]\{\ddot{q}\} = [B]^T \{F_b(q, \dot{q}, t)\}; \qquad (9)$$

The equations of motion of rotor's finite element are derived by applying a Lagrange equation of the second order, which can be written as follows:

$$\left(\left[M_e\right]+\left[B\right]^T\left[M_b\right]\left[B\right]\right)\left\{\ddot{q}\right\}+\left(\left[C_e\right]+\left[G_e\right]\right)\left\{\dot{q}\right\}+\left[K_e\right]\left\{q\right\}=\left\{F_e\left(q,\dot{q},t\right)\right\}+\left[B\right]^T\left\{F_b\left(q,\dot{q},t\right)\right\}; \quad (10)$$

where $[M_e]$, $[M_b]$, $[C_e]$, $[G_e]$, and $[K_e]$ are mass of finite element, mass of blower, damping, gyroscopic and stiffness matrices of the finite element, respectively; $\left\{F_e\left(q,\dot{q},t\right)\right\}$ and $\left\{\vec{F}_b\left(q,\dot{q},t\right)\right\}$ are vectors of forces which affecting rotors finite element and blower.

General equation of all rotating system in matrix form:

$$\left[M\right]\left\{\ddot{q}\right\}+\left[C\right]\left\{\dot{q}\right\}+\left[K\right]\left\{q\right\}=\left\{F\left(q,\dot{q},t\right)\right\} \quad (11)$$

where $[M]$, $[C]$, $[K]$ are the mass, damping and stiffness matrices; $\left\{F\left(q,\dot{q},t\right)\right\}$ is a non-linear force vector; $\left\{q\right\}$, $\left\{\dot{q}\right\}$ and $\left\{\ddot{q}\right\}$ are the displacement, velocity and acceleration vectors of the finite-element assemblage. In an implicit time-integration scheme, the equilibrium of the system (11) is considered at time $t + \Delta t$ to obtain the solution at time $t + \Delta t$. Iteration will be performed in the non-linear analysis (Barzdaitis and Bogdevičius, 2006).

5. RESULTS OF THEORETICAL INVESTIGATION

The calculation results are shown in Fig. 5 and Fig. 6. There is orbit plot of the rotor center O_2, were rotor is attached to air blower, Fig. 5. Numerical calculation results approved that vibration displacement of the rotor are caused not only by unbalance, but by gyroscopic effect too.

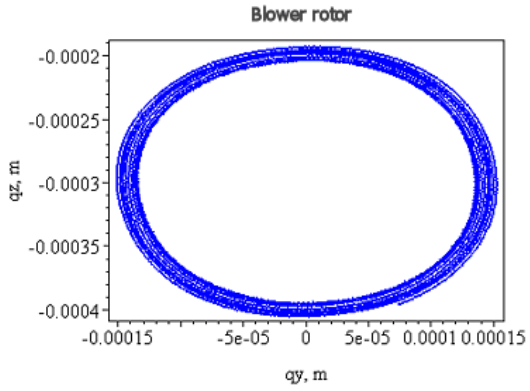

Fig. 5. Orbit of the rotor center point O_2 at nominal rotation speed 3120 rpm, $s_{p\text{-}pmax}$ = 300 μm.

In Fig. 6 are shown orbit of the shafts rotating in 7th and 8th bearings. The four pad tilting-pad journal bearing model of the rotating system was used. The numerical calculation results were acquired with such parameters: coefficients of stiffness of bearing $k_{3Y}=k_{3Z}=200\times10^6$N/m, $k_{2Y}=k_{2Z}=150\times10^6$N/m; coefficients of damping $c_{3Y}=c_{3Z}=40\times10^3$Ns/m, $c_{2Y}=c_{2Z}=20\times10^3$Ns/m; rotor diameter d=0.20m; air blower weight m=1660kg.

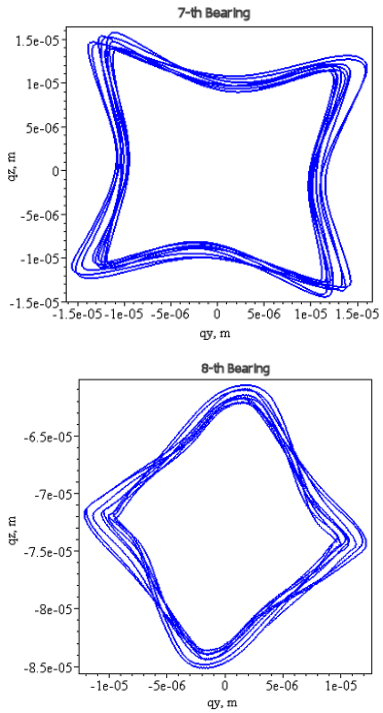

Fig. 6. Simulation results of the journals motion in the bearings at nominal rotating speed 3120rpm. a) – orbit of 7th bearing $s_{p\text{-}pmax}$=31μm, b) – orbit of 8th bearing $s_{p\text{-}pmax}$=25μm

6. CONCLUSIONS

1. The designed theoretical model of the air blower rotating system is based on the finite-element method.
2. Calculation and experimental results indicated that gyroscopic effect is important for long continuous run of
tilting pad journal bearings. Elevated hypothesis is that air blower rotors gyroscopic moment decrease rotor dynamic eccentricity at nominal rotating speed.
3. But during shutdown mode of operation its negative influence of the tilting pad bearing wear is inadmissible too high.
4. Air blower rotating system shutdown time interval must be minimized with additional brake mechanism.

REFERENCES

1. **Barzdaitis V., Bogdevičius M.** (2006), The Dynamic Behavior of a Turbine Rotating System/ Strojniski vestnik, *Journal of Mechanical Engineering*, 5210, 653-661.
2. **Barzdaitis, V., Činikas G. (1998)**, *Monitoring and Diagnostics of Rotor Machines*, Kaunas: Technologija, Lithuania.
3. **Bently D. E.** (2002), *Fundamentals of Rotating Machinery Diagnostics*, Library of Congress Control, Bently Pressurized Bearing Company.
4. **Muszynska A.** (2005), *Rotordynamics*, CRC.
5. **Rao J. S.** (1996), Rotor Dynamics 3th edition, New Age Publishers.

SPEECH CONTROL FOR MOBILE ROBOTIC SYSTEMS

Arkady S. YUSCHENKO, Dmitry N. MOROZOV, Andrey A. ZHONIN

Bauman Moscow State Technical University, 105005, Moscow, 2-nd Baumanskaya str., 5, Russia

robot@bmstu.ru, morozovd@mail.ru, neurofish@yandex.ru

Abstract: The experience and intelligence of human are necessary to fulfill the hazardous and responsible operations by mobile robot in undetermined environment. To make the control process more effective and simple for human the speech control may be used. The operator's interface in this case may be created using the linguistic variables both for commands formalization and for information presentation. The speech controlled robot has to be an autonomous intelligent system capable to re-cognize the current situation and to adopt its behavior to real environment. To adopt the artificial intelligence to the human impression and reasoning the fuzzy logic principles may be used to create the knowledge base of a speech controlled robot. The simple manipulation and locomotion operations may be presented in form of fuzzy production rules. For complicated modes of behavior the procedure of fuzzy AI – planning have been proposed. The procedure of robot learning on the base of fuzzy neural networks has been developed .for the situations when human-operator can not formalize the fuzzy rules of robot behavior beforehand.

1. INTRODUCTION

Mobile robots are widely applied for complicated operations in undetermined environment. Among such operations are mine disarming, fire fighting, rescue operations, medical service, etc. Robotic systems are normally equipped with manipulators, different sensors, including vision systems. Such systems are generally controlled by human operator whose experience and intelligence is necessary to fulfill the hazardous and responsible operations. The control of mobile robots is often realized now as a remote control by human-operator using a kind of joystick to guide the motion of a manipulator or a chassis. This mode of control is difficult for operator working in time and information deficit and often inefficient creating the risk of error due to the "human factor". Thus a task emerged to arrange the control process so that the operator would have to specify only the aim of the operation. The robot is supposed to assess the environment and make decisions that are necessary to ensure the aims posed by the human operator are achieved. Such systems have been traditionally defined as Intelligent Robotic Systems (IRS). It is rational to arrange the IRS control based on speech, which is expected to take the shape of bi-lateral dialogue between the robot and the operator using a problem-oriented language similar to a natural one.

The speech control, in turn, induces a whole range of artificial intelligence control problems including environment scenes and operator's commands recognition, motion planning, knowledge accumulation and IRS training. Theses tasks are suggested to be solved using the same approach based on linguistic variables and fuzzy logic application. Some of the tasks are discussed below.

2. ENVIRONMENT REPRESENTATION

The environment representation in a human-controlled IRS is based on the corresponding representation in human mind. The information necessary for control in a given situation can be expressed using the means of a natural language (NL) and then translated to a formal language of the relevant semiotic model that is used to control the robot. One of the peculiarities of such representation is its structure, i.e. the representation of the environment as a set of objects bearing particular names and linked with particular relations. D.A.Pospelov names 11 types of such relations (including spatial, temporal, quantitative, causal, and others) (Pospelov, 1986). In most cases of mobile robots control, the environment description in IRS based on fuzzy representations includes the description of objects in the environment as well as spatial and temporal relations between them. The human is known to assess these relations using psycho-physiological scales, defined by objective properties of the corresponding receptors in his body. Therefore the most adequate means to describe the spatial-temporal relations is the apparatus of linguistic variables which uses the same scales.

To describe the current scene, extensional and intentional relations are employed. The former are represented by the relations that describe the location and orientation of objects. For example *a1 is far, to the right, to the fore and a little above a2.* The latter include the relations like R_1 *– to be adjacent to;* R_2 *– to be inside of;* R_3 *– to be outside of;* R_4 *– to be in the centre of;* R_5 *– to be on the same line as;* R_6 *– to be on the same plane as;* R_7 *– to have zero projection on,* R_8 *– to be on the surface of.* Two unary relations are also proposed in (Pospelov, 1986) – R_{00} – *to be horizontal* and R_{01} – *to be vertical*, as well as 28 elementary spatial binary relations.

The set of specified objects in the current scene, the relations between them, and transformation rules constitute a formal language for scene representation, that is similar to a natural language. Scene description in this language allows for a formal semiotic representation that uses the spatial-temporal relations logic. So, a complex relation *a_1 is on the surface S far and to the right* can be written as *$(a_1\ R_8\ S)\&(a_0\ d_5\ f_7\ a_1)$,* where a_0 – is the observer, with respect to whom the distance and orientation relations are formulated.

Since the environment is ever-changing due the motion of the observed objects as well as to the motion of the robot itself, the scene description changes in time respectively. This circumstance requires that we take into account not only spatial but also temporal relations in the external world, such as *to be simultaneous with, to be prior to, to follow* etc.

3. OPERATIONS DESCRIPTION

External world description allows to pass on to the description of robot's operations within it (Yuschenko, 2002). We assume that complex operations performed by the robot can be represented as a sequence of relatively few typical consistent operations. These are define in advance and are stored in the IRS knowledge base as frames of typical operations. A frame of this kind contains linguistic variables based description of the aims of an operation, the initial stage scene, and the preconditions for the feasibility of the operation. The latter may depend on the specific situation, the capabilities of the robot in question, and the properties of the object of the operation. Thus, the structure of a typical operation frame is as follows: *<operation name> <operation object> < initial situation (modifier of place)> <target situation> <operation feasibility conditions (preconditions)>.<additional details>***.** For example: *<move> <object A> <object A on B> <object A on C> <object A is free>* **<***install object A shock-free***>**. While performing technological operations this frame should sometimes have an extra slot <operation performance method (modifier of manner)>.

Preconditions are one peculiarity of the discussed operations description approach. Generally, all preconditions can belong to one of at least three types: a) situational, e.g. the condition *object A is free* means that *there are no other objects on object A*; b) preconditions stipulated by the robot's capabilities: *the robot is equipped with the gripper suitable for type and size of the object*; and c) preconditions connected with the peculiarities of the object: *the object is a rigid body and can withstand the force developed by the gripper without any damage*.

The description of typical operations expands the situation description language mentioned above. The operator can control a robotic system directly by giving the names and aims of the typical operations in the problem-oriented language, e.g., *‹move object A to plane C› ‹insert shaft A into orifice O›*. Preconditions description may not always be complete in the sense that some of them may not be defined. For example, it may not be known whether there is free space on plane C, on which object A is to be put. Then a query to the cognitive operations base is formed, and an operation is selected for examining plane C that is supposed to provide for filling in the empty slot. The system can also formulate address queries to the operator, if cognitive actions yield no results or uncertainty persists.

Taking into account the similarity between the proposed language for IRS operations description and the situational control language as formulated by D. A. Pospelov, we shall keep to this term bearing in mind the above mentioned peculiarities of the language for IRS.

4. COMPLEX OPERATIONS PLANNING

We shall use the term complex for the operations that can be represented by a sequence of consistent typical operations that result in achieving the aim. Consistency of operations means that the situation achieved as a result of n-th operation meets the preconditions for the (n+1)-th operation. If after the actual completion of n-th operation the consistency is not achieved, the planning process is repeated, with the current situation being assumed as the initial. A distinctive feature of planning procedure in robotics, as compared to numerous methods of artificial intelligence planning, is the possibility of continuous comparison of the real situation observations and the conditions defined during the planning stage. The comparison can be performed as that of linguistic descriptions of the observed and expected (existing only as a statement) situations. The emerging conflict induces a plan of actions aimed at solving it and hence realization of the desired situation. Thus the aim and the name of each separate typical situation gene-rated by the system based on the comparison of real and expected situations, rather than specified by the operator.

The conflict resolution approach is rather similar to human cognitive activity while planning actions, which is also based on comparing the operative image of the situation and the target image. The conflict resolution principle application requires a further extension of IRS control language. Besides the "vocabulary" of typical operations we now need a "vocabulary" for situational conflicts resolution by means of performing typical operations. If spatial relations are intentional then each type of conflict induces its own typical operation to resolve it.

For example: if the aim is: *$(a_1\ R_8\ S)$,* i.e. object a_1 is on the surface S, while in fact *$(a_1\ \neg R_8\ S)$,* then the conflict induces a typical operation *move a_1 to S* . If the aim is defined as *$(a_1\ R_2\ C)$,* i.e. *shaft a_1 is inside orifice C*, while observation results show *$(a_1\ \neg R_2\ C)$,* then a typical operation is induced: *insert a_1 into C.* If the condition *a1 is free* is necessary for further operations, while in fact we have: *$(a_2\ R_8\ a_1)$,* i.e. *a2 is on a1*, then a typical operation *remove a_2 from a_1* is induced. One can easily proceed with this list of action that resolve intentional type conflicts.

If the relations are extensional there is no need for a special vocabulary for matching the situation with the required typical operation. Conflict can be resolved by performing a typical operation aimed at the relation specified as its precondition. If a mobile robot R is expected to in position *$(R\ d_1\ f_1\ N)$* with respect to observer *N*, while in fact a different conditions holds true: *$(R\ d_2, f_2\ N)$,* then

the required operation will be defined in the form of: *move robot R from position (R d_2 f_2 N) to position (R d_1 f_1 N).*

While planning complex operations there emerges a multi-step procedure of conflicts resolution. At first, the target and the actual situations are compared. If they do not coincide, the conflicts are defined and the actions are devised to resolve the conflicts. Then the preconditions of the resolving actions are checked, as they can also be in conflict the actual situation. They generate new actions and so on, until at least one resolving action meets the necessary conditions. Then this operation is performed (so far on the planning level), and a new situation appears, which is analyzed in a similar way and so on. This procedure can be represented as directed graph, with its root being the target situation (Yuschenko, 2005).

A disadvantage of the existing approach is that the operator has to define the rules for different situations beforehand, hence the situations should also be known in advance. If the operator fails to formulate the IRS operating rules, then the system can be taught instruction. In this case the operator guides the robot through typical situations after which the information is processed in, e.g. teachable fuzzy (hybrid) neural networks (Vechkanov et al., 2002).

5. SPEECH INTERFACE

Speech interface is the main method to transfer the control data to the IRS. In consists of recognition and linguistic blocks. The recognition block is a device for transforming speech signals as well as interpreting them as separate words or phrases. The linguistic block performs the interpretation of statements into situational control language, as well as the representation of these statements in a semiotic form.

At present there are two most widely used methods of speech recognition : Dynamic Time Warping (DTW), or template matching, and hypothesis probability estimation using Hidden Markov Models (HMM). The template matching method can hardly be regarded a continuous speech recognition method. Moreover, it is speaker depen-dent and requires periodical templates refreshment. For continuous speech recognition one can employ template phrases construction, using the information on the grammar of the IRS problem-oriented language. It is possible to increase the number of operators whose commands the system can efficiently recognize, by means of the so-called method of multiple templates.

The HMM method using hypothesis probability estimation with Viterbi algorithm (beam-search) allows to recognize continuous speech almost independent of the speaker. However this method requires a high quality and expensive teaching speech database. Moreover, the hypothesis probability estimation method implies that the a-priori probability distribution of different hypotheses is known in advance, at the same time ignoring the possible similarity of speech messages. In other words, the HMM method is incapable of detecting and using the distinctive features of words or phrases, in contrast with the template matching method.

Operators statements for IRS control can be formulated in the robot situational control language mentioned above. The linguistic analyzer performs the syntactic and semantic decomposition of the statement which is supposed to result in filling the slots of the frame that describes operations.

When passing from speech sound signal recognition to the inner representation of the operator's sentence, the sequence of words-members of the sentence undergo a formalization procedure. Each sentence – except degenerate commands like "stop" – is presented in the form of typed predicative structure. While describing a sentence, that is in fact a command to perform a certain operation, the corresponding verb plays the key role and is described by the higher-order frame. The slots of the frame are filled in with relevant subordinate parts of the command-sentence. Relying on L. Tesniere's *verb-centric theory* we can introduce the obligatory and arbitrary valences for each of the verbs that describe the IRS' operations. Each slot of the higher-order frame can also be an encapsulated frame, which is the case, e.g. with operation object description. This relieves the operator from the necessity to include into the command-sentence all available information on the object in question. Providing only one of the identification tags allows to assign to the object all available data (size, position, e t. c.) on the semantic level of the speech interface without human interference. The linguistic recognition stage output is a set of encapsulated frames that can be uniquely interpreted over the further stages of command-sentence completion.

It was shown above that the sentences represented by linguistic frames can be expressed in the inner semiotic language as a sequence of symbols. Operator's command that arrives through the speech recognition block is in turn a sequence of symbols as well. Thus, the interaction between recognition and linguistic is reduced to transforming one sequence of symbols into another, based on an expert-built grammar. At the same the linguistic analyzer can be represented as finite-state automaton.

The speech recognition block generates a stream of word hypotheses constituting the operator's sentence. For each word a hypothesis is selected that has the higher probability value. The linguistic block after recognizing each separate word is to define a manifold of acceptable ending of the phrase, with each variant of the complete sentence being assigned the corresponding probability. Using this information the recognition block selects the most plausible hypothesis for the next word (or phrase). The advantage of using the DTW method in this case is in the fact that the reduction of number of the hypotheses to be recognized allows us to use the computational adjustment procedure that would choose the most relevant hypothesis of the remaining few.

Note that the recognition block can in some cases result in recognition failure instead of a hypothesis, as is the case when the noise level is high. In this case the IRS requests the operator for the missing information. The operator's answer can in turn pose new questions which brings about the requirement to fit the linguistic block with a separate dialogue-planning module.

6. CONCLUSION

The preliminary research has shown that the implementation of speech control for a robotic system by way of formulating separate commands is inefficient. It is necessary to develop a speech interface meant focused on the use of problem-oriented language similar in its structure to the situational control language. This allows a substantial simplification of the task of robot control, as it no longer requires any special skills from the operator. There are ho-wever a number of tasks in this field that are yet to be solved. In particular, the application of speech interface for teaching the robot, rather than merely controlling it, when the rules of behavior cannot be formalized in advance, is seen as very important. We also attribute crucial importance to the psychological aspects of interaction between a human and an "intelligent" system, connected with "mutual" ideas about the situations and reasonable beha-vior.

REFERENCES

1. **Pospelov D. A.** (1986), *Situational Control: theory and practice*, Nauka – Phys.matt.lith., Moscow.
2. **Vechkanov V. V., Kiselev D. V., Yuschenko A. S.** (2005), Adaptive system for mobile robot fuzzy control, *Mekhatronika*, Vol. 1, 20-26.
3. **Yuschenko A. S.** (2002), Robot distance control using fuzzy concepts, Iskusstvennyi intellect, *Vol. 4, NAS Ukraine*, 388-396.
4. **Yuschenko A. S.** (2005), Intelligent planning in robot operation, *Mekhatronica*, Vol. 3, 5-18.